ISBN 82-471-7826-5 (printed version)
ISBN 82-471-7825-7 (electronic version)
ISSN 1503-8181

Doctoral theses at NTNU 2006:41

Krishna Kanta Panthi

Analysis of engineering geological uncertainties related to tunnelling in Himalayan rock mass conditions

Doctoral thesis
for the degree of doktor ingeniør

Trondheim, February 2006

Norwegian University of Science and Technology
Faculty of Engineering Science and Technology
Department of Geology and Mineral Resources Engineering

NTNU
Innovation and Creativity

Acknowledgements

This study has been conducted at the Department of Geology and Mineral Resources Engineering, Norwegian University of Science and Technology (NTNU) in Trondheim, Norway.

Professor Bjørn Nilsen has been my supervisor for this study. His vast knowledge and experience in the field of engineering geology and tunnelling have very much enhanced my work. His enthusiasm and encouragement in using new methods and approaches for solving the problems and his continuous guidance have played considerably to accomplish the objectives of this thesis. He has provided financial support for the transportation of rock samples from Nepal and also provided financial support for attending Norwegian National Tunneling Congress in November 2004 and World Tunnel Congress in Istanbul in May 2005. I am very indebted to him.

I am grateful to Mr. Shiva Kumar Sharma, General Manager of Himal Hydro and Executive Committee Chairman for Modi Khola Project, Mr. Henning Fjelstad, former Executive Committee Chairman of Civil Construction Consortium for Khimti Project, Mr. Rajendra Nara Singha Pradhan and Mr. Rajeshwor Man Sulpya, Project Director and Director for Kaligandaki "A" Project, Mr. Shashi Raj Shrestha, Project Director for Middle Marsyangdi Project, for giving permission to use documents and data for respective tunnel cases. I am also thankful to Mr. Sarad Pokhrel, Manager for Impregilo SpA - civil contractor for Kaligandaki, Mr. Dibya Raj Panta and Mr. Kaustubh Nepal, Engineering Geologists at Middle Marsyangdi Project and Mr. Ram Hari Sharma of Himal Hydro for their help during my field work.

I express my gratitude to Norwegian State Loan Fund for providing educational loan for three years. I am thankful to Ms. Ragnhild Brakstad, Senior Coordinator – QUOTA Program at the International Office for her administrative support concerning loan and residence permit issues. I am also thankful to Ms. Turid Brak for her help concerning residence permit to my family.

I am grateful to Professor Haakon Støle and Ms. Hilbjørg Sandvik, Professor In-charge and Coordinator for MSc Program on Hydropower Development (HPD) at the Department of Hydraulic and Environmental Engineering for offering me one year financial support in lieu of my teaching contributions in rock engineering to MSc students for last four years. I am also grateful to them for their financial support for attending Hydropower'05 at Stavanger in May 2005.

I am thankful to Ms. Torill Sørløkk, Mr. Trond E. Larsen and Ms. Ingrid Vokes for their help to carry out test for the mechanical properties of rock samples. I am grateful to my friend Mr. Gyanendra Lal Shrestha and also to Mr. Purushottam Shrestha for their fruitful comments on this thesis. I am thankful to Mr. Nghia Trinh for his innovative program on joint rosette.

I am deeply obliged to my father Sobhakhar and mother Nim Kumari Panthi for their continuous effort to bring me to this level. I am grateful to my brothers, sisters, mother-in-law, brother-in-laws and sister-in-laws and other family members for their continuous support and care.

I am indebted to my wife Laxmi for her moral support, encouragement and love and also for her help in reviewing this thesis. I appreciate our daughter Kriti and son Kritagya for keeping our home lively that always encouraged me for next day work.

I dedicate this work to my parents.

Abstract

The need for tunnelling in Nepal, as in the Himalayan region in general, is enormous, particularly for hydropower development. Due to active tectonic movement and dynamic monsoon, the rock mass in the Himalaya is relatively weak and highly deformed, schistose, weathered and altered. Predicting rock mass quality, analyzing stress induced problems, in particular tunnel squeezing, and predicting inflow and leakage often have been found extremely difficult during planning stage. Considerable discrepancies have been found between predicted and actual rock mass conditions, resulting in significant cost and time overrun for most of the tunnelling projects. Finding innovative solutions for quantifying geological uncertainties and assessing risk are therefore key factors for cost effective and optimum future tunnelling through Himalayan rock mass.

In this thesis, a probabilistic approach of uncertainty analyses has been introduced to deal with the most important geological uncertainties reflecting Himalayan rock mass conditions. A geological uncertainty analysis model concept based on the software program @Risk has been applied for this purpose.

The analyses presented in this thesis are based mainly on four headrace tunnel cases from Nepal; 1) 60 MW Khimti I hydropower project, 2) 144 MW Kaligandaki "A" hydroelectric project, 3) 14 MW Modi Khola hydroelectric project, and 4) 69 MW Middle Marsyangdi hydroelectric project. The first three projects have been completed recently and the fourth one is under construction.

The thesis identifies the most crucial aspects of tunnel stability problems (geological uncertainties) by reviewing the engineering geological conditions of the respective cases and the Himalayan geology. It also evaluates the theoretical aspects of the main factors influencing on tunnel stability, reviews the engineering geological conditions, the extent of pre-construction phase engineering geological investigations, evaluates the deviation between predicted and actual rock mass conditions, and describes the laboratory testing that has been carried out for the respective cases. Probabilistic approaches that have been applied in the field of engineering geology in past and the basic theory on statistical analyses are briefly discussed. Main emphasis is then placed on the descriptions of useful probability distribution functions (pdf), the @Risk statistical analysis tool, the applied uncertainty analysis model concept and @Risk analysis for the respective tunnel cases.

The uncertainty analyses include rock mass quality evaluation based on the Q-system of rock mass classification for Khimti and Modi Khola headrace tunnels, tunnel squeezing based on Hoek and Marinos approach for Kaligandaki and Middle Marsyangdi headrace tunnels, and finally analysis of water leakage from the Khimti headrace tunnel. The degree of correlation between simulated results achieved by the @Risk model and values actually measured in the tunnel is discussed and the sensitiveness and effect of variations in the value of each input parameter and sensitivity of equations and methods used to analyze geological uncertainties are evaluated.

It is concluded that the proposed uncertainty analysis approach gives very promising results and has a great potential for analyzing tunnel projects in the Himalayan rock mass conditions, but more cases are needed for conforming the reliability of the methodology.

Table of contents

Chapter 1
Introduction

1.1 BACKGROUND

Nepal is situated within the southern slope of the Himalaya, and is bounded by the two giant countries China and India, see Figure 1-1. The Himalayan region in Asia covers an area of about 594,400 square kilometres, of which Nepal occupies a total land of 147,181 square kilometres. From East to West, Nepal extends for about 890 kilometres and has a width ranging from 150 to 250 kilometres. Within this very short width, the altitude of the country varies greatly from about 100 meters above sea level at its Southern border to its maximum of 8,848 meters above sea level (the Mount Everest) at its North, giving very rough terrain and steep mountainous topography.

Because of the large elevation difference over a very short distance, the climatic conditions of the country also vary greatly. The higher Himalayan range (above 3,500 meters) to the North has an alpine climate and is mostly covered by snow and ice. The climate changes gradually becoming mild and warm at the Mahabharat range (lesser Himalayan range) and finally to sub-tropical hot weather at the deep valleys, the Siwaliks (Churia) and the Gangetic plane (Terai).

Nepal is a landlocked developing country with a population of approximately 23.1 millions and an annual population growth of approximately two percent. If this trend of population growth continues, it will reach approximately 40 millions by the year 2030. On the other hand, there is an increasing migration trend of people towards the urban areas, and it has been estimated that the population at the urban areas will increase by as much as 33 percent by the year 2030 (MoWR, 2003).

The ever increasing population trend and fast urbanization is augmenting pressure and is a major challenge in the economic development of Nepal. The major economic resources of the country are water resources (energy, irrigation and drinking water), agriculture, tourism and agro-tourism based industries. Maximum utilization of these resources is inevitable, and is only possible by developing infrastructures such as hydropower schemes, irrigation systems, road networks, drinking water systems etc. Development of all these infrastructures will indeed demand the need for the utilization of underground space like tunnels and underground caverns.

Figure 1-1. Geographic map of Nepal.

In recent past, the tunnelling activities have increased considerably in Nepal with the development of many medium scale hydropower projects. This increased activity in tunnelling has enabled to gain more knowledge in tunnelling through the Himalayan rock mass. The past tunnelling experience indicated that the majority of the tunnel projects developed have had suffered severe stability problems that made delay in completion and cost overruns.

The following sections aim to brief on the need for tunnelling in Nepal, to highlight major tunnelling challenges that have been faced in Nepal Himalaya, to formulate the scope of this PhD research, to briefly outline the research methodology that will be used in the research and finally to give the outline of this thesis.

1.2 NEED FOR TUNNELLING IN NEPAL

The use of underground space is not new in Nepal. The early miners used underground caverns and tunnels of smaller dimensions to extract ore and minerals such as copper, iron, lead, cobalt, nickel and different types of colour stones. However, the modern and institutionalized tunnelling in Nepal started with the excavation of the tunnels and underground powerhouse for Tinau hydroelectric project located near the town Butwal, see Figure 1-1. Since the completion of Tinau project in the early seventies, approximately 75 kilometers tunnels have been excavated.

There are mainly four areas where tunnels and underground caverns are needed in Nepal. They include; a) water conveying tunnels, b) transport tunnels, c) mining and d)

food storage facilities (Panthi, 2004). For the time being most of the tunnelling is focused on hydropower, and to some extent on mining and irrigation.

1.2.1 Hydropower and tunnelling

Most of the higher Himalayan range (above 3,500 m) of Nepal is mostly covered with snow and glaciers. Depending upon the altitude and monsoon effect the annual rainfall varies from less than 250 mm in the higher Himalaya to more than 4,000 mm in the mid-hills (UNESCAP, 1996). Being snow fed and very steep in their gradient, most of the major rivers originating from the Himalaya have considerable potential in hydropower generation. In particular, those rivers originating from the elevation above 3,500 meters are perennial. For this reason, Nepal has been gifted with considerable hydropower potential, see Figure 1-2.

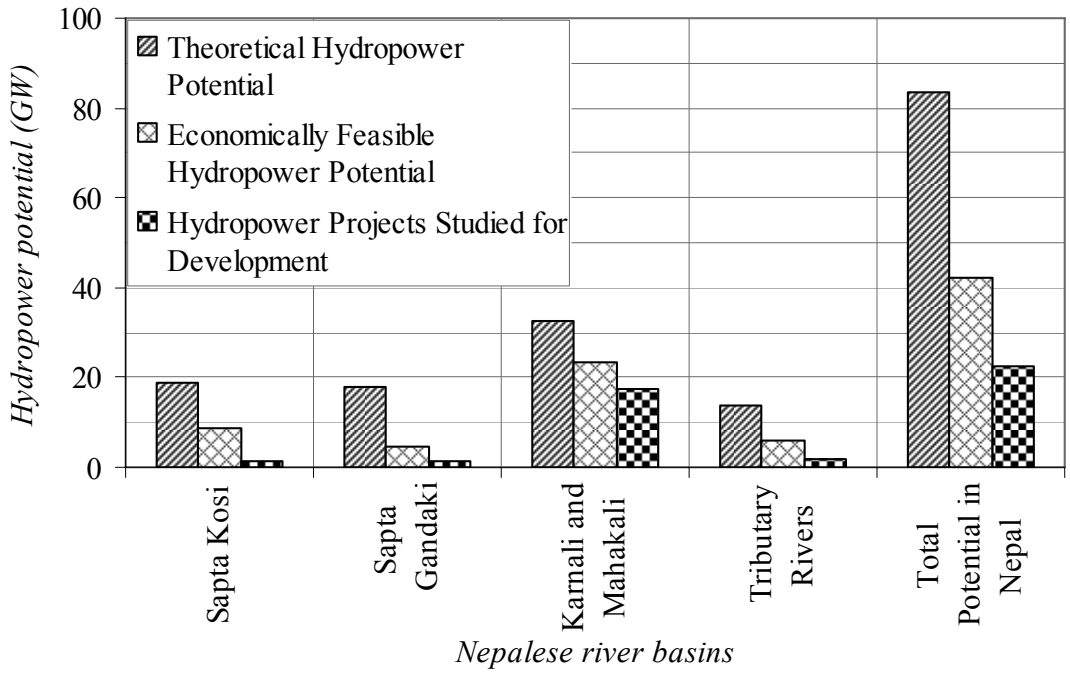

Figure 1-2. An estimated total hydropower potential of Nepal covering different river basins of the country (based on MoWR, 2003).

Nepal has so far managed to develop only about 560 MW hydropower energy, and approximately 40 percent of the total population has got access to it. Apart from the domestic requirements, fast developing India could be an important hydropower energy market for Nepal, since India is experiencing shortage of energy with ever increasing energy demand. Prasad (2003) predicts that by the year 2013 almost 220,000 MW installed capacity of electrical energy is required in India to cope with very rapidly growing economy. Today, the installed capacity of electrical energy in India is approximately 148,000 MW and hydropower contributes only 27,000 MW. Moreover, India is one of the major countries in the world that considerably contributes to global emissions of carbon dioxide (DoE, 2003). Consequently, the hydropower potential that ex-

ists in the Nepal Himalaya could be an alternative and environmentally friendly energy source that could help not only to fulfil the energy demand to India, but also help in reducing the carbon emission to the world (Panthi, 2004).

As can be seen in Figure 1-2, a number of possible hydropower projects have already been studied in different river basins of Nepal and are ready for the materialization. A study carried out by the Water and Energy Commission Secretariat (WECS) of the Ministry of Water Resources (MoWR) indicates that more than 850 kilometres of tunnelling needs to be done to develop already planned hydropower potentials in Nepal (Joshi, 2000). Thus, tunnelling requirement for the development of hydropower is simply enormous in Nepal.

1.2.2 Transport and tunnelling

A balanced, coordinated, well-managed and efficient transport system is a precondition for the sustainable development and economic growth of a country like Nepal. Except for the southern flat land and in some inner valleys, there are many limitations for the development of good air and rail transport in Nepal. Thus, the most suitable mode of transport is an efficient road network. The development of such road network will make it possible to link different parts of the country and commercial hubs, contributing largely for the economic and social development of the country (Panthi, 1998).

At present, A total of approximately 15,000 km of road has been built in Nepal, see Figure 1-3, of which 29 percent are blacktopped with fair to good quality, 25 percent are gravel surfaced and remaining are earthen surfaced (UNESCAP, 1996). The present situation on road network is thus unsatisfactory and poses considerable demands on the need for improving existing road system. The connection of the mountainous part of the country with good quality road to southern flat Gangetic plane, where high level of economic activity exists, is very needy. Such North-South running highways will play an important link between the fast growing economics of India and China.

The Himalayan region as a whole is affected by a constant tectonic uplifting as well as downcutting effects by several river systems. The active tectonic activity and monsoon on the predominantly fragile and deeply weathered rock mass of the Siwaliks and lesser Himalaya make steep mountain slopes highly unstable and erosion prone. Many rock and soil slope failures occurring during monsoon season along the road cut slope not only obstruct the transport movement, but also make considerable human and property damage. Figure 1-4 is one of the many examples of the Prithivi highway, which is the only reliable gateway to capital city Kathmandu from the rest of the country.

Figure 1-3. Existing national road network and major river systems of Nepal (river system added to DoR, 2004).

As shown in Figure 1-4, a major rock/soil slide started to develop in July 1999 at Krishnavir, located 83 kilometres West of Kathmandu. The slide further aggravated during the monsoon 2000 with a massive movement of the slope, and is still active in every monsoon. According to Regmi and Sitaula (2003) almost 360 hours of complete road closure occurred during two monsoon periods in 2000 and 2001 as a result of this major slide, and similar closures are routine in every monsoon period.

Figure 1-4. A major slide at Krishnavir along the Prithibhi highway "a main gateway to Kathmandu valley". Slope protection works with gabion (left) and the extent of slope failure (right).

According to the Nepalese government's 10th national plan, special attention should be placed on regional and sub-regional cooperation for the integrated development of the transport sector in South Asia. The standard of major East-West and North-South highways therefore must be improved so that these highways can be converted into regional commercial routes with high rate of return. The 10th plan also emphasizes on the minimization of investment costs as well as environmental degradation during design, construction, maintenance and rehabilitation of such road systems (NPC, 2003).

The quality target set by the government for major highways is only possible to achieve if road tunnels are introduced on the highways running through mountainous parts of the country. The introduction of such road tunnels will not only reduce the road length, but also make it possible to avoid the areas that are very steep and vulnerable to slope failures and risk of rock falls. As an example of such undertaking that should be mentioned is the planned Kathmandu – Hetauda direct link with an approximately 60 km road length including three road tunnels with total length of 8 km, see Figure 1-3.

If this road project is implemented, it will shorten the existing 224 kilometers long route to only 60 kilometers, making it the shortest connection from the southern flat land to Kathmandu and to Tibet, China (Panthi, 1998).

1.2.3 Other infrastructures and tunnelling

The other areas of infrastructure development where tunnelling is required in Nepal are irrigation, water supply, mining and storage facilities. Even though there are many possibilities for excavation of tunnels and underground caverns in these areas, very little has been done so far, excluding a few kilometers of tunnelling for irrigation and mining. The introduction of underground storage caverns, for example, may help in the reduction of electrical energy.

There are also many tunnelling projects that have been planned for the purpose of improved irrigation and water supply schemes in Nepal. One of the notable tunnelling projects, which requires almost 26 km of tunnelling and has also fallen to national priority, is the Melamchi drinking water supply scheme that aims to supply drinking water to the Kathmandu valley. According to NPC (2003), the drinking water demand of Kathmandu valley at present is about 170 million liter per day and only 140 million liters per day of supply is available. This demand is increasing rapidly and will reach to 250 million liters per day by the year 2007. This shortage is only possible to compensate if the Melamchi project is implemented.

Even though the possibilities for the development of tunnels and underground caverns are huge in Nepal, many uncertainties and challenges exists in this field due to the complex geological setup of the Himalaya.

1.3 TUNNELLING CHALLENGES IN NEPAL

For economically viable tunnelling, it is crucial to have a method characterized by cost effectiveness and flexibility to adopt changing ground conditions, and by accuracy in the prediction of rock mass quality during planning. The design phase decision in selecting tunnel alignment and predicting the rock mass quality and rock support requirement has direct influence on the overall cost and time requirement of any tunnelling project (Nilsen and Thidemann, 1993).

The past tunnelling experience in Nepal shows that the accuracy of planning phase geological investigations for underground works has often been rather poor. In addition, as discussed in Chapter 2, the compressional tectonic stress regime in the Himalaya has resulted in intense deformation of the rock mass, making it highly folded, faulted, sheared, fractured and deeply weathered. This complex geological setting has caused considerable stability problems and is a great challenge for successful tunnelling.

The majority of tunnelling carried out in the Himalaya has suffered severe stability problems, resulting in delayed completion and cost overruns (Panthi and Nilsen, 2005b; Bajracharya and Panthi, 2002; Goel, 2001 and Joshi, 2000). The instabilities in tunnelling in Nepal are related to two major factors; non-geological and geological. The non-geological factors are connected to the level of skill and expertise gained by experience and the interpretation and decision making skills during planning and construction phases of tunnelling projects. The ability to evaluate and tackle the stability issues during planning and construction and the tools, methods and technology used in that process have great significance, since erroneous interpretation may result in loss of millions.

The geological factor is related to the geological complexity of the region. The complexity is represented mainly by four engineering geological characteristics, which have caused major stability problems during tunnelling in Nepal. These are; a) weak rock mass quality, b) high degree of weathering and fracturing, c) rock stresses and d) groundwater effect. The major geological uncertainties and challenges that have been faced in tunnelling in Nepal are briefly summarized below based on four tunnelling projects that have been recently constructed or are under construction, see Figure 1-3, and also represent the project cases for this PhD research.

1.3.1 Rock mass quality

Among the most distinct inherent properties of the rock mass in the Himalaya is the strength anisotropy (schistocity) caused by the preferred orientations of mineral grains or directional stress history. The bedding and foliation that exists in the sedimentary and metamorphic rocks of Nepal have made them highly directional concerning strength and deformability. As a result of this directional behavior with respect to strength and deformability, many rocks in Nepal are highly incompetent. This directional behavior leads to a considerable reduction on the self-supporting capability of the rock masses while tunnelling.

Figure 1-5. Headrace tunnel collapse at Kaligandaki "A" Hydroelectric Project (left) and tunnel face showing thin foliation plane with very weak bond (right) (Photo: Impregilo SpA, 2000).

Figure 1-5 is an example of tunnel collapse caused by this directional anisotropy of a typical Himalayan phyllite. Many such failures occurred in the recently constructed headrace tunnels of 144 MW Kaligandaki "A" hydropower project and 60 MW Khimti I hydropower project in Nepal. The highly deformable rocks such as shale, slate, phyllite, schist and micaceous gneiss show such directional behavior and are weak bonded along the foliation plane.

Another major feature of the highly deformed rock mass of the Himalaya is frequent intercalation between different rocks and shear bands. Such intercalation is observed at interval of even less than 50 centimetres.

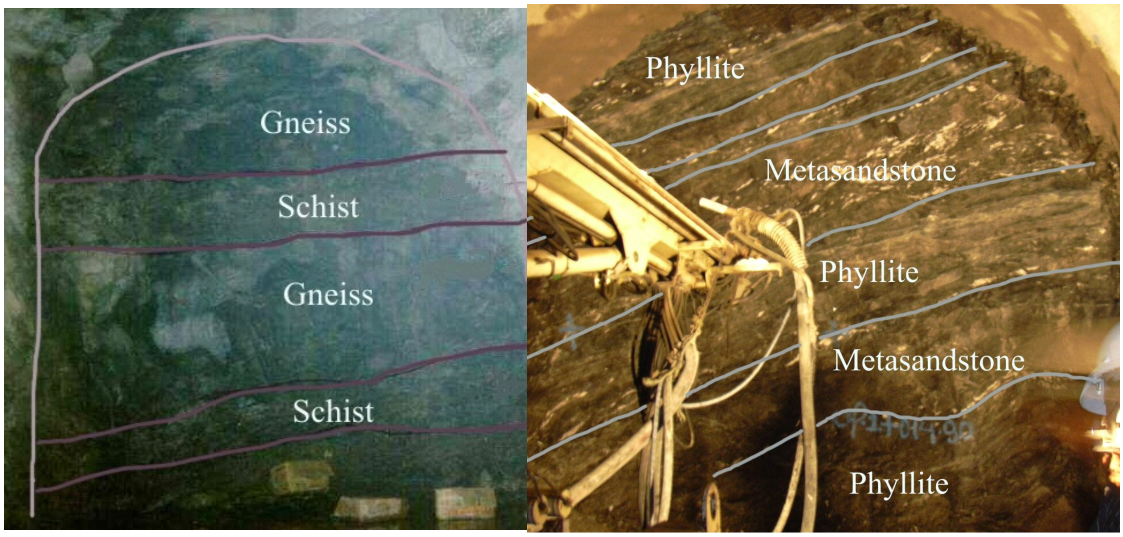

Figure 1-6. Intercalation between gneiss and schist at Khimti headrace tunnel (left) and intercalation between phyllite and metasandstone at Middle Marsyangdi headrace tunnel (right).

In many occasions, thin bands of very weak and highly deformed rocks such as slate, phyllite, schists and sheared mylonites are intercalated within the bands of relatively strong and brittle rocks such as gneiss, quartzite and dolomite. As a result, these small bands of weak rock mass are squeezed and highly sheared within these stronger layers of rock mass (Panthi, 2004), i.e. typical mixed face conditions. Being weaker in their mechanical characteristics and highly schistose, these shear bands lack sufficient bonding / friction and have reduced self-supporting capability. Figure 1-6 is an example of such intercalation observed at the headrace tunnels of Khimti and Middle Marsyangdi hydropower projects in Nepal.

This phenomenon of directional behaviour and intercalation of the rock mass in Nepal, and as a whole in the Himalayan region, has resulted in severe stability problems during tunnel excavation. The anisotropy also has a considerable effect on tunnel blasting, as the attenuation effect makes it extremely difficult to achieve good blasting result.

1.3.2 Weathering and fracturing

In the Himalaya, fracturing is caused either by active tectonic movement or due to gravity effect. The combination of active tectonic movement and complex climatic conditions (dynamic monsoon) of the region lead to aggravated weathering of the fractured rock mass. Being formed from the process of fracturing, shearing and hydrothermal alteration, the fractured rock mass, weakness zones and fault zones provide excellent environment for weathering to intensify. Accordingly, the weathering effect may reach even more than hundred meters below the surface. As an example, in some section of the headrace tunnel of Khimti project, the weathering was so deep that the decomposed organic soil was found at the tunnel face at depth more than hundred meters (Panthi and Nilsen, 2005a). Tunnelling in such environment needs to be well addressed concerning rock mass quality evaluation at planning and implementation stages.

There are two main effects of rock weathering and fracturing with respect to tunnel stability in Nepal. The first is the immediate tunnel collapse during excavation, since the rock mass loses its cohesion (friction) and is unable to selfsustain even for a very short period until the temporary support is placed. Figure 1-7 shows an example of weathering induced instability and a tunnel collapse that was triggered due to deep weathering at the upper pressure shaft of Khimti project.

As shown in Figure 1-7, a sink hole was formed all the way to the surface due to the collapse in this tunnel. Several such collapses were witnessed along the headrace tunnel and pressure shaft of Khimti project. The second effect is the condition that is produced by weathering for water inflow and leakage from the tunnels, since many open channels may be formed along the fractures in the rock mass.

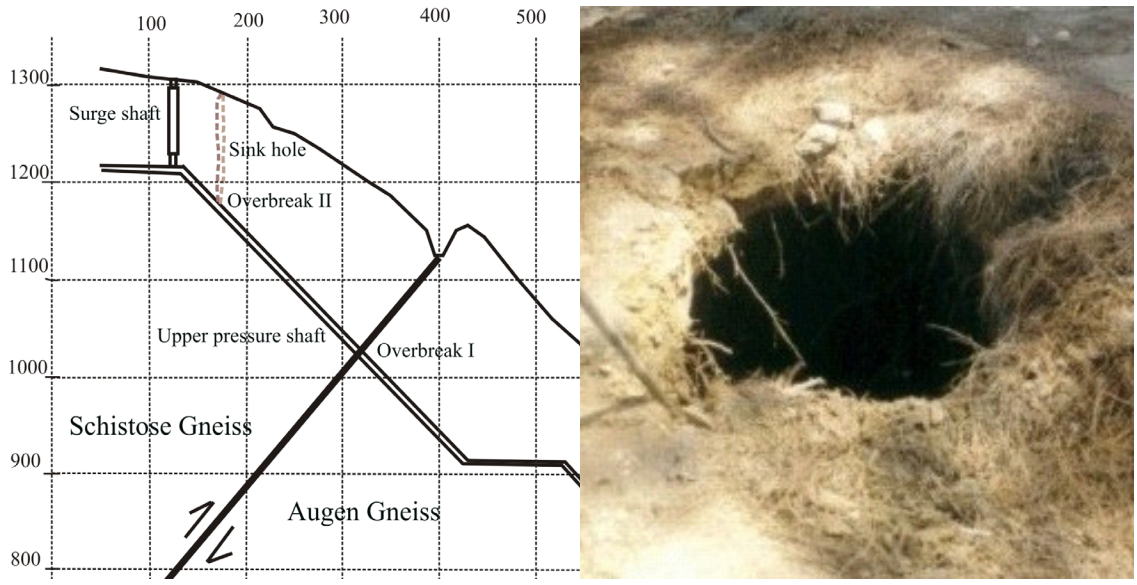

Figure 1-7. Cross section profile of the upper pressure shaft (dimension in meters) showing a tunnel collapse (left) and a sink hole of the same collapse that reached the surface (right) at Khimti Hydropower Project.

1.3.3 Stress induced problems

The third major stability problem faced during tunnelling in Nepal Himalaya is stress anisotropy. Due to topographic reason, most of the tunnel projects are constructed in the Siwaliks and lesser Himalayan zones, where highly deformed rocks such as shale, mudstone, siltstone, slate, phyllite, schist, schistose gneiss and highly sheared fault gouge and mylonites are present. In general, this highly deformed rock mass have very weak rock mass strength, and tunnelling through such rock mass may cause severe squeezing as soon as the overburden stress exceeds the rock mass strength. The severe squeezing has been observed even in relatively low overburden, where tunnels pass through highly sheared fault zones with extremely poor rock mass.

All four tunnel project cases considered for this PhD research are located in the lesser Himalayan zone of Nepal, but in different rock formations, and have experienced tunnel squeezing during excavation. Severe squeezing occurred in the headrace tunnel of Kaligandaki "A" and in the pressure tunnel of Modi Khola projects. At Modi Khola pressure tunnel, the tunnel squeezing observed was very severe with a horizontal convergence close to 1.5 meters, see Figure 1-8 left. At this section, the tunnel passes through highly sheared fault gouge, representing intercalation of highly sheared and decomposed schist mixed with completely crushed quartzite at an overburden of about 75 meters. The squeezing was so severe that the applied support of steel ribs and shotcrete was completely buckled and collapsed (Himal Hydro, 2001).

Figure 1-8. Severe squeezing at Modi pressure tunnel (left) and Kaligandaki headrace tunnel (right) (Photo: Himal Hydro, 2001 and Impregilo SpA, 1989)

In the case of Kaligandaki headrace tunnel, squeezing occurred in many sections. Figure 1-8 right shows a section where more than 50 centimetres of horizontal convergence occurred at an overburden of approximately 450 meters. In this tunnel that passes through highly sheared Himalayan phyllite, a maximum of up to 75 centimetres of tunnel deformation was recorded at a section with an overburden of approximately 600 meters (NEA, 2002b and Panthi and Gouro, 2001).

Severe squeezing in tunnels is extremely difficult to tackle and is a major challenge in tunnelling through the Himalaya rock mass. In fact, no universal solution exists that may be used to control instability caused by tunnel squeezing of such magnitudes. The most effective solution is to predict squeezing as accurately as possible in advance and increase the excavation size for compensating to the predicted squeezing.

1.3.4 Inflow and leakage

As discussed, the combined effect of compressional tectonic movement and shearing and long monsoon cause the rock mass of Nepal Himalaya to be deeply weathered and fractured. As a result, the fault zones, sheared zones and fractured rock mass of the Himalaya are highly permeable and water bearing (Panthi and Nilsen, 2005a). Tunnelling through such permeable zones always represent great difficulties and considerable challenges. Figure 1-9 shows examples of severe water inflow and leakage problems at the Khimti headrace tunnel and the Modi pressure tunnel. As can be seen in the Figure, the severity of the problems caused by inflow and leakage are huge in the Himalaya. In

many occasions several weeks and months and a huge amount of resources were spent to control the inflow and leakage problems.

Figure 1-9. Water leakage from Adit 2 of Khimti headrace tunnel after early water filling (left) and mass inflow of water mixed with debris from a shear fault at the pressure tunnel of Modi Khola (right) (Right Photo: Himal Hydro, 1998).

As seen in Figure 1-9 left, water leakage problems are not only limited to the excessive inflow during tunnelling, but also are relevant for a tunnel constructed for conveying water, where there is a high risk of losing valuable water after the completion due to leakage. About 200 liters per second of water was leaking from one single location of Adit 2 of the Khimti headrace tunnel (Panthi and Nilsen, 2005a). It is a great challenge to establish methods or tools for predicting possible water inflow and leakage so that proper steps for tackling such problems may be considered in advance.

1.4 SCOPE OF THE RESEARCH

It is a fact that the key to the success or failure of any tunnelling project is the quality of the rock mass that the tunnel passes through and the rock support measures that are applied during tunnel excavation. In this respect, accurate evaluation, analysis and interpretation of the rock mass quality play a significant role. Past tunnelling experience in the Himalaya shows that there are many uncertainties and challenges that have to be faced during tunnelling.

A major challenge therefore is to address the geological uncertainties so that cost effectiveness and safer tunnelling may be achieved. In this respect, there is a need for research in the field of engineering geology with maximum focus on uncertainty and risk analysis associated to the rock mass quality evaluation, potential tunnel squeezing and

possible inflow and leakage. The best way to deal with such uncertainties is believed to be to introduce the probabilistic approach of analysis.

In this respect, the following viewpoint from Hoek (1998) is relevant to quote here. "*Given the inherently inhomogeneous nature of rock mass, probabilistic studies enables us to explore the influence of variations in the value of each input parameter and to base our engineering judgements upon the rate of change in the calculated value rather than on a single answer"*.

The main goal of this PhD research is thus to introduce the probabilistic approach to address the issues for tunnelling in the Himalayan rock mass conditions. The research is aiming particularly to fulfil the following three main objectives:

1. Uncertainty analysis to evaluate the rock mass quality by using the Q-system for rock mass classification, making it is possible to identify difficult ground conditions, including weathering and alteration effect.

2. To evaluate the probability of squeezing.

3. To assess leakage from unlined tunnels, making it possible to estimate the probability of valuable water loss.

1.5 RESEARCH METHODOLOGY

Four tunnels cases as shown in Figure 1-3 were selected for this PhD research. For the first three (Khimti I, Kaligandaki "A" and Modi Khola projects) the construction was completed recently, whereas Middle Marsyangdi is still under construction. These projects were selected since they are the most recent and modern tunnelling techniques have been used, but also these cases have all witnessed the challenges described in Section 1.3. In addition, detail information of these projects has been available, and the author was directly involved during their tendering and implementation phases. In particular, the author worked as a construction manager for Khimti I, as a technical auditor for Kaligandaki "A" and as a planning and contracts engineer for Modi Khola and Middle Marsyangdi projects. To meet the objectives described in Section 1.4, the following research methodology is applied in this study:

1. Literature review consisting of;
   i. Review and synthesis of the Himalayan geology including tectonic influence, stress regime, major rock types and weathering effect on the Himalayan rock mass.
   ii. Evaluation of the factors influencing on tunnel stability including discussions on rock mass quality, rock weathering, stress induced problems and water inflow and leakage.
   iii. Review of rock mass classification methods.

iv. Review of the uncertainty and risk analysis related to rock engineering and development of the concept for uncertainty and risk analysis in tunnelling.

2. Project data collection including data and information on project details and engineering geological information on the rock mass conditions of the four tunnel cases. The collected data include reports of planning, tender and design and construction phase investigation and instrumentation reports as well as unpublished data records describing the rock mass quality of the four project cases. The main reports collected from the respective cases are shown in Table 1-1.

Table 1-1. List of project information collected.

Description of data and documents	Khimti I	Kaligandaki "A"	Modi Khola	Middle Marsyangdi
Feasibility study reports	yes	yes	yes	yes
Project definition and design basis	yes	yes	-	yes
Engineering geological investigation reports	yes	yes	yes	yes
Tender stage bill of quantities and costs	yes	yes	yes	yes
Hydraulic fracturing and dilatometer test reports	yes	yes	-	yes
Final design and engineering reports	yes	yes	yes	-
Project completion and instrumentation reports	yes	yes	yes	-
Convergence measurements records	yes	yes	-	yes
Pre- and post injection grouting records	yes	-	-	-
Point load strength measurement records	-	-	-	yes
Geological tunnel logs	yes	yes	yes	yes
Rock support as-built records	yes	yes	yes	-
Contractor's final bill of quantities / cost reports	yes	yes	yes	-
Technical audit report for civil works	-	yes	-	-

3. Field mapping during visits to the respective cases in the summer of 2002, 2003 and 2004. In addition to the collection of project information and data described above, rock samples from the respective four cases were brought to NTNU for laboratory analysis. Surface and tunnel face mapping of Middle Marsyangdi project under construction was also conducted. The geological conditions of the respective cases as well as the results of field mapping and laboratory testing results are discussed in Chapter 4.

4. Uncertainty analysis: A probabilistic approach of uncertainty and risk analysis has been used for analysis and assessment of uncertainty and risk related to rock mass quality, stress induced problems (mainly tunnel squeezing) and water leakage problems through shotcrete lined water tunnel. The Palisade's @RISK advanced risk analysis program - version 4.5 has been used for such analysis.

1.6 THESIS OUTLINE

The discussions and analyses presented in the PhD thesis cover many aspects of stability issues for tunnelling in Himalayan rock mass conditions. Chapter 1 covers the importance of tunnelling in Nepal Himalaya and challenges that have to be faced. Chapter 2 describes and reviews the Himalayan geology, tectonic stress regime, main rock types and their engineering behavior. Chapter 3 covers the factors influencing on the stability in tunnelling. Chapter 4 gives details on the engineering geological conditions of the selected project cases. Chapter 5 reviews uncertainty and risk associated with surface and subsurface structures as well as a model concept developed for the uncertainty and risk assessment of the selected four tunnel cases. Chapter 6 covers the uncertainty and risk analysis part, which is the main objective of this PhD research. Chapter 7 covers the discussion on the research results. Finally, conclusions regarding this research are given in Chapter 8.

Chapter 2
Review of Himalayan geology

2.1 INTRODUCTION

The Himalaya (in Sanskrit "abode of snow") is a mountain system in Asia comprising a series of parallel and converging ranges and forming the highest mountain region in the world. The Himalayan mountain chain and the high relief of the adjacent Tibetan plateau have resulted from the collision of the Indian plate with the Asian plate. The 2,500 km long Himalayan chain of the mountains, see Figure 2-1, forms an arc between the syntaxes of Namche Barwa (7,756 m) in the Southeast Tibet and Nanga Parbat (8,125 m) in the Northwest Pakistan (Patric, 2001). The Himalayan range covers about 594,400 square kilometres in area and is convex towards the Indian shield. The Himalayan range includes of 26 highest mountain peaks of the world and is a typical continent-continent collision zone.

According to Upreti (1999), the wide acceptance of plate tectonic theory in the early seventies inspired many researchers to make a fresh start with intense geological research on most parts of the Himalaya. The main attraction for this was the formation of the Himalaya by the youngest and tectonically active Himalayan-Tibetan orogenesis with excellent rock mass exposures ranging from deep-seated metamorphic rocks to unmetamorphosed fossiliferous rocks.

Even though the systematic geological investigation of the Nepal Himalaya started some time in 1848 after Hooker visited the Tamur valley in the eastern Nepal, the study carried out by Hagen (1968, 1969) was a milestone for further geological research in Nepal. During the past three decades, numerous geological and geophysical investigations have been conducted and discoveries have been made about the orogeny, geomorphology and stratigraphy (Upreti, 1999). However, very limited research has been conducted on the engineering geological aspects of the Himalayan rock mass. In particular, this is the case concerning mechanical characteristics such as jointing and weathering, strength and deformability and directional anisotropy of the rock mass that have direct influence on the stability of surface and subsurface engineering structures.

This chapter aims to review, synthesise and summarize the research work carried out in past on the Himalayan geology. The tectonic influence on the formation of the Himalaya is discussed and major rock types that the Himalaya consists of are highlighted. In this process, focus is also given in the discussion of engineering geological aspects of the Himalayan rock mass.

2.2 FORMATION OF THE HIMALAYA

Many researchers have worked to describe the formation of the Himalaya. The effort made by Patrick (2001) in summarizing the sequence of the Himalayan formation is of particular significance. According to him, the Himalaya was formed as a result of the collision of major lithospheric plates as well as intervening minor plate fragments and arch units from the late Mesozoic times to present date. Following the Permo-Carboniferous break-up of Pangea, the landmass later to become India found itself located deep in the Southern hemisphere with several thousand kilometres of the Neo-Tethys Ocean separating it from the nearest land to the North. The Northern boundary of the Himalaya comprises a series of continental blocks that accreted to the Asian margin during the Palaeozoic and Mesozoic. The most important with respect to the Himalayan evolution is the Lhasa block that collided with the Northern Qiangtang block in Jurassic times along the Bangong suture, see Figure 2-1. At the end of Cretaceous, an oceanic island arc, the Kohistan-Ladakh arc found in the Northwest Himalaya, collided with Asia. Finally, northward moving India collided with the Lhasa block in the Eocene period approximately 70-50 million years back.

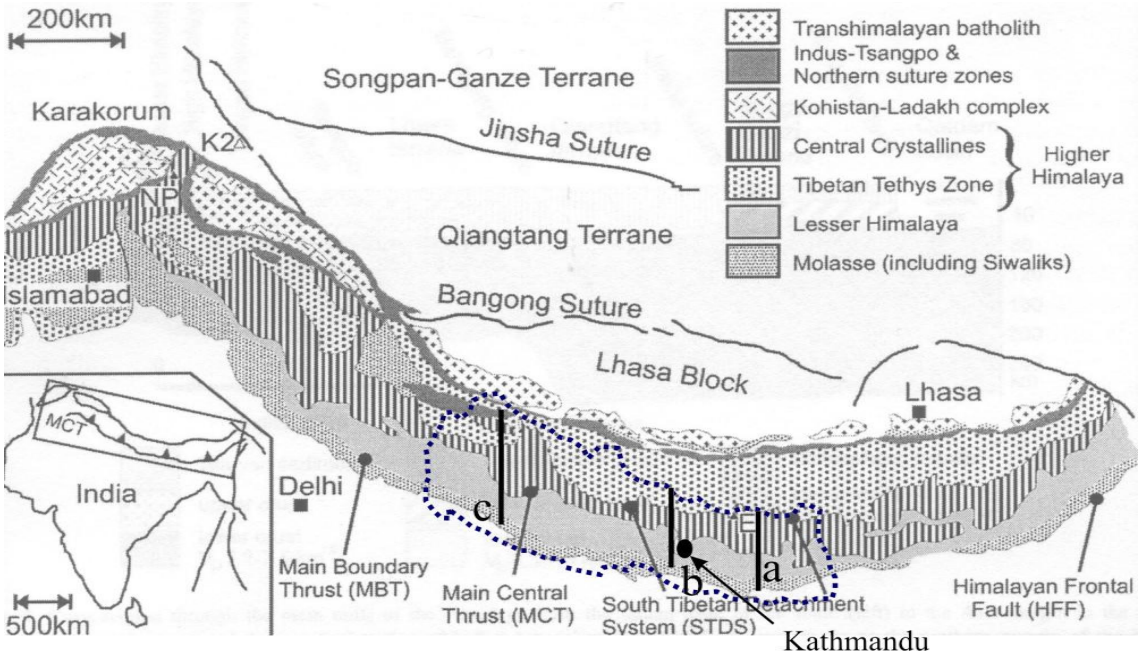

Figure 2-1. Simplified geology of the Himalayan range with main tectonic units. E: Everest; NP: Naga Parbat (Nepal map added to Patrick, 2001). (Note: International boundary is approximate).

The palaeomagnetic record of the Indian Ocean floor indicates that the rate of northward drift of the Indian plate has decreased from the original 15-20 centimetres to about 5 centimetres per annum at the present day (Klootwijk et al, 1992). This continental collision caused crustal imbrications, staking and under-thrusting of the Indian plate beneath the Southern Asian margin and strike-slip movement along faults well away from the collision zone in the North Tibet and Southeast Asia. The main thrust

imbricating the margin of Indian plate, see Figures 2-1 and 2-2, delineates important boundaries between units of different metamorphic character (Deoja et al, 1991b).

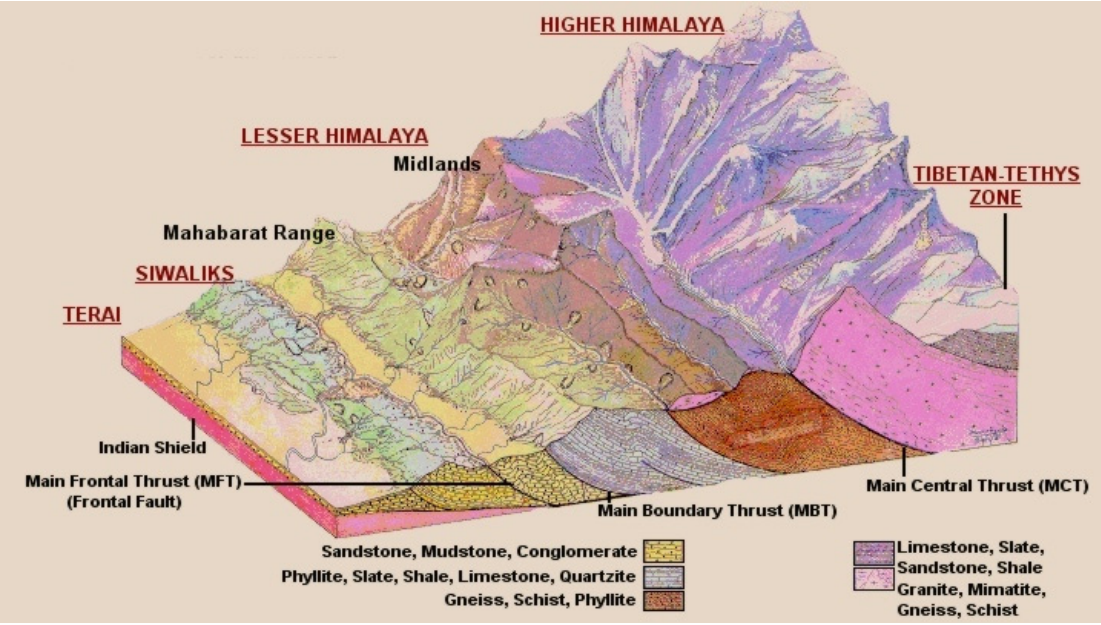

Figure 2-2. Block diagram of the Himalaya giving different litho-tectonic units (Deoja et al, 1991b).

Figures 2-1 and 2-2 show that as a result of collision and tectonic movement, several tectonic thrusts have been developed during the mountain building process. Accordingly, different Northwest-Southeast trending tectonic zones were formed in the Himalaya.

2.3 MAJOR TECTONIC SUBDIVISIONS

As a result of compressional and extensional faulting, the Himalayan belt has several litho-tectonic units with Northwest-Southeast general trend. The altitude varies greatly in the Himalaya, which starts from approximately 100 meters above sea level at its South and reaches to its maximum 8,848 meters above sea level (the Mount Everest). As shown in Figure 2-2, from South to North, the Himalaya can be sub-divided into five major tectonic subdivisions; the Gangetic plane (Terai), the Siwaliks zone, the lesser Himalayan zone, the higher Himalayan zone and the Tibetan-Tethys zone. These tectonic zones are all characterized by special lithology, tectonics, geological structures, and geological history and are made up by different rock types.

2.3.1 Gangetic plane (Terai)

The Gangetic plane represents the Northern edge of vast alluvial Indo-Gangetic foreland basin and belongs to the southernmost tectonic division of the Himalaya, see Figures 2-2 and 2-3. In the North, it is bounded by the Main Frontal Thrust (MFT), whose outcrops are exposed at many places along the Southern front of the Siwaliks range.

The elevation of the Gangetic plane gradually rises from approximately 100 meters at South to 200 meters above sea level at its North.

This zone is made up of Pleistocene to recent alluvium deposits with an average thickness of about 1,500 meters. As shown in Figure 2-3, the Siwaliks-Gangetic foreland basin constitutes a unique present day active foreland system in the geodynamic context of intercontinental collision. The Northern part of the Gangetic plane, which is separated by the MFT from the Siwaliks, represents a Siwaliks mountain in the making (Upreti, 1999). The rocks under the alluvium to the South of the mountain front are very active with respect to tectonic movement. As a result of that a number of thrusts and thrust propagated folds are developed in this belt (Mugnier et al, 1999).

2.3.2 Siwaliks zone

The Siwaliks zone borders the Himalayan range for more than 2,000 km from East India to West Pakistan, see Figure 2-1. The Main Boundary Thrust (MBT) is the major Thrust systems along the entire Himalaya that separates the very young sedimentary rocks of the Siwaliks from the lesser Himalayan zone, see Figures 2-2 and 2-3. Palaeomagnetic studies indicate that the age of the Siwaliks zone is between approximately 14 million years and two million years (Mugnier et al, 1999 and Upreti, 1999).

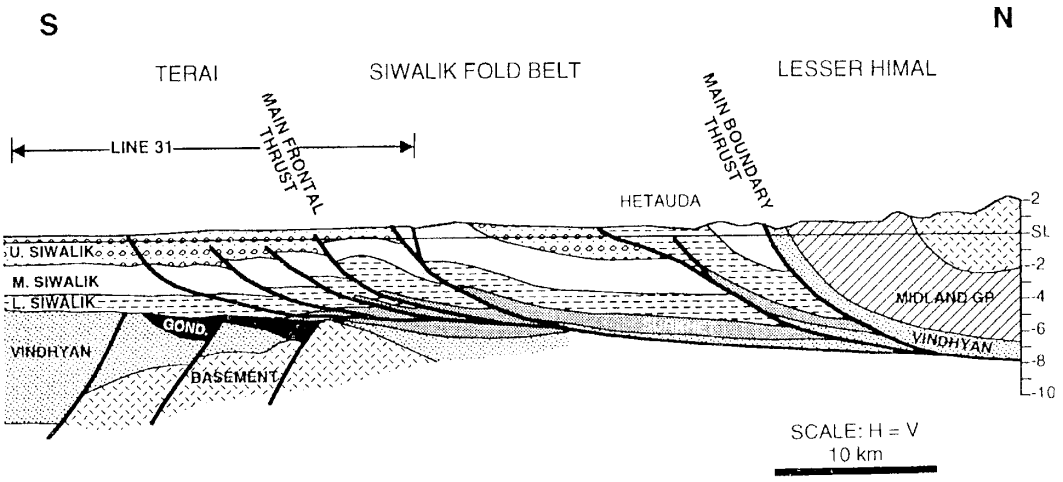

Figure 2-3. Structural cross-section across Gangetic plane, Siwaliks and lesser Himalayan zones (Upreti, 1999). SL: Sea level.

As Figures 2-2 and 2-3 indicate, the Siwaliks zone is sandwiched between the lesser Himalayan zone to the North and the Gangetic plane to the South. The elevation in this zone differs from 200 to about 1,000 meters above sea level. According to Gautem and Rosler (1999) and Upreti (1999), the Siwaliks zone can be subdivided into lower, middle and upper Siwaliks. The lower Siwaliks (LS) zone is composed of fine to medium grained grey sandstones and silty and sandy mud rocks forming nearly uniform sedimentary cycles. The middle Siwaliks (MS) zone consists of medium to coarse grained

grey mica rich sandstones with intercalated siltstones and mudstones. Finally, the middle Siwaliks zone is gradually overlapped by the conglomeratic to sandy conglomeratic facies of the upper Siwaliks (US) zone. In general terms, the Siwaliks rocks are buried beneath the cover of Southward tilted (overthrusted) lesser Himalayan meta-sedimentary rocks along the MBT.

Being sandwiched by two active tectonic thrusts, and also being a very young sedimentary sequence, the rock mass of the Siwaliks are very weak. These rocks are highly deformed, fragile, easily erodeble, porous and intensely folded. Hence, tunnelling through Siwaliks rocks should be regarded as expensive and uneconomical excluding in the areas where bedded and massive sandstones are occasionally present.

2.3.3 Lesser Himalayan zone

The lesser Himalayan zone is a fold and thrust belt bounded by the MBT in the South and the Main Central Thrust (MCT) in the North, see Figures 2-1, 2-2 and 2-4. Paudel and Arita (2000) describe this zone as consisting of low to medium grade meta-sedimentary rocks of late Precambrian to Mesozoic age. In general, the lesser Himalayan zone has a phenomenon of inverted metamorphism. As a result, the zone is folded into a vast post-metamorphic anticline where the Southern flank of the anticline is weakly metamorphosed and the Northern flank has a high degree of metamorphism. Thus, throughout the lesser Himalayan zone, the metamorphic grade appears to increase northwards (structurally upwards toward higher structural level). As Figure 2-4 indicates, in addition to meta-sedimentary rocks, the lesser Himalayan zone also consists of high grade crystalline rocks of the higher Himalaya as nappe over the lesser Himalayan zone (Upreti, 1999).

According to Guillot (1999), the low grade metamorphic rocks situated to the South along and near the MBT are dominated by sheet minerals such as chlorite and biotite, whereas the high grade metamorphic rocks of the North are made of silicate minerals like kyanite and sillimanite excluding highly sheared and mylonitized and schistose rocks along the MCT.

As Figures 2-2 and 2-4 show, the lesser Himalayan zone consists of a variety of sedimentary, meta-sedimentary and crystalline rock formations. The zone can be divided into the outer (Southern), middle and inner (Northern) belts. The rocks in the outer belt, i.e. along and near the MBT, are highly sheared and brecciated and have a very low grade of metamorphism. The rocks in the middle belt are intercalated with medium and high grade metamorphic rocks, whereas the rocks in the inner most belt of the lesser Himalaya are intensely sheared and mylonitized along the MCT.

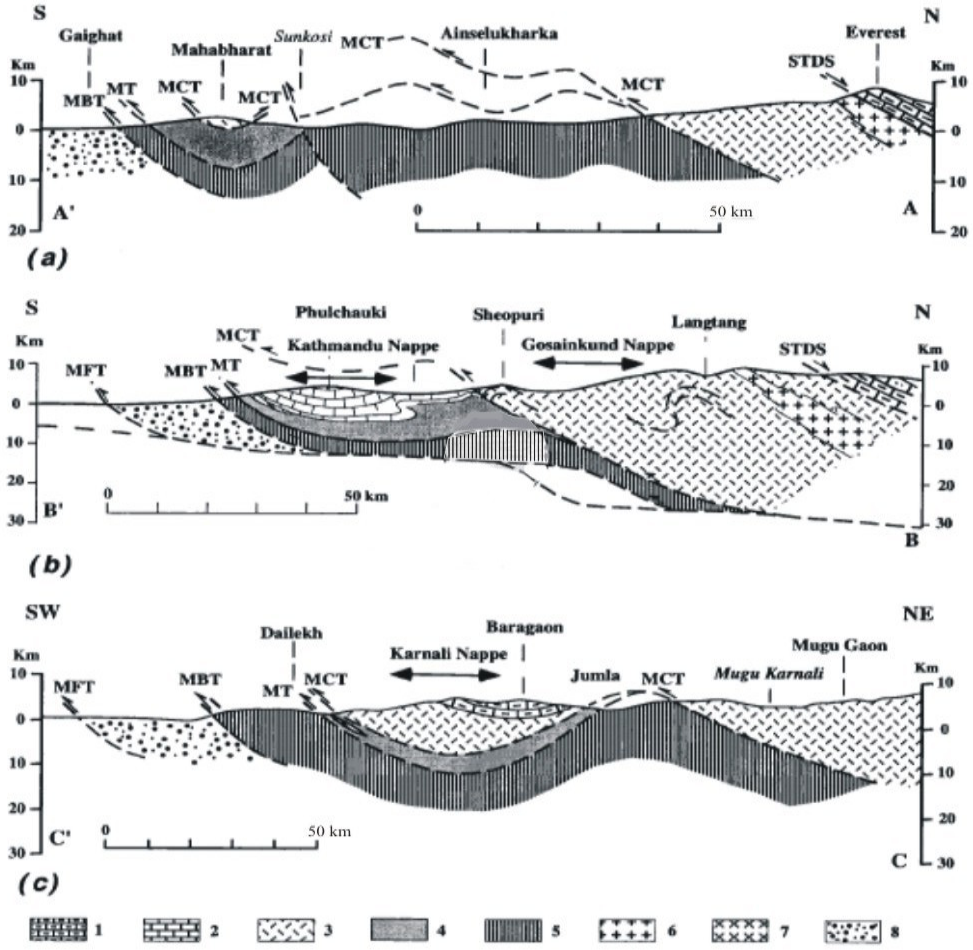

Legends: 1. Tibetan Tethys sediments, 2. Lesser Himalayan meta-sediments of Phulchauki group, 3. Higher Himalayan Crystalline, 4. Low to medium grade meta-sediments of Bhimphedi group, 5. Low grade metamorphic rocks of Nawakot complex, 6. Higher Himalayan Granite, 7. Lesser Himalayan granite and 8. Swaliks sedimentary sequence

Figure 2-4. North-south geological cross-section of the Himalaya (for section location reference is made to Figure 2-1). (a) Eastern Everest section, (b) Central Langtang- Kathmandu section, (c) Western section (after Upreti, 1999).

Due to active tectonic movement the rock mass in this zone is in general intensely fractured, folded, sheared and highly schistose. As a result, it varies greatly with respect to engineering geological characteristics and has varying impact on tunnel stability.

2.3.4 Higher Himalayan zone

The higher Himalayan zone corresponds to the higher Himalayan crystalline rocks. This zone lies to the North of, and above, the MCT and below the sedimentary sequence of the Tibetan-Tethys zone, see Figures 2-1, 2-2 and 2-4. This zone mainly consists of a high-grade metamorphic sequence of various kinds of gneisses. Biotite-sillimanite gneiss, garnet-biotite gneiss and quartzite are the dominant rocks in the higher Himalaya. At the lower (southern) part along and near by the MCT, highly sheared, intensely deformed and mylonitized green-schist and schistose mica gneiss are

present (Robyr et al, 2002). Also granite and amphibolite plutons and dykes, which are composed of biotite-muscovite bearing gneiss and amphibolite, are emplaced in the upper part of the higher Himalayan zone. These rocks are close to the boundary between the metamorphic and sedimentary sequences, which are separated by a normal fault system called the Southern Tibetan Detachment Fault System (STDFS) (Carosi et al, 1999).

In general, the rocks in this zone are more competent, stronger and more isotropic than the other zones. Hence, tunnelling through these competent rocks should have less stability problems, except for the rock mass situated along and nearby the MCT.

2.3.5 Tibetan-Tethys zone

The Tibetan-Tethys zone lies between the STDFS and the Indus-Tsangpo Suture zone (ITS), see Figures 2-1, 2-2 and 2-4. This zone is the northernmost tectonic zone of the Himalaya and occupies a wide belt consisting of sedimentary rocks known as the Tethys sedimentary series (TSS). In general, the rocks in this zone have undergone very little metamorphism, except for the base close to the higher Himalayan crystalline rocks, and consist of a low-grade meta-sedimentary sequence of late Proterozoic to early Cambrian age (Carosi et al, 1999). Shale, sandstone, meta-sandstone, phyllite and some crystalline limestone (marbles) are the major types of rocks in this zone (Deoja et al, 1991). Since most of the highest peaks of the Himalaya including the Mount Everest are located in this zone, the rock mass of this zone is obviously strong and fresh.

2.4 TECTONIC STRESS REGIME

Due to the convergence of the Indian and the Asian tectonic plates, the Himalayan region has been undergoing persistent compression for more than 50 million years. As a result, the Himalaya is one of the most seismically active regions of the world. Only in the last century the Himalayan arc has witnessed four great earthquakes with a Richter scale magnitude of more than eight (Sarkar and Chander, 2003).

The deformation pattern in the Himalaya is mostly characterized by reverse faulting mechanism with minimum contribution by normal and strike-slip faulting. In contrast, the Northern Tibetan belt is characterized by normal and strike-slip faulting and complete absence of reverse fault mechanism. Focal mechanism (fault plane) analysis (an analysis used to interpret the type of fault systems using compressional and dilational seismic waves of earthquakes plotted on a lower-hemisphere equal area projection) of the Himalaya also reveals that the Indian plate under-thrusts the Asian plate, see Figure 2-5. This under-thrusting is at a shallow angle and is dipping towards Northeast (Rao et al, 2003).

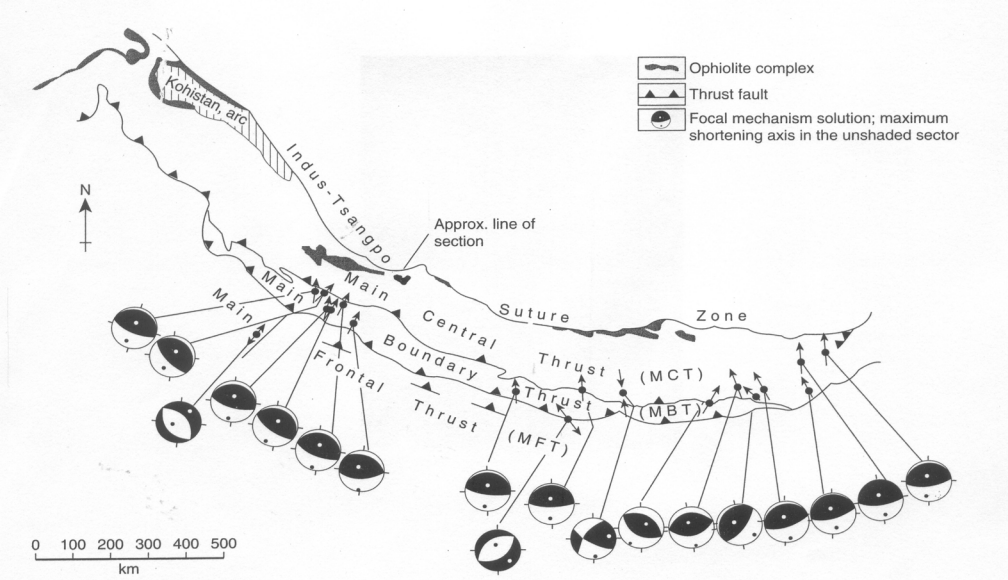

Figure 2-5. The major principle thrust and focal mechanism solution of earthquakes in the Himalaya (Moores and Twiss, 1995).

By analysing the earthquake regime of the Himalaya, Sarkar and Chander (2003) concluded that the plate subduction process in this region is causing large, moderate and small scale earthquakes. The annual rate of long-term tectonic stress change induced by the subduction process is estimated to be in the order of few kilo-Pascals.

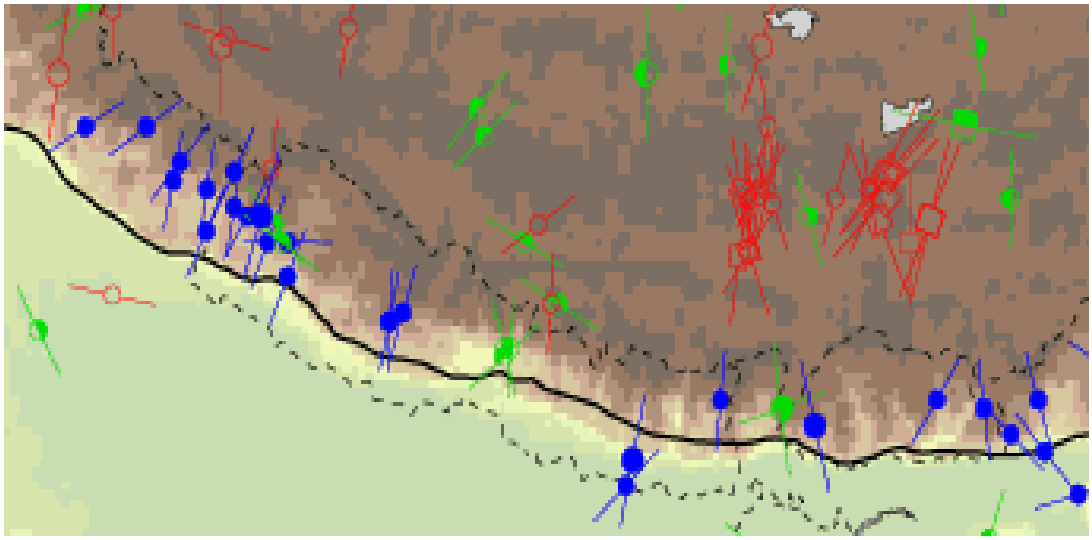

Figure 2-6. Stress map of the Himalaya and adjacent region (from World Stress Map, 2003).

The compressional tectonic deformation and active reverse faulting mechanism have considerable influence on the magnitude of major tectonic principal stress in the Himalaya. As shown in Figure 2-6, the tectonic principal stress in the Himalaya is oriented

horizontally with Northeast-Southwest trend. Figures 2-5 and 2-6 also illustrate that there is an ongoing shortening between the Indian and Asian plates.

Due to the compressional tectonic stress regime, the sedimentary and metamorphic rocks of the Himalaya have undergone intense deformation causing faulting, folding, jointing and shearing of the Himalayan rock mass. Therefore, the rock masses of the region are highly sheared, schistose and anisotropic.

2.5 MAJOR ROCK TYPES

The major rock types in the Himalaya, that are in principle bounded within the five tectonic zones as described in Section 2.3, are summarized in Table 2-1.

Table 2-1. Types of Himalayan rocks and their geomorphic units (based on Upreti, 1999).

Geomorphic Units	Width (km)	Altitude (m)	Main Rock Types	Age
Gangetic plane and inner Terai valleys	20-50	100-200	Alluvial deposits, coarse gravel at the foot of the Siwaliks mountain.	Recent
Siwaliks zone	15-30	200-1,000	Sandstone, mudstone, siltstone, shale, conglomerates etc.	Mid-Miocene to Pleistocene
Lesser Himalayan zone	70-165	200*-5,000	Shale, slate, phyllite, limestone, dolomite, marble, schist, quartzite, gneiss and granite.	Precambrian to Mesozoic
Higher Himalayan zone	10-60	>5,000	Gneiss, schist, marble, granite, quartzite, amphibole etc.	Precambrian
Tibetan-Tethys zone	-----	>2,500	Gneissic schist, marble, shale, slate, limestone, sandstone etc.	Late Proterozoic to early Cambrian

* In the lesser Himalayan valleys the elevation ranges from 200 to 2000 meters.

As indicated by the table, the very young rocks are in the southernmost Himalaya (in the Siwaliks) and the geological age gradually increases towards the North. The rocks in the Siwaliks represent a young sedimentary sequence, in the lesser Himalaya the rocks represent a meta-sedimentary to crystalline metamorphic sequence, in the higher Himalaya a crystalline metamorphic and igneous sequence and finally in the Tibetan-Tethys they represent a very old sedimentary sequence.

2.5.1 Sedimentary rocks

The sedimentary rocks in the Himalaya vary from weak, loose and easily erodable to massive, thickly bedded rocks, see Table 2-1. The rocks in the Siwaliks are the youngest in the region and as a result Siwaliks rocks such as sandstone, mudstone, siltstone

and conglomerates are in general very weak, fragile, easily erodable, porous and highly weathered. The minerals of these young sedimentary rocks are usually softer and their bonding is also weaker. Stronger sedimentary rocks such as black shale, limestone, sandstone and dolomite are found in the southernmost belt of lesser Himalaya and Tibetan-Tethys zone.

The major types of sedimentary rocks are briefly described below (see also Table 2-1).

Conglomerates: Conglomerates, also termed Rudaceous rock, are found as very young in the upper Siwaliks. Conglomerates consist of at least 30% rounded particles coarser than 2 mm, and the space between the rounded particles are filled with either fine detrital sand/clay or siliceous cement (Goodman, 1993). The conglomerates of the Siwaliks are generally massive and without any distinct bedding. Structurally, these rocks are very permeable and erode easily when in contact with water, and thus can be characterized as very fragile rocks.

Mudstone/Siltstone/Sandstone: These rock types are also found as very young rocks of the Siwaliks zone. The mudstones in the Siwaliks zone are brown-purple or dark grey in color and consist of minerals like quartz, feldspar, clay, chlorite and biotite. The sandstones are fine to medium grained, bedded, tilted and rich in quartz and feldspar (Mugnier et al, 1999). The most fine-grained of these rocks were formed after the lithification of argillaceous (clay or silt) material transported by the rivers and deposited in the flood plains. In general, the mudstones/siltstones are structurally very weak and deformable. The sandstones are generally uniformly graded, bedded and massive.

Shale: The shale is found along the MBT and in the Tibetan- Tethys Zone of the Himalaya. Along the MBT, the shale appears as shale mylonites intercalated with thick bedded meta-sandstone. These shale mylonites are some times described as sheared and crushed mudstones or shale forming gouge (Deoja et al, 1991a). The shale found in the Tibetan-Tethys zone is more competent but intensely folded and thinly bedded, and therefore displays fissility and slaking and is highly anisotropic.

Limestone/Dolomite: The limestone and dolomite are wide-spread rocks in the Himalaya and mostly found in the lesser Himalayan and Tibetan-Tethys zones. The Himalayan limestone has distinct bedding. In general, the surface exposed limestone and dolomite are heavily jointed and highly to moderately weathered. The fresh dolomites of the Himalaya are massive, strong and very stable rocks.

2.5.2 Metamorphic rocks

The degree of metamorphism of the metamorphic rocks varies greatly depending upon the location. Low to medium grade metamorphic (meta-sedimentary) rocks are found in the southern belt of lesser Himalaya adjacent to the MBT and also in the middle part of the lesser Himalaya. Stronger and high grade metamorphic rocks are found in the inner

(northern) part of the lesser Himalaya and in the higher Himalaya. As a result of thrusting and faulting, the metamorphic rocks in the lesser Himalayas have undergone intense deformation. Therefore, these rocks are distinctly anisotropic, strongly folded, foliated and jointed. The crystalline rocks of the higher Himalaya are stronger and more isotropic, except for the rocks along the MCT, which are intensely sheared and mylonitized.

The engineering geological aspects of the metamorphic rocks of the Himalaya are very important for this research since the great majority of the completed as well as future tunnelling projects are situated either in the lesser Himalayan or lower (southern) part of the higher Himalayan zones. The main types of metamorphic rocks found in the Himalaya are briefly described below (see also Table 2-1).

Slate: The slate is found immediately North of the MBT and in the middle part of lesser Himalaya. This rock is formed from shale by the alteration of its constituent particles with relatively low grade metamorphism. The slate is highly altered, folded and strongly cleaved and has a high degree of anisotropy. The slate is flaky in its nature and can easily be split with a chisel into very thin plates. According to Deoja et al (1991a), most of the slates found in Himalaya are black, dark blue and gray in colors. The slate containing considerable amount of graphite is black, whereas the slate containing chlorite is greener in color.

Phyllite: Phyllite is found immediately North of MBT and also in the inner part of the lesser Himalayan zone. The phyllite consists of numerous small scale folds with anticlines and synclines and is thinly foliated (Deoja et al, 1991a). This rock is the product of further metamorphism of slates that has developed almost visible crystals of muscovite parallel to the foliation plane. Apart from mica minerals, the phyllite found in the Himalaya also contains chlorite, graphite, talc and quartz.

Schist: This rock is very common in the Himalaya and is found in both lesser and higher Himalayan zones. The highly sheared, mylonitized and ductile zone of the MCT is one of the major sources of Himalayan schist. The schist in the Himalaya is strongly foliated, anisotropic, deformed and flaky. In most of the areas schist is intercalated within stronger rocks such as quartzite and gneiss formations (Nasseri et al, 2003 and Deoja et al, 1991a). The schists found in the Himalaya are coarse-grained mica-schist, quartz mica-schist and chlorite-schist.

Quartzite: This rock is commonly found in the lesser and higher Himalayan zones. Depending upon the degree of metamorphism, the quality and type of quartzite can vary from low to medium metamorphosed meta-sandstone to highly metamorphosed fine grained, massive and pure quartzite (Sharma, 1990). For instance, meta-sandstone, schistose quartzite and phyllitic quartzite belong to the category of low to medium grade metamorphic rocks. The rocks of this category are schistose, foliated and interca-

lated with other rocks like schist, phyllite and gneiss. Pure quartzite is massive, strong, isotropic and abrasive when unweathered.

Marble: The marble is found in narrow bands in the lesser Himalayan and Tibetan-Tethys zones. These rocks were formed by metamorphism of limestone and dolomite. Depending upon the mineral composition, both calcitic and dolomitic marbles can be found in the region (Deoja et al, 1991a). The marbles of the Himalaya are anisotropic due to bedding or foliation and often weathered.

Gneiss: Crystalline, medium to coarse grained gneisses are very common rocks in the Himalaya and found in both lesser and higher Himalayan zones. The gneisses located along and near by the MCT have a distinct schistocity. The main types of gneisses found in the Himalaya are coarse grained kyanite-bearing banded gneiss, augun mica gneiss and granitic gneiss (Paudel and Arita, 2000). The banded gneiss and augen mica gneiss of the Himalaya are formed as a result of high grade metamorphism of sedimentary rocks and are distinctly anisotropic. The granitic gneiss is formed by metamorphism of igneous intrusions and is more isotropic.

2.5.3 Igneous rocks

Igneous rocks are formed by the solidification of liquid melt or magma. Only a few plutons and dykes of igneous rocks are found in the lesser and higher Himalayan zones, see Table 2-1. The notable rocks in this category are granites and gabbros. Most of the granites in the Himalaya have been further metamorphosed and converted into granitic gneisses and the gabbro has been converted into amphibolite. The fresh crystalline granite is in general pink to gray in color and contains feldspar, quartz and mica. Amphibolites are occasionally formed at the inner part of the lesser Himalaya (Sharma, 1990). In general, the igneous rocks of the Himalaya are massive and isotropic. However, exceptions are found at the surface where granites are exfoliated, jointed and weathered due to steep topography.

2.6 WEATHERING EFFECT

Rock weathering is a natural phenomenon and is simply a response of the dynamic earth to a changing environment. The compressional tectonic stress regime that contributes to the continued convergence and uplift of the Himalaya has resulted in great relief and steep and rough topography. Aside from being squeezed by tectonic stress, the rock mass in the region has undergone intense folding, faulting and jointing. In addition, the climatic conditions vary greatly in the Himalaya. The weather at the southernmost Gangetic plane is tropical and it changes gradually towards sub-tropical at the Siwaliks and to alpine in the northernmost higher Himalaya. As a result of high temperature variation, change in climatic conditions and presence of an active monsoon, rock weathering (both physical and chemical) is very active in the Himalayan region.

Three spatial scales of downward gravitational transfer of rock material occur in the Himalaya during the weathering process (Shroder and Bishop, 1998). The first is the tectonic extensional failure of the surface bedrock known as tectonic denudation, passing downward into deep-seated ductile zones of the subsurface known as major thrust zones. The second is the system of extensional failure at shallow depths, involving mountain settlement along lines of internal foliation and fracture that ultimately leads to a lateral expansion of the mountains. The third is the smallest system of extensional failure with shear movements, passing steeply downward from the high and steep slopes. In addition, chemical weathering of the mica and feldspar rich rocks of the Himalaya in the sub-tropical environment is also significant. The surface is highly weathered and dominated by clay material, and then there is a gradual reduction of weathering as depth increases. This gradual reduction leads to less and less altered parent material at depth until the bedrock is reached (Gardner and Walsh, 1996).

Thus, the weathering in the Himalaya is very significant and the rocks in this region are deeply weathered. The deep weathering has led to a significant reduction in the strength and deformability properties of the rock mass. The rock weathering is particularly deep in the relatively flat hills, in the valleys and in thrust faults, shear and weakness zones. Consequently, weathering induced instability in tunnelling is one of the major challenges in tunnelling in the region.

2.7 CONCLUDING REMARKS ON HIMALAYAN GEOLOGY

In summary, the Himalaya has a complex geological set-up and there is a significant tectonic influence on the rock mass conditions. The engineering geological characteristics of the rocks of this region therefore vary greatly. The major areas of concern with respect to the engineering geological behaviour of the Himalayan rock mass may be summarized as follows:

1. Due to under-thrusting of the Indian plate beneath the Asian plate, the rock mass in the region has undergone intense deformation. This deformation has led to intense folding, faulting, shearing and fracturing of the rock mass.

2. The folding, faulting, shearing and jointing have resulted in high degree of anisotropy and reduction of strength and deformability properties of the rock mass.

3. The combined effect of compressional tectonic movement and tough climatic conditions in the Himalaya has contributed to deep weathering. As a result of deep weathering, the fracture zones and fault zones in the rock mass are highly permeable, and rock weathering is therefore a key factor for ground water induced instability in the tunnels.

Chapter 3
Evaluation of factors influencing on stability

3.1 INTRODUCTION

A rock mass is a heterogeneous medium with many associated variables. The two main features characterizing the rock mass are; 1) rock mass quality and 2) the mechanical processes acting on the rock mass. These two features are not independent, but very much interlinked to each other. The rock mass quality is related to rock mass strength, deformability, strength anisotropy, presence of discontinuities and weathering effect. On the other hand, the mechanical processes that have an effect on tunnel stability are linked to rock stresses and groundwater. The stability of tunnels and underground caverns is therefore a function of these two features as illustrated in Figure 3-1. In addition, the tunnel stability is influenced by project specific characteristics such as size, shape, location and its orientation.

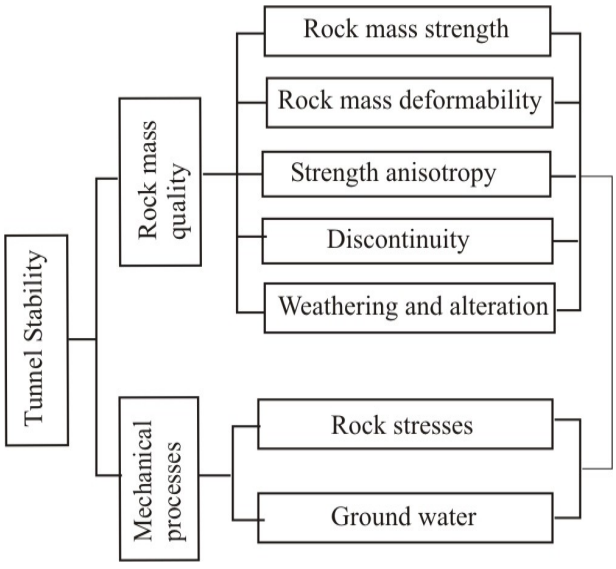

Figure 3-1. Factors influencing on tunnel stability.

In general terms, tunnel stability can be defined as ability to sustain failure after the excavation. According to Hoek and Brown (1980), the stability of an underground excavation is interdependent with the structural condition in the rock mass, degree of weathering of the rock mass and the relationship between rock stresses and the rock mass strength. Hudson (1993) suggests that there are mainly two modes of failure that

occur in underground excavations. These are: block failure when pre-existing blocks in the roof and side walls become free to move after the excavation has been made and stress failure when induced stresses around the excavation exceed the rock mass strength. Thus, tunnel instabilities are depth dependent. In the deeper ground the spacing between discontinuities is generally reduced, and the in-situ stresses are high and control the stability, while near the surface, the stress magnitudes are low, and discontinuities mainly control the stability.

This chapter is aiming at discussing the importance of the variables given in Figure 3-1.

3.2 ROCK MASS QUALITY

The quality of the rock mass is mainly governed by rock mass strength, deformability properties, strength anisotropy, the mechanical characteristics of the discontinuities and the degree of weathering. Rock mass classification systems are used to describe the quality of rock masses. The most commonly used classification systems are reviewed in Appendix A.

3.2.1 Rock mass strength

The rock mass strength can be defined as an ability to withstand stress and deformation. The strength of rocks is often influenced by discontinuities and foliation or schistocity planes, and the orientation of these features relatively to the direction in which the strength is assessed. As discussed by Bieniawaski and Van Heerden (1975), rock mass strength and deformation are different from the strength and deformation of an intact rock specimen. An intact rock specimen is usually strong and homogeneous with few discontinuities, and much stronger than the rock mass. Hence, a small specimen does not represent the rock mass strength and deformation, but there is a distinct scale effect.

To address the influence of sample size on the rock strength, Hoek and Brown (1980) analyzed published strength data of different rock specimen sizes and suggested a correlation between uniaxial compressive strength (σ_c) of a rock specimen with a diameter (d), and the uniaxial compressive strength (σ_{ci50}) of a rock specimen with 50 mm diameter, see Figure 3-2 left. Medhurst and Brown (1998) carried out triaxial test of highly cleaved coal of Moura mine in Australia that also indicated significant decrease in rock strength with increasing sample size, see Figure 3-2 right. Figure 3-2 is an example of great significance that demonstrates considerable reduction on rock strength by the increase in sample size. As Figure 3-2 left indicates, by increasing the specimen diameter from 50 mm to 200 mm, the rock strength is reduced by almost 25 percent.

The size dependency of rock strength is influenced by the degree of metamorphism or gneissocity in the rock mass. Crystalline unweathered rocks have relatively small size effect, while highly schistose, foliated and deformed rocks of sedimentary and metamorphic origin such as shale, slate, phyllite and schist have considerable size as well as directional effect on their strength (Hoek and Brown, 1997).

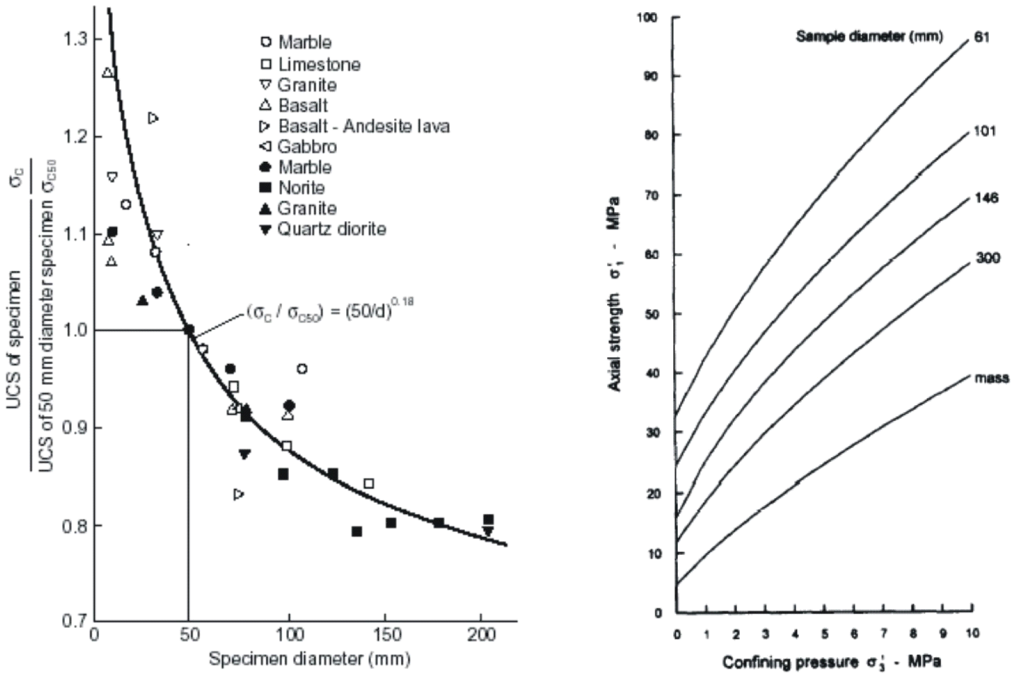

Figure 3-2. Influence of specimen size on the strength of intact rock (left) (Hoek and Brown, 1980) and peak strength of Australian Moura coal (right) (Medhurst and Brown, 1998).

The rock mass strength is difficult to estimate directly in the field or by laboratory testing, and many authors therefore have suggested empirical formulae for the estimation of rock mass strength. Among the most used empirical relations are Rock Mass Rating (RMR) (Bieniawaski, 1989 and 1993), Hoek-Brown relationship (Hoek et al, 2002) and Q-value correlation (Barton, 2002). These empirical relationships are presented in Table 3-1. As can be seen, the determination of intact rock strength for 50-mm diameter rock specimen is essential to estimate the rock mass strength using these equations.

Table 3-1. Empirical formulae for estimation of rock mass strength.

Proposed by	Rock mass strength and its relationship with rock mass classifications
Bieniawaski (1993)	$\sigma_{cm} = \sigma_{ci} \times \exp\left[\frac{RMR - 100}{18.75}\right]$
Hoek et al (2002) and Hoek (1994)	$\sigma_{cm} = \sigma_{ci} \times s^a = \sigma_{ci} \times \left[\exp\left(\frac{GSI - 100}{9}\right)\right]^a = \sigma_{ci} \times \left[\exp\left(\frac{RMR - 105}{9}\right)\right]^a$
Barton (2002)	$\sigma_{cm} = 5\gamma \times Q_c^{1/3} = 5\gamma \times \left[\frac{\sigma_{ci}}{100} \times Q\right]^{1/3} = 5\gamma \times \left[\frac{\sigma_{ci}}{100} \times 10^{\frac{RMR-50}{15}}\right]^{1/3}$

Where; σ_{cm} is the unconfined compressive strength of rock mass in MPa, σ_{ci} is the uniaxial compressive strength of intact rock (50 mm core diameter) in MPa, RMR is the Bieniawaski's rock mass rating, *s* and *a* are the material constant related to Hoek-Brown failure criteria (the value of *a* ranges from 0.5 for GSI value 100 to 0.58 for GSI value 10), GSI is the geological strength index, γ is the rock density in t/m^3, Q_c is the normalized rock mass quality rating and Q is the rock mass quality rating.

To achieve correlation between rock mass strength and strength of an intact rock specimen of 50 mm diameter, these empirical relations have been related to the Bieniawski's RMR system, see Table 3-1. For this, the material constant *a* is estimated as 0.5 for massive rocks (GSI = 100) and 0.58 for very poor and highly deformed rock mass (GSI < 10). A value of 2.65 t/m^3 has been used for rock density.

Based on the formulae in Table 3-1, an analysis is performed to estimate the correlation between the rock mass strength and the intact rock strength. The results of this analysis are shown in Figure 3-3. Equation 3-1 defined by the power curve best representating the correlation has been established.

$$\sigma_{cm} = \frac{\sigma_{ci}^{1.50}}{60} \qquad (3\text{-}1)$$

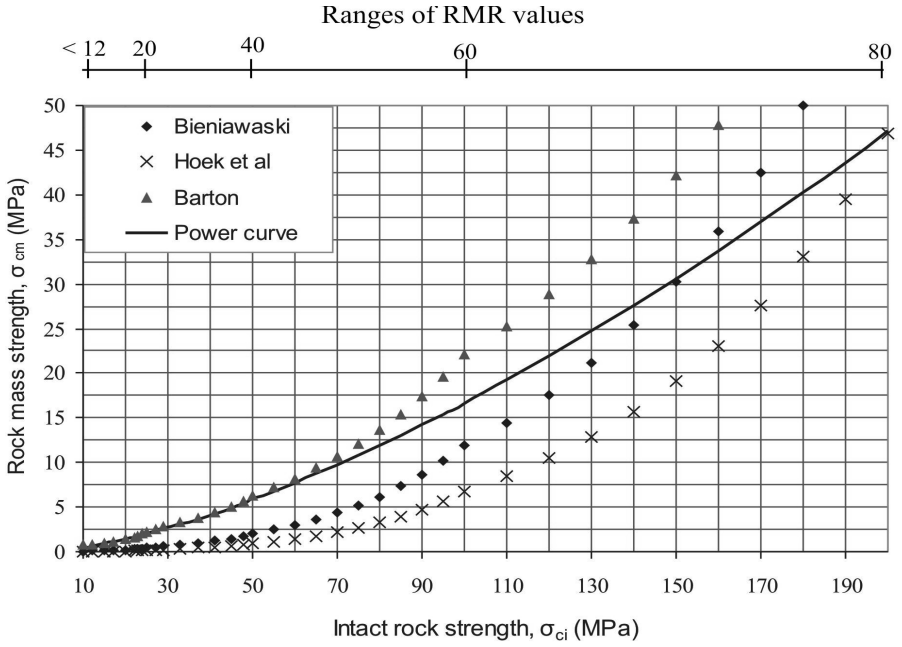

Figure 3-3. Correlation between rock mass strength, σ_{cm} and intact rock strength, σ_{ci}.

Figure 3-3 shows that the rock mass strength calculated based on Barton's and Hoek et al's relations give highest and lowest estimate, respectively. As can also be seen, the rock mass strength achieved for intact rock strength less than 60 MPa according to Hoek et al's and Bieniawaski's equations give conservative results (less than 3 MPa).

Equation 3-1 gives reasonable correlation between the rock mass strength and intact rock strength. This correlation may be used for an approximate estimation of the ranges of rock mass strength for highly schistose, foliated, thinly bedded and anisotropic rocks of metamorphic and sedimentary origin with low compressive strength. For more isotropic, crystalline and massive rocks with less schistocity, the rock mass strength should be in the range of 50 percent of intact rock strength as suggested by Palmstrøm (1995).

3.2.2 Rock mass deformability

The Commission of Terminology of ISRM (1975) describes *modulus of deformation (E_m)* as the ratio of stress to corresponding strain during loading of the rock mass, including elastic and inelastic behaviour, and the *modulus of elasticity (E_{ci})* as the ratio between applied stress and corresponding strain within the elasticity limit. The fact that jointed rock mass does not behave elastically has prompted the use of the term modulus of deformation rather than modulus of elasticity or Young's modulus (Bieniawski, 1978). According to Hudson and Harrison (1997), the deformation modulus of jointed rock mass is very low compared to the elasticity modulus of intact rock (may reach as low as 10 percent of the elasticity modulus of intact rock specimen).

The deformation modulus may be measured directly in the field using the methods such as Plate Jacking Test (PJT), Plate Loading Test (PLT), Goodman Jack Test (GJT), Flat Jack Test (FJT), Cable Jack Test (CJT), Radial Jack Test (RJT) and Dilatometer Test (DT) (Palmstrøm and Singh, 2001). However, all these methods are time-consuming and imply notable cost and operational difficulties. Also, the values obtained from different tests often differ considerably (Nilsen and Palmstrøm, 2000). Therefore, many authors have proposed empirical equations for estimating the rock mass deformation modulus, see Table 3-2.

Table 3-2. Empirical formulae for the estimation of rock mass deformation modulus.

Equation purposed by	Relationship to estimate rock mass deformation modulus
Bieniawaski (1978)	$E_m = 2RMR - 100$
Serafim and Pereira (1983)	$E_m = 10^{\frac{(RMR-10)}{40}}$
Palmstrøm (1995)	$E_m = 5.6 \times RMi^{0.375}$
Hoek and Brown (1997)	$E_m = \sqrt{\frac{\sigma_{ci}}{100}} \times 10^{\frac{GSI-10}{40}}$
Barton (2002)	$E_m = 10 \times Q_c^{1/3} = 10 \times \left(\frac{Q \times \sigma_{ci}}{100} \right)^{1/3}$

Where; E_m is the rock mass deformation modulus in GPa and *RMi* is the Palmstrøm's rock mass index.

During the planning phase of tunnelling projects rock mass classification is mostly based on surface observations and borehole data, and may not be as reliable as during construction. In contrast, many rock samples representing different rock formations are often collected and the intact rock strength (σ_{ci}) and elasticity modulus (E_{ci}) are determined by laboratory testing at this early phase of planning. It, therefore, would be a great advantage if the deformation modulus of rock mass was linked to the intact rock strength (σ_{ci}) and elasticity modulus (E_{ci}).

For isotropic, homogeneous and massive rock mass the ratio between rock mass strength and intact rock strength, and the ratio between deformation modulus and elasticity modulus should theoretically be equal, i.e. it should be possible to express the rock mass deformation modulus (E_m) by the following equation:

$$E_m = E_{ci} \times \left(\frac{\sigma_{cm}}{\sigma_{ci}} \right) \tag{3-2}$$

By substituting equation 3-1 into 3-2, the rock mass deformation modulus may be estimated based on intact rock strength and elasticity modulus as:

$$E_m = \frac{1}{60} \times E_{ci} \times \sigma_{ci}^{0.5} \tag{3-3}$$

Equation 3-3 may be useful for estimating the rock mass deformation modulus for schistose, foliated and bedded rocks with low compressive strength. For massive and isotropic rocks, the deformation modulus should be considered approximately fifty percent of the elasticity modulus as suggested by Palmstrøm and Singh (2001).

3.2.3 Strength anisotropy

Strength anisotropy is common in many rocks mainly as a result of preferred orientations of mineral grains and directional stress history. Distinct anisotropy is very common for sedimentary and metamorphic rocks as a result of bedding, foliation and schistocity (Goodman, 1989).

As discussed in Chapter 1, the rocks of the Himalaya are highly directional concerning strength and deformability. In many occasions, thin bands of very weak and highly sheared rocks such as slate, phyllite and schists are intercalated within the bands of relatively strong and brittle rocks such as gneiss, quartzite and dolomite. Being weaker in their mechanical characteristics and highly schistose, these weak rocks lack sufficient bonding / friction and have reduced self-supporting capability, and as a result severe stability problems have been faced during tunnelling.

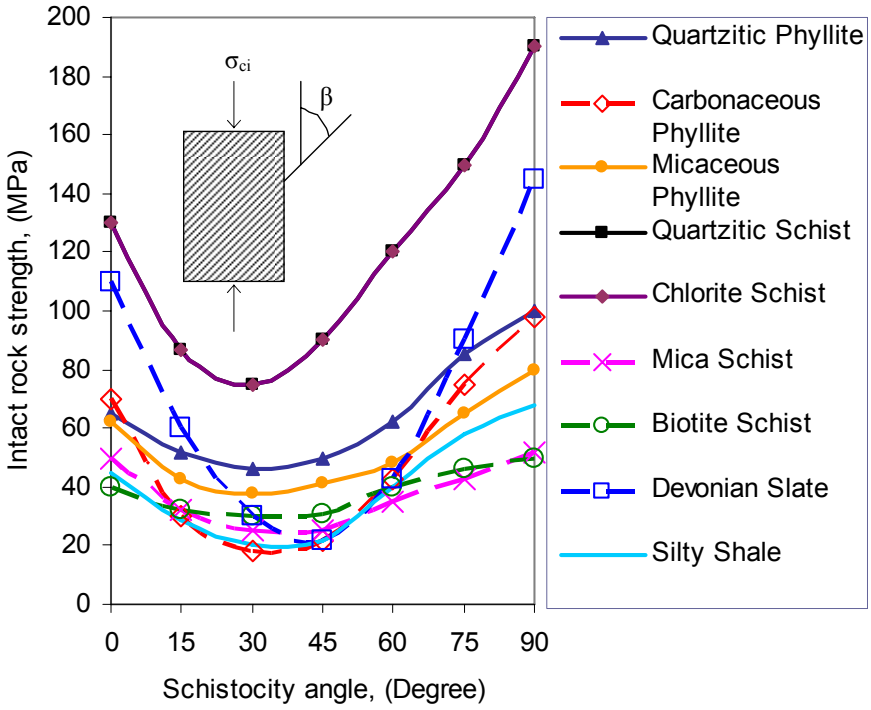

Figure 3-4. Uniaxial compressive strength at different angle of schistocity plane (based on Ramamurthy, 1993; Hawkins, 1998; Ajalloeian and Laskaripour, 2000 and Nasseri et al, 2003).

Figure 3-4, which is based on research for different rocks of the Himalaya and other part of the world, illustrates that the uniaxial compressive strength of intact rock specimens is smallest when the schistocity plane is inclined at around 30 degrees from the direction of loading (β = 30 degrees), and is greatest when the schistocity plane is perpendicular to the direction of loading (β = 90 degrees). Figure 3-4 clearly shows that schistose rocks consisting of sheet minerals like mica, biotite/muscovite, chlorite, graphite and talc have considerable strength anisotropy.

As Figure 3-4 indicates, compressive strength measured on cores drilled parallel and normal to the schistocity plane may give false impression of an isotropic material. Similarly, it is not always easy to core or obtain rock samples with schistocity angle in oblique direction. In this respect, the point load test, measuring induced tensional strength, gives maximum strength at a loading direction normal to the plane of schistocity and a minimum strength parallel to the plane of schistocity and therefore is more reliable in estimating strength anisotropy (index I_a) (Greminger, 1982 and Broch, 1983).

Based on the I_a index and Tsidzi (1987) foliation index, the strength anisotropy of the rocks can be classified in five categories as given in Table 3-3.

Table 3-3. Classification of rock strength anisotropy (after Palmstrøm, 1995 and Tsidzi, 1987).

Class	Descriptive class	Strength anisotropy index (I_a)	Typical rock types
I	Isotropic or close to Isotropic	1.0 – 1.2	Rocks having platy/prismatic minerals < 10% with shape factors <2 and platy minerals in random orientation. *Rock Types: Most of the igneous rocks and very high grade metamorphic rocks, i.e. diorite, granite, gabbro, quartzite, granitic gneiss , granulite etc.*
II	Slightly anisotropic	1.2 – 1.5	Rocks having platy/prismatic minerals 10 – 20 % with shape factors 2-4 and platy minerals in compositional layering. *Rock Types: High grade metamorphic rocks and some strong sedimentary rock, i.e. quartz-feldspatic gneiss, marble, migmatite, sandstone, limestone, etc.*
III	Moderately anisotropic	1.5 – 2.5	Rocks having platy/prismatic minerals 20 – 40 % with shape factors 4-8 and foliation plane distinctly visible. *Rock Types: Medium-high grade metamorphic rocks, i.e. mica gneiss, quartzitic schist, mica schist, biotite schist, etc.*
IV	Highly anisotropic	2.5 – 4.0	Rocks having platy/prismatic minerals 40 – 60 % with shape factors 8-12 and very closely foliated. *Rock Types: Low - medium grade metamorphic rocks such as phyllite, silty slate, etc.*
V	Extremely anisotropic	>4.0	Rocks having platy/prismatic minerals >60 % with shape factors >12 and fissile rocks. *Rock Types: Low grade metamorphic and argillaceous sedimentary rock, i.e. slate, carbonaceous phyllite, shale, etc.*

3.2.4 Discontinuity

Discontinuity is a structural or geological feature that changes the homogeneity in the rock mass. Most discontinuities are formed as a result of movement in the rock mass caused by geological events at different times and at different stress stages. According to ISRM (1978), discontinuity is the general term for any mechanical discontinuity in the rock mass having zero or low tensile strength. It is also the collective term for most types of joints, bedding planes, foliation planes, schistocity planes, weakness zones and fault zones (Nilsen and Palmstrøm, 2000).

The mechanical characteristics of a discontinuity surface are represented by roughness, alteration, weathering, spacing and persistence (Barton et al, 1985 and Hudson, 1989). ISRM (1978) recommended ten parameters to be considered for describing the discontinuity characteristics in the rock mass. These are illustrated in Figure 3-5.

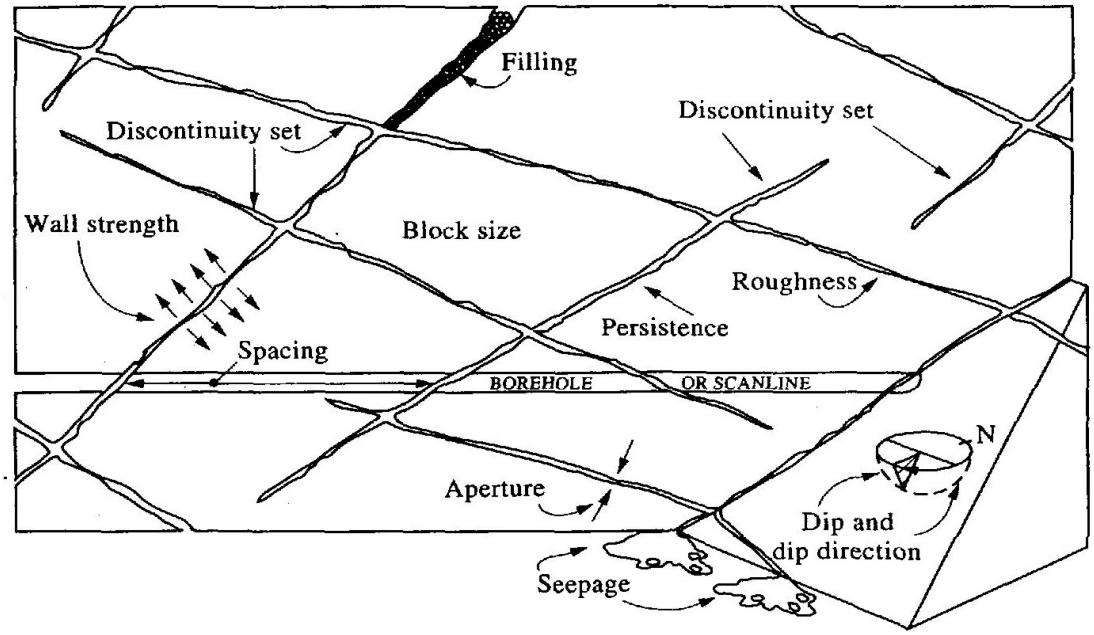

Figure 3-5. Discontinuity characteristics in the rock mass (Hudson and Harrison, 1997).

The discontinuity roughness, alteration, weathering, type and amount of filling material and susceptibility to groundwater flow may vary greatly along a discontinuity surface.

3.2.4.1 Discontinuity characteristics

Surface roughness: Roughness can be characterized by waviness or smoothness. The great majority of discontinuities in the rock mass have irregularities (waviness) that cause dilation for shear displacement. There also are small asperities, which are damaged during shear displacement unless the joint wall strength is high or the stress level is low (ISRM, 1978). To characterize the surface roughness of the discontinuities numerically, Bandis et al (1981) have introduced an empirical index called joint roughness coefficient (JRC), see Figure 3-6.

As shown in Figure 3-6, the discontinuity roughness may vary from rough to slickenside, giving different numerical ratings.

Alteration and infilling: Through geological history the discontinuity surfaces may undergo processes of weathering, hydro-thermal alteration and shearing cycles. The filling material on the discontinuity surfaces therefore may either be gouge material formed as a result of shear movement or material transported by groundwater through open joints in the rock mass (Bandis, 1993). Alternative type of discontinuity surfaces that may be observed in the field are shown in Figure 3-7.

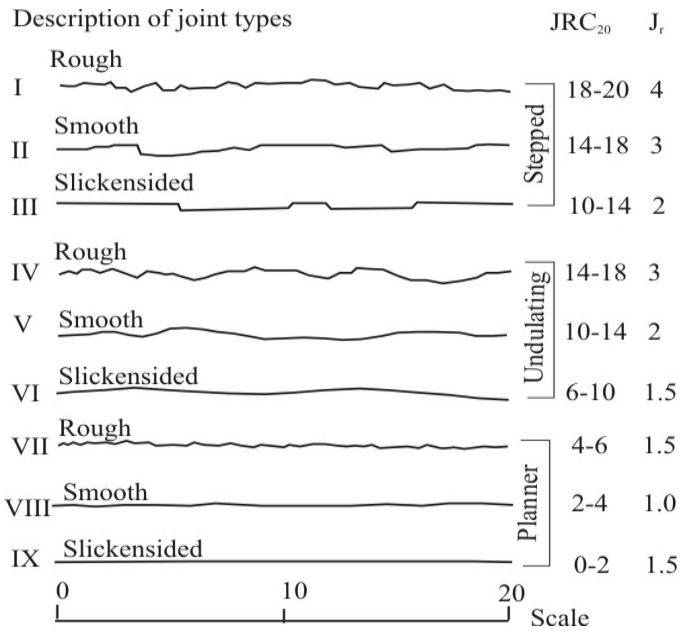

Figure 3-6. Discontinuity description and joint roughness coefficient (JRC) estimation, left and scale effect correlation for JRC, right (Barton and Bandis, 1990).

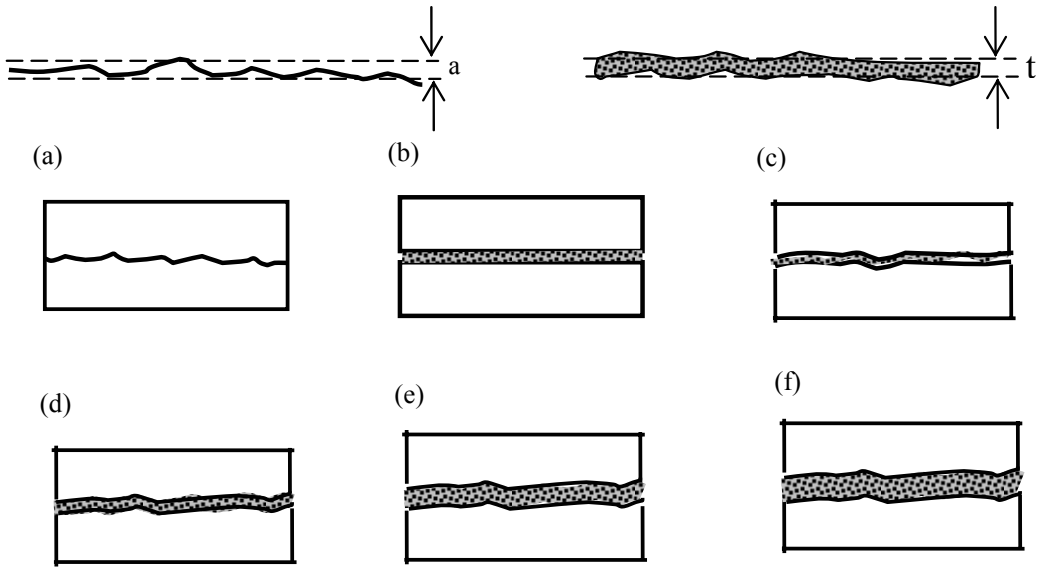

Figure 3-7. Nature of discontinuity surfaces (after Bandis, 1993).

The alternatives in the figure may be described as; (a) rough and interlocked discontinuity surface, (b) planar (slickensided) discontinuity surface with no rock contact, (c) non-planar discontinuity surface with almost immediate rock contact ($t << a$), (d) non-planar discontinuity surface with possible rock contact after some shearing ($t < a$), (e) non-planar discontinuity surface with no rock contact ($t > a$), and (f) discontinuity sur-

face dominated by filling material, and where influence by surface roughness is not possible (t >> a).

Testing carried out by Goodman in 1970 on artificially produced saw-tooth discontinuity surfaces filled with varying thickness of crushed mica showed considerable reduction in shear strength with increasing ratio between infilling thickness (t) and asperity (a) (Barton, 1974). Similar tests on discontinuity surfaces with commercial bentonite as infilling material and asperity height 2.5 mm carried out by Indraratna et al (1999) showed similar results. The results of the two test series are shown in Figure 3-8.

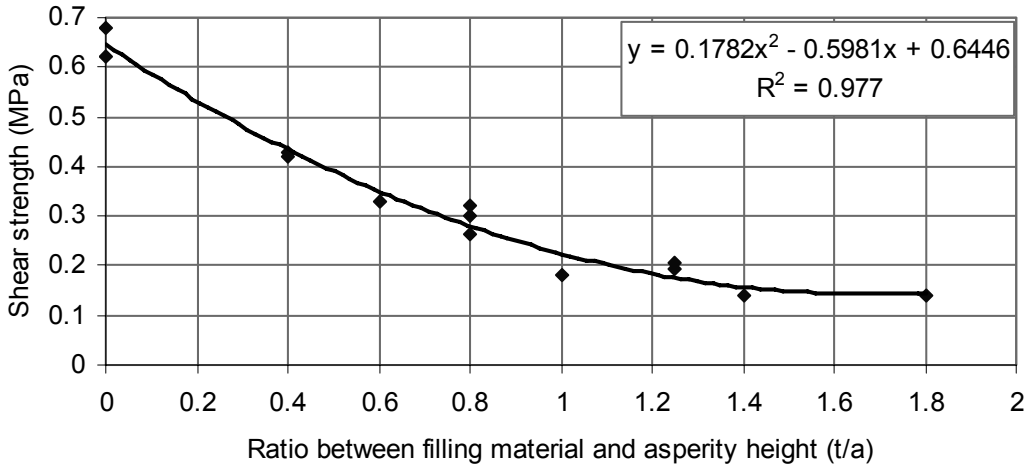

Figure 3-8. Effect of filling thickness on shear strength of the discontinuity surface (based on data in Goodman, 1970 and Indraratna et al, 1999).

As shown in Figure 3-8, when the filling thickness (t) on the discontinuity surface relatively to the asperity height (a) is increasing, the shear strength is reduced considerably.

Wall strength: Measurement of wall strength is crucial as the thin layer of altered and weathered rock adjacent to the discontinuity surface has major impact on the strength and deformation properties of the rock mass (Barton and Choubey, 1977). The term joint compressive strength (JCS) introduced by Barton (1973) is being widely used to characterize the wall strength of the discontinuity surface. The relevant value of JCS can be measured using Schmidt Hammer applied directly to the exposed joint walls as described by ISRM (1978).

Spacing and block size: The spacing between discontinuities determines the size of individual rock block. Factors such as compressive strength, deformation modulus, permeability, shear stiffness and failure modes are all influenced by discontinuity spacing and block size of the rock mass (Palmstrøm, 1995). Closely spaced discontinuities lead to reduction of the interlocking effect and increase in rock mass permeability and seep-

age characteristics (ISRM, 1978), which again lead to decrease in cohesion that may result in complete rock mass failure due to revelling ground conditions.

3.2.4.2 Large scale discontinuities

Weakness and fault zones are major discontinuities in the rock mass, and normally considered as the weakest link and the preferred channels for circulating groundwater. Since they are often very weak and highly conductive, they may have considerable influence on tunnel stability, and often represent the major safety risk during excavation. Therefore, knowledge on type of weakness zones and their process of origin is important. Ernest M. Anderson classified three fundamental categories of faults on the basis of their direction of principal stresses (Hatcher, 1995). These are strike-slip - (wrench), normal - (dip-slip) and reverse - (thrust) faults, see Figure 3-9.

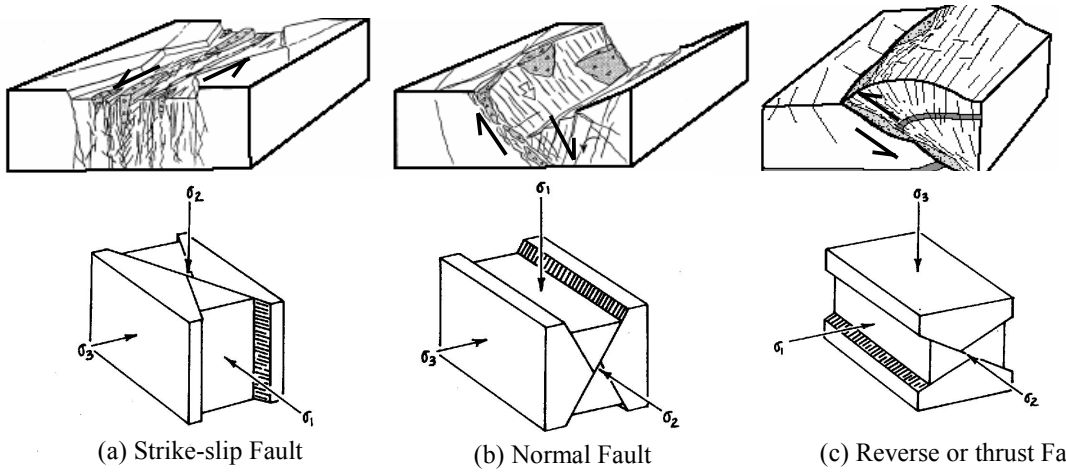

(a) Strike-slip Fault (b) Normal Fault (c) Reverse or thrust Fault

Figure 3-9. Anderson's classification of faults (after Braathen and Gabrielsen, 2000 and Rowland and Duebendorfer, 1994).

In rock engineering, the weakness and faults zones are often also divided into two main categories according to their character. The first category includes layers of particularly weak or highly schistose rock within a series of strong rocks, and referred to as zone of weak rock. The second category includes zones of crushed rock formed by faulting or tectonic events (Nilsen and Thidemann, 1993 and Palmstrøm, 1995).

Zones of weak rock: This category includes zones represented by excessive content of weak minerals such as clay, mica, talk, graphite, serpentine, etc. and also zones that have become weak due to alteration.

Fracture/weakness zones: Zones of heavily jointed to completely crushed rock mass fall in this category of weakness zones. The mechanism of formation of fracture zones is generally associated with two types of actions; 1) the formation of tensional and shear fractures, 2) hydrothermal alteration and weathering (Gudmundsson et al, 2002).

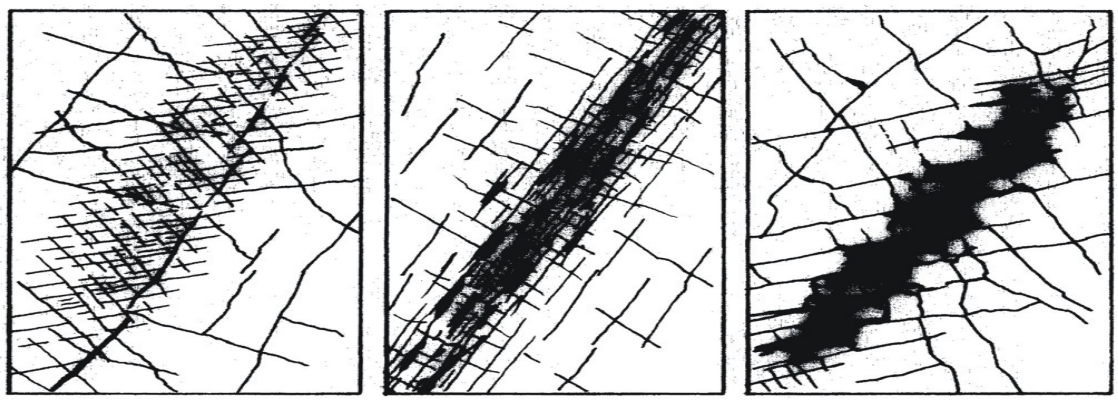

Figure 3-10. Structural features of fracture zones (ISRM, 1978).

As indicated by Figure 3-10, fracture zones typically consist of a central core and transition zone. The central core is made up of completely crushed and altered rock mass and primarily consists of silt or clay infilling. The damaged zone (transition zone) is represented by rock fractures of various sizes.

As discussed, weakness and fault zones are the weakest parts in the rock mass, and may cause severe stability problems in tunnelling. Their mechanical characteristics and engineering behaviour may vary greatly depending upon their type and origin. The weakness and fault zones act as conduits for groundwater flow and are the sources for accelerated hydrothermal alteration.

Zones of weak rock are very weak and often anisotropic, mostly ductile and highly deformable. They are relatively impermeable and homogeneous in their nature (Hoek et al, 1998). Stability problems in such zones are thus associated with rock squeezing and tunnel buckling or collapse of the roof and side walls due to very weak bond and reduced self supporting capability of the rock mass.

Weakness and fracture zones formed by tectonic stress and hydrothermal activity have varying mechanical characteristics from core to damaged zone. Unlike zones of weak rock mass, the weakness and fracture zones are heterogeneous and inhomogeneous. The stability problems in tunnelling are therefore more severe, and may vary from squeezing to water ingress and revelling ground conditions (Palmstrøm, 1995).

Due to topographic and other project specific constraints, it may not always be possible to avoid weakness and faults zones while planning underground excavations. Therefore, the length of tunnel crossing through such zones should be as short as possible, and the tunnel alignment should be oriented at an angle as high as possible. Large underground caverns should not be located in or in the vicinity of weakness and fault zones. Mistakes made may lead to excessive time and cost overrun and in extreme case to complete failure.

3.2.5 Rock weathering

Rock weathering is a natural process and a response of the dynamic earth to a changing environment. Rock weathering is analogous to corrosion in conventional engineering materials, and generally is most aggressive near the surface and gradually decreases with depth as shown in see Figure 3-11.

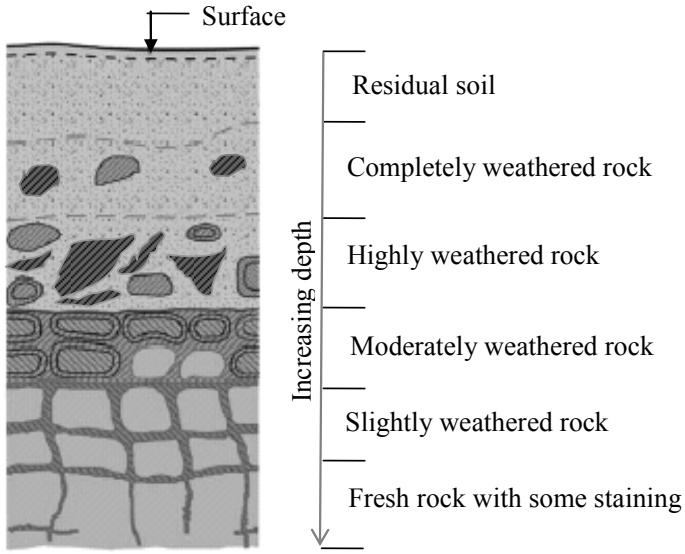

Figure 3-11. Typical rock weathering profile from the surface (after Rhardjo et al, 2004).

3.2.5.1 Weathering process

Rock weathering is a process of disintegration and decomposition of the rock material. Rocks may weather in different ways: by physical disintegration and by chemical decomposition. Physical weathering involves mechanical breakdown of the rock mass and is mainly controlled by discontinuities, grain boundaries and mineral cleavages. Chemical weathering involves decomposition and dissolution.

Mechanical and chemical weathering act together, but depending upon the environment and climatic regime, one or other of these aspects may be dominant (ISRM, 1978). In humid climatic conditions disintegration and decomposition act together, whereas in arid climatic conditions disintegration is dominant. In many occasions topography has also significant influence on rock weathering since it controls the rate of run-off and rate of water intake. On the other hand, weathering processes occurring at greater depth are largely chemical in origin and are related to dissolution, oxidation and hydrothermal alteration.

Physical weathering is caused by four main physical processes in the rock mass that lead to the fragmentation. These are; frost wedging, expansion due to a change in stress regime, thermal expansion and dynamic activity. Physical weathering results in rock

mass breakage, formation of new discontinuity surfaces and fracturing of individual mineral grains (Brattli, 2002).

Chemical weathering changes the chemical and mineralogical composition in the rock mass. The decomposition of minerals caused by chemical weathering eventually may change rock fragments into clay minerals. Chemical weathering may also lead to leaching or solution of calcite, anhydrite and salt minerals (Beavis, 1985 and Nilsen and Palmstrøm, 2000).

3.2.5.2 Weathering effect on the rock mass

As a general rule, the weathering process in the rock mass starts from its discontinuities and migrates to the rock minerals. There are five factors that are important in the process of weathering in the rock mass; discolouration and staining, change in texture and fabric, disintegration, decomposition and strength reduction (Gupta and Rao, 2000). If the rock mass is fresh, the discontinuity surfaces are very tight and slightly stained. If the discontinuity sets become more closely spaced and are open to weathering agents, the degree of weathering increases considerably, making discontinuity surfaces highly altered and filled with clay minerals of various kinds (Beavis et al, 1982).

There may be considerable variation in the degree of weathering of the rock mass and in weathering zones. This variability is assessed based on classification of weathering grade in the rock mass. ISRM (1978) classifies weathering grade in six categories as shown in Table 3-4.

Table 3-4. Weathering classification according to ISRM, 1978.

Term	Description of rock mass conditions	Weathering grade
Fresh rock	No visible sign of rock material weathering; perhaps slight discolouration on major discontinuity surfaces.	I
Slightly weathered	Discolouration indicates weathering of rock material and discontinuity surfaces. All the rock material may be discoloured by weathering and may be some what weaker externally than in its fresh condition.	II
Moderately weathered	Less than half of the material is decomposed and/or disintegrated to a soil. Fresh or discoloured rock is present either as a continuous framework or as corestones.	III
Highly weathered	More than half of the rock material is decomposed and/or disintegrated to a soil. Fresh or discoloured rock is present either as a discontinuous framework or as corestones.	IV
Completely weathered	All rock material is decomposed and/or disintegrated to soil. The original mass structure is still largely intact.	V
Residual soil	All rock material is converted to soil. The mass structure and material fabric are destroyed. There is a large change in volume, but the soil has not been significantly transported.	VI

As discussed in section 3.2.4, weakness and fault zones are often significantly influenced by weathering. Being formed by fracturing, shearing and hydrothermal alteration, the weakness and fault zones provide excellent environment for intensified weathering to take place, since such zones act as a medium for ground water flow.

Weathering reduces properties such as rock mass strength, deformability, slaking durability and frictional resistance. At the same time it may increase permeability considerably. Beavis (1985) and Gupta and Rao (2000) evaluated the weathering effect on the rock mass properties such as porosity, density, tensile strength, uniaxial compressive strength and elasticity modulus and concluded that there is a considerable reducing effect as illustrated in Figure 3-12.

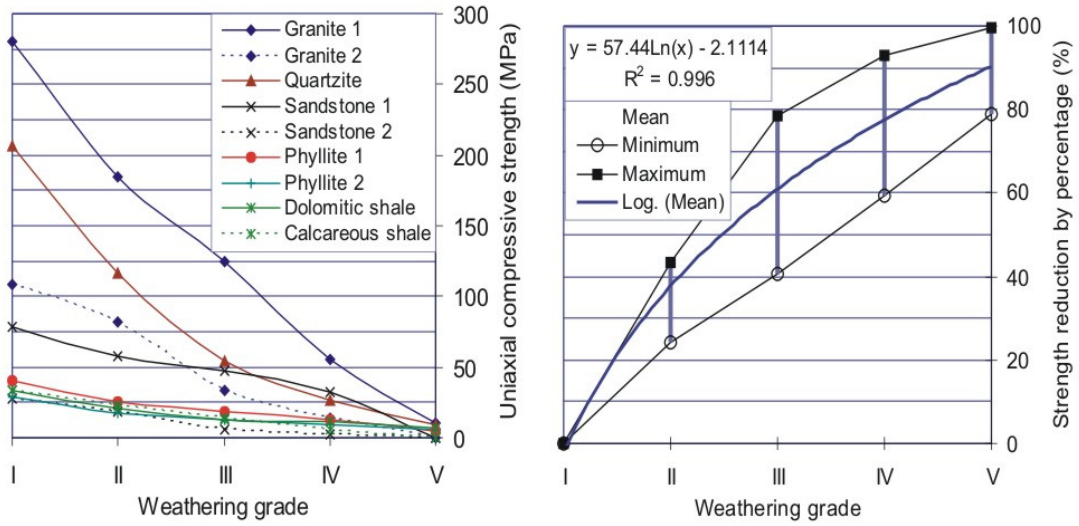

Figure 3-12. Compressive strength of rock (left) and strength reduction in percentage (right) as function of weathering grade (based on data in Beavis et al, 1982; Beavis, 1985 and Gupta and Rao, 2000).

As Figure 3-12 left indicates, there is a considerable variation in the influence of weathering on the unconfined compressive strength. As shown in Figure 3-12 right, moderate weathering may cause reduction of the intact rock strength by almost 40 percent in sedimentary and meta-sedimentary rocks, and 80 percent in crystalline rocks. Almost similar trends may be found regarding elasticity modulus. In addition, as Figure 3-8 indicated, there is a considerable reduction on the shearing resistance of the discontinuity surfaces caused by increased weathering.

Since rock weathering is one of the major aspects that has significant effect on tunnel stability in the Himalaya, it needs to be addressed in rock mass quality evaluation and stability analysis of underground excavations.

3.3 ROCK STRESSES

Unlike other materials used in engineering design, geological materials are preloaded by in-situ stresses. While excavation is made in the rock mass, the in-situ stresses are redistributed, inducing tangential stresses in the vicinity of the underground opening (Hoek and Brown, 1980). As discussed in section 3.2, the situation is complicated by the fact that structural features such as joints, fractures, bedding, and schistocity planes play important roles in the reduction of rock mass strength and deformability properties. As soon as the rock mass strength becomes less than induced tangential stress, there is a risk of overstressing leading to instability in an underground opening. Therefore, the magnitudes of in-situ stresses should be known for the assessment of stress induced instabilities in the tunnel.

3.3.1 In-situ rock stresses

The principle origins of in-situ stresses in the rock mass are gravity, plate tectonics and surface topography. The most important stress related parameters for stability analysis of underground openings are the magnitudes and directions of major and minor principle stresses.

The gravity induced vertical and horizontal stresses may be calculated as:

$$\sigma_v = \gamma \times H \tag{3-4}$$

$$\sigma_h = \frac{\nu}{1-\nu} \times \gamma \times H \tag{3-5}$$

Where, σ_v and σ_h are the vertical and horizontal stresses in MPa, γ is the specific weight in MN/m^3, H is the depth in meters and ν is the Poisson's ratio.

Hoek and Brown (1980) have found that the ratio (*k*) between horizontal and vertical in-situ stresses vary greatly and that the average horizontal stress near the surface is in must cases greater than the vertical stress, see Figure 3-13. While the ratio k is greater than one at shallow depths, it is less than one and approaches a constant value at great depths (McCutchen, 1982). This means that the magnitude of average horizontal stress (σ_h) is to a great extent influenced by plate tectonic movements.

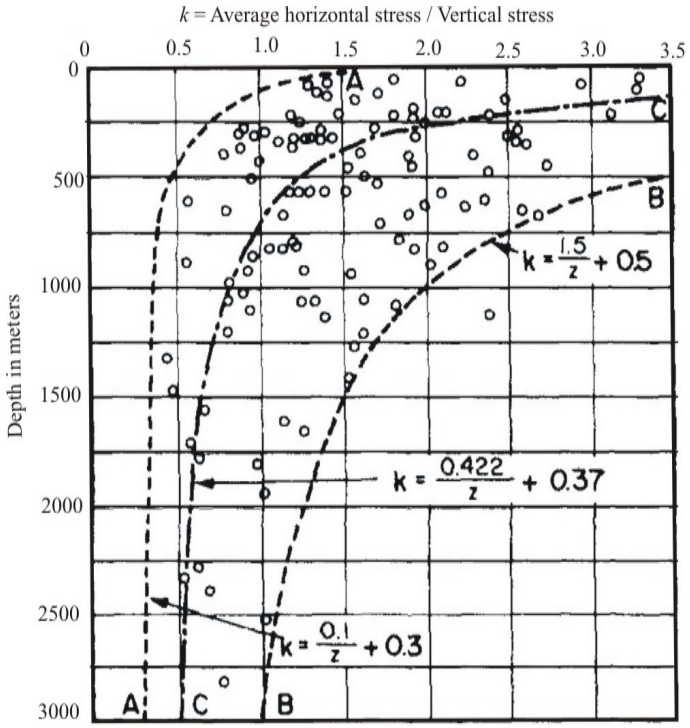

Figure 3-13. Variation of ratio of average horizontal to vertical stress with depth below surface (after Hoek and Brown, 1980).

3.3.2 Rock stress redistribution around a tunnel

After excavation of an underground opening, the in-situ stresses in the rock mass are disturbed. Stresses are redistributed along the periphery of the excavation. According to *Kirsch solution*, the redistribution of stresses around a circular opening in an elastic material in isostatic stress conditions ($\sigma_h = \sigma_v = \sigma$) may be expressed as shown in Figure 3-14.

As shown in Figure 3-14 (right), the tangential stresses (σ_θ) and the radial stress (σ_R) at the periphery of a circular opening in fully isostatic stress condition and for elastic rock material will be twice and zero times the isostatic stress respectively. Stresses become normalized as the ratio between radial distance (R) and opening radius (r) increases. The magnitudes of σ_θ and σ_R are:

$$\sigma_\theta = \sigma \times \left(1 + \frac{r^2}{R^2}\right) \tag{3-6}$$

$$\sigma_R = \sigma \times \left(1 - \frac{r^2}{R^2}\right) \tag{3-7}$$

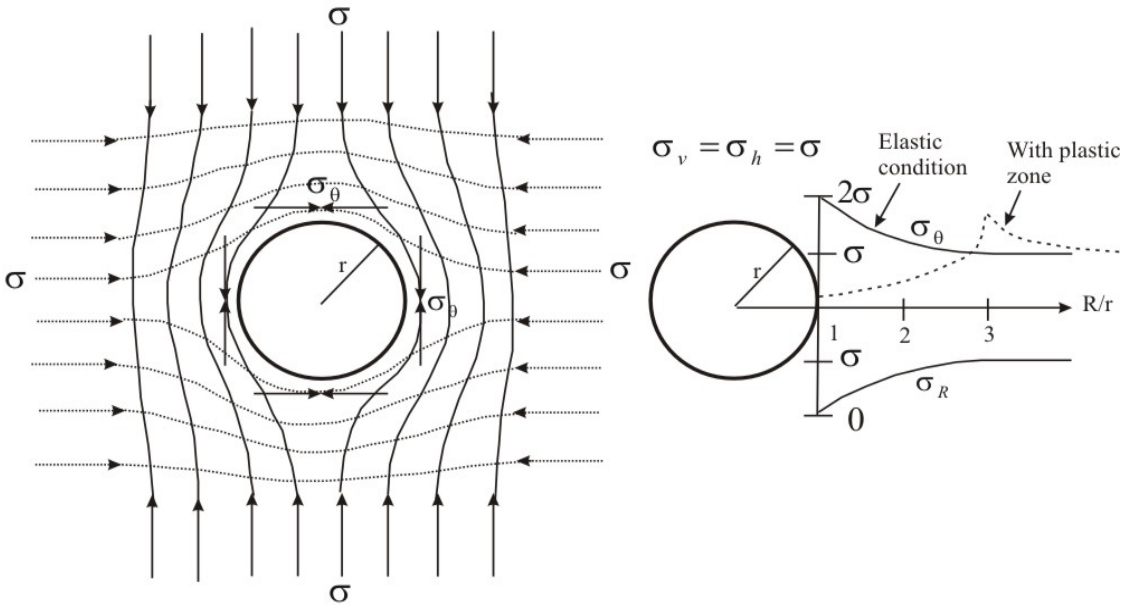

Figure 3-14. Stress trajectories in rock mass surrounding a circular opening (left) and tangential and radial stress distribution in elastic and non elastic conditions (right) (based on Hoek and Brown, 1980; Nilsen and Thidemann, 1993 and Bray, 1967).

However, the stress conditions are seldom isostatic and a different magnitude of major principal stress (σ_1) and minor principal stress (σ_3) give variation in the magnitude of tangential stresses. According to *Kirsch solution* the tangential stress will reach its maximum value ($\sigma_{\theta max}$) where the σ_1 direction is tangent to the contour, and its minimum value ($\sigma_{\theta min}$) where the σ_3 direction is tangent. The actual values will be as follows:

$$\sigma_{\theta \max} = 3\sigma_1 - \sigma_3 \tag{3-8}$$

$$\sigma_{\theta \min} = 3\sigma_3 - \sigma_1 \tag{3-9}$$

Equations 3-6, 3-7, 3-8 and 3-9 are valid for homogeneous, isotropic and elastic rock mass having widely spaced and tight joints. In weak and anisotropic rocks, the gradual reduction in strength caused by destruction and cracking by the tangential stresses drives the zone of broken rock deeper into the contours forming a plastic zone. In such rock mass, as shown in Figure 3-14 right with dotted lines, the maximum tangential stresses are moved further until the elastic zone is reached. Therefore, a solution for stresses and displacements derived from the theory of plasticity may provide a useful basis for the analysis in such rock mass condition (Goodman, 1989).

3.3.3 Stress induced instability

Instability induced by rock stresses are generally caused by induced stresses exceeding the rock mass strength. There are mainly two forms of instability caused by induced stresses; 1) rock burst / rock spalling, and 2) tunnel squeezing or deformation.

Rock spalling is fracturing parallel to the tunnel periphery occurring typically in strong and brittle rock masses. If the fracturing process is accompanied by loud noises and vibrations, this phenomenon is referred to as rock burst.

Assessment of risk for rock burst or spalling in a tunnel is generally based on the ratio between maximum tangential stress given by Equation 3-8 and the rock mass strength (approximately 50 percent of the uniaxial compressive strength). Several authors, for instance Hoek and Brown (1980), Broch and Sørheim (1984) and Grimstad and Barton (1993), have proposed criteria for assessment of rock burst and spalling in tunnels. Analysis and risk assessment of rock burst or spalling is however not an objective of this research, and the discussion below is therefore mainly focused on squeezing, which is very relevant for Himalayan rock mass conditions.

3.3.3.1 Tunnel squeezing

Weak rocks such as shale, slates and phyllite, and weakness / fracture zones, behave very differently from isotropic and stronger rocks when subjected to tangential stresses. In such rock mass, when the strength is less than induced tangential stresses along the tunnel periphery, gradual formation of micro-cracks along the schistocity or foliation plane will take place. As a result, a visco-plastic zone of micro-fractured rock mass is formed deeply into the walls as shown in Figure 3-15, and the induced maximum tangential stresses are moved beyond the plastic zone (Bray, 1967).

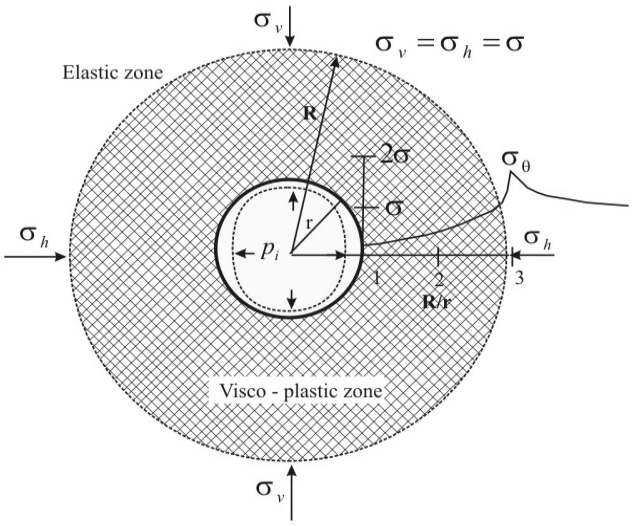

Figure 3-15. An illustration of squeezing in a circular tunnel (based on Bray, 1967). In the figure, r is the tunnel radius, R is the radius of visco-plastic zone and p_i is the support pressure.

As a result, a time dependent inward movement of rock material will take place and support in the opening will experience gradual build up of pressure. This time-dependent inward movement (plastic strain or creep) of the rock material towards the tunnel when subjected to tangential stresses (illustrated by dotted lines in Figure 3-15) is defined as tunnel squeezing.

In many occasions, temporary support provided in the tunnel has failed to sustain large deformations and the applied temporary support is damaged (an example of this is shown in Figures 1-8 and 4-10). In extreme cases a new state of equilibrium is achieved after complete closure of the tunnel (Kovari, 1998 and Steinar, 1996). Therefore, unless a reliable prediction of rate and extent of squeezing is made in advance, it is not possible to develop a strategy for controlling large deformations caused by squeezing.

In an effort to predict tunnel squeezing, several methods have been developed. Basically, these methods include empirical methods such as Singh et al (1992), Grimstad and Barton (1993), Goel et al (1995), Palmstrøm (1995); semi-analytical methods such as Hoek and Marinos (2000), Kovari (1998), Adyan et al (1993); and analytical methods (convergence confinement methods) such as Carranza-Tores and Fairhust (2000). Singh et al (1992), Goel et al (1995) and Hoek and Marinos (2000) are the most commonly used empirical and semi-analytical methods, respectively, and represent the basis for uncertainty analysis of squeezing discussed in Chapter 6, and therefore will be described in some detail below

3.3.3.2 Alternative approaches for predicting tunnel squeezing

Singh et al approach: The empirical criterion proposed by Singh et al (1992) is based on the relationship between rock mass quality (Q) and overburden for Himalayan tunnels, see Figure 3-16. Based on this criterion, tunnels plotting above the indicated line are likely to be affected by squeezing.

Goel et al approach: Among the six parameters of the Q-system, the stress reduction factor (SRF) considers the effect of rock stress. Hence, the criterion in Figure 3-16 has double account of the stress effect. To avoid this contradiction, Goel et al (1995) proposed a new criterion for squeezing, which is related to rock mass number N, see also Figure 3-17:

$$H \geq 270 \times N^{0.33} \times B^{-0.1} \qquad (3\text{-}10)$$

In Equation 3-10, H is the overburden height in meters, N is the Q-value without SRF and B is the span (width or diameter) of the underground opening.

This empirical criterion indicates whether squeezing will occur or not. However, it can not be used for estimating the magnitude of tunnel convergence, and therefore has limited application.

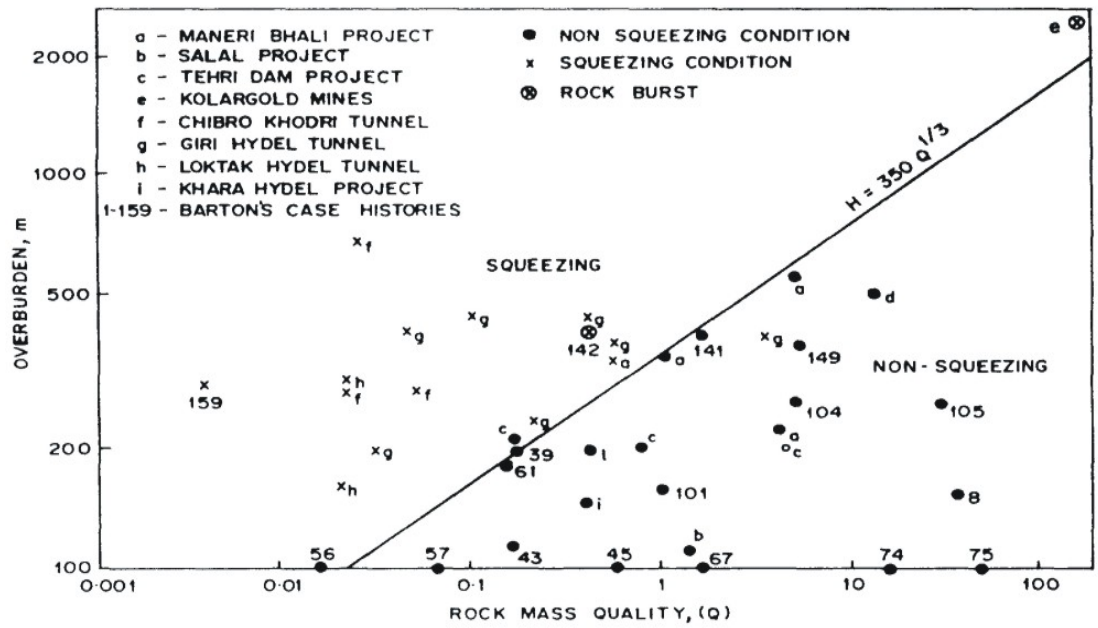

Figure 3-16. Criteria for predicting squeezing proposed by Singh et al, 1992.

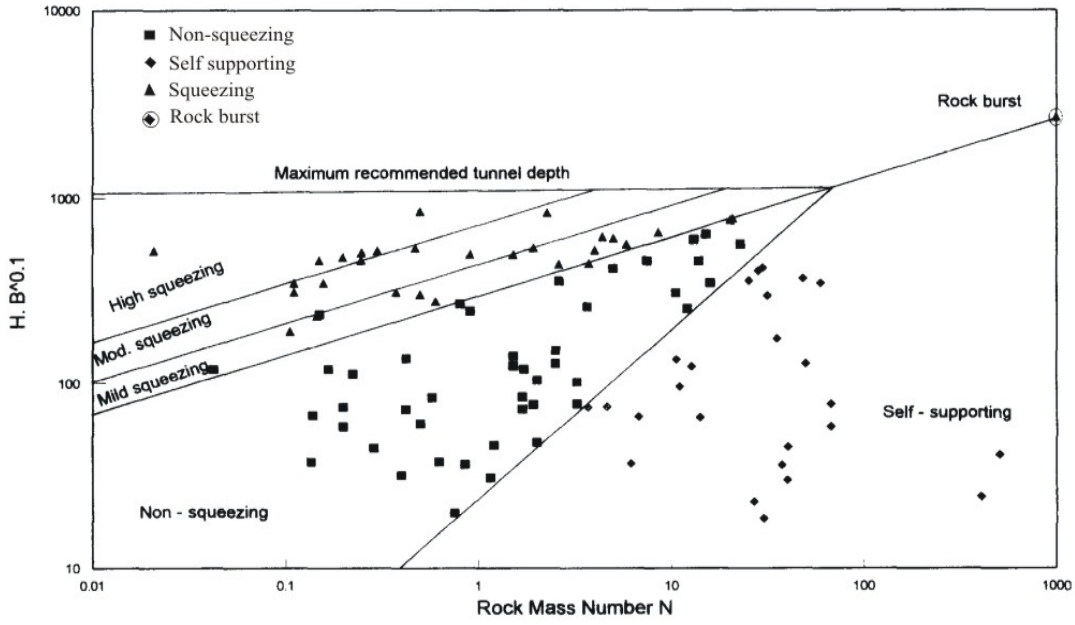

Figure 3-17. Criteria for predicting squeezing proposed by Goel et al, 1995 (after Singh et al, 1997).

In practice, a reliable assessment of N and Q values is often difficult during planning of underground openings in the Himalaya since information about rock mass quality below the weathering surface is often limited.

Hoek and Marinos approach: The extent of squeezing is not only related to overburden pressure. According to Kovari (1998) the changing strength and deformability properties of the rock mass over time have far greater consequence on tunnel squeezing than the overburden pressure. Therefore, a semi-analytical approach of predicting tunnel squeezing proposed by Hoek and Marinos (2000) is considered to be more reliable than the purely empirical criterion.

The rock mass strength and the overburden pressure are the two key parameters for estimating tunnel squeezing (total strain) of an underground opening. In view of this, Hoek and Marinos (2000) suggested a relationship that gives total tunnel strain (the ratio of tunnel closure versus tunnel diameter), which is function of the ratio between rock mass strength and in-situ overburden pressure. The criterion is based on circular tunnel and isostatic stress condition. This relation is also based on Monte Carlo analysis of a very wide range of rock mass properties and in-situ stress conditions, see Figure 3-18 left.

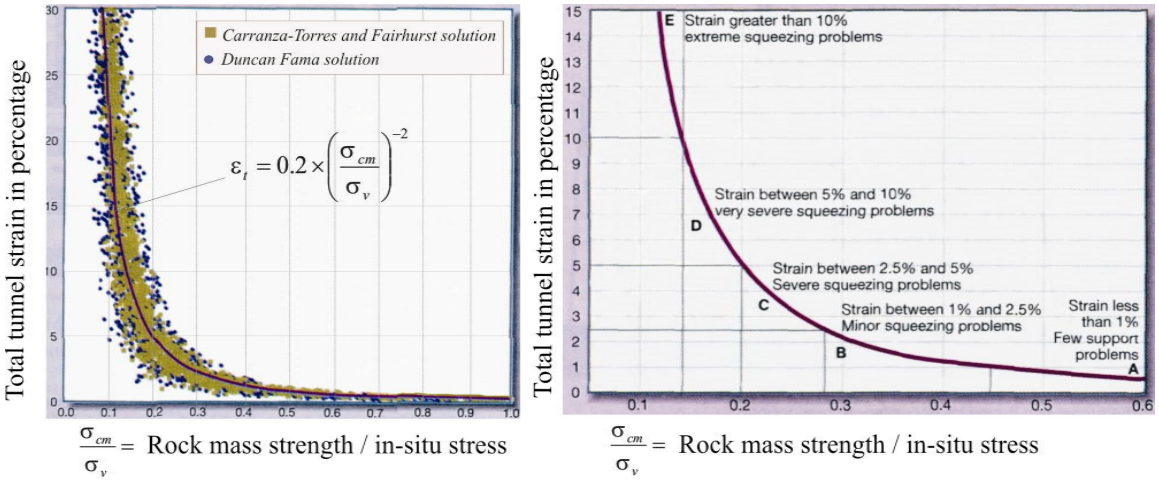

Figure 3-18. Tunnel convergence against the ratio of rock mass strength and in-situ stress (left) and tunnel convergence against the degree of difficulties associated with tunnel squeezing (right) (Hoek and Marinos, 2000).

Hoek and Marinos define the size of the plastic zone (R) and the total tunnel strain (ε_t) by the following two equations.

$$R = r \times \left(1.25 - 0.625 \times \frac{p_i}{\sigma_v}\right) \times \left(\frac{\sigma_{cm}}{\sigma_v}\right)^{\left(\frac{p_i}{\sigma_v} - 0.57\right)} \tag{3-11}$$

$$\varepsilon_t = \frac{\delta_t}{2r} \times 100 = \left(0.2 - 0.25 \times \frac{p_i}{\sigma_v}\right) \times \left(\frac{\sigma_{cm}}{\sigma_v}\right)^{\left(2.4 \times \frac{p_i}{\sigma_v} - 2\right)} \tag{3-12}$$

Where; ε_t is the total inward tunnel strain in percentage, δ_t is total inward tunnel deformation in meters, p_i is support pressure in MPa and other parameters have already been described above.

For support pressure (p_i) equivalent to zero, i.e. total squeezing without rock support, Equations 3-11 and 3-12 may be rewritten as follows:

$$R = 2.5 \times r \times \left(\frac{\sigma_v}{\sigma_{cm}} \right)^{0.57} \tag{3-13}$$

$$\varepsilon_t = \frac{\delta_i}{2r} \times 100 = 0.2 \times \left(\frac{\sigma_{cm}}{\sigma_v} \right)^{-2} \tag{3-14}$$

Hoek and Marinos (2000) assumed that very weak rock masses are incapable of sustaining significant differential stresses and that failure occurs until the in-situ horizontal and vertical stresses have been equalized. This is the main reason for their consideration of overburden pressure instead of the tangential stress, which is always greater in magnitude than the overburden pressure, for estimating tunnel squeezing. For defining approximate guidelines to characterize the degree of difficulties that can be encountered at different levels of tunnel strains as shown in Figure 3-18 right, they used Figure 3-18 left and Equation 3-14.

Since it is not possible to predict exactly the magnitude of rock mass strength, and since it may vary greatly in the area of concern, the author is of the opinion that uncertainty analysis should be carried out while using Equations 3-12 and 3-14.

3.3.3.3 Estimating support pressure

One of the most important aspects concerning tunnel squeezing is to make a strategy regarding stabilizing measures in order to minimize the stability problems. In this respect, the behavior of the support and its influence on the rock support pressure (p_i) is very important. When tunnel support is placed immediately behind the tunnel face, it does not carry the full pressure since a part of the pressure will be carried by the face itself. As the tunnel face advances (i.e. away from the installed support), the face effect decreases and the support must carry most of the pressure that the face carried earlier (Carranza-Torres and Fairhurst, 2000). This situation may be described by the ground reaction curve (GRC) as shown in Figure 3-19 left.

In the figure, p_i is the support pressure provided by the rock mass through which the tunnel is being advanced. At a distance of approximately one diameter ahead of the tunnel, the rock mass is not influenced by the presence of the tunnel and the support pressure equals the in-situ stress ($\sigma_v = \sigma_h = \sigma$), corresponding to point A on the ground reaction curve. As the tunnel advances, the support provided by the rock mass de-

creases and the rock mass responds elastically up to point B, at which the plastic failure of the rock mass initiates. Eventually, the support pressure (p_i) becomes close to zero and the radial convergence (δ_t) reaches its final value at a distance of approximately two tunnel diameters from the face. If tunnel support is installed after the tunnel has converged a distance value δ_0, the system reaches its equilibrium at point C, where the ground reaction curve and the provided support reaction line (SRL) intersect (Hoek 2001).

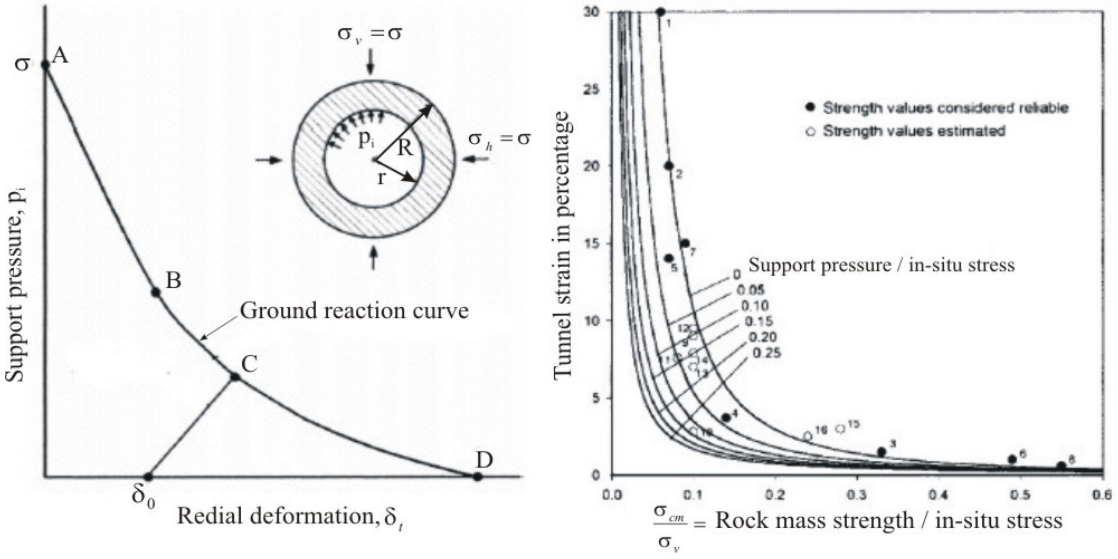

Figure 3-19. Ground reaction curve for a circular tunnel in hydrostatic conditions (left) and influence of support pressure on tunnel strain in weak rock mass (right) (Hoek, 2001).

Hoek (2001) also compared deformations observed for tunnels from Venezuela, Taiwan and India and values calculated according to Equations (3-12 and 3-14) with different rock support pressures, see Figure 3-19 right. As can be seen, the results are in reasonable agreement. However, according to Hoek, one of the problems in interpreting field observations of tunnel squeezing is the influence of tunnel support. It is particularly difficult, when applied support capacity is exceeded and there is a considerable damage on the applied support such as buckling of steel sets, cracking of shotcrete and excessive yielding of rock bolts.

3.4 GROUND WATER

The rock mass is a jointed aquifer where water moves through the most permeable discontinuities or through open channels along them. In general, the rock mass close to the surface is more jointed and the joints are more open than deeper in the rock mass. Visual observations in many ungrouted tunnels indicate that most water leakage occurs in the part of the tunnel which is closest to the surface and that it is mainly confined in fractures, faults and weathered zones (Nilsen and Thidemann, 1993 and Karlsrud, 2002).

3.4.1 Hydraulic conductivity of the rock mass

In the rock mass, the degree of jointing and the character of joint surfaces largely govern the hydraulic conductivity (coefficient of permeability). As shown in Figure 3-5, if joint sets in the rock mass are interlinked to each other, and have wide aperture and are open or filled with permeable materials, the hydraulic conductivity is high. In general, the degree of jointing, spacing between joints and wideness of aperture in the rock mass are depth dependent. With the increase in depth, joints become tighter with reduced aperture, and often there is an increase in joint spacing and reduction in the joint set numbers. As a result, the hydraulic conductivity of the rock mass decreases with increased depth as shown in Figure 3-20.

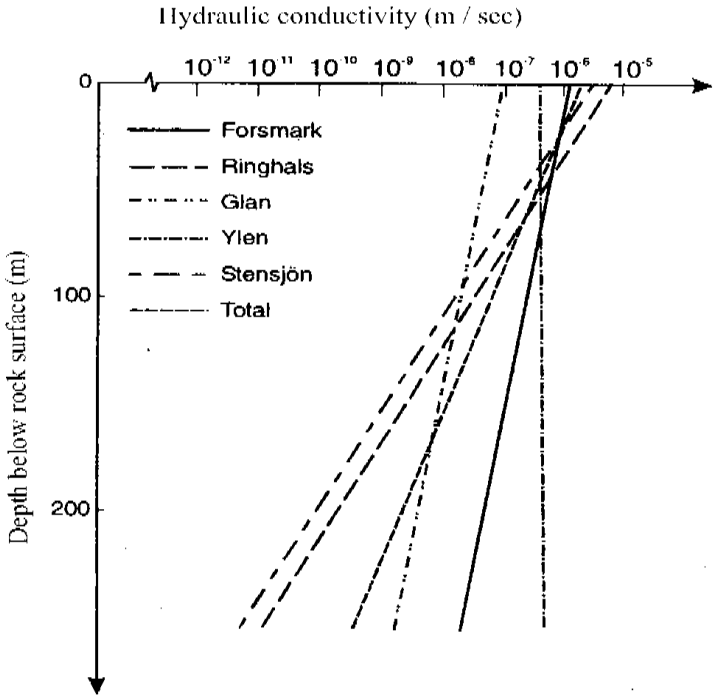

Figure 3-20. Hydraulic conductivity as a function of depth for Swedish test sites in Precambrian rocks (after Carlsson and Olssen, 1977).

Different rocks have different characteristics with respect to hydraulic conductivity. Jointed but strong and brittle rocks such as granite, quartzite and gneiss may have a hydraulic conductivity corresponding to the value of clean sand as shown in Figure 3-21, while unjointed rocks of similar category may have permeability lower than that of marine clay. Similarly, very weak, highly folded and highly sheared rocks such as shale, phyllite and schist have low hydraulic conductivity. On the other hand, rocks such as limestone and marble, with calcite as the mineral, have a tendency of dissolution when in contact with acid water. As a result, large water inflow as well as leakage may occur through karst channels.

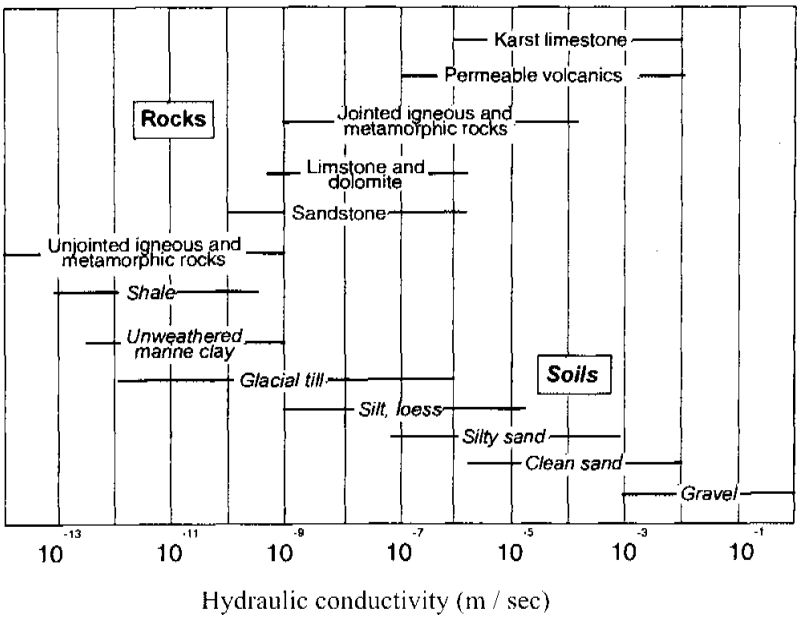

Figure 3-21. Hydraulic conductivity of rocks and soils (Freeze and Cherry, 1979).

Therefore, problems related to ground water differs depending upon the type of rocks, jointing characteristics in the rock mass, and depth from the surface.

3.4.2 Problem associated with inflow and leakage

Water inflow and leakage problems are not new issues in tunnelling. At the tunnel face, water inflow during excavation may reduce work safety considerably and drilling and detonation may become very difficult. Stability of the tunnel may be reduced considerably due to reduction in the rock mass strength. Excessive inflow through weakness / fracture zones may cause severe stability problems and in extreme cases tunnel may be lost due to heavy inflow as illustrated in Figure 1-9, right.

Similarly, leakage from water tunnels during operation may reduce the stability of the rock mass, and also valuable water may be lost from the tunnel, causing huge economic loss to the project, see Figure 1-9, left. According to Kassana and Nilsen (2003), some notable projects, which have suffered excessive water leakage problems are Chivor II (Columbia), Whatshan (Canada), Askora and Bjerka (Norway) and Kihansi (Tanzania). Therefore, water leakage control plays a vital role not only in improving the rock mass quality, but also in saving economic loss caused by leakages.

Control of water inflow during excavation through difficult ground conditions is often possible to achieve by high pressure grouting techniques. Such techniques have also made it possible to control and reduce the amount of leakage from water tunnels to a target level. The systematic preinjection grouting not only improves the hydraulic con-

ductivity of the rock mass closest to the tunnel periphery by many folds, but also considerably improves the quality of the rock mass (Panthi and Nilsen, 2005a).

Due to considerable improvement in tunnelling techniques and need for more underground space for various purposes, future tunnels will often be located in weak and heterogeneous rock masses, and tunneling through zones of weakness, fractures and faults will more and more become a matter of reality. In this respect, predicting inflow and leakage during planning plays a key role. Such predictions are even more needy in the Himalaya, where the rock mass are highly heterogeneous and more and more tunnelling are required to develop hydropower potential that exists in this region.

3.4.3 Estimating inflow and leakage

Predicting possible inflow and leakage in a planned underground excavation is very difficult. Permeability testing and geo-electrical methods may give some indication for potential inflow and leakages. However, the difficult part of the problem is the scale effect, i.e. conversion of the test results to large scale conditions (Nilsen and Palmstrøm, 2000).

Prevailing inflow theories based on inflow from single joints or weakness zones generally do not correspond well with real ground conditions. Equations based on rock mass permeability are more relevant, but few such equations have been found in literature. An equation proposed by Tokheim and Janbu (1984) seems to be the one most often referred to in literatures and will be briefly discussed below. This equation is based on basic flow theory and is expressed as follows:

$$Q_w = \frac{2\pi \times K \times L \times p}{\mu_w \times G} \tag{3-15}$$

Where; Q_w is the inflow or leakage rate in m^3 / s, K is the specific permeability in m^2, L is the length of tunnel in meters, p is the active head in Pa, μ_w is dynamic viscosity of water (9.81 x 10^{-10} N / m. s. for pure water at 10^0C), G is the geometry factor describing flow pattern relative to the geometry of the tunnel and is expressed by the following equation:

$$G = \ln \frac{(2D - r) \times (L + 2r)}{r \times \left[L + 2 \times (2D - r)\right]} \tag{3-16}$$

Where; D is the distance between the length axis of the excavation and ground water table in meters and r is the equivalent radius in meters (the radius of cylinder with a surface area equivalent to the surface area of the tunnel).

As can be seen, the specific permeability of the rock mass has to be known for estimating possible water leakage using Equation 3-15. By theory, the specific permeability is given by the following equation:

$$K = \frac{k_w \times \mu_w}{\rho_w \times g} = \frac{k_w \times \mu_w}{\gamma_w} \tag{3-17}$$

Where; k_w is the hydraulic conductivity in m / s, g is the acceleration due to gravity in m / s^2, ρ_w is the density of water in kg / m^3 and γ_w is the specific weight of water in N / m^3.

By substituting equation 3-17 into 3-15, the specific leakage (q), described in l /min. / m tunnel, through an unlined or shotcrete lined tunnel may be expressed as:

$$q = \frac{60000 \times 2\pi \times k_w \times p}{\gamma_w \times G_1} = \frac{120000 \times \pi \times k_w \times \gamma_w \times h_{static}}{\gamma_w \times G_1} = \frac{3.77 \times 10^5 \times k_w \times h_{static}}{G_1} \tag{3-18}$$

Where; q is specific leakage in l / min. / m tunnel, h_{static} is the static head in meters and G_1 is the geometry factor for one meter tunnel length (L = 1 in equation 3-16).

Equation 3-18 may be useful for estimating specific leakage through an unlined or shotcrete lined tunnel in full hydrostatic condition. However, one of the major difficulties in using this equation is reliable quantification of hydraulic conductivity (k_w). The value k_w varies considerably depending upon the degree of jointing in the rock mass and also upon the type of rocks as shown in Figure 3-21.

Alternative approaches, which are used to estimate inflow and leakages, are field measurements such as Lugeon test, water pressure measurements and water inflow registration through exploratory drilling. Such measurements play a key role in estimating leakage from tunnels during excavation. At the planning stage field measurements are generally limited to selected locations. This is due to the fact that extensive exploratory drilling and excavation of test adits at the planning stage are limited by economic constraints.

As discussed in Chapter 1, one objective of this research is to evaluate the probability of water leakage from unlined or shotcrete lined water tunnels in the Himalaya. The main area of interest here is to estimate the amount of leakage that may occur through unlined / shotcrete lined water tunnels passing through fractured rock mass. The linkage between possible leakage, rock mass quality and quantity of grout material required for reducing the leakage to a target level is of great importance. Without knowledge about this linkage, it is not possible to optimize and estimate the cost and time required for systematic grouting.

Very little literature on such correlation except for Equation 3-15 has been found. An attempt therefore will be made to find an empirical relationship based on data from a recently constructed shotcrete lined headrace tunnel in the Himalaya, where pre- and postinjection grouting have been successfully used to solve such problems. The results of such analysis are given in Chapter 6.

3.5 CONCLUDING REMARKS ON STABILITY FACTORS

As have been reviewed and discussed in this chapter, there are many factors that influence on the rock mass conditions and thereby on the stability of underground excavations. The importance of these factors may vary from project to project and there is no universal way of defining these factors that are applicable to all tunnelling projects. Since the quality of rock mass may vary considerably even within similar lithology, uncertainly and risk analysis may be very useful when analyzing stability problems for Himalayan rock mass condition.

Chapter 4
Engineering geological conditions of the cases

4.1 INTRODUCTION

The rock mass condition along the alignment of any tunnel project is decisive with respect to its final cost and the construction time required. To carry out a study on the economic viability of a tunnel project, the rock mass quality along the tunnel alignment has to be examined and estimated quantitatively during the pre-construction phase. This is done by engineering geological investigation conducted at this stage of planning and design. Due to the fact that the rock mass is a complex material with many variable parameters, it is generally expected that there will be some degree of deviations between predicted and actual rock mass conditions. This deviation should, however, be within the acceptable limit so that excessive cost overruns and required construction time are controlled (Panthi and Nilsen, 2005b). Nevertheless, it is not always an easy task to predict and estimate the rock mass conditions along the tunnel alignment accurately enough in advance so that variations can be kept within the acceptable limit.

The only way to control quality deviation is to have a well planned and organized pre-construction phase engineering geological investigation. If the procedures have satisfactorily high quality, the final investigation results with desired limit of deviations are possible to obtain in spite of geological uncertainties and difficulties. In regards to the Himalaya, four major tunnel projects in Nepal representating selected cases for this PhD research have not shown such results. To a great extent these tunnel projects have encountered ground conditions quite different from what was anticipated during pre-construction phase planning and design. This has caused additional cost and considerable delay in the project completions and also has led to claims and contractual fight between the client and the contractor.

This chapter reviews and examines the engineering geological conditions of headrace tunnels of the four selected tunnel project cases shown in Figure 4.1. These projects include; 1) Khimti I hydropower project, 2) Kaligandaki "A" hydroelectric project, 3), Modi Khola hydroelectric project and 4) Middle Marsyangdi hydroelectric project. The first three of these projects were recently completed and are now in commercial operation and the fourth, the Middle Marsyangdi hydroelectric project is under construction. In addition to project locations and Himalayan geology, Figure 4-1 also shows the three major river systems of Nepal Himalaya. It should be noted here that there are more than

6,000 rivers and rivulets in Nepal and only the major ones originating from the Himalayas are shown in Figure 4-1.

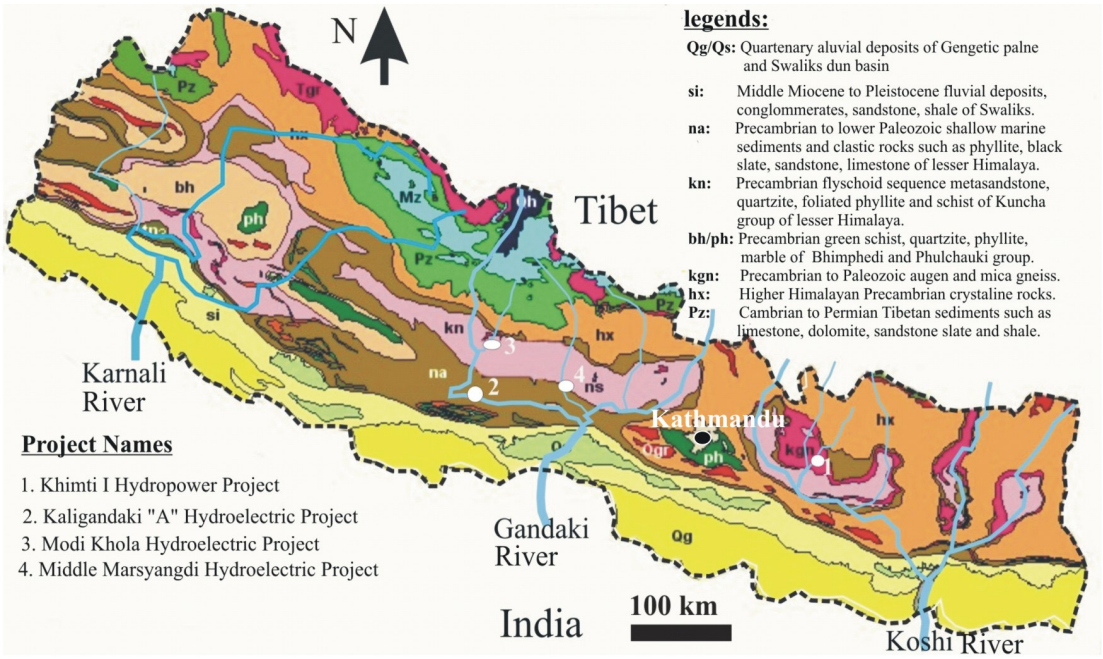

Figure 4-1. Location of the four selected project cases in Nepal Himalaya. (The project locations and the three major river systems are added by the author on the geological map of Nepal prepared by Department of Mines and Geology given in Galay et al, 2001).

This chapter particularly aims to describe the engineering geological conditions of the project cases, to evaluate predicted and actual rock mass conditions and to discuss the effect of rock mass quality deviation. A review of the level of pre-construction phase engineering geological investigations carried out for these projects is made. The pre-construction phase engineering geological investigations required for future tunnel projects in Nepal are also discussed. Project reports, various unpublished project data and information on pre-construction and construction phases (see Table 1-1) as well as the author's own experience have been used as main basis for the review. Characterizations of the rock mass are made based on laboratory testing and analyses conducted by the author during his PhD research.

4.2 ROCK MASS CLASSIFICATION SYSTEM USED FOR THE CASES

Rock mass classification systems are used extensively to quantitatively describe the quality of rock mass in underground excavations in Nepal Himalaya both during planning and implementation phases. Basically, the Barton's Q-system and the Bieniawski's RMR-system (discussed in Appendix A) are the most widely used rock mass classification systems in the country. These two methods were and are being extensively used at Khimti, Modi and Middle Marsyangdi projects to quantitatively de-

scribe the quality of rock mass and also to design tunnel rock support during pre-construction and construction phases. The use of these methods for the Kaligandaki project was more limited to pre-construction phase rock mass quality evaluation and rock support predictions. During construction, the use of classification system for deciding tunnel rock support was found difficult due to high squeezing pressure and presence of very weak rock mass along the whole headrace tunnel alignment (Panthi and Gauro, 2001). The GSI-system was applied at Kaligandaki for estimating the rock mass strength and deformability properties by back analysis since these properties were needed for the design of final concrete lining (NEA, 2002b).

It is generally accepted that rock mass classification systems are important tools for monitoring, recording and comparing predicted and actual rock mass conditions. To allow for homogeneous review, analysis and comparison, the rock mass along the four tunnels are divided into classes as shown in Table 4-1 based on Q and RMR values. The relationships published by Bieniawaski (1989) and Barton (1995) between Q and RMR systems have been used for the classification.

Table 4-1. Rock mass classes used for comparison of the four tunnel projects.

$RMR \approx 9 \times \ln Q + 44$ (Bieniawaski, 1989) $RMR = 15 \times \log Q + 50$ (Barton, 1995)

Descriptions		Range of Q-values		Range of RMR-values	
Rock Class	Quality descriptions	Minimum	Maximum	Minimum	Maximum
Class 1	Very good to excellent	100	1000	85	100
Class 2	Good	10	100	65	85
Class 3	Fair to good	4	10	56	65
Class 4	Poor	1	4	44	56
Class 5	Very poor	0.1	1	35	44
Class 6	Extremely poor	0.01	0.1	20	35
Class 7	Exceptionally poor	0.001	0.01	5	20

It is important to mention here that the rock mass classification systems for designing tunnel rock support during construction have been adopted cautiously, and have been based supplemented by additional inputs from observation and engineering judgment of the real ground conditions.

4.3 BRIEF DESCRIPTIONS OF THE CASES

As discussed in Chapter 1, most of the major rivers originating from the high and snow covered Himalaya have considerable potential in hydropower generation. This means that many underground powerhouse caverns and tunnels are likely to be built in the future in Nepal. However, there are many challenges in tunnelling with high degree of uncertainty and risk posed by the complex geological setup of the Himalaya. Therefore, describing the engineering geological conditions and tunnel instability in the selected four tunnel cases is an important aspect of this research.

4.3.1 Khimti I hydropower project

The Khimti I hydropower project is located in the lesser Himalayan region about 100 kilometers east of Kathmandu, see Figure 4-1. The Civil Construction Consortium (CCC), a consortium between Statkraft Anlegg of Norway (now NCC) and Himal Hydro of Nepal carried out the construction work of this project on a turn key basis. The construction work was completed in 2000 and since than the project has been in commercial operation. The project is owned by Himal Power Limited (HPL) and is the first privately invested and owned hydropower projects in Nepal under the BOOT concept. The project has an installed capacity of 60 MW and generates approximately 350 GWh electrical energy annually. The Khimti I is a high head scheme with a design discharge of 10.75 m³/s and a gross head of 684 meters. The total tunnel length of the waterway is approximately 10 kilometers (CCC, 2002), see Figure 4-2.

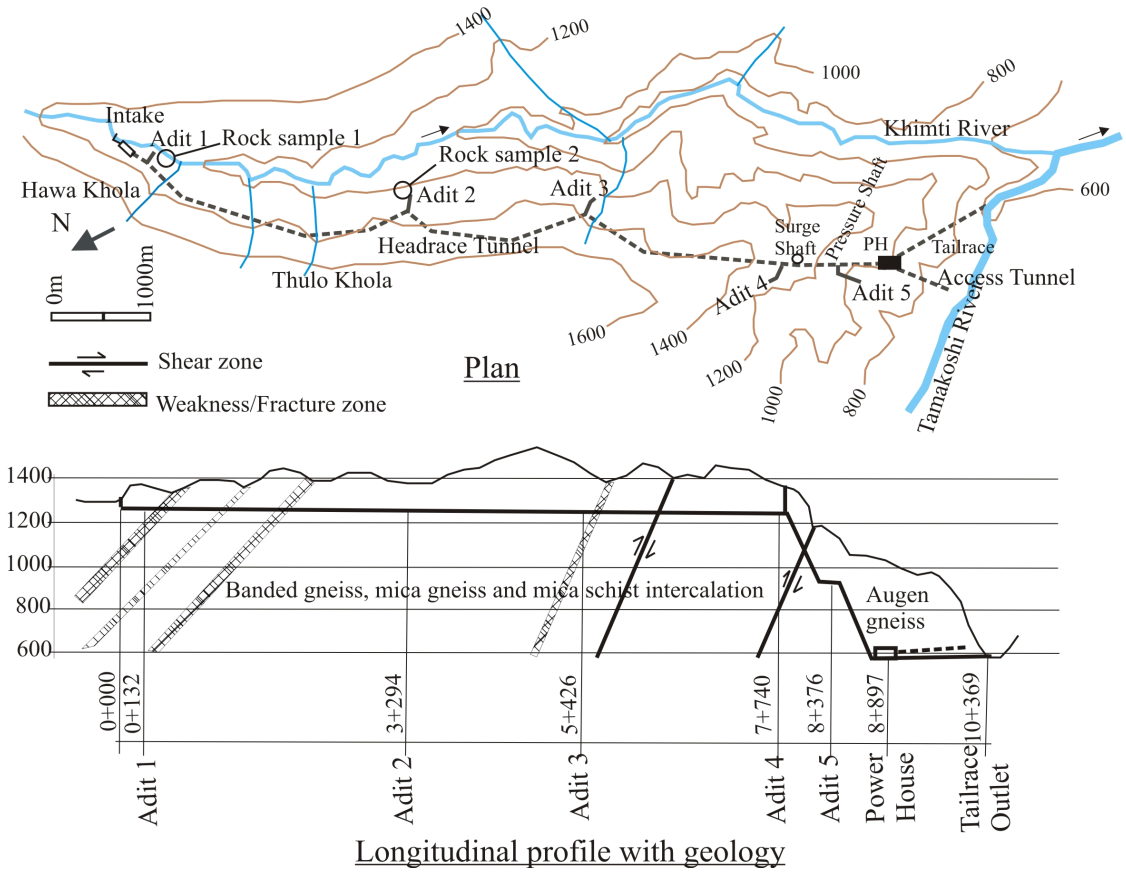

Figure 4-2. Project topography and longitudinal profile with geological description of the Khimti I hydropower project.

As shown in Figure 4-2, the Khimti headrace tunnel is a pressurized tunnel with maximum and minimum static water head of 4 bars and 1.1 bars at its downstream and upstream end respectively. The headrace tunnel is approximately 7.9 kilometers long with inverted D-shape and 14 square meters in cross-section. Except first downstream end of 418 meters with full reinforced concrete lining, the tunnel is built based on Norwegian

tunnelling principles and is unlined or shotcrete supported. Modern support means such as pre- and post-grouting, steel fiber shotcrete, spiling and rock-bolts have been used as temporary and final tunnel rock support.

4.3.1.1 Project geology

Geologically, the project lies in the crystalline Tamakoshi gneiss complex of the lesser Himalaya. Structurally, the area is bounded or surrounded by a major fault system of the Himalaya called "the Main Central Thrust (MCT)", see Figures 4-1 and 4-3. As indicated in these Figures, the rocks in the project area are mainly comprised by banded granite gneiss and augen mica gneiss. These gneisses have been subjected to frequent intercalation and shearing with chlorite and talcose mica schist.

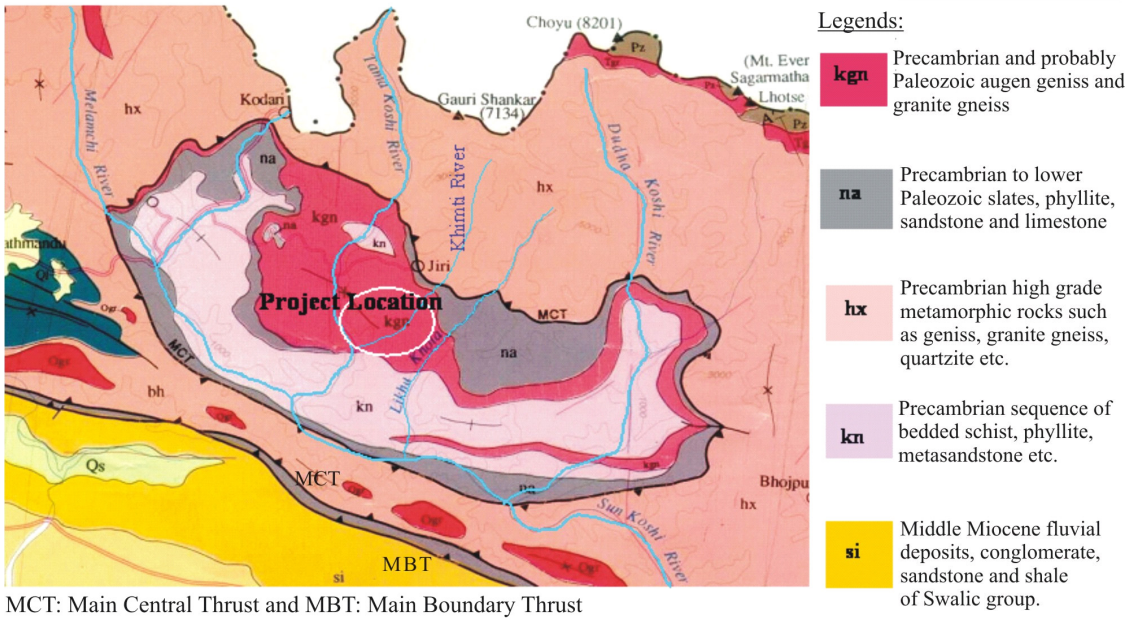

Figure 4-3. Geological environment of the Khimti I hydropower project.

This intercalation is most frequent, with an interval of approximately 5-10 meters at the downstream end of the headrace tunnel, whereas at the upstream stretch the interval is longer and banded gneiss and augen gneiss are more fractured and open-jointed (Panthi and Nilsen, 2005a). The foliation planes are generally striking Northeast – Southwest and dipping towards Northwest, see Figure 4-4. Since the project area is bounded by the Main Central Thrust (MCT) the rock mass along the headrace tunnel is highly jointed, sheared, deeply weathered and deformed. The geology along the headrace tunnel is also influenced by several minor faults and weakness zones represented by very weak sheared schist and crushed zones, see Figure 4-2.

4.3.1.2 Rock mass conditions

The planning phase investigations and predictions of the rock mass conditions along the headrace tunnel and as a whole of the Khimti project were rather poor, see Table 4-3. The Design Basis Memorandum (HPL, 1995), which was the main guideline used by the contractor for detail design of the project, stated that most of the tunnel length would be in sound rocks. Exceptions were described to be the construction adits, the initial section close to the intake, the downstream end of the headrace tunnel and some weakness zones, where the tunnel was predicted to be in weathered rock and lining might be needed. Accordingly, the estimated rock support requirement was much too low with no measures for water leakage control. Huge deviations were found on the rock mass quality and rock support requirement during construction, see Section 4.4.

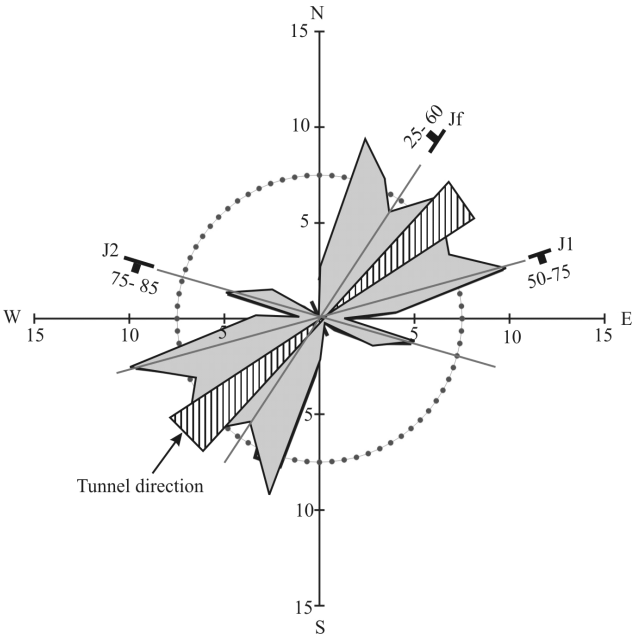

Figure 4-4. Orientations of main joint sets and Khimti headrace tunnel.

As shown by Figure 4-4, three major joint sets with frequent random joints were observed along the tunnel alignment during excavation. The general strikes of the main foliation joints (J_f) were found varying from N15^o to 60^{o}E. As can be seen in the Figure, this is not very favorable relatively to the headrace tunnel alignment, which also is oriented in Northeast / Southwest direction. The foliation joints are mostly dipping towards Northwest with a varying dip angle of 50 to 60 degrees at the Southern part of the tunnel (adit 4 area), and this trend changes gradually making the dip angle more flat with almost 25 degrees at its Northern part (adit 1). The joint set number one (J_1) is oriented with almost the same strike direction as the foliation joints and is very close to parallel to the tunnel alignment but dipping opposite to the foliation joints (dip angle 50 to 75 degrees towards Southeast). Joint set number two (J_2) is oriented in Northwest Southeast direction with very steep dip angle (70 to 85 degrees) towards Southwest.

With respect to joint filling and alteration, most of the discontinuities at the Southern section of the headrace tunnel (downstream from Adit 3) are filled with clay and bands of chlorite and talcose schist and have been characterized as impermeable with respect to water leakage. In contrast, the discontinuities present at the Northern section of the headrace tunnel are either open or filled with coarse grained permeable silt materials. The intercalation effect of mica schist is also present there, but at greater intervals. In this northern section several open joints with aperture up to 10 cm have been observed during tunnelling. The degree of weathering along the tunnel alignment also varies greatly and is classified as medium to highly weathered according to ISRM (1978b). In some sections the degree of weathering was so deep that decomposed and highly sheared organic clay was found in the tunnel. Especially the tunnel section 500 meters downstream from Adit 2 (between chainage 3450 – 3900) was deeply weathered (CCC, 2002). The valley side slope in this stretch of the tunnel is flatter (about 25 degrees) and the rock cover is slightly more than 100 meters, see Figure 4-2.

4.3.1.3 Tunnel stability problems

In the Khimti headrace tunnel, there were two areas of major tunnel stability problems. The first one was related to tunnel collapse caused by the presence of thick bands of highly weathered and sheared chlorite and talcose mica schist intercalated between relatively strong but fractured gneiss that allowed ground water to move into such bands, see Figure 4-5 left. The second one was related to large leakage through open and permeable joints present in the gneisses and loss of valuable water from the tunnel during operation, see Figure 4-5 right. Such possible loss of water also may cause tunnel instability due to weakening and disintegration of weak rock mass strata consisting of mica schist.

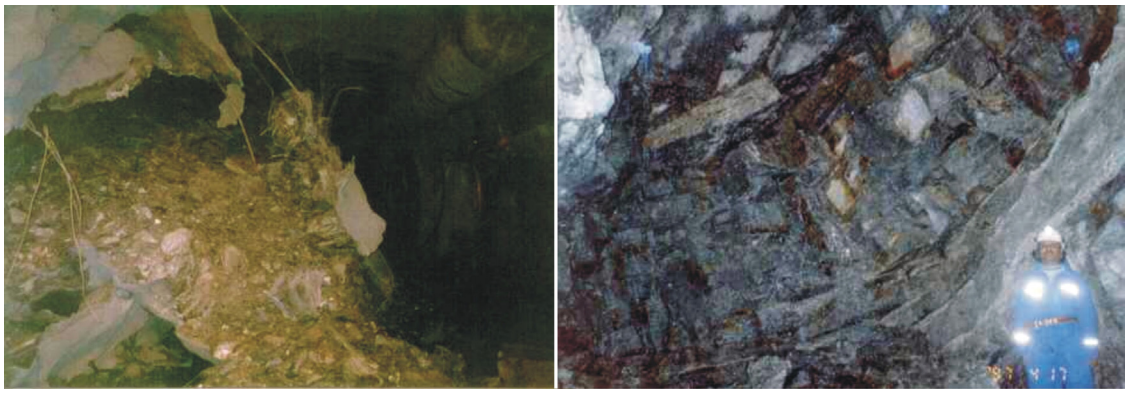

Figure 4-5. Tunnel instability situations; tunnel collapse after application of tunnel support (left) and open and permeable joints within gneiss (right).

In addition to these two types of instability, minor tunnel squeezing was also observed in some locations of the headrace tunnel where chlorite and talcose mica schist was dominant. Such areas were mainly observed at relatively high overburden (above 200 meters) areas upstream and downstream of adit 3 and at the weakness zones (below

Hawa Khola, see Figure 4-2) downstream of adit 1 with relatively low overburden (approximately 100 meters).

4.3.2 Kaligandaki "A" hydroelectric project

The Kaligandaki "A" hydroelectric project is also located in the lesser Himalaya but in the western part of Nepal about 200 km West of Kathmandu, see Figure 4-1. This project is the largest run-of-river scheme ever constructed in Nepal. It has an installed capacity of 144 MW and is capable of generating 842 GWh electrical energy annually. To generate this energy, the project utilizes a 45 kilometers long loop of a relatively flat bedded Kaligandaki river in a shortcut. The water is diverted by a concrete gravity dam with a height of 43 meters and is conveyed through three settling basins, approximately 6 km long headrace tunnel, a vertical penstock tunnel of 97 meters height and a semi underground powerhouse, see Figure 4-6. The excavated cross section of the headrace tunnel is approximately 60 square meters with horse-shoe shape and 8.4 meters diameter. The final fully concrete lined shape of the headrace tunnel is circular and has 7.4 meters diameter. The project is a medium head scheme (net head 115 meters) with a rated design discharge of 141 m^3/s (NEA, 2004a).

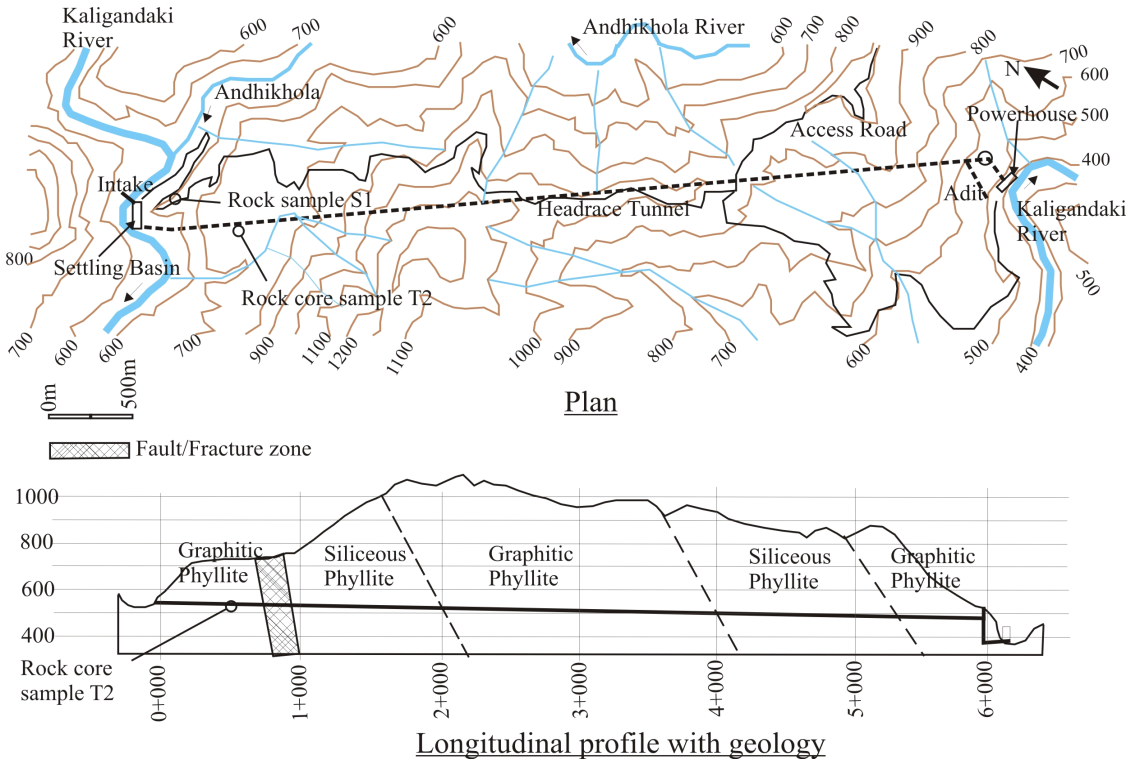

Figure 4-6. Project topography and longitudinal profile with geological description of the Kaligandaki "A" hydroelectric project.

The civil work contract was awarded to Impregilo SpA of Italy in January 1997 and the project was completed in the summer of 2002. This project is owned by Nepal Electricity Authority (NEA), an undertaking of the His Majesty's the Government of Nepal.

4.3.2.1 Project geology

Geologically, the project area lies in the lesser Himalayan highly deformed rock formation and is relatively close to the Main Boundary Thrust (MBT). The rocks in the project area are mainly comprised of Precambrian to lower Paleozoic shallow marine sediments. Rocks in this group are mainly represented by dark slate, graphitic and siliceous phyllite and siliceous dolomite, see Figure 4-7. As shown in Figure 4-6, the headrace tunnel of the project mostly passes through highly deformed graphitic phyllite, siliceous phyllite and phyllitic slate intercalation. The first few hundred meters upstream section of the headrace tunnel consists of highly fractured and weathered siliceous dolomite in intercalation with graphitic phyllite. The mineral composition of these rocks and the degree of metamorphism vary considerably (NEA, 1992).

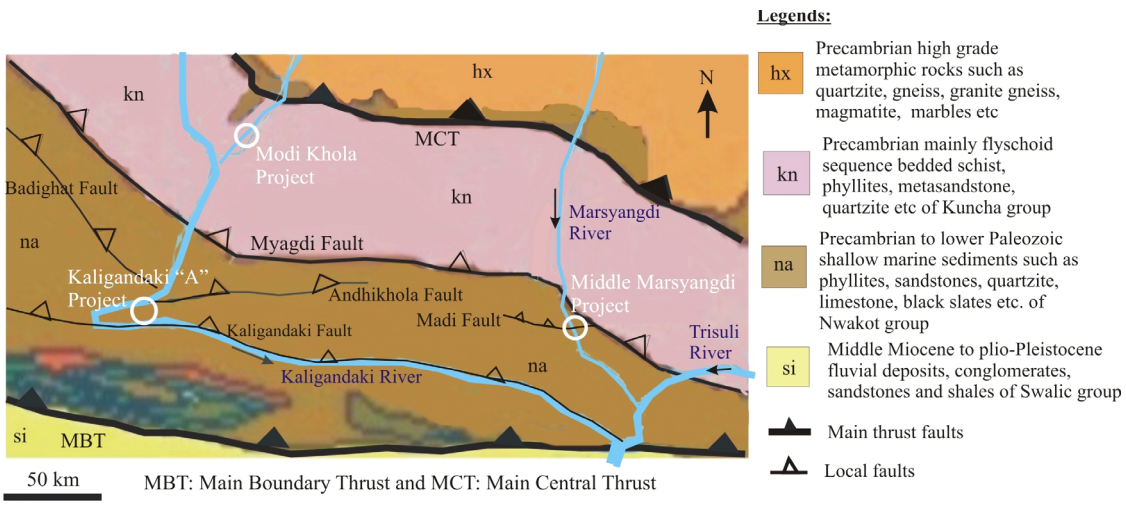

Figure 4-7. Geological environment of Kaligandaki "A", Modi Khola and Middle Marsyangdi projects. The local faults are added based on feasibility reports of respective projects.

Figure 4-7 indicates that the project area is very close to several local faults, namely Badighat, Andhikhola and Kaligandaki faults. The splay (branch) of Andhikhola fault crosses the headrace tunnel at about 700 meters from the intake, see Figure 4-6.

4.3.2.2 Rock mass conditions

The planning phase investigation and predictions of the rock mass conditions along the headrace tunnel indicated that the upstream one kilometer section of the headrace tunnel would meet small fault and weakness zones. It was predicted that the tunnel might be subjected to heavy squeezing at this upstream section. The rest of the tunnel alignment was assumed to have fair to good quality rock mass except for some sections with

highly sheared and deformed rock mass. It is interesting to note that most of the engineering geological investigations conducted during pre-construction phases were at headworks and powerhouse areas, see Table 4-3. The geological investigations along the headrace tunnel alignment were limited only to engineering geological mapping and petrographic and mineralogical analysis of a limited number of rock samples (NEA 1992). Accordingly, the estimated temporary tunnel rock support was also relatively small in comparison to as built, see Section 4.4. However, the rock mass observed during excavation was found to be very weak, highly sheared, thinly foliated and intensely folded, see Figure 4-8.

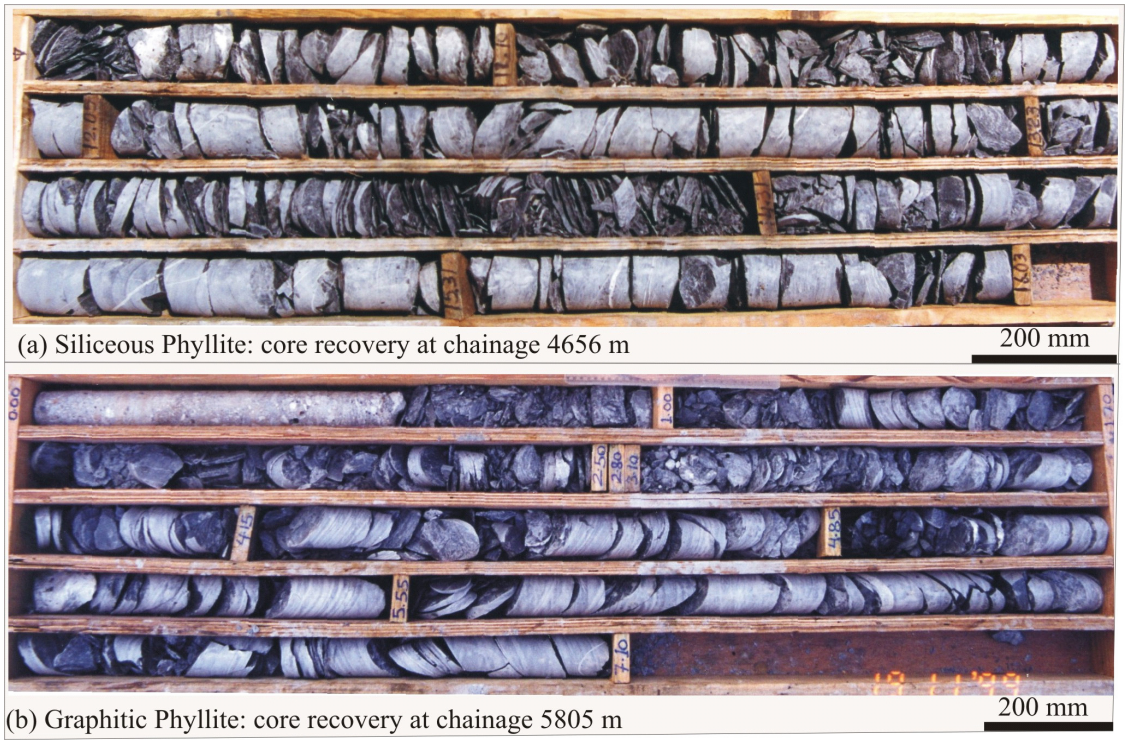

Figure 4-8. Example of core recovery during excavation indicating the quality of rock mass along the headrace tunnel of Kaligandaki (Photo: Impregilo SpA, 1999).

As Figure 4-8 indicates, the RQD values of the cored samples are close to zero and during tunnel mapping it was always found to be less than 15 to 20 percent, except for some sections of the upstream end of the headrace tunnel where intercalation of bands of dolomite was present (NEA, 2002b). An almost similar situation was observed by a SINTEF team who carried out hydraulic fracturing and dilatometer tests in test adit at downstream end of the headrace tunnel in 1993. Out of the five exploratory drill holes totaling 78 meters drilled, only three samples having length greater than 15 centimeters were recovered (SINTEF, 1993).

As a result of active tectonic movement and presence of several local faults, the rock mass in the area has been subjected to shearing, folding and faulting. In addition, the maximum elevation difference between the top of the hill and the tunnel alignment is as

much as 600 meters and more than 80 percent of the tunnel alignment has overburden exceeding 200 meters, see Figure 4-6. During tunnel excavation, most of the rock mass along the tunnel alignment was found to be of poor to extremely poor quality and demanding heavy rock support. As a result, considerable deviations between predicted and actual rock mass quality were witnessed and the need for tunnel rock support exceeded considerably what was predicted at planning, see Section 4.4.

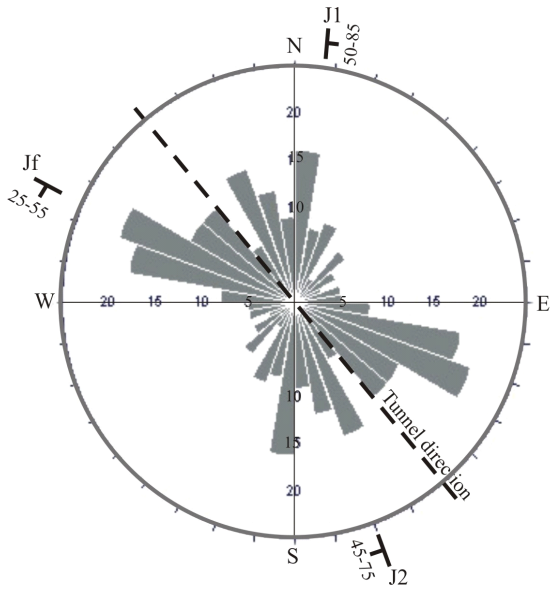

Figure 4.9. Orientation of main joint sets and Kaligandaki "A" headrace tunnel.

As Figure 4-9 indicates, the orientation and dip of the joints sets are highly scattered due to extreme folding and shearing giving no distinct joint system except for foliation joints. In general, the foliation joints are oriented with strike varying from N85^{o} to140^{o}E with dip angles between 25-55 degrees towards Southwest. The alteration and weathering of discontinuity surfaces are considerable and the joints are filled with highly sheared clay, quartz and calcite veins.

4.3.2.3 Tunnel stability problems

There were two major factors that played significant roles for stability at the Kaligandaki headrace tunnel. The first was related to very weak and thinly foliated phyllite with high degree of strength anisotropy that led to considerable reduction on the self supporting capability of the rock mass. As a result of this, frequent small to medium scale tunnel collapses occurred. The second one was related to tunnel squeezing. Due to high overburden stress and the presence of weak phyllite rock mass, especially graphitic phyllite with low compressive strength, the tunnel squeezed severely at many locations, see Figure 4-10. For more discussion of this, reference is made to Chapter 6.

Figure 4-10. Collapse due to strength and stress anisotropy (left) and cracks formed by high squeezing pressure (right) (Photo: Impregilo SpA, 1999).

4.3.3 Modi Khola hydroelectric project

The Modi Khola hydroelectric project is located on the right bank of Modi river, a tributary of the Kaligandaki river, also to the West of Kathmandu, see Figure 4-1. The project has an installed capacity of 14.7 MW and is capable of generating 91 GWh electrical energy annually. The project is a run-of-river scheme with a medium head of approximately 67 meters and a design discharge of 27.5 m^3/s (NEA, 2000a). This project is also owned by the Nepal Electricity Authority (NEA).

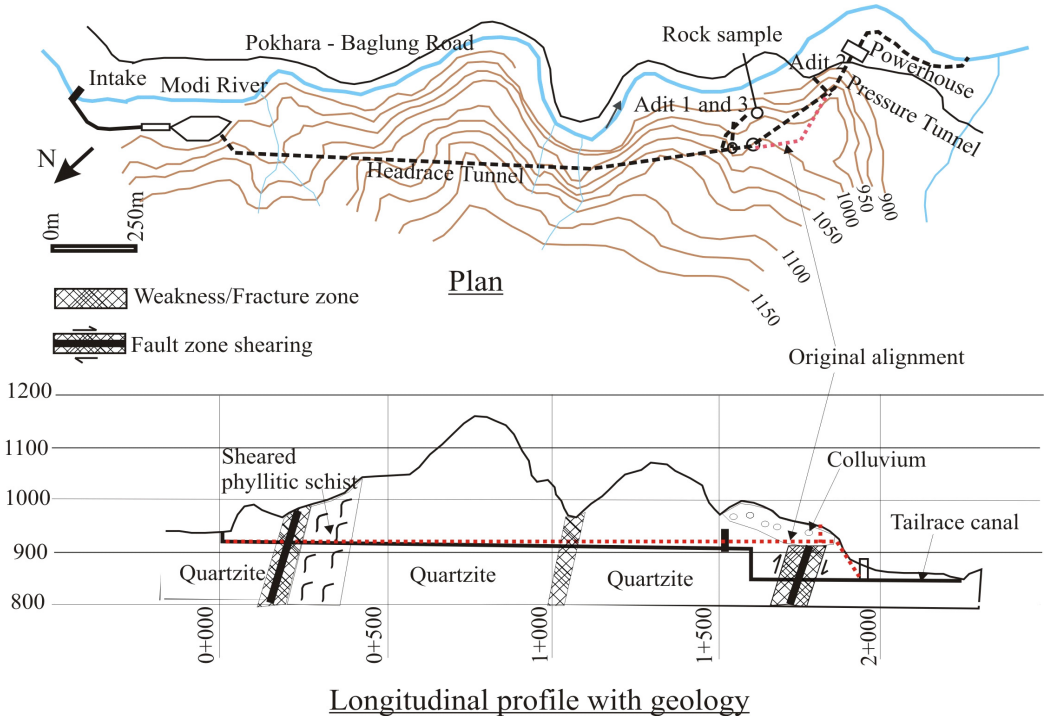

Figure 4-11. Project topography and longitudinal profile with geological description of the Modi Khola hydroelectric project.

As Figure 4-11 indicates, the project has a total underground waterway length of approximately 2 kilometers. The tunnel system includes a 1,503 meters long headrace tunnel with a cross section of approximately 15 square meters, a 50 meters deep vertical pressure shaft and a 430 meters long pressure tunnel. The construction work for the underground section of the project was carried out by a joint venture of Himal Hydro, Nepal and Statkraft Anlegg (now NCC), Norway and was completed in 2001.

4.3.3.1 Project geology

Geologically, the project area lies in the Precambrian sequence of the lesser Himalayan meta-sedimentary rock formations, see Figures 4-1 and 4-7, and is relatively close to the Main Central Thrust (MCT). The area is influenced by many local faults and the rock mass is fractured and deformed. The bedrock along the underground waterways of this project is mainly dominated by fractured but abrasive greenish quartzite (Himal Hydro, 2000). As shown in Figure 4-11, the first 500 meter upstream section of the headrace tunnel passes through a fracture zone consisting of highly fractured quartzite and highly sheared and deformed phyllitic green schist. Similarly, the pressure tunnel also crosses a major shear fault consisting of decomposed quartzite fragments and highly sheared green schist (Poudel et al., 1998).

4.3.3.2 Rock mass conditions

For this medium scale project, the planning phase engineering geological investigations were mostly limited to surface mapping and a few hundred meters of probe-hole drilling at the surge tank and powerhouse areas, see Table 4-3. With the well exposed rock along the Modi river, the rock mass conditions along the headrace tunnel alignment were not difficult to predict. As a result, the deviation between predicted and actual rock mass condition was not found to be significantly high, see Section 4.4.

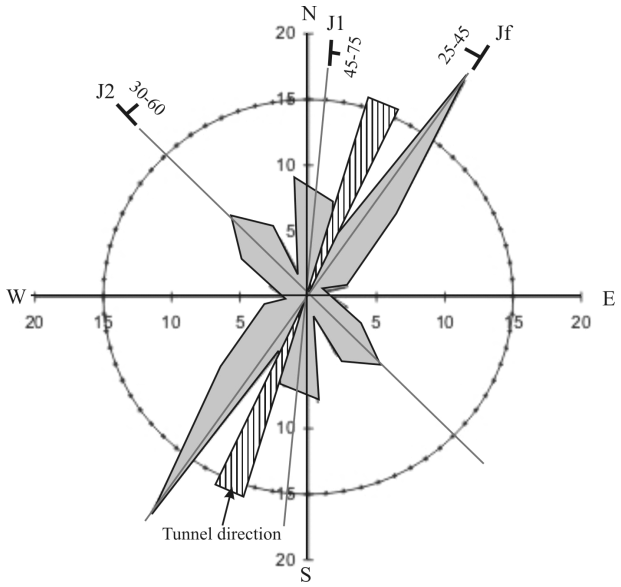

Figure 4-12. Orientation of main joint sets and Modi headrace tunnel.

The rock mass conditions observed during tunnel excavation along the headrace tunnel and vertical shaft were found to be of good quality greenish to white quartzite, excluding the tunnel section passing through weakness and fracture zones as indicated in Figure 4-11.

As can be seen in Figure 4-12, the tunnel direction is not favorably oriented relatively to foliation joints (J_f) and joint set number one (J_1). Three sets of joints and occasional random joints were encountered along the tunnel alignment. The discontinuities were found to be slightly to moderately weathered with some degree of alteration. Most of the discontinuities were smooth undulating to smooth planner. Mostly these discontinuities were filled with a thin layer of silty clay fragments. In addition, thin bands of decomposed green to dark grey mica schist were found intercalated within massive quartzite at some locations.

4.3.3.3 Tunnel stability problems

During tunnel excavation, the pressure tunnel and the headrace tunnel had to cross weakness and fault zones. Severe tunnel instabilities related to rock squeezing and ground water inflow had occurred, where the pressure tunnel crossed a highly sheared fault zone (between chainage 1700 – 1800) as indicated in Figure 4-11. Otherwise, the excavation of the headrace tunnel and the vertical shaft went relatively smoothly with few surprises. However, frequent small scale wedge failures occurred at the headrace tunnel due to unfavorably oriented tunnel alignment and presence of more than two joint sets. The weakness zones located near the intake, at approximate chainage 1050 of the headrace tunnel as indicated in Figure 4-11, were crossed without major difficulties (Himal Hydro, 2000).

4.3.4 Middle Marsyangdi hydroelectric project

The Middle Marsyangdi hydroelectric project is also located in the western development region of Nepal, see Figure 4-1. The project is on the right bank of the Marsyangdi river, which is a major tributary of the Gnadaki river system. The project is a medium sized run-of-river scheme with planned installed capacity of 69 MW and will be capable of producing 380 GWh electrical energy annually. The project is a medium head scheme with a gross head of approximately 110 meters and a design discharge of 80 m^3/s (NEA, 1998).

This project is also owned by Nepal Electricity Authority (NEA). The design and construction supervision of the project is being carried out by a joint venture of FICHTNER, Germany and Statkraft Grøner (Sweco Grøner), Norway. The civil works contract was awarded to the joint venture of Dywidag, Dragados and CWE (DDC). The construction work of the project started in early 2002 and is still going on.

The project consists of a 68 meters high dam, three underground settling chambers, a 5,300 meters long headrace tunnel, a surge shaft, various construction adits, a 385 meters long penstock and a semi-underground powerhouse, see Figure 4-13.

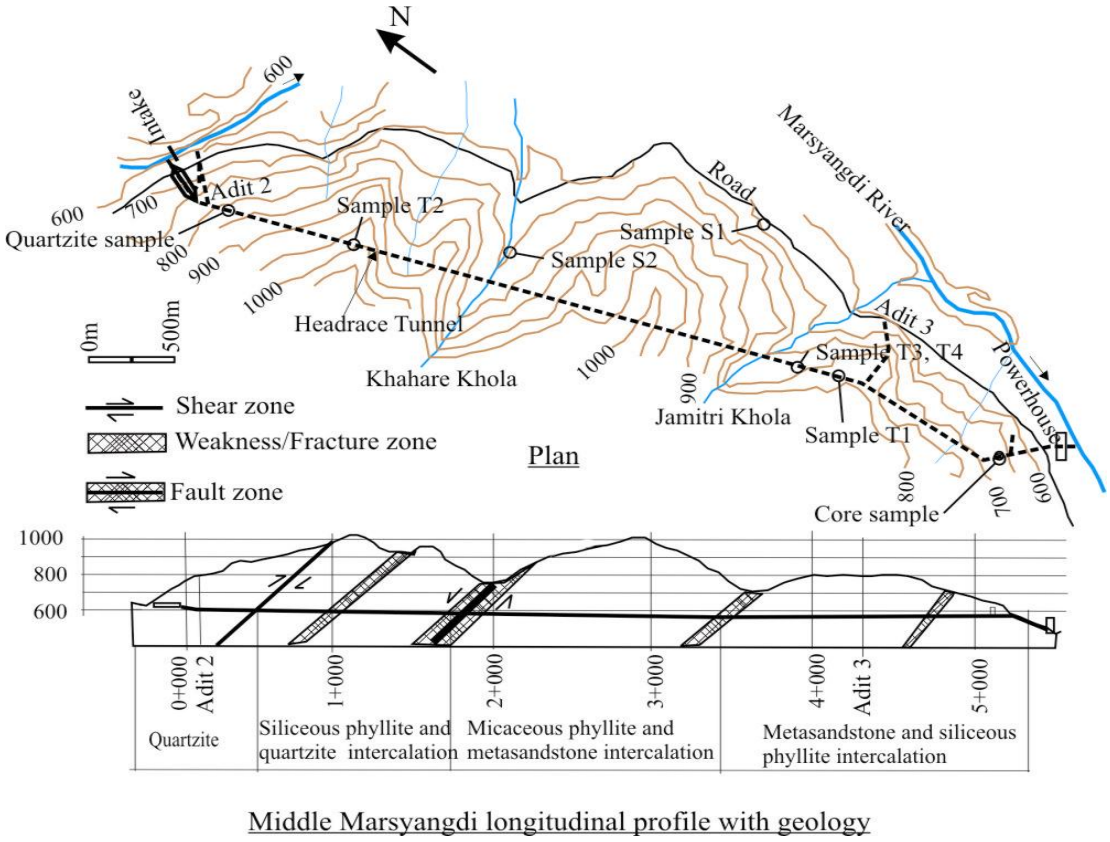

Figure 4-13. Project topography and longitudinal profile with geological description of the Middle Marsyangdi hydroelectric project.

The headrace tunnel is designed with 6.4 meters excavation diameter and 34 square meters cross-section (horse-shoe shaped). To reduce the friction loss, the tunnel will be fully concrete lined and have a circular shape with 5.4 meters in diameter.

4.3.4.1 Project geology

Geologically, this project also lies in the same regional geological formation as of Kaligandaki "A", i.e. the lesser Himalayan meta-sedimentary rocks, see Figures 4-1 and 4-7. The main rock types of the project are quartzite, phyllite and metasandstone. As shown in Figure 4-13, the upstream short section of the headrace tunnel, intake, underground settling basins and diversion facilities of the project are situated in quartzitic rocks. The remaining downstream section of headrace tunnel and other underground structures are mostly passing through micaceous and siliceous phyllite and metasandstone intercalations. The headrace tunnel is crossing some weakness and fault zones, including a major fault system called Madi fault that passes along the Khahare Khola.

4.3.4.2 Rock mass conditions

The planning phase engineering geological investigations carried out for this project were more comprehensive than for the other projects discussed above, see Table 4-3. In addition to surface mapping of the headrace tunnel alignment, a test adit of approximately 120 meters length was excavated at Bhote Odar (near by adit 3) during the updated feasibility study. The aim was to carry out in-situ dilatometer and flat jack tests and also to evaluate the condition of the phyllitic rock mass expected to be representative of the planned headrace tunnel alignment. With respect to surface mapping, many rock exposures were found along the access road and along the many local streams on the valley slope, see Figure 4-13. Moreover, approximately 1100 meters of 2D-geoelectrical profiling was conducted along the headrace tunnel with particular focus on the Khahare Khola (NEA, 2000b).

In general, the rock mass along the headrace tunnel is highly fractured, tectonically disturbed and sheared. The first approximately 500 meters from the intake passes through fractured and thinly foliated quartzite. During excavation, the quartzite was found to be of fair to good quality according to the Q and RMR- systems. After that, siliceous phyllite in intercalation with thin bands (less than 1 meter) of quartzite and highly sheared micaceous phyllite are predominant until the headrace tunnel reaches Khahare Khola fault (Madi fault). The micaceous phyllite bands are highly sheared, micro-folded and deformed and of extremely poor quality, see Figure 4-14. The bands of siliceous phyllite and quartzite are fresher but also fractured and of poor to fair quality.

Figure 4-14. Rock mass conditions at Middle Marsyangdi: thinly foliated and fracture quartzite (left) and siliceous phyllite in intercalation with thin bands of metasandstone and micaceous phyllite (right).

As shown in Figure 4-13, between Khahare Khola and Jamitri Khola, the rock mass is predicted to be dominated by highly sheared, micro-folded and deformed micaceous phyllite with intercalation of thin bands of fractured metasandstone and siliceous phyllite. Downstream from Jamitri Khola, metasandstone and siliceous phyllite with occasional bands of highly sheared micaceous phyllite have been encountered.

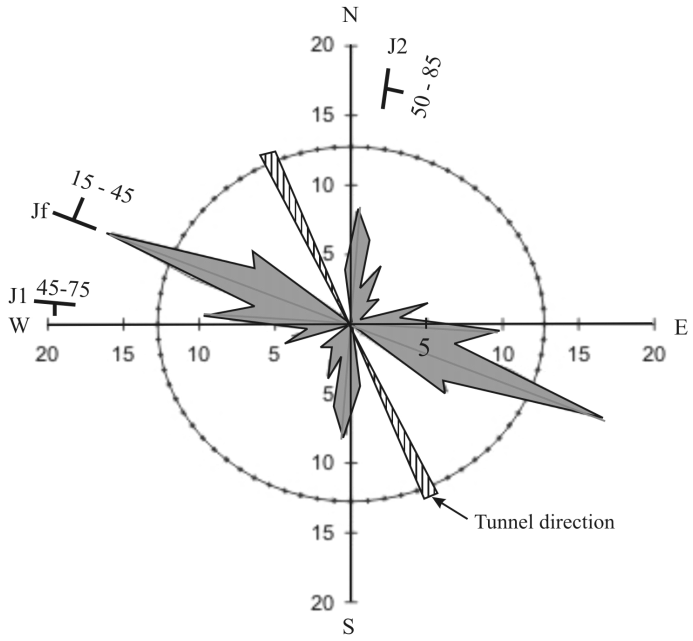

Figure 4-15. Orientation of the main joint sets and Middle Marsyangdi headrace tunnel.

As shown in Figure 4-15, the headrace tunnel is aligned favorably relatively to the major three joint sets. Three main joint sets with random joints occur in the rock mass, especially in quartzite. Since the micaceous phyllite is highly sheared and micro-folded, the phyllitic rock mass in most of the headrace tunnel has foliation as the main joint set. With respect to the character of discontinuities, the joint surfaces in the quartzite rock mass are smooth planar to rough undulating with an aperture of less than 5 mm and are mostly filled with silty clay fragments. The joint surfaces in the phyllite rock mass are slickensided and have undulating surface due to high deformation, micro-folding and shearing.

4.3.4.3 Tunnel stability problems

The already excavated tunnel sections (approximately 1100 meters upstream section, approximately 500 meters upstream from adit 3 and section between adit 3 and surge tank) have not faced significant tunnel instability. However, minor instability caused by intercalation effect has been observed quite frequently, even though very careful excavation with rounds not exceeding 1.5 meters has been applied. Very low strength bands of micaceous phyllite within stronger siliceous phyllite and metasandstone have been experienced to have very low self supporting capability. As soon as bands of micaceous phyllite have been encountered at the crown of the tunnel, immediate failures have occurred in such locations. In addition, minor scale tunnel deformation has been recorded at the contact zone between quartzite and phyllite. It is expected that major tunnel stability problems will occur at the section between Jamitri and Khahare Kholas, see Fig-

ure 4-13, where the rock mass is dominated by micaceous phyllite. At this stretch of the headrace tunnel the overburden is relatively high (up to approximately 400 meters), and the weak micaceous phyllite is expected not be able to sustain the overburden pressure. Therefore, rock squeezing problems are expected to occur. Moreover, the tunnel has to cross the Madi fault, which is likely to represent a challenge in tunnel excavation.

4.4 PREDICTED VERSUS ACTUAL ROCK MASS CONDITION

Due to the complexity of the rock mass, it can hardly be avoided to end up with some degree of discrepancy between the predicted and actual rock mass conditions and between the predicted and actual rock support. However, this deviation should be within acceptable limits so that the tunnel cost and construction time are kept well under control (Panthi and Nilsen, 2005b). As discussed above and in Section 4.5, the levels of pre-construction phase engineering geological investigations at the respective four tunnel cases are quite different. In the following, these differences will be discussed and an attempt will be made to analyze and explain the main discrepancies between predicted and as-built conditions.

4.4.1 Rock mass quality deviation

The characterization of rock mass quality is very essential during pre-construction phase geological investigations, since it is the key for estimating required tunnel rock support and construction time. Without estimating needed quantity of rock support and construction time it is not possible to evaluate the economic viability of a tunnel project during planning.

As shown in Figure 4-16, there are considerable differences between predicted and actual rock mass quality for the respective four tunnel cases. It is interesting to note that the discrepancy for Modi headrace tunnel seems slightly smaller than for the other three projects, even though the difference for class 4 is quite significant. This may be explained by the fact that this tunnel is located in very steep topography (see Figure 4-11) where the rock mass is well exposed.

The headrace tunnel of Middle Marsyangdi also seems to have relatively small discrepancy. However, it is too early to come to a final conclusion for Middle Marsyangdi since the comparison is based on only approximately 50 percent tunnel (2,461 meters) that has been completed by August 2004. Given the high level of pre-construction phase investigations and the good rock exposure represented by the road that passes almost parallel to the tunnel alignment, the relatively small discrepancy is, however, not very surprising.

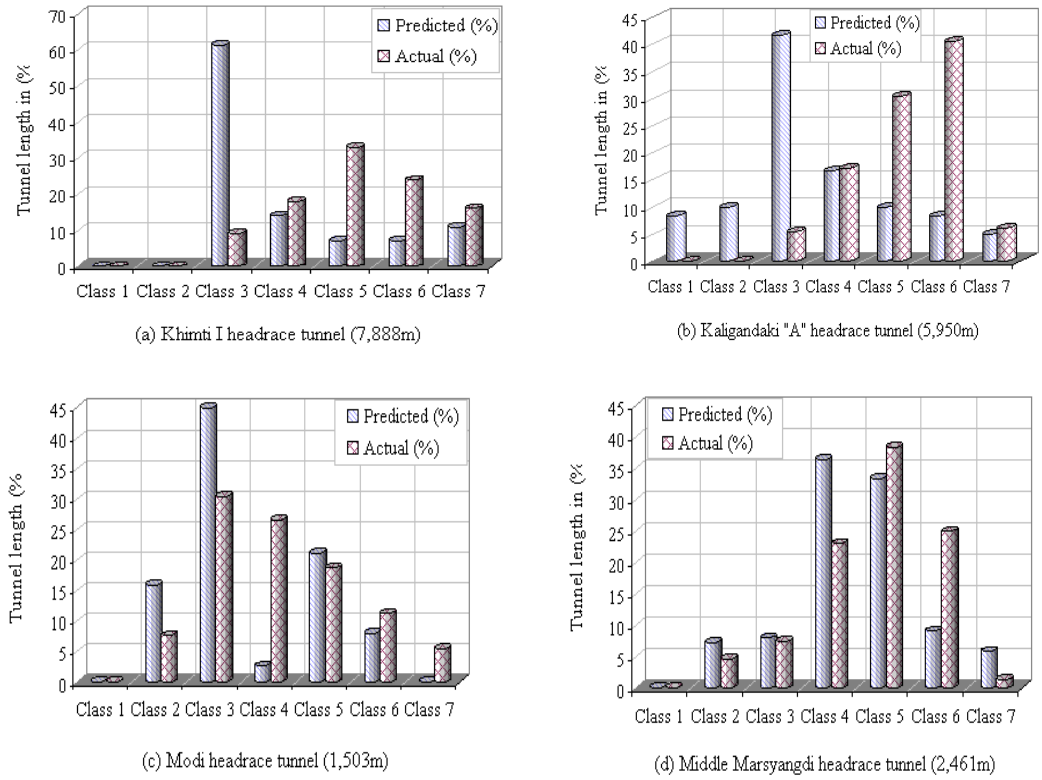

Figure 4-16. Predicted and actual rock mass conditions of the four tunnel cases (rock class rating according to Table 4-1).

In contrast to Modi and Middle Marsyangdi, the discrepancies for Khimti I and Kaligandaki "A" headrace tunnels are found to be unexpectedly high. As a result of large discrepancy between predicted and actual rock mass quality, the differences between predicted and applied tunnel rock support are also large for these two projects.

4.4.2 Discrepancy in tunnel rock support

Only the Khimti I and the Kaligandaki "A" headrace tunnels are considered in the following for the comparison between predicted and as-built tunnel rock support. The main reason for this is that the Modi headrace tunnel had insignificant deviation, whereas the final rock support data for Middle Marsyangdi headrace tunnel are not yet available due to undergoing construction. As can be seen in Table 4-2, the greatest discrepancy has been experienced for rock bolts and shotcrete for both Khimti and Kaligandaki headrace tunnels. The discrepancy concerning concrete for the Kaligandaki "A" headrace tunnel is rather small. This is logical since the whole headrace tunnel was planned with a final concrete lining at planning phase to improve tunnel smoothness and to reduce friction loss.

Table 4-2 confirms the findings of Figure 4-16a and 4-16b; that the actual rock mass quality was much poorer than it was predicted during planning.

Table 4-2. Predicted versus actual tunnel rock support per meter tunnel excavation.

Type of rock support	Unit	Khimti I headrace tunnel		Kaligandaki "A" headrace tunnel	
		Predicted	Actual	Predicted	Actual
Rock bolting	no./m	1.5	6.9	5.9	6.6
Shotcreting	m^3/m	0.1	1.4	3.2	9.7
Steel ribs	no./m	NA	NA	0.3	0.4
Concrete lining	m^3/m	0.3	0.6	17.0	15.3

Note: NA means not applicable. At Khimti, no steel ribs were used as tunnel support.

As shown in Figure 4-17, the coefficient of variation between predicted and actual rock support is significant for these two tunnels. Not surprisingly, the large increase in rock support requirement resulted in considerable increase in tunnel construction costs and time.

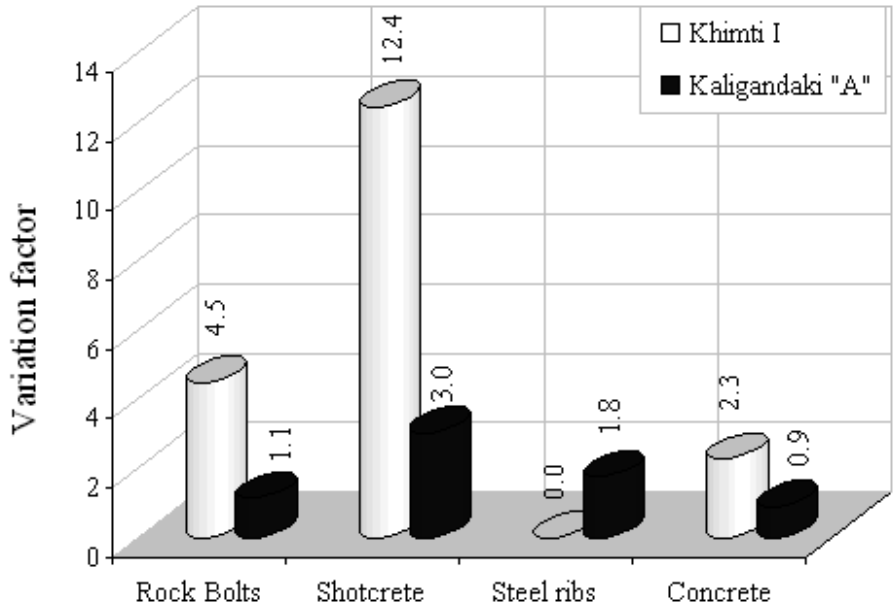

Figure 4-17. Variation factors between predicted and actual tunnel rock support for Khimti I and Kaligandaki "A" headrace tunnels (variation factor is the ratio between applied and predicted tunnel rock support).

Due to the considerable deviation in rock mass quality and increase in tunnel rock support for the headrace tunnels of Khimti I and Kaligandaki "A", the final rock support cost was approximately five and two times, respectively, of what was estimated during planning. The discrepancies also had considerable impact on the construction time. For instance, the Kaligandaki "A" project was delayed by almost one and half years and for the Khimti headrace tunnel the contractor was forced to open a new construction adit (adit 3) and accelerate the excavation work to meet the construction target set in the turn-key project contract.

4.5 SUMMARY OF PRE-CONSTRUCTION PHASE INVESTIGATIONS

A summary of the pre-construction phase engineering geological investigations carried out for the respective four tunnel cases is shown in Table 4-3.

Table 4-3.Pre-construction phases engineering geological investigations of tunnel cases.

Projects / Descriptions		Khimti I	Kali-Gandaki "A"	Modi Khola	Middle Marsyangdi	Remarks if any
Feasibility stage	Desk studies based on existing geological information and pre-feasibility study	yes	yes	yes	yes	Very limited geological investigations were done during pre-feasibility.
	Aerial photo studies and interpretations	yes	yes	yes	yes	Available in scale 1:50,000 and 1:125,000.
	Surface geological mapping	yes	yes	yes	yes	Of the project area.
	Refraction seismics	yes	yes	yes	yes	At specified locations. Mostly at surge tank and headwork areas.
	Electrical resistivity	-	-	-	yes	At the suspected Madi fault area and intake.
	Core drilling	yes	yes	yes	yes	Focused mainly on intake, surge shaft and powerhouse area.
	Laboratory testing	yes	yes	-	yes	Involving rock strength parameters and mineralogical testing.
Design and contract stage	Review of the feasibility study investigations	yes	yes	-	yes	
	Detailed surface mapping	yes	yes	-	yes	Few days of surface investigation at Khimti project.
	Additional core drilling	-	yes	-	yes	Concentrated to intake and powerhouse areas
	Additional geophysical investigations	-	-	-	yes	Electrical resistivity survey on the suspected fault zone areas.
	Exploratory test adit excavation	-	yes	-	yes	
	Rock stress measurements	-	yes	-	yes	Hydraulic fracturing test at Kaligandaki and small jack test at Middle Marsyangdi.
	Laboratory testing	-	yes	-	yes	Further investigation, including dilatometer test.

Table 4-3 illustrates the variations in level and types of engineering geological investigations for the respective tunnel cases. As can be seen, the level of investigations carried out at Khimti and Modi Khola projects is relatively low and much lower than for

the other two projects. Moreover, most of the geophysical investigations, core drilling and laboratory testing for the projects were for headworks, surge tank and powerhouse areas, except for Middle Marsyangdi project. This indicates that the rock mass quality assessment, stability analysis and rock support quantity predictions were mainly based on desk studies, aerial photo interpretation and surface geological mapping. As can be seen from the table, the main reasons for high discrepancy between predicted and actual rock mass conditions and predicted and as-built rock support discussed in Section 4-4 may be insufficient pre-construction phase engineering geological investigations.

The author would like to emphasize that the main goal of any pre-construction phase engineering geological site investigations for underground hydropower projects is to characterize the rock mass conditions of the project site and to locate tunnels and other underground openings in as good rock quality as possible. In addition, the location of tunnel projects is not always based on the geological conditions alone. In many cases, topographic as well as hydrological and hydraulic conditions play an important role in fixing the inlet and outlet of hydropower tunnels.

Moreover, the geological conditions of the site of interest may vary widely as each site will have its own characteristics, and thus there is no standard investigation procedure that will be the only correct way in all cases. However, by thorough investigation, design and planning, it is in theory always possible to find the best alternative and the most cost effective solution (Nilsen and Palmstrøm, 2000). Optimization and risk assessment is therefore a key issue not only for reducing the unforeseen risk and uncertainty associated with the tunnel stability, but also for reducing the project cost and construction time.

4.6 EVALUATION ON INVESTIGATION APPROACH

It is logical that large discrepancies in rock mass quality have a direct effect on the project cost and time. Such discrepancy gives room for claims from the contractor since he will need additional resources to deal with more difficult conditions and to accomplish additional amount of rock support needed to stabilize the ground conditions. As a result, the client and contractor may end up with unnecessary contractual debate and dispute. Consequently, the completion of the project within stipulated construction schedule may not be possible with considerable delay as the result. Such unpleasant situation may also lead to additional economic loss due to revenue lost by delayed start of the project operation and by increased interest in investment during construction.

The cases discussed in this chapter are therefore important lessons for the planning of future projects. As a planning tool for new projects, assessment of the cost implication that may be caused by changes in rock mass conditions will be very useful. Based on the evaluation and analysis of actual excavation and rock support costs of the cases described in this chapter, such a tool has been developed and is presented in Figure 4-18. This figure defines the relative rock support cost for different rock mass classes as de-

scribed in Table 4-1 and illustrates the cost impact caused by change in rock mass quality. As can be seen, as soon as the rock mass quality decreases (higher class), there is a dramatic increase in the rock support cost. For example, for very poor (class 5) and exceptionally poor (class 7) rock mass quality, the rock support cost can be more than 250 and 350 percent respectively of the excavation cost. It needs to be noted that Figure 4-18 does not include additional cost due to additional time required for excavation and rock support installation, and not the cost related to pre and post grouting used at Khimti I headrace tunnel.

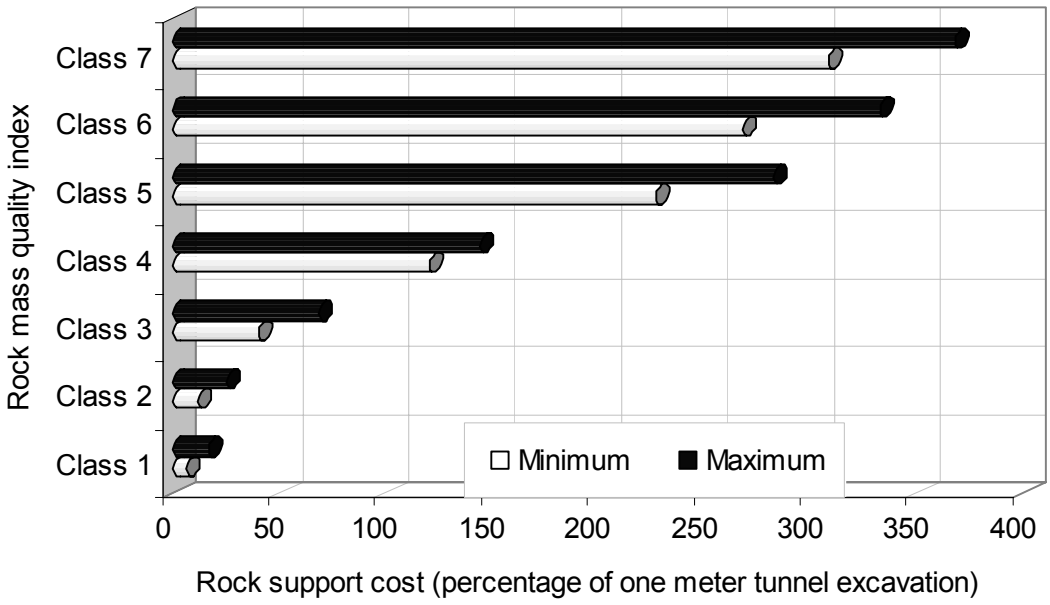

Figure 4-18. Approximate rock support cost for different rock mass classes (minimum and maximum for small and large section tunnels, respectively).

Since every tunnel project is unique, the rock mass conditions and the required level of pre-construction phase engineering geological investigation will vary from one project to another. However, all tunnelling projects require engineering geological investigations giving a satisfactory knowledge about the geology of the area of concern.

Based on the cases reviewed above, it is assumed that the large discrepancies between the predicted and actual rock mass conditions have been caused by three main factors; 1) poor or insufficient engineering geological investigations and testing carried out during planning and design phases, 2) complex geological conditions with deep weathering making it difficult to predict actual rock mass conditions by surface mapping and 3) insufficient level of experience in tunnelling and lack of engineering geological investigation technique suitable for Himalayan geological conditions. In author's opinion, if a thorough, stepwise procedure of geological investigations as shown in principle in Figure 4-19 is followed, it should be possible to increase the level of accuracy in evalu-

ating and predicting the quality of rock mass. The additional investigation cost normally will be small compared to what would be saved during construction phases.

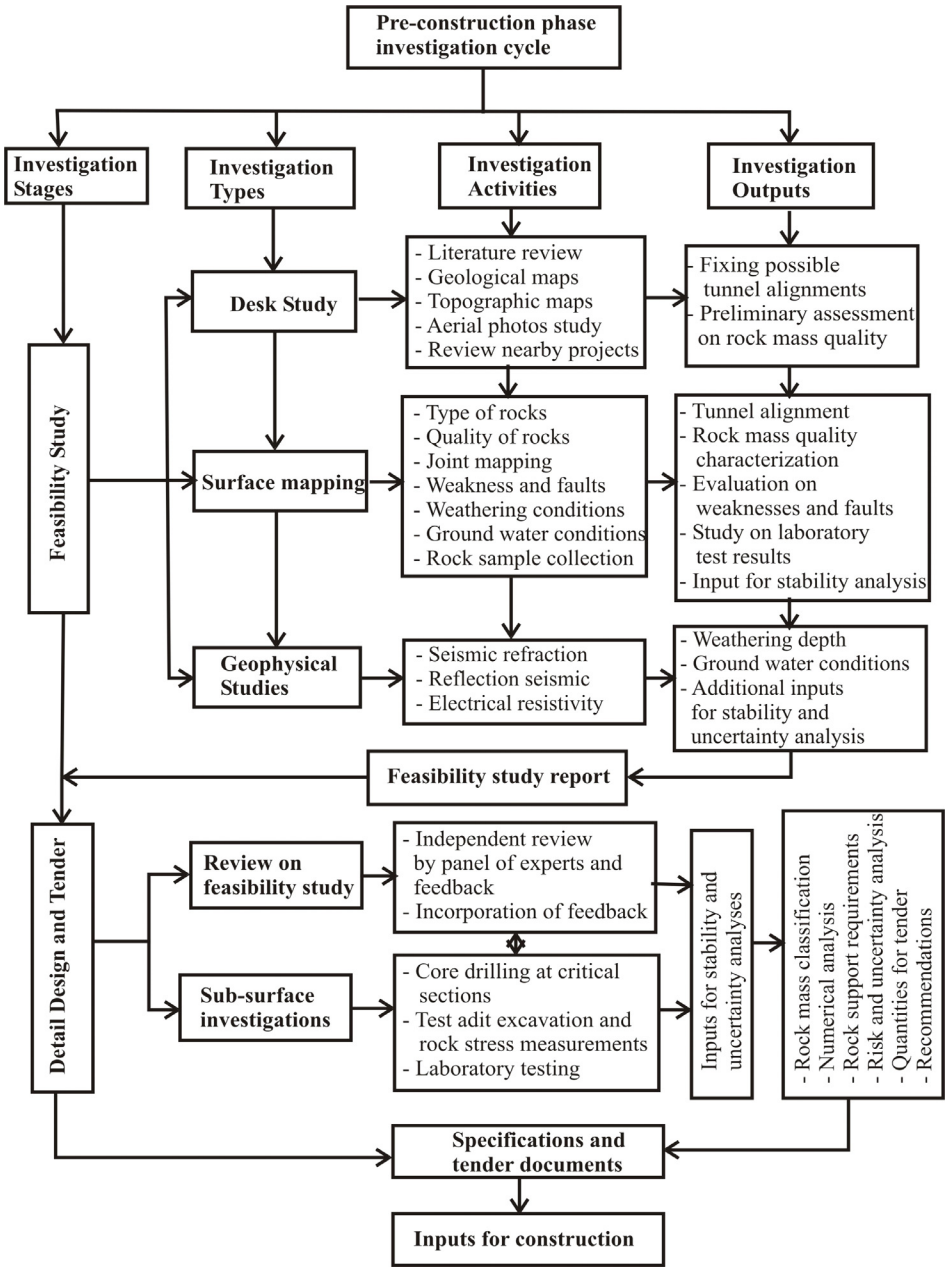

Figure 4-19. Recommended pre-construction phase engineering geological investigations for underground projects in the Himalaya.

It should be emphasized that engineering geological mapping, instrumentations and following up during excavation are crucial for a successful completion of any tunnel project. Even when very detailed investigations have been carried out from the surface, this is of great importance.

4.7 SUPPLEMENTARY TESTING FOR ROCK CHARACTERIZATION

As discussed in Section 4-3 to 4-6, the four tunnel cases used in this research are located in various rock types with different degrees of tunnel stability problems. The most important factors that influence on tunnel stability are the engineering characteristics of the rock mass and external factors such as induced rock stress and ground water. The first factor, the engineering characteristics of the rock mass, is mainly governed by intact rock properties and the conditions of discontinuities. To characterize the intact rock properties of main rock types of the respective cases, the author collected representative rock samples from the tunnel cases during field vists and conducted laboratory testing at the laboratory of the Department of geology and mineral resources engineering. The tests give valuable input for describing and characterizing the mechanical characteristics of intact rock. Details of the samples are given in Table 4-4.

Table 4-4. Rock samples collected for laboratory testing.

Project names	Rock types	Location/reference	Means of collection
Khimti I hydropower project	Banded gneiss	Headrace tunnel, adit 1 spoil tip, see Figure 4-2	Rock pieces from tunnel excavation.
	Augen mica gneiss	Headrace tunnel, adit 2 spoil tip, see Figure 4-2	
Kaligandaki "A" hydroelectric project	Siliceous dolomite	Cores from desander back slope, see Figure 4-6	Cores by probe drilling and small rock pieces from surface.
	Graphitic phyllite	Headrace tunnel sample T2 and surface S1, see Figure 4-6	
Modi Khola hydroelectric project	Quartzite	Headrace tunnel, adit 1 spoil tip, see Figure 4-11	Rock pieces from tunnel excavation.
Middle Marsyangdi hydroelectric project	Quartzite	Headrace tunnel from adit 2, see Figure 4-13	Rock pieces from tunnel excavation. T2 only for slake durability test.
	Siliceous phyllite	Headrace tunnel, sample T1 and T2, see Figure 4-13	
	Metasandstone	Surge tank, see Figure 4-13	Cores by probe drilling.
	Micaceous phyllite	Headrace tunnel from adit 3, samples T3 and T4 plus samples from surface S1 and S2, see Figure 4-13	These samples were used only for slake-durability test.

It is emphasized here that the laboratory testing was limited due to economic constraints, and the results therefore should be taken as indicative and not as a complete characterization of intact rocks of the cases. Moreover, finding undisturbed samples that could be cored in sufficient length for the weaker rocks such as graphitic phyllite, sheared mica gneiss and micaceous phyllite was very difficult.

4.7.1 Laboratory tests and results

The laboratory testing program included mineralogical analysis, intact rock strength and deformability, intact rock strength anisotropy, drillability and slake durability properties. Most of the tests were conducted in accordance with the ISRM standards. For drillability properties, which are not defined in the ISRM standard, the standard developed by the Norwegian University of Science and Technology was used.

4.7.1.1 Mineralogical analysis

The first step to characterize the rock mass is to identify the mineralogical composition, texture and fabric (ISRM, 1978a). The best way to carry out such analysis is to conduct thin section analysis and X-ray diffraction (XRD) investigation. Since the aim of the test here was to verify approximate mineralogical composition of the rocks only XRD investigation was conducted. The results are given in Table 4-5.

Table 4-5. Mineral composition of rocks of the project cases.

Rock type	Mineral composition in (%)								
	Quartz	Plagioclase	k-feldspar	Mica	Chlorite	Pyrite	Calcite	Dolomite	Muscovite
Banded gneiss	40	30	16	10	-	4	-	-	-
Augen mica gneiss	37	23	-	37	-	2	1	-	-
Siliceous dolomite	35	24	-	9	6	3	-	23	-
Graphitic phyllite*	20	-	-	35	7	3	-	-	8
Quartzite	99	1	-	-	-	-	-	-	-
Siliceous phyllite, T1 and T2	22	47	-	18	6	3	-	-	-
Metasandstone	53	36	-	7	3	1	-	-	-
Micaceous phyllite, S1, S2 and T3	45	-	-	42	6	-	-	-	-

Note: the locations are according to Table 4-4. *Remaining material is mainly carbonate.

The engineering properties of the rock mass vary considerably in the Himalaya, even within the same rock category, since the rock mass in the region are subjected to active tectonic movement and weathering effects. Especially, the rocks that are composed of clay and sheet minerals such as chlorite and mica have reduced strength and deformability properties and have considerable strength anisotropy. In addition, such conditions have significant impact on drilling and blasting. The mineralogical analysis therefore helps for evaluating the mechanical character of the rock mass, particularly concerning strength anisotropy, flakiness, slaking and weathering properties.

4.7.1.2 Strength and deformability properties

The most significant characteristics of the rock mass are their strength and deformability properties. Due to practical reasons in-situ measurement of rock mass strength and deformability properties is difficult. The normal way to estimate rock mass strength is therefore based on the relationship between rock mass strength and intact rock strength of small specimens as discussed in Chapter 3.

ISRM (1979b) defines 50mm as a reference diameter for laboratory testing of strength and deformability properties for intact rock material. The procedure suggested by ISRM (1979b) has been applied for intact rock strength, elasticity modulus, density, porosity and sonic velocity tests. The mean values and their standard deviations are shown in Table 4-6 and the details are given in Table B-1 (Appendix B).

Table 4-6. Density, porosity, strength and deformability properties of the rocks of the cases.

Rock type	Density (gm/cm^3)	Porosity (%)		Longitudinal sonic velocity (km/sec)		Poisson's ratio (ν)	Young's modulus, E (GPa)		UCS, σ_{c50} (MPa)	
	mean	mean	St. dev.	mean	St. dev.	mean	mean	St. dev.	mean	St. dev.
Banded gneiss	2.68	0.87	0.1	3.7	0.3	0.12	25	3	50	5
Augen mica gneiss	2.73	0.76	0.1	3.0	0.2	0.10	22	4	38	6
Siliceous dolomite	2.82	0.44	0.1	4.3	0.5	0.12	57	6	165	31
Graphitic phyllite	2.78	0.45	0.03	3.8	0.4	0.10	27	2	39	5
Modi quartzite	2.60	0.22	0.04	5.7	0.02	0.13	83	2	221	23
Marsyangdi quartzite	2.62	0.30	0.04	4.7	0.05	0.10	46	3	190	16
Siliceous phyllite	2.86	0.77	0.1	3.7	0.15	0.05	14	1	39	5
Metasandstone	2.65	0.81	0.2	3.8	0.23	0.14	46	14	73	39

Note: the locations are according to Table 4-4.

The results for sonic velocity, uniaxial compressive strength, Young's modulus and Poisson's ratio in Table 4-6 are for saturated conditions. The dimensions of the rock specimens used for testing are given in Table B-1 (Appendix B).

As shown in Table 4-6, the mechanical characteristics of the different rocks vary greatly. The Poisson's ratios of the rock specimens have been found to be relatively low. The uniaxial compressive strength (UCS) results for banded and augen mica gneiss of Khimti project are also relatively low. The main reason for this may be the high degree of schistocity and presence of considerable amount of mica, see Table 4-5. Based on ISRM (1978b) the rocks can be classified into categories as shown in Table 4-7.

Table 4-7. Rock characterization according to compressive strength based on ISRM (1978b).

Classification	Field identification	Approximate range of UCS, σ_{c50} (MPa)	Rock types of the project cases
Extremely weak	Indented by thumbnail.	0.25 – 1	Highly sheared fault gouge*.
Very weak	Crumbles under firm blows by geological hammer, can be pilled by pocket knife.	1 – 5	Extremely weak mud stone and shale.
Weak	Can be pilled by pocket knife with difficulty.	5 - 25	Highly sheared slate, phyllite and schist**.
Medium strong	Can not be scraped by a pocket knife but can be fractured by single blow of geological hammer.	25 - 50	Micaceous phyllite**, siliceous phyllite, graphitic phyllite, and augen mica gneiss.
Strong	Requires more than one blows of geological hammer to fracture.	50 - 100	Banded gneiss and metasandstone.
Very strong	Requires many blows of geological hammer to fracture.	100 - 250	Siliceous dolomite and quartzite.
Extremely strong	Can only be chipped with geological hammer.	> 250	

Note: * based on field observation and ** based on field observation and point load test

It needs to be emphasized here that due to high degree of schistocity, the author has experienced difficulties to achieve cores of sufficient length for the testing of the rock samples, except for quartzite. Even getting more than three cores longer than 80 mm from each rock sample of approximately 15 kilograms became extremely difficult. The author also faced same difficulties in finding cores of sufficient length (longer than 80mm) from exploratory drilling for the Kaligandaki "A" and Middle Marsyangdi projects.

4.7.1.3 Strength anisotropy properties

Another important engineering characteristic of the rocks in the Himalaya is strength anisotropy caused by preferred orientations of mineral grains or directional stress history. The point load test was conducted both axially (perpendicular to foliation) and diametrically (parallel to foliation) in accordance with ISRM (ISRM, 1985) to identify the degree of strength anisotropy of the rock samples defined in Table 4-4. The mean values of the test results are given in Table 4-8.

As shown in Table 4-8, graphitic phyllite of Kaligandaki "A" classifies as highly anisotropic. Even though the average anisotropy index of augen mica gneiss of Khimti and siliceous phyllite of Middle Marsyangdi classify as moderately anisotropic, their high

ranges of standard deviation indicate that these rocks may also behave very highly anisotropically.

Table 4-8. Point load strength and strength anisotropy of the rocks of project cases.

Rock type	Diametrical point load strength, I_{s50} (MPa)		Axial point load strength, I_{sa50} (MPa)		Strength anisotropy index, I_a		Strength anisotropy class*
	Mean	St. dev.	Mean	St. dev.	Mean	St. dev.	
Banded gneiss	2.8	0.4	4.7	0.6	1.7	0.3	Moderate
Augen mica gneiss	2.2	0.9	4.1	0.9	1.9	1.1	Moderate to high
Siliceous dolomite	9.4	1.9	10.7	1.4	1.2	0.2	Slight
Graphitic phyllite	1.4	0.4	3.8	0.7	2.7	0.9	High
Modi quartzite	13.3	0.5	13.5	1.3	1.0	0.1	Isotropic
Marsyangdi quartzite	14.4	1.2	14.6	1.2	1.0	0.1	Isotropic
Siliceous phyllite	3.1	0.9	6.2	1.3	2.0	0.9	Moderate
Metasandstone	4.1	1.1	4.9	1.0	1.2	0.2	Slight

* Five strength anisotropy classes are defined in Chapter 3, Table 3-3

4.7.1.4 Drillability properties

In tunnelling, drillability is one of the key factors that may influence on the overall cost (Nilsen and Thidemann, 1993). At the same time, drillability properties can also be indicative measures for evaluating how deformable the rock mass is. The drillability testing carried out has been based on the standard procedures developed at the laboratory of the Norwegian University of Science and Technology (NTNU). The standard procedure for drillability testing including brittleness value (S_{20}), Siever's J-value (SJ), abrasion value (AV and AVS) is described in Dahl (2003).

Drillability testing has been conducted for the six rock types (see in Table 4-8, excluding dolomite and micaceous phyllite). A summary of the results of drilling rate index (DRI) and bit wear index (BWI) is shown in Figure 4-20. As can be seen, the correlation between these two parameters is relatively poor, but generally, the rocks having low drilling rate index (DRI) tend to have high bit wear index (BWI). The rocks having low DRI have high quartz content, causing the life of bit and cutter to be much lower than for those having higher DRI values.

This is a very important message, since it indicates on the abrasiveness properties of the rock mass. In principle, the rocks tested can be classified in three categories with respect to their abrasiveness. Highly abrasive rocks having BWI more than 40 and DRI less than 50, medium abrasive rocks having BWI between 20 to 40 and DRI between 50 to 60 and low abrasive rocks having BWI less than 20 and DRI above 60.

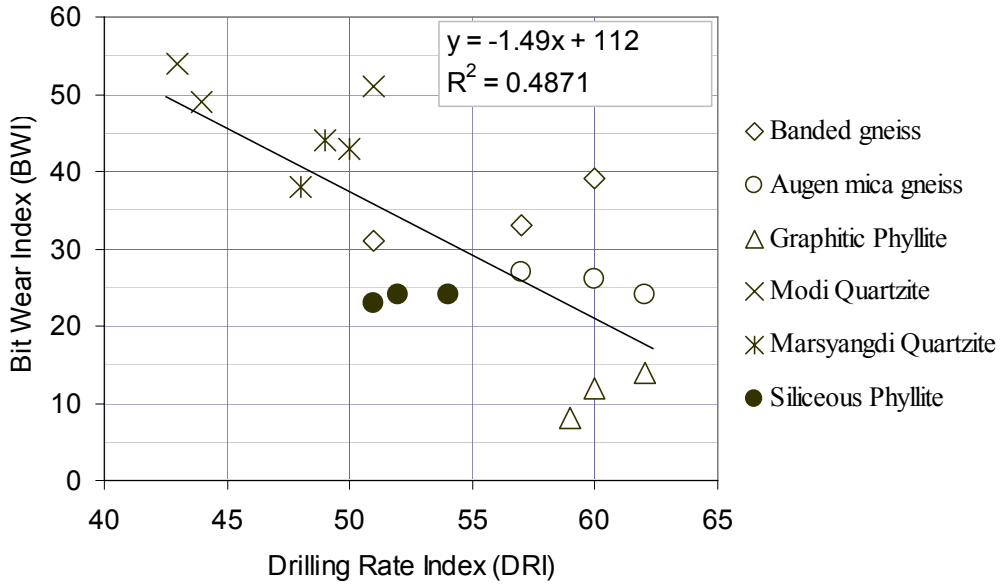

Figure 4-20. Correlation between drilling rate index (DRI) and bit wear index (BWI).

As can be seen in Figure 4-21, the highly abrasive rocks with high percentage of quartz have very low penetration rate in comparison to the rocks with high percentage of mica and low percentage of quartz. From this figure it can also be interpreted that high Siever's J-value means highly deformable rocks since they are mostly made of weak minerals such as chlorite and mica.

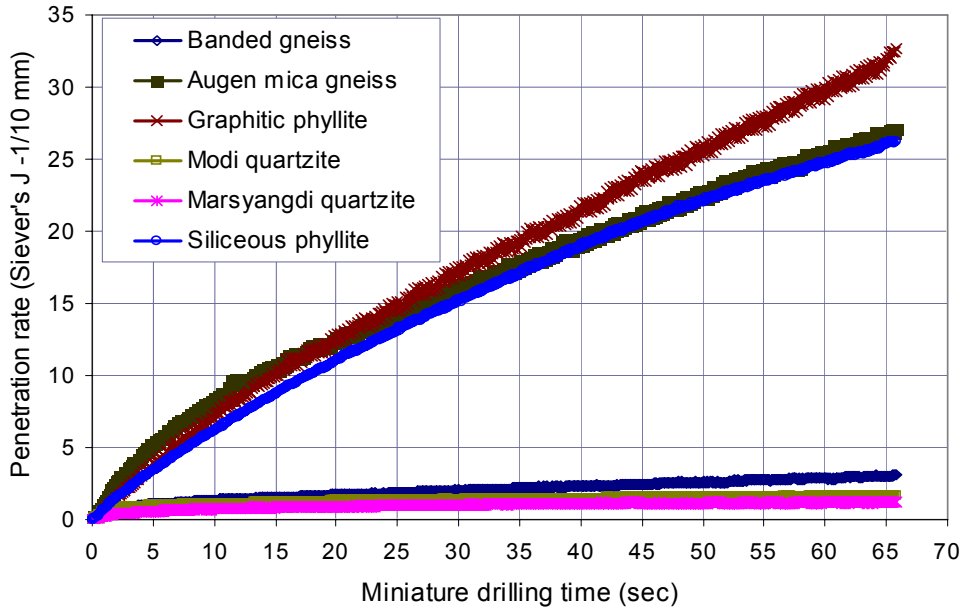

Figure 4-21. Miniature penetration rate with respect to miniature drilling time.

4.7.1.5 Slake durability properties

By definition, slaking is the deterioration, weakening and breakdown of a rock material when subjected to cycles of drying and wetting. As a result of shearing produced by volume change associated with wetting and drying, the fissile and micaceous rocks quickly loose their corners and become polished or slickensided and also develop concentric fractures (Goodman, 1993). The slaking durability at some rocks of sedimentary origin discussed in ISRM (1979a) is presented in Figure 4-22.

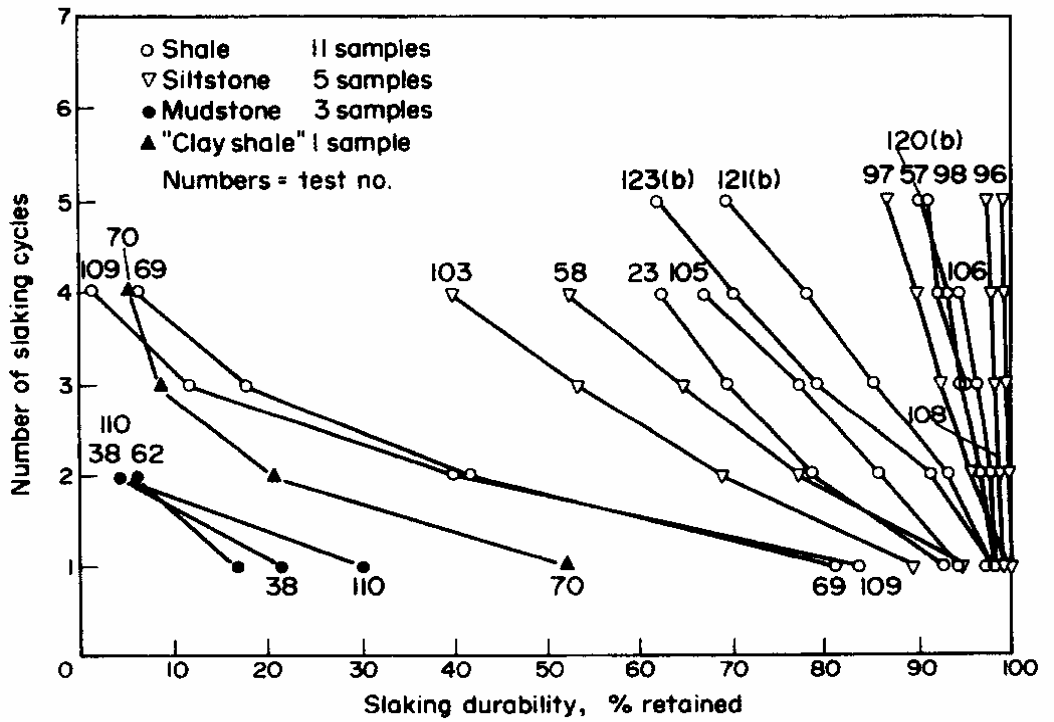

Figure 4-22. Influence of the number of slaking cycles on slake-durability (ISRM, 1979).

As can be seen in Figure 4-22, there is a considerable influence on slake-durability of the rocks by the number of slaking cycles. This suggests that rock mass subjected to long term drying and wetting during weathering is subjected to weakening of the mechanical properties. Thus, the slake durability test makes it possible to assess the resistance of rock material against weakening and disintegration when subjected to cycles of drying and wetting.

According to ISRM (1979a), the slake durability index is defined by two cycles of drying and wetting and is calculated as percentage ratio of final to initial dry sample mass as given by:

$$I_{d2} = \frac{C - D}{A - D} \times 100 \qquad (4\text{-}1)$$

Where; I_{d2} id the slake-durability index of second cycle, A is the mass of ten pieces of rock lumps (each weighing approximately 40 to 60 grams) after drying in an oven at 105°C for about 2 to 6 hours plus mass of apparatus drum, C is the mass of remaining rock lumps after two cycles of drying and rotation in slaking fluid (tap water at approximately 20°C) at 200 revolutions in 10 minutes plus mass of apparatus drum, and D is the mass of the clean apparatus drum.

The highly sheared and deformable rocks of the Himalaya such as siltstone, mudstone, shale, slate, phyllite, schist and mica gneiss, which largely are made of flaky minerals, are also likely to disintegrate and weather as soon as they are exposed to the cycles of drying and wetting. It is well known fact that the weathering and shearing effects are high in the Himalaya due to active monsoon, great temperature variations and active tectonic movement.

To find the slaking durability of the rock mass of the project cases, slake durability test was conducted in accordance to the procedure defined by ISRM. A slake durability testing apparatus, see Figure 4-23, was designed in accordance to ISRM (1979a) and manufactured at the mechanical workshop of the Norwegian University of Science and Technology (NTNU). The test samples, see Table 4-4, were from tunnel as well as surface of the respective cases.

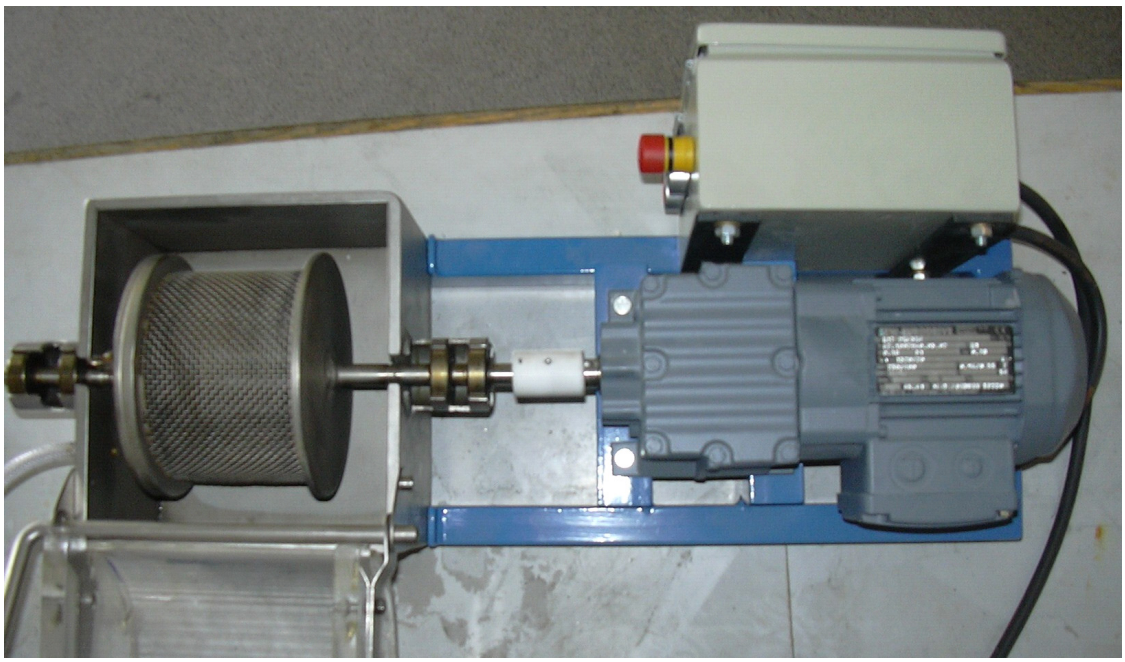

Figure 4-23. Slake durability testing apparatus designed based on ISRM (1979).

As previously described, most of the rock mass of the project cases are of metamorphic origin and thus have in principle higher slake durability than rocks of sedimentary ori-

gin like illustrated in Figure 4-22. For that reason, four cycles of slaking and drying were performed to make it easier to evaluate the weathering effect.

Table 4-9 shows the slake-durability indices (I_{d2}) of the respective rock samples. The table also characterizes the tested rock samples of the respective project cases according to ISRM (1979a) that classifies rocks into six categories ranging from very high slake-durability to very low slake-durability. In the table, the fourth cycle slake-durability (I_{d4}) is also included for comparison purpose.

Table 4-9. Slake-durability indices of the tested rocks.

Rock type	Project name	Sample location	Slake-durability indices		Classification according to ISRM (1979)*
			I_{d4}	I_{d2}	
Quartzite	Middle Marsyangdi (MM)	Headrace tunnel, adit 2 DS	99.2	99.6	Very high (98 – 100)
Banded gneiss	Khimti I (KHP)	Headrace tunnel, adit 1	97.9	98.7	
Augen mica gneiss		Headrace tunnel, adit 2	96.1	97.2	High (95 – 98)
Siliceous phyllite	Middle Marsyangdi (MM)	Headrace tunnel, samples T1	91.8	96.1	
		Sample T2	92.1	96.0	
Micaceous phyllite	Middle Marsyangdi (MM)	Headrace tunnel, sample T3	88.2	93.3	Medium high (85 – 95)
		Headrace tunnel, sample T4	87.6	92.5	
		Surface, sample S1	81.3	88.4	
		Surface, sample S2	80.0	87.2	
Graphite phyllite	Kaligandaki "A" (KGA)	Headrace tunnel, sample T2	88.9	95.0	
		Surface, sample S1	78.9	86.2	

* ISRM (1979a) defines slake durability 98 – 100as very high, 95 – 98 high, 85 – 95 medium high, 60 – 85 medium, 30 – 60 low and < 30 as very low.

Slake-durability versus cycle of drying and wetting of the rock samples is plotted in Figure 4-24 (see also Table B-2 in Appendix B). The figure clearly indicates that multiple drying and wetting has a considerable effect on the slake-durability. Even for metamorphic rocks with high slake-durability index (I_{d2}) the long term weathering effect leads to considerable weakening and disintegration of the rock mass. This is especially the case for rocks with flaky minerals, such as phyllite, schist and mica gneiss.

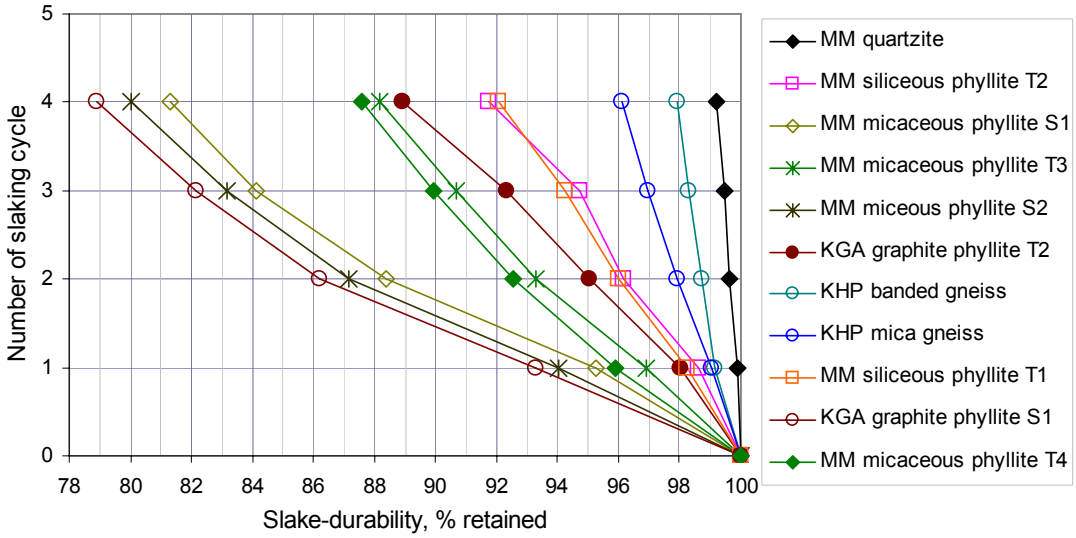

Figure 4-24. Slake-durability versus cycle of drying and wetting.

As also shown in Figure 4-24, graphitic and micaceous phyllite from the tunnel have lost more than 10 percent mass after four cycles of drying and wetting. This means that disintegration and weakening may be even greater for such rock masses located at considerable depth, if they are subjected to drying and wetting.

4.7.2 Field measurements and analysis

In addition to the laboratory testing of the rock samples collected from the respective project cases, field measurements of Schmidt hammer rebound using N/NR type Schmidt hammer was conducted during site visits (2003 and 2004) at the Middle Marsyangdi hydroelectric project. The aim was to measure weathering grade of the rock, and to establish correlation between Schmidt rebound numbers and point load strength values of lump samples. The tested rocks included quartzite, metasandstone, siliceous and micaceous phyllite of Marsyangdi headrace tunnel. The point load tests on the lump samples were conducted regularly at site by the project authority at certain intervals of tunnel excavation. Details of the measured Schmidt hammer rebound numbers and point load test results for lump samples are given in Table B-3 and B-4 in Appendix B.

The testing was done perpendicular to the foliation for both Schmidt rebound and point load tests. The rebound numbers include measurements taken at the tunnel face and on rock exposures along road cut slopes. Fresh rock exposures comparable to the tunnel rocks were selected for Schmidt rebound measurement along cut slope.

The Schmidt hammer rebound numbers that could be recorded by the N/NR type hammer ranged from 10 to 60. The lowest numbers apply to weak rock like micaceous

phyllite and the highest numbers to very strong rock like quartzite. Getting rebound on highly deformed and weathered micaceous phyllite was found extremely difficult. The results presented here for micaceous and siliceous phyllite are from relatively fresh rock exposures and represent rocks having point load strength index between 1.4- 3.5 MPa. The higher values are for metasandstone and quartzite. A summary of the results is shown in Figure 4-25.

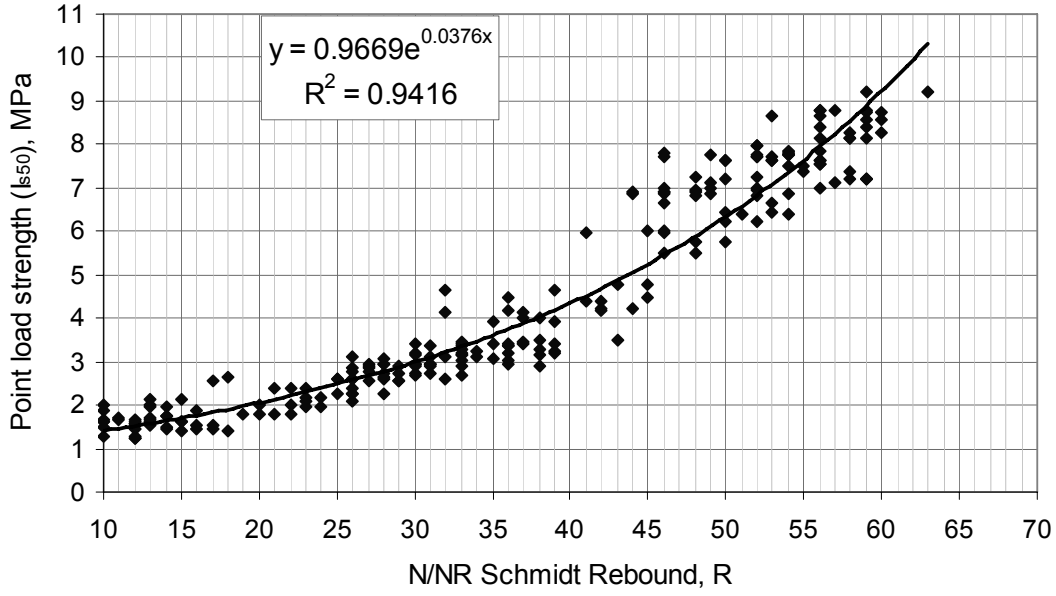

Figure 4-25. Correlation between N/NR type Schmidt rebound number and point load strength.

As can be seen, a fairly good correlation between Schmidt rebound and point load strength index has been found. Since a correlation between point load strength and uniaxial compressive strength (UCS) exists, Schmidt rebound values therefore may be used to estimate uniaxial compressive strength of intact rock.

4.8 CONCLUDING REMARKS

The review made in this chapter of the geological conditions of the selected four tunnel cases has revealed high discrepancies in predicted versus actual rock mass quality and also in predicted versus actual rock support. Particularly this is the case for Kaligandaki "A" and Khimti headrace tunnels, where much poorer rock quality than expected have caused significant impact on the overall cost and construction time. The review also shows that there have been considerable differences in the type and level of investigations carried out.

All tunnel projects are unique in their nature. Consequently, the type and level of pre-construction phase engineering geological investigation should always be adjusted to the geological complexity and the type of project. If a planned tunnel project is relatively short and is situated in good quality rock formation, and the rocks in the area are

well exposed, review of the geological conditions based on published literature, study of aerial photographs and a few days of surface investigations by an experienced team of engineering geologists may give sufficient information. However, in most cases the project site is not so ideal in the Himalaya. Due to active tectonics and monsoon effect, the rock mass in the region often is highly fractured, faulted, intercalated and weathered, and also soil-covered. As has been indicated by the results of laboratory testing, the mechanical characteristics of the rocks also vary considerably due to high degree of schistocity.

Therefore, a thorough, stepwise investigation approach as suggested in Figure 4-19 should be adopted. This approach may slightly increase engineering geological investigation cost, but may help saving millions during construction. Risk and uncertainty analysis also should be carried out for realistic prediction and evaluation of rock mass quality and for analyzing the stability conditions of a planned tunnel project.

Chapter 5
Methodology for analyzing uncertainty

5.1 INTRODUCTION

It is a well known fact that the rock mass is a heterogeneous medium usually made up of an interlocking matrix of discrete blocks. The blocks are generally separated by the sets of discontinuities such as bedding planes, foliation planes and other systematic or random joints and faults oriented in different directions. The discontinuities in the rock mass are subjected to lateral movement and shearing caused by tectonic or other mechanical course of actions occurred during their geological life time. Such movements always cause alteration and weathering to the rock mass to varying degrees and the contact surfaces between the blocks may vary from very clean, fresh and rough to clay filled, smooth and slickensided (Hoek 1998). Thus, the mechanical characteristics of rock mass are not uniform and vary greatly.

Rock mass quality predictions and stability analysis for underground structures are based normally on very limited information established by surface and subsurface site explorations and laboratory testing. As a result, the degree of uncertainty and risk remain higher while predicting and evaluating the quality of rock mass at planning phase. Consequently, both rock quality knowledge and level of uncertainty are time dependent and project stage based as shown Figure 5-1.

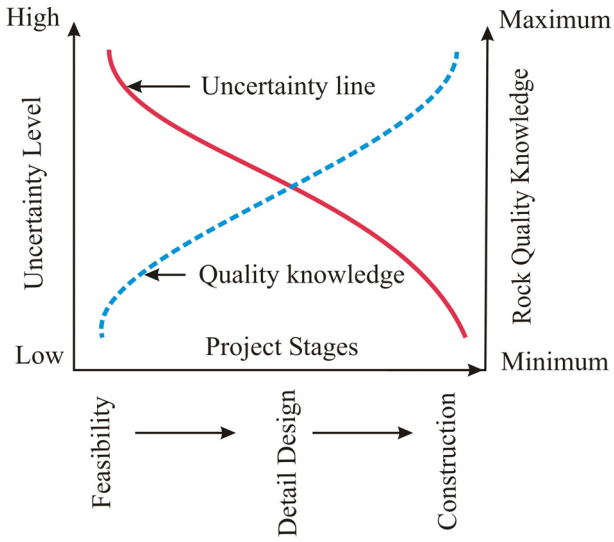

Figure 5-1. Schematic illustration of uncertainty level and rock quality knowledge at different project stages.

As indicated in Figure 5-1, the ability to better comprehend the rock mass conditions increases as project development stage moves on. This is because the level of engineering geological investigations, site explorations and in-situ as well as laboratory testing activities increase steadily. In fact, the actual rock mass condition of an underground structure is fully known only after the completion of its excavation work. Conversely, basic design and economic viability evaluation of any underground project has to be made during its feasibility study stage. On the basis of technical and economic feasibility further recommendations are made for detail design and implementation. Since the degree of uncertainty related to the geological condition is much higher at an early stage of planning, there exists high risk of large variations on the estimated and actual rock mass condition, refer Chapter 4. Therefore, the real challenge is on how to minimize this level of uncertainty and reduce possible risk of large deviations between predicted and actual rock mass condition.

The traditional empirical, deterministic as well as numerical approaches of rock mass quality evaluation and stability analysis are generally based on single point estimate that give single answer, and the possibility for considerable deviation from reality is therefore high. In this respect, probabilistic approach of analysis may provide better answer to such analyses and prove to be a better tool to help reduce large deviations and discrepancies. However, due consideration should be given to the fact that even the most sophisticated analysis can become a meaningless exercise if the geological information upon which it is based is inaccurate or inadequate (Hoek, 1998). Thus, the importance of judgment based on past experience of similar projects and expertise gained in rock engineering is of high value.

This chapter aims to discuss the basic concept of the probabilistic approach for evaluation and analysis of projects related to engineering geology. The discussion covers history, rationale and basic theory of statistics and the probabilistic approach on uncertainty analysis. The most useful probability distribution functions that may be used for such analyses are also discussed, and brief introduction to the Palisade's @Risk statistical analysis program that has been used for the uncertainty analysis of selected cases in Chapter 6 is given. On top of that, an appropriate @Risk model or process useful for the uncertainty and risk analysis related to the evaluation of rock mass quality and stability analysis is introduced.

5.2 PROBABILISTIC APPROACH USED IN ROCK ENGINEERING

The use of probabilistic approach in engineering geology has been recognized since it was acknowledged that a single answer from the conventional analytical design may give highly uncertain solution to the problem due to large range of variations of properties used in such analytical design. According to Einstein (2003), the basic concept of probabilistic approach of analysis in the field of engineering geology was developed as early as in the late 1960's. In this connection the Casagrande's well-known Terzaghi Lecture (Casagrande, 1965) where he extensively discussed on the role of "calculated

risk" and uncertainties may be considered as one of the earliest attempts on the use of probabilistic approach of thinking. In that lecture Casagrande defined "calculated risk" as the taking of a carefully considered risk which is based largely on an analysis of factors that require experience and judgment for their evaluation. His definition broadly follows two distinct steps;

1. Use of imperfect knowledge, guided by judgment and experience, to estimate the probable ranges for all pertinent quantities that enter into the solution of a problem.

2. Decision on an appropriate margin of safety, or degree of risk, taking into consideration of economic factors and magnitude of losses that would result from failure.

Thus, Casagrande's definition about calculated risk can be considered as a corner stone that gave new sights on the use of probabilistic approach of analysis in engineering geology and geotechnical engineering. Although, Casagrande was not certain and optimistic that the risks could literally be calculated or even quantified (Whitman, 2000).

Wu and Kraft (1967) introduced probability theory that could be applied in the rational analysis of foundation safety and computation of probability of safety of the foundation. In their work, they considered applied load and soil strength as random variables. They defined probability distribution functions of soil properties empirically by fitting the data from laboratory analysis, admitting however that their calculations represent merely a first approximation and should be considered qualitative due to the use of limited statistical data that did not permit precise calculation of the distribution functions. Their further work of 1970 (Wu and Kraft, 1970) developed the concept of quantifying sources of geotechnical uncertainties, and they incorporated these uncertainties for the optimum and reliable analysis of factor of safety against slope failure. The concept to use normal and log-normal probability distribution of soil properties to calculate an optimum safety probability of a soil slope was a kind of milestone in the use of probability theory in geotechnical engineering.

There are mainly three areas where the probabilistic approach of analysis has been widely used since then in rock engineering. These areas cover; factor of safety and reliability analysis of rock slopes, assessment of variability in rock mass properties, and uncertainty and risk assessment of time and cost for underground structures. Some of the land mark research works and scientific papers produced in 1970's and 1980's describing probabilistic and statistical analysis methods and parameter distribution models applicable to engineering geology are Beacher (1972), Einstein et al. (1978) and Einstein and Beacher (1982 and 1983).

In the early 1990's the concept and methods developed previously were extensively upgraded. Most of the probabilistic and statistical analyses were focused particularly on rock slope stability and reliability analysis and on characterizing the properties of rock

mass on the basis of laboratory testing, as described by Nikraz and Press (1993), Lashkaripour and Dusseault (1993), Fell (1993) and Low (1997).

It has been recognized that further upgrading and improvements were needed in this field not only because the probability and reliability analysis can facilitate in characterizing pertinent uncertainties and in analyzing their effects on the geotechnical performance, but also because the society at large was demanding more explicit assessment of risk (Tang, 1993). However, until the middle of 1990's, the computational capabilities of computers were not sufficiently strong, causing limitations on the use of the probabilistic approach. As a result, the probabilistic approach of analysis was mostly considered to be very tedious, time and effort consuming.

Nevertheless, after the middle of 1990's there has been tremendous improvement and innovative development in computational and simulation capabilities of the computers followed by development of more sophisticated and advanced statistical analyzing tools and software. Similarly, the concept and theoretical models of probabilistic and statistical analyses have been refined and to some extent simplified (Einstein, 2003). Accordingly, probabilistic and statistical analyses have become much more accessible in the areas of reliability (safety) analysis, rock mass characterization and analysis of cost and time domains. An example of such tools is the use of statistical program @Risk developed by Palisade Cooperation in 1996 and 1997. Hoek (1998) used this program first to calculate probability of failure of the rock slope and later followed by Nilsen (1999), Pathak (2002), Pathak and Nilsen (2004) and many others.

In recent years, efforts have been made to use probabilistic approach of analysis for underground construction. Nilsen et al. (1999) used so-called Lichtenberg's method of uncertainty analysis in estimating cost and time for a sub-sea tunnel in Norway. Hoek (2000) carried out Monte Carlo simulation for the analysis of reliable first estimate on a severity of potential squeezing problems using @Risk. Martin et al. (2003) performed stability analysis of rock stresses particularly for rock spalling using @Risk. Kim et al. (2003) attempted to exploit the @Risk program to revaluate the RMR system of rock mass classification with main focus on multiple regression analysis for defining the contribution made by each input parameters in the total RMR value. This is a manifestation that the potential capabilities of @Risk and other statistical analyzing tools are very diverse and may provide answers to many uncertainties that exist in underground construction.

5.3 PROBABILITY THEORY

Data on rock mass properties and rock quality evaluation parameters are in general scattered and random. There is no way of predicting exactly what the value of these parameters will be at any given location. The best way to describe this randomness is to use probabilistic mathematical models. The use of such models gives better understanding of the distribution pattern and also of the corresponding uncertainties associated

with their engineering performance. The basic concepts of the probability theory used for analyzing uncertainties in the field of engineering geological and geotechnique are described by Wu and Kraft (1967 and 1970), Einstein and Beacher (1982 and 1993), Tang (1993) and Christian et al. (1994), and Beacher and Christian (2003).

Therefore, this author feels that it is not necessary to discuss the discipline of probability theory too deeply or to dig deeply into the mathematics. Nevertheless, a brief discussion of the basics of statistics and probability theory are presented below.

5.3.1 Statistical data analysis

The term "statistics" refers to any mathematical function of a set of measured data such as arithmetical average, the largest value (x_{max}), the smallest value (x_{min}) and so forth. Depending on the methodology of statistics used, the set of operating principles therefore may differ (Einstein and Beacher, 1982 and Beacher and Christian, 2003). The most common measures of central tendency used in engineering geology are however *mean*, *median* and *mode* and the most common measures of central dispersions are the *standard deviation*, *range* and *inner quartiles* of the frequency distribution.

The *mean* is an arithmetic average of a set of data and also is a centre of gravity of the probability distribution along x-axis. The mean ($\bar{x}$) of the set of "n" data ($x = x_1, x_2....x_n$) is given by:

$$\bar{x} = \frac{1}{n}\sum_{i=1}^{n} x_i \qquad (5\text{-}1)$$

The *median* of the set of data is that value of x_n for which half the data are less and half are more or in other words midpoint of the data when listed in increasing or decreasing order. Consequently, the cumulative distribution evaluated at the median is 0.5:

$$F_x(x_{0.5}) = 0.5 \qquad (5\text{-}2)$$

The *mode* is the most common value or most likely value of data sets. The use of this term is very useful, particularly to characterize the input with its maximum, minimum and most likely value.

The term *standard deviation (s)*, which is very common in statistical analysis, is the root-mean-square (rms) of the difference between a particular data within the set of data and their mean, and is expressed as:

$$s = \sqrt{\frac{\sum_{i=1}^{n}(x_i - \bar{x})^2}{n-1}} \qquad (5\text{-}3)$$

Theoretically, the denominator for the calculation of standard deviation should be (n) rather than (n-1). However, (n-1) is generally used for the finite number of samples to correct the statistical bias (Beacher and Christian, 2003). Accordingly, it is logical and valid to use this expression in rock engineering.

The *variance* or second moment about the mean (s^2) of the set of data is the square of standard deviation (s) and is given by:

$$s^2 = \frac{1}{n-1}\sum_{i=1}^{n}(x_i - \bar{x})^2 \tag{5-4}$$

The *coefficient of variation* (COV) of a set of data is defined as the standard deviation (s) divided by the mean ($\bar{x}$). COV is dimensionless and is particularly useful to measure uncertainty. A small value of COV represents a small level of uncertainty.

$$COV = \frac{s}{\bar{x}} \tag{5-5}$$

The *range* of a set of data (r) is the difference between the largest and smallest values. In general the range has poor statistical properties and is sensitive to extreme values. However, this term is very useful in rock mass classification. The range is given by:

$$r = \left| x_{\max} - x_{\min} \right| \tag{5-6}$$

The *inner quartiles* of a set of data are the values for which one-quarter of the data are smaller and one-quarter larger. This term is particularly useful in describing cumulative probability distribution functions.

5.3.2 Useful probability distribution models

In rock engineering, the interpretation of probability should be done in terms of relative frequency as well as degree of belief. The relative frequency is the frequency of occurrence of some events or properties in a long series of similar trails that give individual irregularity with aggregate regularity (Beacher and Christian, 2003). An example is the measurement of rock strength of a particular rock type. In contrast, the degree of belief reflects an understanding of the probability of occurrence or outcome of the event drawn upon judgment, past experience and information of events. The degree of belief is therefore more subjective, and thus more knowledge based. For example, the probability of a solution cavity that may exist along a tunnel passing through calcitic rock formation such as limestone can only be estimated based on personal judgment and past experience of such events. The degree of belief also involves consideration of effects of the possible range of values of the parameters, and the possible occurrence of these parameters within the expected range.

Since the uncertainties encompass natural variability, randomness and lack of knowledge, the best way to quantitatively analyze these uncertainties is to use probability (frequency) distribution models that are expressed by the term probability density functions (pdf). A probability density function describes the relative likelihood that a random variable may assume a particular value. The selection of such mathematical distribution models in uncertainty analysis should always be based on numerical calculations, experimental or field measured results and logical judgment made by observation (Whitman, 2000 and Einstein, 2003). The most useful probability density functions that might be used in rock mass quality evaluation and stability analysis are:

Normal distribution: Normal or Gaussian distribution is a well known type of probability distribution. This is a bell-shaped curve, see Figure 5-2a, and many random variables have been found to confirm to this distribution. This distribution requires a physical property (x) whose value may range from (- ∞) to (+ ∞) with x-values showing a strong tendency to cluster around their mean ($\bar{x}$) (Borradaile, 2003). To use this distribution, the dispersion about the mean ($\bar{x}$) has to be defined by the standard deviation (s) or by the variance (s^2). The normal distribution is often being used for probability study in the field of engineering geology unless other distribution functions are specifically designated (Kim et al., 2003). The probability density function (pdf) of this type of distribution is defined by:

$$f(x) = \frac{\exp\left[-\frac{1}{2}\left(\frac{x-\bar{x}}{s}\right)^2\right]}{s\sqrt{2\pi}} \qquad (5\text{-}7)$$

Lognormal distribution: Some random variables (input parameters) in engineering geology can not be represented by normal distribution due to their positively skewed distributions that give long tail towards high values of measurements, and are defined as lognormal distributions. The random variables conforming to lognormal distribution have many small values, commonly with a peak near the lower limit and large values occurring less often, giving a long tail, see Figure 5-2b. Spacing of discontinuities often conforms to the lognormal distribution (Einstein and Beacher, 1983). This distribution also requires a physical property (x) whose value may range between (- ∞) to (+ ∞) and the plot of logarithm of x-values show a strong tendency to cluster around their mean of *log x*. To use this distribution, the dispersion about the *log x* mean (α) and standard deviation (s) have to be defined (Borradaile, 2003). The probability density function (pdf) of this distribution is defined by:

$$f(x) = \frac{1}{sx\sqrt{2\pi}} \cdot \exp\left[-\frac{(\log x - \alpha)^2}{2s^2}\right] \qquad (5\text{-}8)$$

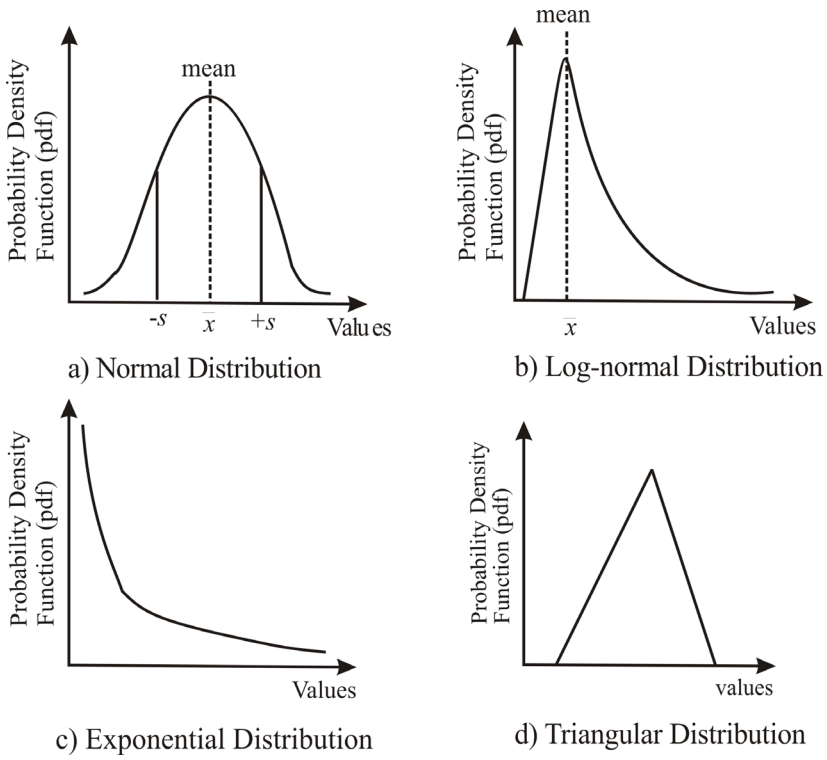

Figure 5-2. Useful probability distribution models for uncertainty analysis in rock engineering.

Exponential distribution: There are some random variables that may give an exponential distribution of their frequencies as shown in Figure 5-2c. In engineering geology, parameters such as earthquake events and ground water pressure may be modeled by using this distribution. In general, the parameters fitting to exponential distribution indicate that the lower values (above zero) occur more frequent and the larger values rear. In theory, a random variable x is said to have an exponential distribution with a mean value parameter $\beta>0$ with a variance β^2 and its probability density function is given by:

$$f(x) = \frac{e^{-\frac{x}{\beta}}}{\beta} \tag{5-9}$$

Triangular distribution: Another common probability density function that could be used in rock engineering is the triangular distribution, see Figure 5-2d. This distribution may be useful particularly for modeling certain random variables having their range within narrow space. The random values that need to be quantified for using this probability density function are minimum (x_{min}), maximum (x_{max}) and most likely value (x_{mlik}). The probability density function of this distribution is given by:

$$f(x) = \frac{2(x - x_{\min})}{(x_{mlik} - x_{\min})(x_{\max} - x_{\min})} \qquad (x_{min} < x < x_{mlik}) \qquad (5\text{-}10)$$

$$f(x) = \frac{2(x_{\max} - x)}{(x_{\max} - x_{mlik})(x_{\max} - x_{\min})} \qquad (x_{mlik} < x < x_{max}) \qquad (5\text{-}11)$$

The above mentioned probability distribution functions are the distributions that most commonly give good estimate on the randomness characteristics of engineering geological parameters. In general, during estimation of engineering geological parameters, their ranges are specified by their maximum and minimum values. Therefore, while specifying probability density function (pdf) of most of these parameters it is useful to truncate the parameters within their maximum and minimum range to avoid model error that may occur during the use of statistical programs such as @Risk.

5.4 PALISADE'S @RISK APPROACH

The software program @Risk is an advanced statistical risk analysis software system introduced by Palisade Corporation in 1996 and updated in 2002 (version 4.5). The @Risk is a Windows based program that is capable in performing risk analysis and simulation of technical and business situations impacted by many uncertainties. This is an Add-Inn software system compatible for the industry standard spreadsheet package, Microsoft Excel. The program is relatively convenient and easy to handle, and can be used to develop a suitable excel design model and is capable of simulating, quantifying and solving many issues subjected to uncertainties and risk. The main features of @Risk version 4.5 are given below (for details about @Risk recommendation is made to @Risk user manual Palisade; Corporation, 2002):

1. The program is an Add-Inn to the Microsoft Excel program, linking directly to the Excel in adding risk analysis capabilities.

2. It allows for defining almost any type of uncertainties as cell values in the Excel sheet. The program includes 37 probability distribution functions (pdf) that a user may specify or define, and it is also possible to make a best-fit out of available statistical data.

3. The program can produce high resolutions graphics to present the output distributions from the simulations. The simulation results can be plotted as frequency histograms, cumulative curves, summary graphs and reports and also can be exported to excel sheet.

4. The program has sophisticated capabilities for specifying and executing simulations of Excel models using both ***Monte Carlo*** and ***Latin Hypercube*** simulation tech-

niques, and is capable of any numbers of iterations per simulation and any number of simulations in a single analysis.

5.4.1 Monte Carlo simulation method

The Monte Carlo simulation is a traditional method of simulation technique developed during World War II. This simulation method uses random or pseudo-random numbers to sample from different types of probability distribution functions specified on the input variables. This method uses pseudo-randomly generated points to cover the range of values that enter into the calculation, and may fall anywhere within the range of input distribution that respects the assumed probability distribution curve (Palisade Corporation, 2002). The Monte Carlo method of simulation technique can be employed to study both stochastic and deterministic systems, and the computation is entirely based on the hit and miss approach (Beacher and Christian, 2003).

On the course of simulation process samples are more likely to be drawn from the areas of distribution that have higher probability of occurrence, and each sample uses a new random number between 0 and 1 from cumulative distribution curve of input variables. The main advantage of this technique is that it is relatively easy to implement on a computer and can deal with wide range of functions. The major disadvantage is its slow convergence that is specially pronounced when a distribution includes low probability outcomes which could have major impact on the results (Beacher and Christian, 2003).

5.4.2 Latin Hypercube simulation method

A relatively recently developed simulation technique is the Latin Hypercube sampling technique that gives comparable results to Monte Carlo sampling technique, but with fewer samples. This simulation technique was introduced by Imam and others in 1980 (Hoek, 1998). The Latin Hypercube technique constitutes part of a Monte Carlo procedure for the propagation of uncertainty. This method can be viewed as a compromise procedure that incorporates many of the desirable features of random sampling and stratified sampling. The key to this sampling technique is that the range of each variable input parameter is divided into intervals of equal probability on the cumulative probability scale (between 0 and 1), and one value is selected at random from each interval (Helton and Davis, 2003). In that way sampling is forced to recreate the input probability distribution and the technique being used during sampling is “sampling without replacement”.

The main advantage of Latin Hypercube simulation technique is that it offers great benefits in terms of increased sampling efficiency and faster runtimes due to fewer iterations. It also aids the analysis in situations where low probability outcomes are represented in the input probability distributions. In addition, the concept of convergence is used to test a sampling method. At the point of convergence, the output distributions become stable (Palisade Corporation, 2002).

5.5 UNCERTAINTY ANALYSIS MODEL USING @RISK

An optimum prediction of rock mass quality along the tunnel alignment is one which enables to minimize the variation between predicted and actual rock mass conditions. Likewise, an optimum design of the tunnel project is one that allows to foresee in advance the probability of possible instability situations that may occur during construction. If a realistic probabilistic model of uncertainty analysis is followed, it is virtually possible to get an answer close to both these situations. In this respect, an uncertainty analysis model as illustrated in Figure 5-3 represents the optimum process for the evaluation of rock mass quality as well as for the analyses of stability problems.

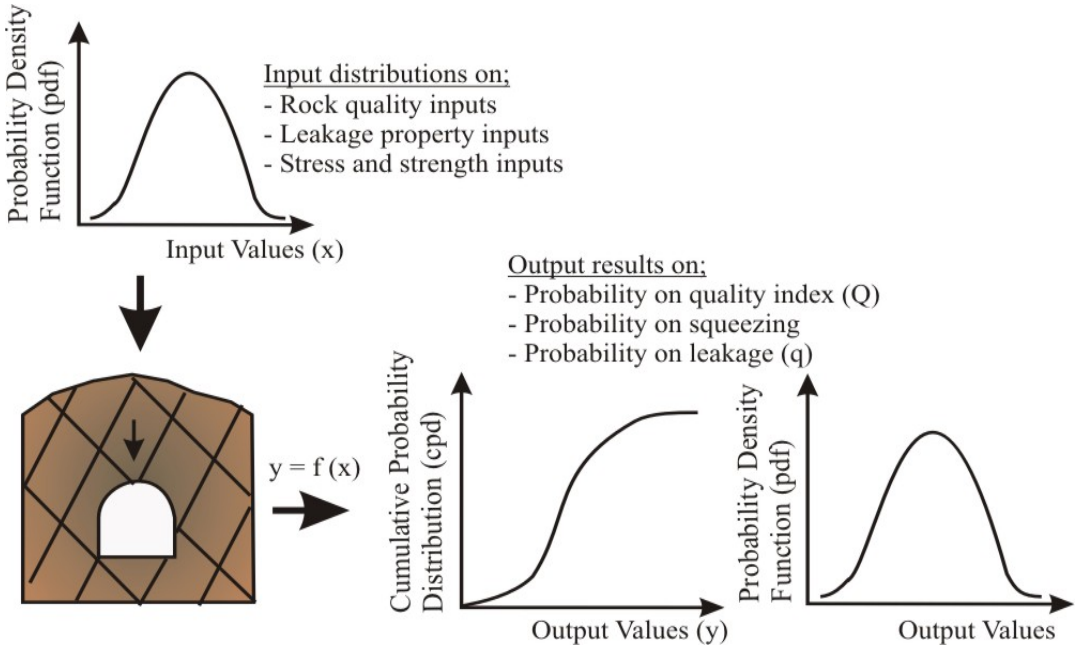

Figure 5-3. Principle sketch of uncertainty analysis model for a tunnel project.

As shown in Figure 5-3, while carrying out any uncertainty analysis it is very important to characterize the most representative probability distribution of the input parameters. Representative probability density functions of the input parameters will make it possible to reliably and quantitatively predict the probability distribution of the output results. This is the most important aspect that needs to be carefully considered for the successful use of @Risk in uncertainty and risk analysis. More importantly, the @Risk always seeks for relationship between output and input parameters and gives quantitative simulation results of the uncertainties.

5.6 CONCLUDING REMARKS

The model concept illustrated in Figure 5-3, based on Palisade's @Risk is used in Chapter 6 for evaluation of rock mass quality, probability of tunnel squeezing and probability of leakage for the selected tunnel cases from Nepal Himalaya.

Chapter 6
Uncertainty analyses for selected cases

6.1 INTRODUCTION

Given the heterogeneous nature of rock mass, it is not possible to eliminate all uncertainties that may exist in it while planning and designing tunnel projects. The uncertainties are mainly related to spatial variability of rock mass behavior, limitations in the field exploration, measurements and testing techniques and human and analysis model errors. More reliably quantified uncertainty or probability of occurrence is therefore a useful tool for the communication between tunnel engineers / engineering geologists and the client / contractor.

In regards to tunnelling, uncertainty analysis allows exploring the influence of variations of each input parameter interlinked to the rock mass quality evaluation and stability analysis. Hence, uncertainty analysis improves the base of our engineering judgment and makes it possible to foresee the possible consequences of variations that ultimately reflect project economy. In principle, an uncertainty analysis for a tunnel project should follow the steps given in Figure 5-3 and 6-1.

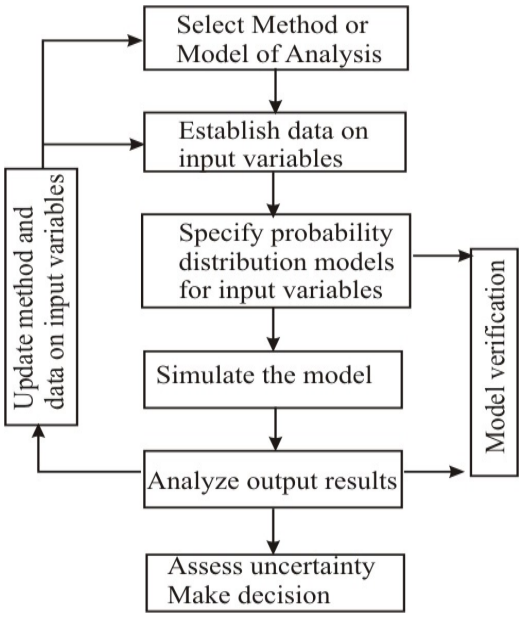

Figure 6-1. Uncertainty analyzing cycle.

With respect to tunnelling through tectonically active Himalayan rock mass, the main areas of concern on tunnel stability are the existence of weak and highly deformed rock mass, high degree of weathering and fracturing of the rock mass, possibilities for stress induced problems such as tunnel squeezing, and potential inflow and leakage (see Chapter 1 and 4). The best way to reliably analyze stability issues is therefore to carry out uncertainty analyses with maximum focus on the effect of variation in each input parameter and to incorporate these input variations with sufficient comprehension.

This chapter therefore will focus on uncertainty analyses of stability and water leakage issues for the four tunnel cases from Nepal Himalaya described in Chapter 1 and 4. Main emphasis is given on uncertainty analysis related to:

1. Rock mass quality;
2. Tunnel squeezing;
3. Water leakage through unlined tunnel.

It needs to be emphasized here that covering all these aspects for all projects described in Chapter 4 is not possible within the scope of this thesis. Therefore, the cases are prioritized based on main areas of uncertainties and available data information.

For instance, at Khimti and Modi headrace tunnels no major problems associated with tunnel squeezing were faced during tunnelling. On the other hand, as discussed in Chapter 4, these two tunnels represent large and small deviation, respectively, with respect to predicted and actual rock mass conditions. Therefore, these two tunnels have been selected for the uncertainty analysis concerning rock mass quality.

At Kaligandaki headrace tunnel the major stability problem was associated with tunnel squeezing, which was the major cause for large deviation between predicted and actual rock mass conditions as discussed in Chapter 4. In the case of Middle Marsyangdi, it is expected that some degree of tunnel squeezing will occur in the geological section between Jamitri and Khahare Khola, see Figure 4-13. Therefore, these two headrace tunnels have been selected for the uncertainty analysis concerning tunnel squeezing.

Khimti headrace tunnel is the only project where the unlined / shotcrete lined concept with preinjection grouting technique for controlling water leakage has been used. Therefore, uncertainty analysis on assessment of water leakage is made only for this tunnel. Since this analysis is carried out for only one single project from the Himalaya, particular uncertainty will be associated with the water leakage analysis.

The probabilistic approach is used for quantification of the probable distribution of rock mass quality indexes (Q), tunnel strain (ε_t) and specific leakage (q). The Palisade's 2002 version of @Risk statistical analysis software program discussed in Chapter 5 is used as a tool for the analysis. While carrying out uncertainty analysis by using the @Risk model, great emphasis has to be placed on trustworthy estimation of possible range of the input pa-

rameters and their probability density functions (pdf). The basic theory of the probability density functions (pdf) used in this research is described in Chapter 5.

While carrying out uncertainty analysis, the selection of representative probability density functions are based on logical judgment and use of the best fit tool of @Risk program. Concerning rock mass quality and water leakage, large numbers of mapped observations in tunnels are available for each input variable, and both logical judgement and the best fitting tool of @Risk program are used to select probability density functions for evaluating rock mass quality index (Q) and estimating water leakage (q). Logical judgment is used for defining probability density functions of each input variable in estimating tunnel strains (ε_t). Truncation has been applied by fixing possible maximum and minimum ranges for each input variable. This allows @Risk model to select random value within truncated range and helps to minimize model error.

6.2 ROCK MASS QUALITY

As discussed in Chapter 4, review of the rock mass conditions of the selected four tunnel project cases from Nepal Himalaya has indicated high discrepancies between predicted and actual rock mass quality. Such discrepancies not only led to considerable increase in rock support requirements, but also to a need for increased quantities of tunnelling machinery compared to what were anticipated during planning. Minimizing such discrepancies in advance (at project planning) and controlling possible large variations of estimated cost and time is very essential, and also challenging.

Natural outcrops, excavated road cut slopes, borehole cores, geophysical investigation results and tunnel mapping are the most common sources of information for classifying rock mass quality according to Q, RMR, RMi and GSI systems discussed in Appendix A. It is generally accepted that quantifying the input parameters involved in these classification methods are subjective and very much dependent on the personal judgement of the user. The subjectivity and the extent of variations between the observers in quantifying input parameters of these classification systems are discussed by Nilsen et al. (2003). The most crucial and difficult part of giving representative rating often is the assessment of the effect of weathering and alteration of the rock mass.

The probabilistic approach may be a good alternative for giving reliable quantification of the distribution of rock mass quality indexes. In the following two Sections 6.2.1 and 6.2.2 of this research, the probabilistic approach is introduced to evaluate the probability distribution of rock mass quality indexes for Khimti and Modikhola headrace tunnels. The Q-system of rock mass classification, which was used to quantify the quality of rock mass in these two projects, is used here as a basis for analysis. However, there is no restriction to use any type of rock mass classification systems that give quantitative quality index on the basis of numerically quantified input parameters.

The rock quality index (Q) is a function of six variable input parameters and is described by the following equation:

$$Q = f(x) = \frac{RQD}{J_n} \times \frac{J_r}{J_a} \times \frac{J_w}{SRF} \qquad (6\text{-}1)$$

In the Q-system; *RQD* is the rock quality designation that represents degree of jointing and its rating varies from 10 to 100, J_n is the joint set number that varies from 20 to 0.5, J_r is the joint roughness number that varies from 0.5 to 4, J_a is the joint alteration number that varies from 20 to 0.75, J_w is the joint water reduction factor that varies from 0.05 to 1 and *SRF* is the stress reduction factor that varies from 400 to 1. The details concerning characterization of these parameters are given in Table A-1 of Appendix A.

It should be emphasized here that higher rating numbers to the denominator in Equation 6-1 (J_n, J_a and *SRF*) contribute to reduction of the Q-value. Therefore, while assigning probability density functions (pdf) representating denominators J_n, J_a and *SRF* it should be kept in mind that the higher values give smallest value with respect to rock quality index (Q).

In terms of probabilistic approach, the rock mass quality index (Q) should be considered as an uncertainty that is dependable on these six variable input parameters, and all these six variables are considered to be independent to each other. This means that the main principle of uncertainty analysis based on Q-value is to characterize the uncertainties that exist while estimating these six variable input parameters. The characterization of these uncertain input variables is done by assigning probability density functions to each of them. Logical judgement, mapped input variables in the tunnel during excavation given in the geological tunnel log and the best fit tool of @Risk program are used to define probability density function for each input variables.

To avoid @Risk model error, a truncation is applied for each input variable. The possible range of each input variable for Q is discussed above and these values are used for the truncation, except for stress reduction factor. For SRF a truncation is defined with values 1 and 10. The main reason for this is that the SRF value is mainly used to describe weakness zones or shear bands, since both headrace tunnels have moderate overburden (less than 250 meters) and less stress effect according to the Q-system.

The main source of information in defining statistical ranges of each input variable for Khimti and Modi Khola is project information such as investigation phase geological reports and geological tunnel logs. Planning phase detail information on predicted input variables of Q-value was not available for Khimti headrace tunnel, except for jointing characteristics and rock mass class defined as shown in Table 4-1. Therefore, predicted statistical ranges of input variables for this tunnel are assumed based on Table A-1 in Appendix A. Actual statistical ranges are calculated from actually mapped input variables in the tunnel.

6.2.1 Khimti headrace tunnel

The approximately 7.9 kilometers long Khimti headrace tunnel, see Figure 4-2, passes through highly fractured gneiss that has frequent intercalation of chlorite and talcose mica schist. At the planning and design phase of the project it was believed that the gneiss was more homogeneous and competent (Panthi and Nilsen, 2005a and 2005b). However, due to intercalation effect and deep weathering, large discrepancies between predicted and actual rock mass quality were experienced (see Chapter 4 for detailed descriptions of project geology, level of planning phase investigations and discrepancies between predicted and actual rock mass conditions along the headrace tunnel).

For the purpose of uncertainty analysis based on @Risk model, three tunnel sections representating extremities with respect to rock mass quality index (Q) have been selected, see Figure 6-2. It is believed that uncertainty analysis of these three sections illustrate the general potential and reliability of the probabilistic approach. Probable causes of variations between predicted and actual rock mass quality are discussed in Chapter 7.

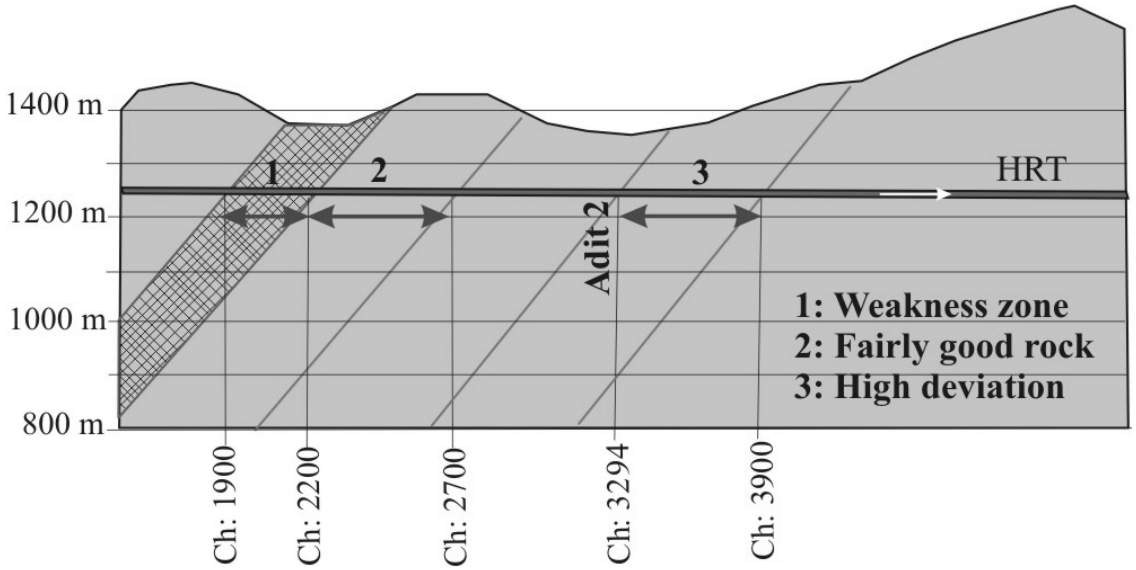

Figure 6-2. Three extreme sections of the Khimti headrace tunnel, two sections upstream and one section downstream of Adit 2 junction.

In Figure 6-2, section 1 represents a highly fractured weakness zone that was predicted at planning and design phase and was actually observed during excavation. Section 2 represents a section of the tunnel where fair to good quality rock mass was predicted, and the actually found quality was close to predicted. Section 3 represents a section where prediction was made for fair to good quality rock mass, but the conditions were found to be exceptionally poor to poor during tunnel excavation.

6.2.1.1 Weakness zone (Chainage 1900 - 2200)

This is a fracture zone represented by a small stream named Thulo (Chyama) khola on the surface, see Figure 4-2 and 6-2. During planning, this section was considered to be a highly fractured and sheared weakness zone with a potential of moderate ground water inflow in the tunnel. In reality, the rock mass was found to be highly weathered and weak, and representating a fractured weakness zone. In the tunnel, the rock mass in this section was found mainly to consist of highly fractured and extremely weathered mica gneiss with frequent intercalation of extremely weak, highly weathered and altered talcose mica schist. In addition, moderate groundwater inflow was observed between chainage 1930 to 2045 meters.

Defining probability density function (pdf): The predicted and actual ranges of input variables for Q-value with their minimum, maximum, mean and most likely values are given in Table 6-1. In addition, assumed probability density functions of each input variable and mapped value for simulation by @Risk model are given.

Table 6-1. Predicted and actual ranges of input parameters for Q-value with assumed probability density functions (pdf) for weakness zone (chainage 1900-2200) in the Khimti headrace tunnel.

Descriptions of Q-value parameters	Rating ranges of Q-value parameters					Assumed probability density function (pdf)
	Min. (x_{min})	Max. (x_{max})	Mean / most likely	St. dev. (s)	@Risk value	
A. Predicted						
RQD	10	30	20	10	21.41	Lognormal, Truncate (10;100)
J_n	20	9	15		14.67	Triangular, Truncate (1;20)
J_r	0.5	1.5	1	0.5	1.07	Lognormal, Truncate (0.5;4)
J_a	15	6	10	4	9.68	Lognormal, Truncate (0.75;20)
J_w	0.33	0.66	0.5		0.51	Triangular, Truncate (0.05;1)
SRF	10	5	7.5		7.50	Triangular, Truncate (1;10)
Q-value	0.001	0.147	0.01		0.011	
B. Actual						
RQD	10	50	30	15	34.82	Same as above
J_n	20	9	15		14.67	
J_r	0.5	2	1	0.75	1.16	
J_a	15	4	10	5	9.32	
J_w	0.5	1	0.66		0.74	
SRF	10	2.5	7.5		6.67	
Q-value	0.001	1.111	0.021		0.033	

In Table 6-1, lognormal probability density function is assumed for the input variables *RQD*, J_r and J_a. For very weak quality rock mass representing fractured weakness zone like here, the input variables *RQD* and J_r are characterized by low ratings and their mean values in general try to cluster towards smaller values. In contrast, the input variable J_a, which is denominator in the equation 6-1, clusters towards higher values. Therefore, lognormal

probability density function, as discussed in Chapter 5, is believed to be the most representative distribution model for these three input variables in the rock mass representating weakness zones. As seen in the table, a truncation is applied for all input variables of Q as described earlier.

A triangular distribution of probability density function is assumed for the input variable J_n. For a very fractured weakness zone like in Figure 6-2, it is logical to predict that there will be more than three joint sets, and it is most likely that four or more joints will represent the heavily jointed rock mass. In extreme situations the rock mass could be highly crushed. Consequently, it is predicted that the maximum J_n value is in the range of 9, the most likely value is 15 and the extreme minimum value is 20, see Table 6-1. The actual ranges of J_n values given in Table 6-1 were calculated based on the records from tunnel excavation. For such narrow space of rating, the most representative probability density function for J_n is believed to be a triangular distribution.

A triangular distribution is assumed also for the input variable J_w. It is a well known fact that the fracture zone represents high permeability that may give large inflow with considerable pressure. The overburden at this location is, however, slightly more than 100 meters (see Figure 6-2) and the maximum groundwater pressure therefore will not exceed 10 bars. For that reason, most likely J_w rating of 0.5 and maximum and minimum value of 0.66 and 0.33, respectively, have been used for the predicted values, see Table 6-1. Actual ranges of J_w with a most likely rating of 0.66, maximum 1 and minimum 0.5 were established based on records from the tunnel mapping, see Table 6-1.

Also for the stress reduction factor (*SRF*) a triangular distribution is assumed. The main reason for this is that this weakness zone mostly consists of fractured rock mass with intercalation of multiple bands of shear zone, representating talcose mica schist, and it is located at a moderate overburden of 100 meters. Based on this, the predicted most likely value of *SRF* is estimated to be in the range of 7.5, representating weakness zone with multiple shear zones in fairly competent but highly fractured rock mass. The maximum and minimum ratings of *SRF* are estimated at 5 and 10, respectively, which represent single shear zone in competent rock mass and multiple occurrences of shear zones containing chemically disintegrated rock mass. Actual ranges of *SRF* with a most likely rating of 7.5, maximum 2.5 and minimum 10 were calculated based on records from tunnel mapping, see Table 6-1.

Achieved simulation results: The @Risk uncertainty analysis model was run after defining and assigning the probability density functions (pdf) for each input variable of the quality index Q as given in Table 6-1. The simulation settings of the @Risk model were specified to single number of simulation and maximum iterations of 5000. The Latin Hypercube simulation technique that selects single value at random from each interval was selected; see section 5.4.2 in Chapter 5.

The outcomes of the pseudo-randomly distributed quality index Q achieved after simulation by @Risk are shown in Figure 6-3. The figure shows the relative frequency (probability density) and cumulative distribution of Q-values representating the iteration results of @Risk for predicted and actual rock mass conditions. The cumulative diagram also includes the distribution of Q-values actually mapped during excavation. The cumulative curve for actually mapped Q-values was constructed based on each segment of tunnel representing a given Q-value divided by the length of fracture zone (in this case 300 meters), and the frequency values were added with increasing value of Q to convert into cumulative form.

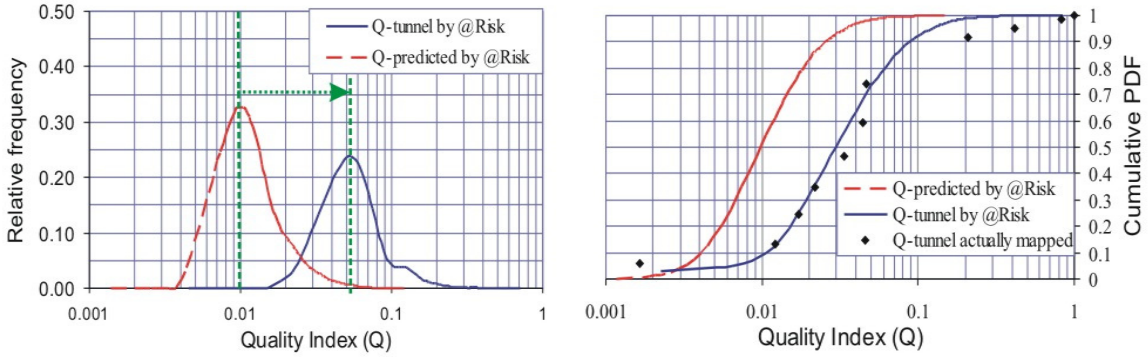

Figure 6-3. Distribution of quality index Q between chainage 1900-2200 of the Khimti headrace tunnel.

Figure 6-3 shows that the probability distributions based on @Risk for actual and predicted ranges of the rock mass conditions are slightly different. The rock mass was found to be of slightly better quality than anticipated based on prediction. However, this variation is not as big as it seems since almost ninety percent of Q-values are lower than 0.1, indicating very poor rock mass (see also Table 6-1).

The cumulative probability distribution as calculated from actual data by @Risk and the distribution of actually mapped values of the quality indexes Q are found to be in close agreement, see Figure 6-3 right. As indicated, the assigned probability density functions of input variables in Table 6-1 are fairly representative of the real ground conditions.

6.2.1.2 Section with fairly good rock (Chainage 2200 - 2700)

This is a tunnel section located upstream of Adit 2, see Figure 6-2. During planning the rock mass in this section was predicted to be of fair to good quality. In reality, the rock mass was found to be poor to fair. In the tunnel, the rock mass was found to consist mainly of fresh to moderately weathered and jointed mica gneiss in intercalation with thin bands (less than 1 meter) of weak, highly weathered and deformed talcose mica schist.

Defining probability density function (pdf): The predicted and actual ranges of input variables for Q-value with their minimum, maximum, mean and most likely values are given in

Table 6-2. In addition, assumed probability density functions of each input variable and mapped value for the simulation by @Risk are given.

Table 6-2. Predicted and actual ranges of input parameters for Q-values with assumed probability density functions (pdf) between chainage 2200-2700 of the Khimti headrace tunnel.

Descriptions of Q-value parameters	Rating ranges of Q-value parameters					Assumed probability density function (pdf)
	Min. (x_{min})	Max. (x_{max})	Mean / most likely	St. dev. (s)	@Risk value	
A. Predicted						
RQD	50	80	65	15	64.62	Normal, Truncate (10;100)
J_n	12	4	9		8.33	Triangular, Truncate (1;20)
J_r	1.5	4	3	1	2.73	Normal, Truncate (0.5;4)
J_a	4	2	3	1	3.03	Normal, Truncate (0.75;20)
J_w	0.66	1	1		0.89	Triangular, Truncate (0.05;1)
SRF	2.5	1	1		1.50	Triangular, Truncate (1;10)
Q-value	0.431	40	7.222		4.130	
B. Actual						
RQD	40	85	65	15	64.62	same as above
J_n	15	6	9		10.00	
J_r	1	3	1.5	0.5	1.53	
J_a	4	2	3	1	3.03	
J_w	0.5	1	1		0.83	
SRF	2.5	1	2.5		2.00	
Q-value	0.133	21.25	1.444		1.357	

For fair to good quality rock mass, most of the mapped ratings for *RQD*, J_r and J_a in the tunnel have indicated clustering to the center or towards their mean. Therefore, normal probability density function is assumed for *RQD*, J_r and J_a, see Table 6-2,

The input variable *RQD* is described with a rating between 50 to 90, and its mean value is somewhere between 60 and 70. Likewise, most of the discontinuities in such rock mass are described to be rough - undulating to rough – planar with rock wall contact. For that reason, a mean or most likely J_r rating of 3 with minimum and maximum values of 1.5 and 4, respectively, are used for the predicted values. Similarly, with respect to alteration, most of the discontinuities in fair to good quality rock mass are described to have no mineral filling, only coating. Therefore, a mean or most likely J_a rating of 3 with maximum and minimum values of 2 and 4 are used for the predicted values. The actual ranges of RQD, J_r *and* J_a values given in the Table 6-2 are calculated based on recording in the tunnel during excavation.

A triangular distribution of probability density function is assumed for the input variable J_n, J_w and *SRF*. The arguments are the same as in Section 6.2.1.1.

For fair to good quality rock mass, it is logical to predict that there will be less than three joint sets. As discussed in Chapter 4, the rock mass at Khimti are highly fractured and has

three prominent joint sets. Consequently, it is predicted that the maximum J_n value is in the range of 4, the most likely value is estimated as 9, and for extreme conditions the minimum value is estimated to 12, see Table 6-2. Actual ranges of J_n values given in Table 6-2 are calculated based on recordings from the tunnel during excavation.

Since there are no water sources above this tunnel section that feed the rock mass, it is logical to assume that this tunnel section will mostly be in dry conditions but with occasional inflow during the monsoon. For that reason, most likely J_w rating is in the range of 1.0, and the maximum and minimum values are estimated to 1.0 and 0.66, respectively, see Table 6-2. In the table, the actual ranges of J_w with a most likely rating of 1, maximum of 1 and minimum of 0.5 are established from mapping in the tunnel during excavation.

The overburden in this section of the tunnel is less than 200 meters, giving no stress induced problem, but it is most likely that thin bands of sheared talcose mica schist may be present in the rock mass. For that reason, it is logical to assume a most likely SRF value of 1 and maximum and minimum values 1 and 2.5, respectively, see Table 6-2. In the table, actual ranges of SRF with a most likely rating of 2.5, maximum 1 and minimum 2.5 are established from mapping in the tunnel.

Achieved simulation results: The @Risk uncertainty analysis model was run after defining and assigning the probability density functions (pdf) for each input variable of the quality index Q as given in Table 6-2. The simulation settings of @Risk were specified as discussed in Section 6.2.1.1. The outcomes for pseudo-randomly distributed quality index Q based on simulation by @Risk are shown in Figure 6-4.

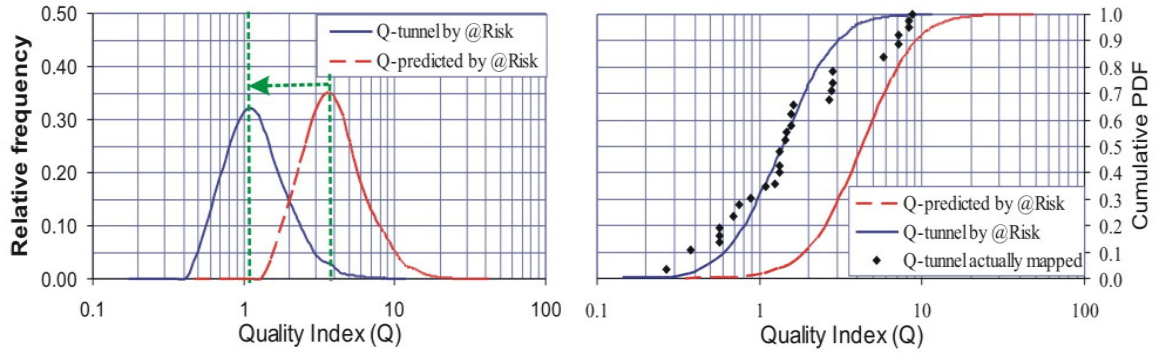

Figure 6-4. Distribution of quality index Q between chainage 2200-2700 of the Khimti headrace tunnel.

The figure shows relative frequency (probability density) and cumulative distributions of Q-values for predicted and actual rock mass conditions. The cumulative curve for actually mapped Q-values in the tunnel is based on summarizing segments of the tunnel with a given Q-value and dividing by the selected tunnel length (in this case 500 meters). The frequency values are added with increasing value of Q to convert into cumulative form.

Figure 6-4 shows that the probability distributions based on @Risk are slightly different for actual and predicted ranges of the rock mass conditions. The rock mass was found to be more altered and weathered with frequent intercalation of thin bands of talcose mica schist than anticipated during prediction.

The cumulative probability distribution as calculated from actual data by @Risk, and the distribution of actually mapped values of Q, are found to be in fairly good agreement, see Figure 6-4 right. This indicates that the assigned probability density functions of input variables in Table 6-2 are fairly representative of the real ground conditions.

6.2.1.3 Section with high deviation (Chainage 3294 - 3900)

This is a tunnel section representating Adit 2 junction and 600 meters downstream, see Figure 6-2. During planning, the rock mass in this section was predicted to be of fair to good quality. In reality, the rock mass was found to be of exceptionally poor to poor quality, i.e. to deviate considerably from what was predicted. In the tunnel, the rock mass was found to consist mainly of moderately to highly weathered and highly fractured mica gneiss in intercalation with multiple thick bands (more than 1 meter) of very weak, highly altered, weathered and highly deformed talcose mica schist.

Defining probability density function (pdf): The predicted and actual ranges of input variables for Q-value with their minimum, maximum, mean and most likely values are given in Table 6-3. In addition, the assumed probability density functions of each input variable and the mapped values for simulation by @Risk are given.

Since fair to good quality rock mass was predicted during planning, the assumed probability density functions for predicted input variables of Q were considered to be as described in Section 6.2.1.2. In reality, the rock mass in the tunnel can be regarded as a weakness zone. Actually mapped ratings of input variables *RQD*, J_r and J_a in the tunnel were found to be randomly scattered, with most of the values clustered towards the lower ranges of their rating, representating lognormal distributions. Thus, the probability density functions of actual rock mass are considered similar to those described in Section 6.2.1.1.

During planning, the rock mass in this section was described to be more fractured than discussed in Section 6.2.1.2. For that reason, the *RQD* was estimated to have a rating between 40 and 70, and a mean value of 50 to 60. Most of the discontinuities were described to be rough - undulating to rough – planar with rock wall contact. For that reason, a mean or most likely J_r rating of 3 and maximum and minimum values of 4 and 1.5, respectively, were estimated. Similarly, a mean or most likely J_a rating of 3 and minimum and maximum values of 6 and 2 were predicted. Actual ranges of *RQD*, J_r *and* J_a values as shown in Table 6-3 were calculated based on mapping in the tunnel during excavation.

Table 6-3. Predicted and actual ranges of input parameters for Q-values with assumed probability density functions (pdf) between chainage 3294-3900 of the Khimti headrace tunnel.

Descriptions of Q-value parameters	Rating ranges of Q-value parameters					Assumed probability density function (pdf)
	Min. (x_{min})	Max. (x_{max})	Mean / most likely	St. dev. (s)	@Risk value	
A. Predicted						
RQD	40	70	55	15	55	Normal, Truncate (10;100)
J_n	12	6	9		9	Triangular, Truncate (1;20)
J_r	1.5	4	3	1	2.73	Normal, Truncate (0.5;4)
J_a	6	2	3	2	3.49	Normal, Truncate (0.75;20)
J_w	0.33	1	0.5		0.61	Triangular, Truncate (0.05;1)
SRF	2.5	1	1		1.50	Triangular, Truncate (1;10)
Q-value	0.110	23.33	3.361		2.001	
B. Actual						
RQD	10	55	30	20	30.42	Lognormal, Truncate (10;100)
J_n	20	6	12		12.67	Triangular, Truncate (1;20)
J_r	0.5	3	1	0.5	1.07	Lognormal, Truncate (0.5;4)
J_a	15	3	10	5	9.32	Lognormal, Truncate (0.75;20)
J_w	0.5	1	0.66		0.74	Triangular, Truncate (0.05;1)
SRF	10	2.5	7.5		6.67	Triangular, Truncate (1;10)
Q-value	0.001	3.667	0.022		0.030	

As discussed, the rock mass at this section is highly fractured and has three prominent joint sets. Consequently, a maximum J_n value is in the range of 6, a most likely value of 9 and an extreme minimum value of 12 were predicted, see Table 6-3. The actual ranges of J_n values given in Table 6-3 are calculated based on actually mapped values during excavation.

This section of tunnel is located below a gentle surface slope (less than 25 degrees) and a paddy field where small water springs are located. This means that the ground water table is close to the surface, representating maximum water pressure of up to 15 bars. For that reason, a most likely J_w rating in the range of 0.5 and maximum and minimum values of 1.0 and 0.33, respectively, are assumed, see Table 6-3. Actual ranges of J_w with most likely rating of 0.66, maximum 1 and minimum 0.33 were established based on actually mapped values in the tunnel.

The overburden at this section of the tunnel is less than 150 meters and represents no stress induced problem. Since the predicted rock mass quality was fair to good, SRF values similar to those in Section 6.2.1.2 were predicted, see Table 6-3. Actual ranges of SRF with most likely rating of 7.5, maximum 2.5 and minimum 10 were established based on actually mapped values in the tunnel.

Achieved simulation results: The @Risk uncertainty analysis model was run after defining and assigning the probability density functions (pdf) for each input variable of the quality index Q as given in Table 6-3. The simulation settings of the @Risk model were specified

as described in Section 6.2.1.1. The outcomes for the pseudo-randomly distributed quality index Q achieved based on simulation by @Risk are shown in Figure 6-5.

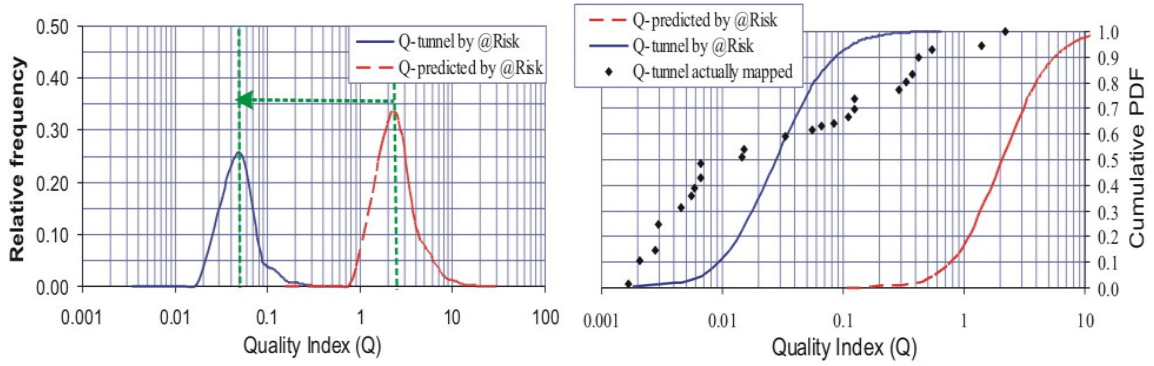

Figure 6-5. Distribution of quality index Q between chainage 3294-3900 of the Khimti headrace tunnel.

The figure shows relative frequency (probability density) and cumulative distributions of Q-values representating the iteration results based on @Risk for predicted and actual rock mass conditions. The cumulative diagram also includes the distribution of Q-values for this section of tunnel (606 meters) actually mapped during excavation.

Figure 6-5 shows that there is a great discrepancy between probability distributions for actual and predicted ranges of the rock mass conditions. The rock mass actually found in the tunnel was highly altered and weathered with frequent intercalation of thick bands (above 1 meter) of talcose mica schist. This was not anticipated during prediction, and in reality the rock mass condition of this tunnel section is poor to exceptionally poor with a quality index Q range between 0.001 and 2 (sees also Table 6-3).

As shown by Figure 6-5 right, the cumulative probability distribution calculated from actual data by @Risk and the distribution of actually mapped values of the quality indexes Q are found not to be in close agreement. This indicates that for rock mass with high degree of deviation with respect to quality index Q, it is not easy to assign probability density functions (pdf) of input variables that give results close to real ground conditions. Nevertheless, as shown in Table 6-3, the mean values of Q-tunnel calculated by @Risk (0.03) and actually measured (0.022) are not very different.

6.2.2 Modi Khola headrace tunnel

The uncertainty analysis carried out in Section 6.2.1 indicates that the probabilistic approach is a useful tool for evaluating rock mass quality. As discussed, quantifying input parameters for the rock quality index (Q) is subjective and very much dependent on the personal judgement of the user. Keeping this in mind, the probabilistic approach will now be used for evaluating rock mass quality at two sections of Modi Khola headrace tunnel. At

this tunnel, both rock formation and the team of engineering geologists involved in the construction are different from Khimti.

As discussed in Section 4.3.3, of the 1,492 meters long headrace tunnel, the uppermost section (up to 325 meters) consists of extremely fractured and highly weathered quartzite with intercalation of extremely sheared and decomposed phyllitic schist. The remaining section of the headrace tunnel mostly passes through very hard, abrasive and fractured quartzite, see Figure 6-6. The discrepancy between predicted and actual rock mass conditions for this headrace tunnel was found to be relatively small, see Figure 4-16.

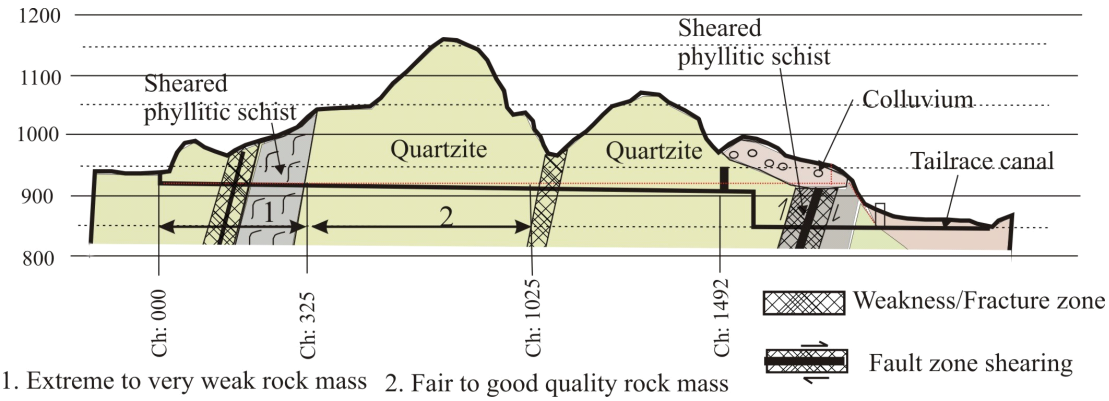

Figure 6-6. Modi tunnel profile indicating two tunnel sections used for the uncertainty analysis.

As shown in Figure 6-6, two sections of the headrace tunnel representating two extreme situations with respect to rock mass quality are selected for the uncertainty analysis.

6.2.2.1 Section with extreme to very weak rock mass (Chainage 0 - 325)

This section of the tunnel has relatively low overburden (less than 100 meters), see Figure 6-6. During planning this section was considered to be a highly fractured zone with a potential of moderate ground water inflow. In reality, the rock mass was found to be highly weathered and extremely weak, representating a weakness zone. In the tunnel, the rock mass in the upstream section of approximately 225 meters was found mainly to consist of highly fractured and extremely weathered quartzite with frequent intercalations of bands of extremely weak, highly sheared phyllitic schist. After this, the rock mass was dominated by a shear zone consisting of highly sheared and decomposed phyllitic schist until chainage 325.

Defining probability density functions (pdf): The predicted and actual ranges of input variables for Q-value with their minimum, maximum, mean and most likely or median values are given in Table 6-4. In addition, assumed probability density functions of each input variable and mapped value for the simulation of @Risk model are given. Since this tunnel section represents a fracture zone the assumed probability density functions are considered to be the same as described in Section 6.2.1.1.

Table 6-4. Predicted and actual ranges of input parameters for Q-value with assigned probability density functions (pdf) for chainage 0-325 of the Modi Khola headrace tunnel.

Descriptions of Q-value parameters	Rating ranges of Q-value parameters					Assumed probability density function (pdf)
	Min. (x_{min})	Max. (x_{max})	Mean / most likely	St. dev. (s)	@Risk value	
A. Predicted						
RQD	10	40	25	15	26.28	Lognormal, Truncate (10;100)
J_n	20	9	15		14.67	Triangular, Truncate (1;20)
J_r	0.5	1.5	1	0.5	1.07	Lognormal, Truncate (0.5;4)
J_a	15	8	15	5	13.47	Lognormal, Truncate (0.75;20)
J_w	0.5	0.66	0.5		0.55	Triangular, Truncate (0.05;1)
SRF	10	5	7.5		7.50	Triangular, Truncate (1;10)
Q-value	0.001	0.110	0.007		0.010	
B. Actual						
RQD	10	55	25	15	26.28	Same as above
J_n	20	12	15		15.67	
J_r	0.5	2	1	0.5	1.07	
J_a	20	6	12	5	11.09	
J_w	0.5	1	0.66		0.72	
SRF	10	2.5	6.3		6.25	
Q-value	0.001	0.611	0.015		0.019	

Achieved simulation results: The @Risk uncertainty analysis was run after defining and assigning the probability density functions (pdf) for each input variable of the quality index Q as shown in Table 6-4. The simulation settings of the @Risk model were specified to single number of simulation and maximum iterations of 5000. The Latin Hypercube simulation technique that selects single values at random from each interval was selected, see Section 5.4.2. The outcomes of the pseudo-randomly distributed quality index Q based on simulation by @Risk are shown in Figure 6-7.

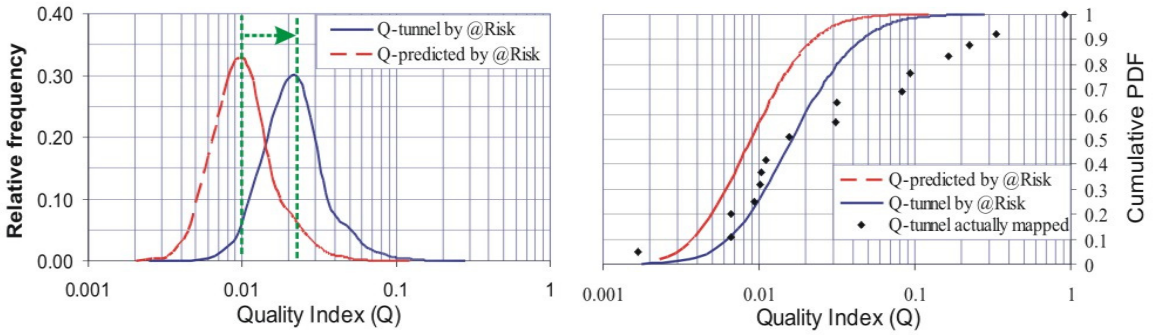

Figure 6-7. Distribution of quality index Q between chainage 0-325 of the Modi Khola headrace tunnel.

The figure shows relative frequency (probability density) and cumulative distributions of Q-values representating the iteration results based on @Risk for predicted and actual rock mass conditions. The cumulative diagram also includes the distribution of actually mapped Q-values recorded during excavation for the 325 meters long tunnel section.

Figure 6-7 shows that the probability distributions for actual and predicted ranges of the rock mass conditions are very close to each other. The rock mass actually encountered was of slightly better quality than anticipated during prediction. The main reason for this was the thickness of sheared phyllitic schist, which was less than estimated during planning.

The cumulative probability distribution as calculated from actual tunnel data by @Risk and the distribution of actually mapped values of the quality indexes Q in the tunnel are found to be in close agreement for lower ranges (Q-values less than 0.02), see Figure 6-4 right. For higher Q-values (above 0.03) the actually mapped Q-values do not show good correlation with the cumulative distribution of Q-values calculated by @Risk.

6.2.2.2 Section with fair to good quality rock mass (Chainage 325-1025)

This section of the Modi Khola headrace tunnel has moderate overburden (between 75 and 250 meters). The rock mass mainly consists of very hard, abrasive, fresh to slightly weathered but highly jointed quartzite, see Figure 6-7. The discontinuity surfaces in the tunnel were observed to be altered and filled with silt and clay, but the overall quality of rock mass observed in the tunnel was found to be of fair to good quality, as predicted during planning.

Defining probability density functions (pdf): The predicted and actual ranges of input variables for Q-value with their minimum, maximum, mean and most likely values are given in Table 6-5. In addition, assumed probability density functions of each input variable and mapped value for simulation by @Risk are given. Since this tunnel section represents rock mass having fair to good quality, the assumed probability density functions are considered to be similar to those described in Section 6.2.1.2.

Achieved simulation results: The @Risk uncertainty analysis model was run after defining and assigning the probability density functions (pdf) for each input variable of the quality index Q as given in Table 6-5. The simulation settings of the @Risk model were specified as described in Section 6.2.2.1. The outcomes of the pseudo-randomly distributed quality index Q achieved after simulation by @Risk are shown in Figure 6-8.

Figure 6-8 shows relative frequency (probability density) and cumulative distributions of Q-values representating the iteration results based on @Risk for predicted and actual rock mass conditions. The cumulative diagram also includes the distribution of Q-values recorded during excavation, in this case for a 700 meters long tunnel section.

Table 6-5. Predicted and actual ranges of input parameters for Q-value with assigned probability density functions (pdf) for chainage 325-1025 of the Modi Khola headrace tunnel.

Descriptions of Q-value parameters	Rating ranges of Q-value parameters					Assumed probability density function (pdf)
	Min. (x_{min})	Max. (x_{max})	Mean / most likely	St. dev. (s)	@Risk value	
A. Predicted						
RQD	60	90	75	15	73.45	Normal, Truncate (10;100)
J_n	9	4	6		6.33	Triangular, Truncate (1;20)
J_r	1	3	2	1	2.08	Normal, Truncate (0.5;4)
J_a	3	1	2	1	2.20	Normal, Truncate (0.75;20)
J_w	0.66	1	1		0.89	Triangular, Truncate (0.05;1)
SRF	2.5	1	1		1.50	Triangular, Truncate (1;10)
Q-value	0.58	67.50	12.50		6.48	
B. Actual						
RQD	50	85	65	10	65.00	Same as above
J_n	12	9	9		10.00	
J_r	1	3	2	1	2.08	
J_a	4	1	2	1	2.20	
J_w	0.66	1	1		0.89	
SRF	1.5	1	1		1.17	
Q-value	0.45	28.33	7.22		4.67	

Figure 6-8 shows that the probability distributions based on @Risk are very close to each other for actual and predicted ranges of the rock mass conditions. The actual rock mass was found to be slightly more altered and weathered than what was anticipated.

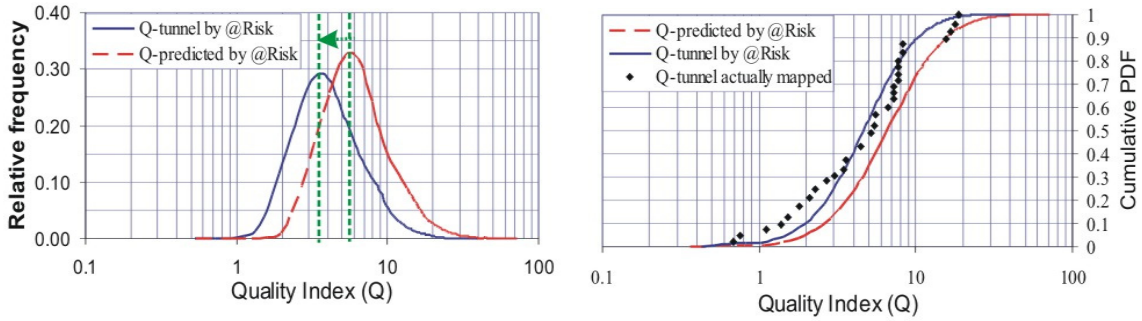

Figure 6-8. Distribution of Q between chainage 325-1025 of the Modi Khola headrace tunnel.

The cumulative distribution as calculated from actual data by @Risk and the distribution of actually mapped values of Q are also found to be in close agreement, see Figure 6-8 right. As seen in the left figure, there is a good overlap in the frequency distributions for predicted and actually mapped Q-values. This indicates that the assigned probability density functions of input variables in Table 6-5 are representative of the real ground conditions.

6.3 TUNNEL SQUEEZING

Severe tunnel squeezing is extremely difficult to tackle, and is a major challenge in tunnelling through Himalaya rock masses. As discussed in Chapters 1, 2 and 4, the rock masses in the region are weak, highly deformable and anisotropic in their character. Severe tunnel squeezing is very common in weak rocks such as shale, slate, phyllite and schist of the lesser Himalayan and Siwaliks zones, and in weakness / fault zones.

All the cases described in Chapter 1 and 4 have been affected by tunnel squeezing of different magnitudes. Severe tunnel squeezing occurred at Kaligandaki headrace tunnel and at a fault zone of Modi pressure tunnel. At Khimti headrace tunnel, there were only three locations where the tunnel convergence exceeded one percent, with a maximum 4.5 percent below Hawa Khola, see Figure 4-2 and 6-9. In the Middle Marsyangdi headrace tunnel, minor squeezing (up to one percent) has been experienced at some locations of already excavated tunnel. It is however expected that more severe tunnel squeezing will occur while tunnelling through the geological sections between Jamitri and Khahere Khola, see Figure 4-13. This section consists of rock mass of poor quality; mainly micaceous phyllite in intercalation with bands of siliceous phyllite and metasandstone. In addition, the headrace tunnel has an overburden as high as 410 meters.

The following two Sections of this research are focusing on the use of the probabilistic approach for estimating degree of tunnel squeezing for Kaligandaki and Middle Marsyangdi headrace tunnels. Hoek and Marinos (2000) approach for predicting tunnel squeezing as discussed in Section 3.3 and Equation 3-1 for estimating rock mass strength are used as a basis for the analysis. Equations 3-12 and 3-14 as also given in Table 6-6, intact rock properties as given in Section 4.7, test results of the project implementation phases of respective projects and measured tunnel deformations of Kaligandaki headrace tunnel are the key factors used in the analysis.

Table 6-6. Basic equations used for squeezing analysis.

Equation no.	Equations	Remarks
3-1	$\sigma_{cm} = \frac{\sigma_{ci}^{1.5}}{60}$	For calculating ranges of rock mass strength.
3-12	$\varepsilon_t = \left(0.2 - 0.25 \times \frac{p_i}{\sigma_v}\right) \times \left[\frac{\sigma_{cm}}{\sigma_v}\right]^{\left(2.4 \times \frac{p_i}{\sigma_v} - 2\right)}$	Tunnel strain in percent with support pressure.
3-14	$\varepsilon_t = 0.2 \times \left(\frac{\sigma_{cm}}{\sigma_v}\right)^{-2}$	Tunnel strain in percent without support pressure.

For Kaligandaki headrace tunnel, a section with overburden exceeding 400 meters and consisting of weak graphitic phyllite is selected (between chainage 1964 – 4032, see Figure 4-6). At this section of the headrace tunnel, severe tunnel squeezing occurred during tunnel excavation. Since actually measured tunnel deformations are available, main emphasis is

placed on verifying the reliability of Hoek and Marinos approach for Kaligandaki. After this verification, prediction is made on anticipated degree of tunnel squeezing in Middle Marsyangdi headrace tunnel for a section between Jamitri and Khahare Kola (between chainage 2000 -3400, see Figure 4-13).

In terms of probabilistic approach, the tunnel strain (ε_t) defined by Equation 3-12 and 3-14 is considered as an uncertainty that is dependable mainly on three variable input parameters; i.e. rock mass strength (σ_{cm}), overburden stress (σ_v) and rock support pressure (p_i). This means that the main principle of uncertainty analysis based on Hoek and Marinos approach is to define the uncertainties of these variable input parameters. The tunnel strain is expressed in percentages, and is defined as:

$$\varepsilon_t = \frac{\delta_t}{B} \times 100 \qquad (6\text{-}2)$$

Where; δ_t is total horizontal convergence in meters and B is the excavation width or diameter of the tunnel in meters.

6.3.1 Tunnel squeezing pattern

As discussed in Chapter 3, weak rock masses are incapable of sustaining high tangential stress. When the rock mass strength becomes less than overburden stress, a time dependent creep (deformation) occurs along the periphery of the tunnel. Immediately after tunnel excavation, most of the rock pressure is carried by the face itself. As excavation advances, there is a gradual decrease in face effect and tunnel deformation (inward movement) increases until it reaches its final value some distance from the face.

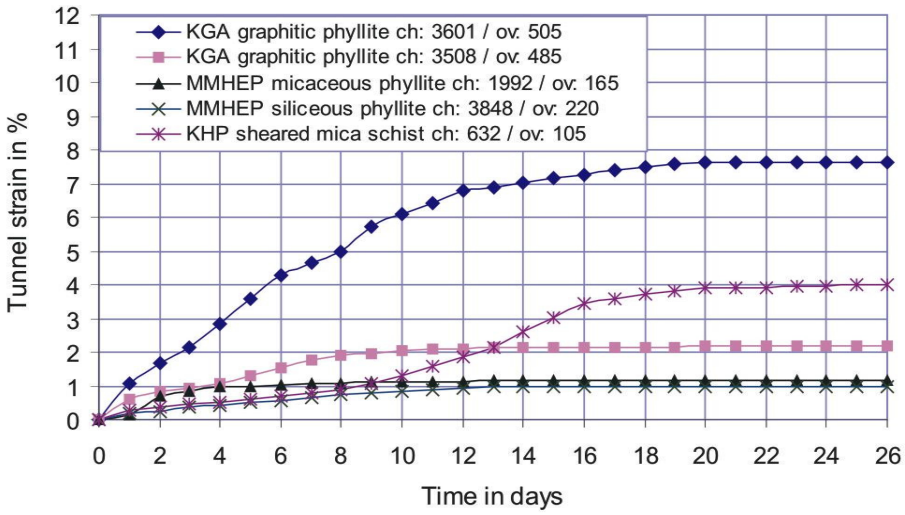

Figure 6-9. Measured time dependent tunnel strains in some selected sections of the project cases. KGA = Kaligandaki "A", MMHEP = Middle Marsyangdi and KHP = Khimti headrace tunnels, ch: = chainage and ov: = overburden.

Figure 6-9 shows a typical example of tunnel convergence pattern at some selected sections of three of the project cases. As seen in the figure, most of the inward movement (tunnel strain) occurred within 20 days of excavation. In the case of Khimti, the deformation intensified after 10 days of excavation. At this section, the Khimti headrace tunnel met a fault zone (Hawa Khola), see Figure 4-2, and there was a considerable delay in tunnel advancement caused by considerable water inflow into the tunnel (CCC, 2002).

Tunnelling experience from the cases discussed in Chapter 4 suggests that average achievable tunnel advancement in difficult ground conditions for tunnels having cross section less than 60 m^2 is between 1 and 1.5 meters a day. Hence, based on Figure 6-9 it seems logical to assume that most of the tunnel deformation (more than 90 percent) occurs less than approximately two tunnel diameters behind the face.

6.3.2 Squeezing analysis for Kaligandaki headrace tunnel

For the uncertainty analysis of tunnel squeezing at Kaligandaki headrace tunnel, a slightly more than two kilometers long tunnel section between chainage 1964 and 4032 is selected. At this section, the headrace tunnel passes through highly schistose graphitic phyllite, and has overburden ranging from 425 to 620 meters.

6.3.2.1 Measured tunnel deformation (Chainage 1964-4032)

During tunnel excavation, this section of the headrace tunnel experienced severe stability problems caused by tunnel squeezing. The measured horizontal convergence (δ_t) along the BC line (see Figure 6-10) of this section of the headrace tunnel is given in Table 6-7.

Out of 214 convergence measurement stations along the headrace tunnel, 129 stations were located within this section of the headrace tunnel. Convergence readings were made by using tape extensometer with 2, 4, 5 and 7 pins system as shown in Figure 6-10. According to NEA (2002b), the horizontal convergence measured in this tunnel stretch was mostly highest for the BC line, which indicates domination of overburden stress on total tunnel strain.

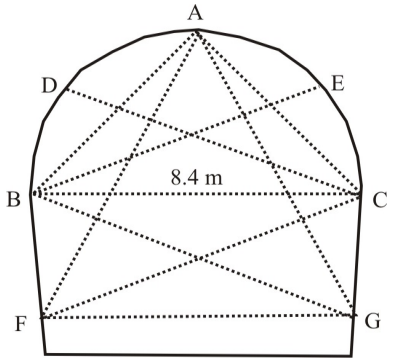

Figure 6-10. Headrace tunnel section indicating tape extensometer measuring points (NEA, 2002b).

Table 6-7. Measured horizontal convergence along the BC line of Kaligandaki headrace tunnel between chainage 1964 – 4032 (based on NEA, 2002b).

Chainage (m)	Convergence (cm)	Chainage (m)	Convergence (cm)	Chainage (m)	Convergence (cm)	Chainage (m)	Convergence (cm)	Chainage (m)	Convergence (cm)	Chainage (m)	Convergence (cm)	Chainage (m)	Convergence (cm)
1964	25.3	2282	31.8	2594	31.8	2894	7.21	3250	7.8	3522	9.4	3736	26.4
1992	12.1	2295	14.8	2613	16.2	2910	10.8	3259	9	3538	21.3	3744	22.8
2009	5	2301	23.6	2622	17.7	2928	6.5	3278	6.7	3548	17.6	3754	22.1
2020	19.6	2326	25.1	2640	36.4	2945	6.1	3289	9.3	3563	20.9	3764	33.8
2060	12	2337	51.8	2655	47.7	2965	6.8	3302	8.3	3581	20.1	3774	43.4
2073	14.1	2346	35.3	2662	41.5	2988	16.9	3311	7.8	3588	22.6	3786	23.7
2121	16.1	2361	20.7	2676	25.7	3008	13.3	3327	16.2	3596	49.6	3800	21.9
2138	14.1	2371	22.4	2704	16.3	3028	12	3342	31.7	3601	64.4	3815	21.7
2156	42.8	2385	21	2719	25.9	3071	8.7	3349	30.4	3612	65.1	3836	17.1
2167	74.6	2392	17.5	2729	65.4	3110	16.7	3358	23.5	3624	21.7	3865	14.9
2184	68	2416	11.1	2743	51	3137	7.6	3369	16.8	3636	55.3	3872	14.8
2195	55	2434	27	2750	28.7	3158	5.4	3387	31.4	3645	40.9	3914	16.5
2208	71.2	2446	21.9	2763	10.7	3167	5.9	3406	10	3654	32	3937	13.1
2217	38	2464	16	2778	18.4	3174	4.9	3416	6	3662	46.2	3982	6.6
2229	35.5	2487	11.2	2811	11	3183	4.5	3442	9.7	3676	19.4	4032	9.8
2243	21.9	2532	11.6	2820	5.2	3203	7	3460	7.8	3688	16.5		
2258	22.6	2549	20.4	2841	3.4	3214	8.5	3473	14.8	3703	12		
2270	30.7	2566	20.6	2862	3.6	3223	6.4	3494	14.9	3713	15.2		
2275	33.8	2579	28.6	2875	4.5	3236	4.8	3508	18.2	3727	23.8		

The horizontal convergence given in Table 6-7 is converted to strain (ε_t) by using Equation 6-2. The calculated tunnel strains for respective instrumentation chainage are shown in Figure 6-11. The figure also shows the overburden height.

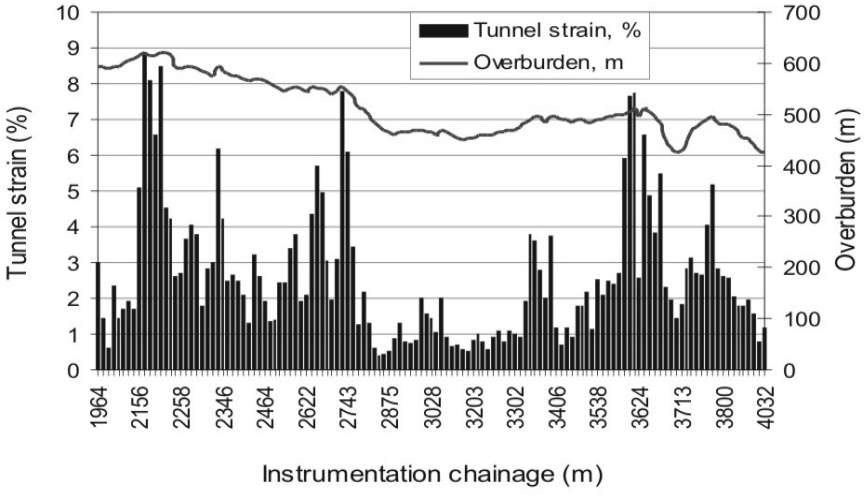

Figure 6-11. Horizontal strain in % between chainage 1964 and 4032 in Kaligandaki headrace tunnel (based on the data in Table 6-7 and Figure 4-6).

Figure 6-11 shows that the magnitudes of horizontal tunnel strain vary considerably within this section of the headrace tunnel. The figure also illustrates that even within similar overburden height there is a considerable difference in degree of tunnel squeezing. This suggests that the quality of rock mass, and in particular rock mass strength, varies greatly within short tunnel distances.

Figure 6-12 shows the measured tunnel strains as cumulative curve. This cumulative curve is based on adding segments of identical tunnel strain in ascending order and dividing by the tunnel length (in this case 2068 meters). In this process, an approximation is based on the assumption that similar magnitude of tunnel deformation occurred for a tunnel segment representating 50% length at each side of the instrumentation chainage given in Table 6-7.

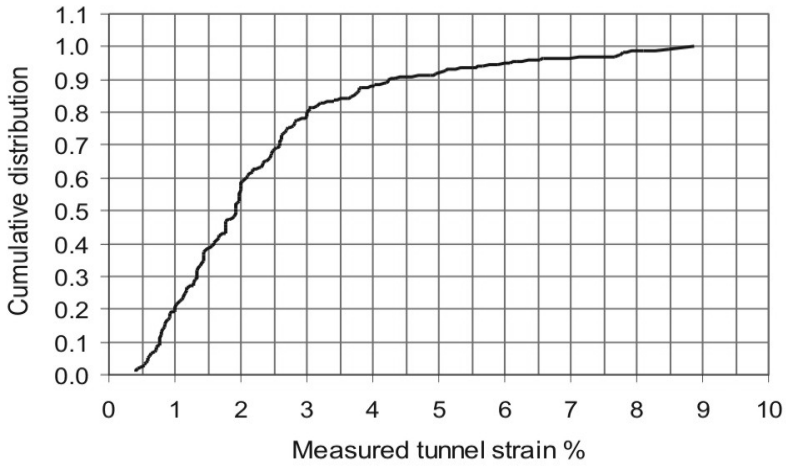

Figure 6-12. Cumulative distribution of calculated tunnel strain in % between chainage 1964 and 4032 of Kaligandaki headrace tunnel calculated by using data from Table 6-7 and Equation 6-2.

As shown by the figure, approximately 10 percent of the tunnel length has tunnel strain between 5 - 9 percent and approximately 20 percent has tunnel strain between 2.5 – 5 percent. This indicates very severe and severe squeezing, respectively, according to Hoek and Marinos classification of degree of difficulties (see Figure 3-18 right). This means that out of 2068 meters tunnel length approximately 620 meters had severe to very severe squeezing condition.

6.3.2.2 Estimation based on @Risk (Chainage 1964-4032)

In the following an uncertainty analysis is performed to estimate tunnel squeezing between chainage 1964 and 4032 of the Kaligandaki headrace tunnel. The @Risk tool described in Chapter 5 and Hoek and Marinos approach for estimating tunnel strain are used for this purpose. The simulation results of tunnel strain achieved by @Risk by using equation 3-12, 3-14 and 3-1 (see Table 6-6 and Chapter 3) will be compared with the actual tunnel strain shown in Figure 6-11 and 6-12.

Ranges of input variables for graphitic phyllite: There are mainly four variable input parameters that need to be defined for the estimation of tunnel strain (ε_t) based on Equation 3-12 and 3-14. These are; 1) rock mass strength (σ_{cm}), 2) specific weight of the rock (γ), 3) overburden height (h) and 4) rock support pressure (p_i).

Laboratory tested intact rock strength of graphitic phyllite as given for 50 mm equivalent diameter in Table 4-6 is used as mean value. As minimum and maximum intact rock strength, laboratory tested results given by NEA (2002b) are used. Specific weight of graphitic phyllite is calculated by using density of the same rock as given in Table 4-6. The total pressure cell measurements conducted at five locations of the headrace tunnel during construction (NEA, 2002b) indicated rock support pressure (p_i) ranging between 0.46 and 1.27 MPa. Table 6-8 defines the input variables with their statistical ranges.

Table 6-8. Estimated input variables for graphitic phyllite of Kaligandaki headrace tunnel.

Description of input variables	Units	Minimum	Maximum	Mean	Standard deviation
Overburden height (h)	m	425	620	505	60
Rock density	gm/cm^3	-	-	2.77	-
Specific weight (γ)	MN/m^3	-	-	0.027	-
Overburden pressure ($\sigma_v = \gamma h$)	MPa	11.47	16.74	13.63	2.1
Intact rock strength (σ_{ci})*	MPa	28	50	39	8.5
Support pressure (p_i)**	MPa	0.46	1.27	0.71	0.3

* Mean values of UCS test at Ch: 1881 = 28.3, Ch: 1883 = 49.5, Ch: 1984 = 46.1, Ch: 2077 = 35.6 MPa.
** Five total pressure cell embedded in shotcrete lining gave results of 0.58, 0.64, 0.46, 0.56 and 1.27 MPa in 520 days. Source NEA (2002b).

Defining probability density function (pdf): As shown in Table 6-8 a constant value of specific weight for graphitic phyllite is used. The variation of density is generally small and its effect on the overburden pressure is therefore considered insignificant. The estimated statistical ranges of input variables based on Table 6-8, Equation 3-1, 3-12 and 3-14 are given in Table 6-9. The table highlights the minimum, maximum and mean values of input variables and the respective tunnel strain (ε_t). In addition, the assigned probability density function for each input variable and the most likely value of each input variable achieved by @Risk are also shown in the table.

In Table 6-9, exponential probability density function is assumed for the input variable inverse to overburden pressure ($1 / \gamma h$). In fact, the higher the overburden (h), the smaller the value of $1 / \gamma h$, but the more likely squeezing is to occur. Similarly, the lower the overburden (h), the higher the value of $1 / \gamma h$, but the less likely squeezing is to occur. Therefore, exponential probability density function is considered to be the most representative distribution model for $1 / \gamma h$. At this section of the headrace tunnel, it is unlikely to have an overburden (h) higher than 620 meters and lower than 400 meters, see Figure 4-6 and 6-11. Therefore, a truncation is applied for $1 / \gamma h$ with minimum and maximum values of 0.057 and 0.09, respectively.

Table 6-9. Statistical ranges of input variables for graphitic phyllite of Kaligandaki headrace tunnel and assumed probability density functions (pdf).

Description of input variables	Minimum	Maximum	Mean	Standard deviation	@Risk values	Assumed pdf
$1/\sigma_v = 1/\gamma h$	0.060	0.087	0.073	0.011	0.076	Exponential, Truncate (0.057; 0.09)
σ_{cm} (Eq. 3-1)	2.47	5.89	4.05	1.21	4.28	Normal, Truncate (1.0; 10)
p_i	0.46	1.27	0.71	0.3	0.75	Normal, Truncate (0.3; 1.5)
$\sigma_{cm} / \gamma h$	0.148	0.51	0.29		0.34	
ε_t (Eq. 3-12)	7.85	0.54	1.82		1.43	
ε_t (Eq. 3-14)	9.20	0.76	2.26		1.75	

Note: minimum and maximum values of $1/\gamma h$ are the values with highest and lowest overburden, respectively.

As shown in the table, a normal probability density function is assumed for the input variable σ_{cm}. As for a laboratory tested population of intact rock strength, most of the values of rock mass strength should in general cluster towards their mean value, and with a certain dispersion from it representating the standard deviation. Therefore, normal probability density function is considered to be the most representative distribution model for rock mass strength. A truncation is applied with minimum and maximum values of 1.0 and 10 MPa, assuming that it is unlikely to have rock mass strength lower and higher than these fixed values.

Due to small population of measured support pressure (p_i), the distribution pattern is not clearly known. In such uncertain situation, it has been considered logical to use normal probability distribution as described in Section 5.3.2. It is reasonable to assume that when rock support is installed in a tunnel subjected to squeezing condition, this represents some degree of disturbance of the free inward movement of the rock mass. A truncation is therefore applied with minimum and maximum values of 0.3 and 1.5 MPa, respectively. It has been assumed that it is unlikely to have rock support pressure lower and higher than these fixed values.

Achieved simulation results: The @Risk uncertainty analysis model was run after defining and assigning the probability density functions (pdf) for each input variable as given in Table 6-9. The simulation settings of the @Risk model were specified to single number of simulation and maximum iterations of 5000. The Latin Hypercube simulation technique that selects single value at random from each interval was selected. The outcomes for the pseudo-randomly distributed tunnel strain (ε_t) achieved after simulation based on @Risk are shown in Figure 6-13 (see also Table 6-9).

Figure 6-13 shows relative frequency distributions (probability distributions) and cumulative distributions of tunnel strain (ε_t) for 2068 meters of the headrace tunnel (between chainage 1964 and 4032). The figure also incorporates the cumulative curve given in

Figure 6-12 representating tunnel strain calculated based on actually measured horizontal convergence given in Table 6-7.

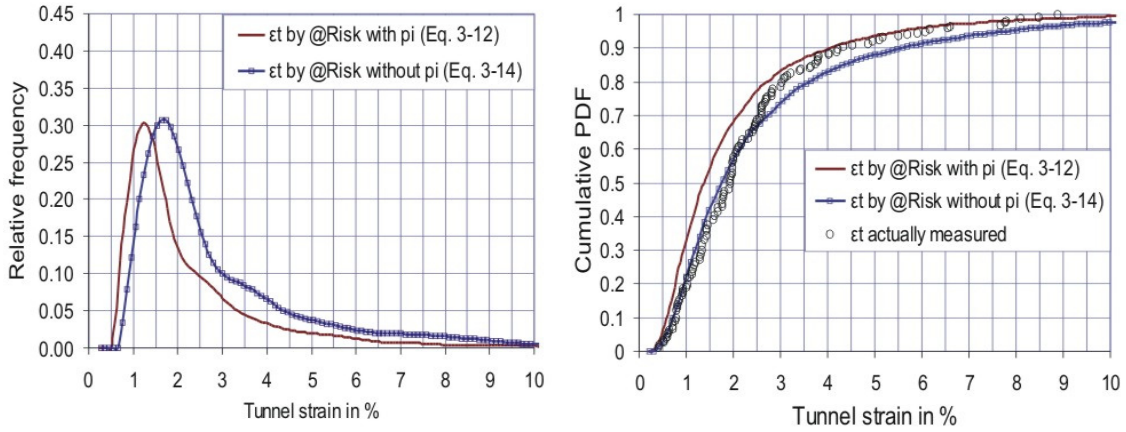

Figure 6-13. Achieved distribution results of tunnel strain between chainage 1964-4032 of Kaligandaki headrace tunnel. The figure to the right also shows actual tunnel strain as given in Figure 6-12.

As shown in Figure 6-13 right, the cumulative probability distribution of the pseudo-randomly calculated tunnel strain based on @Risk and the calculated cumulative distribution of tunnel strain based on actually measured horizontal convergence are found to be in very close agreement. This indicates that the assigned probability density functions for the input variables are realistic.

Figure 6-13 also indicates that the tunnel strains with magnitudes higher than 2.5 percent based on actually measured horizontal convergence are in close agreement with the simulation results of tunnel strain calculated by @Risk based on Equation 3-12. On the other hand, the calculated tunnel strains with magnitudes less than 2.5 percent are in close agreement with the simulation results of tunnel strains achieved by @Risk based on Equation 3-14. Possible reasons for this will be discussed below.

Theoretically, in tunnel sections with low degree of squeezing, the rock mass is not very far away from the elasticity limit. As a result, the rock support pressure (p_i) induced by the rock mass on applied support in principle should be lower in magnitude. In tunnel sections experiencing a high degree of squeezing this is opposite, since the rock mass in such sections is more visco-plastic and there is consistent pressure on the applied support until it fails.

The slight deviation in Figure 6-13 right may also be explained by the fact that the rock mass strength calculated by Equation 3-1 and tunnel strain calculated by Hoek and Marinos approach can not be expected to give results with hundred percent accuracy. In addition, there is a certain degree of uncertainty in the assigned probability density function (pdf)

too. The assigned probability distribution functions assume smooth transition from one segment to another and do not reflect hundred percent accuracy.

The most important aspect of this uncertainty analysis was however to verify the applicability of Equation 3-1, Hoek and Marinos approach and the assigned probability distributions. The correlations achieved for Kaligandaki are considered to be quite good, and a similar approach is believed to be relevant also for predicting the degree of tunnel squeezing in other tunnels passing through weak rock masses.

6.3.3 Estimating squeezing at Middle Marsyangdi (Chainage 2000 – 3400)

The same principle of uncertainty analysis as used for Kaligandaki has been exploited to estimate probable tunnel squeezing for Middle Marsyangdi headrace tunnel. The headrace tunnel section between Jamitri and Khahare Khola (between chainage 2000 and 3400) is selected for this purpose. As discussed in Section 4.3.4, this section of the tunnel passes through rock mass consisting of highly schistose and weak micaceous phyllite in intercalation with thin bands (less than one meter) of siliceous phyllite and highly fractured metasandstone. In addition to weak rock mass, this segment of the headrace tunnel has an overburden varying from 180 to 410 meters, see Figure 4-13.

Recent communication with the project (e-mail from project engineering geologist dated 23rd October 2005) tells that the tunnel crew has reached the Khahare Khola fault. As predicted in Chapter 4, stability problems connected to tunnel squeezing have been experienced at this fault zone. As shown in Figure 6-9, tunnel strain of approximately one percent in magnitude has been recorded at chainage 1992. The recorded tunnel strain is slightly lower in magnitude than what was expected. This may be due to relatively low overburden and very careful excavation with extensive rock support (steel ribs at one meter spacing, 250 mm thick reinforced shotcrete and radial bolting).

Ranges of input variables: Intact rock strength tests for siliceous phyllite and metasandstone have been carried out with results as shown in Table 4-6. As can be seen, the intact rock strength for siliceous phyllite has a mean value of 39 MPa and a standard deviation of 5 MPa. The intact rock strength of metasandstone has a mean value of 73 MPa and a standard deviation of 39 MPa. The highly scattered intact rock strength of metasandstone indicates a high degree of variability.

Due to the highly schistose character of the micaceous phyllite, no cores with sufficient length were possible to achieve for intact rock strength test. The point load test conducted on lump samples on a regular basis by the project (NEA, 2004c) indicates that the I_{s50} for micaceous and siliceous phyllite varies between 1.4 to 3.5 MPa, see Figure 4-25 (in the figure lower range of I_{s50} represents phyllite). Based on these results it is logical to assume that the intact rock strength varies between 20 to 50 MPa in this tunnel section.

The headrace tunnel between Jamitri and Khahare khola has an overburden varying between 180 and 410 meters and a mean value of 296, see Figure 4-13. The density of siliceous phyllite given in Table 4-6 is considered representative for the rock mass in this tunnel section and is used for the estimation of specific weight. For rock support pressure, the results of total pressure cell measurement of Kaligandaki headrace tunnel given in Table 6-7 are considered representative also for this tunnel since the geological conditions are similar. The issue of estimating support pressure in advance is discussed in Section 7.3.2. Table 6-10 defines the input variables used for the uncertainty analysis of the degree of tunnel squeezing.

Table 6-10. Assumed input variables for Middle Marsyangdi headrace tunnel (Ch: 2000-3400).

Description of input variables	Units	Minimum	Maximum	Mean	Standard deviation
Overburden height (h)	m	180	410	296	70
Rock density	gm/cm^3	-	-	2.86	-
Specific weight (γ)	MN/m^3	-	-	0.028	-
Overburden pressure ($\sigma_v = \gamma h$)	MPa	5.04	11.48	8.36	2.1
Point load strength (I_{s50})	MPa	1.4	3.5	2.5	0.70
Intact rock strength ($\sigma_{ci} = 14 \times I_{s50}$)*	MPa	20	50	35	9.5
Support pressure (p_i)	MPa	0.46	1.27	0.71	0.3

* According to Nilsen and Palmstrom (2000) for weak rocks.

Defining probability density function (pdf): The statistical ranges of the input variables based on Table 6-10 and calculation according to Equation 3-1 are given in Table 6-11. The table mainly highlights minimum, maximum and mean values of input variables, and calculated tunnel strains (ε_t). In addition, the assigned probability density functions for each input variable and the most likely or expected value based on @Risk are shown in the table.

Table 6-11. Statistical ranges of input variables for the phyllite at Middle Marsyangdi headrace tunnel and assumed probability density functions (pdf).

Description of input variables	Minimum	Maximum	Mean	Standard deviation	@Risk values	Assumed pdf
$1/\sigma_v = 1/\gamma h$	0.087	0.198	0.121	0.013	0.134	Exponential, Truncate (0.085; 0.21)
σ_{cm} (Eq. 3-1)	1.49	5.89	3.45	1.45	3.59	Normal, Truncate (1.0; 10)
p_i	0.46	1.27	0.71	0.30	0.75	Normal, Truncate (0.3; 1.5)
$\sigma_{cm} / \gamma h$	0.13	1.17	0.38		0.50	
ε_t (Eq. 3-12)	9.27	0.11	1.03		0.59	
ε_t (Eq. 3-14)	11.87	0.15	1.36		0.81	

Note: minimum and maximum values of $1/\gamma h$ are the values with highest and lowest overburden, respectively.

Since the assumed probability density function (pdf) for Kaligandaki headrace tunnel gave good results and the geological conditions are similar, it is considered logical to use similar probability distributions for the uncertainty analysis of Middle Marsyangdi headrace tunnel.

As for Kaligandaki, an exponential probability density function is assumed for the input variable inverse to overburden pressure (1 / γh). At this stretch of headrace tunnel, it is unlikely to have an overburden (h) higher than 420 meters and lower than 170 meters, see Figure 4-13. Therefore, a truncation is applied for 1 / γh with truncated minimum and maximum values representating 0.085 and 0.21, respectively. A normal probability density function is assumed for the input variable σ_{cm}. A truncation is also applied here with truncated minimum and maximum values of 1.0 and 10 MPa, respectively. Correspondingly, a normal probability density function is assumed for the input variable p_i. A truncation is also applied, with truncated minimum and maximum values representating 0.3 and 1.5 MPa, respectively.

Achieved simulation results: The @Risk uncertainty analysis model was run after defining and assigning the probability density functions (pdf) for each input variable as given in Table 6-11. The simulation settings of the @Risk model were specified as described in Section 6.3.2.2. The outcomes for the pseudo-randomly distributed tunnel strain (ε_t) based on @Risk simulation are shown in Figure 6-14 (see also Table 6-11). The figure shows relative frequency distribution and cumulative distribution of the tunnel strain (ε_t) for 1400 meters of the headrace tunnel between chainage 2000 - 3400.

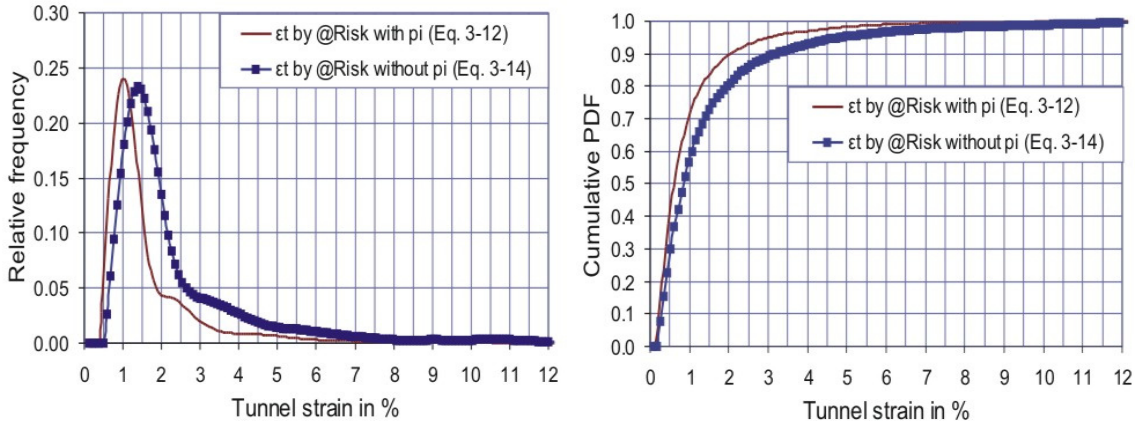

Figure 6-14. Achieved distribution results of tunnel strain between chainage 2000-3400 of Middle Marsyangdi headrace tunnel.

At this tunnel section, a very careful excavation method (round length less than 1.5 m) is being applied with extensive rock support (steel ribs at one meter spacing, 20 - 25 cm thick reinforced shotcrete and radial bolting). Hence, it is logical to use tunnel strain results based on Equation 3-12 (with support pressure) for interpreting probable tunnel squeezing.

Figure 6-14 right indicates that out of the 1400 meters long headrace tunnel between Jamitri and Khahare Khola, 70 percent of the tunnel length (approximately 980 meters) has a probability of tunnel squeezing with a magnitude less than one percent, 25 percent tunnel length (approximately 350 meters) has a probability of squeezing with a magnitude of 1 and 2.5 percent and 5 percent tunnel length (approximately 70 meters) has a probability of squeezing with a magnitude of 2.5 and 5. It needs to be noted here that the intercalation of metasandstone within phyllite most likely will have a positive effect on the extent of tunnel squeezing. Therefore, the risk of exceeding a tunnel strain with a magnitude higher than 5 percent is considered as low.

The information provided by Figure 6-14 is very useful for classifying anticipated degree of difficulties caused by tunnel squeezing as illustrated in Table 6-12. This classification of degree of difficulties is based on Figure 3-18 right.

Table 6-12. Estimated probability of squeezing and its possible effect on applied rock support in the Middle Marsyangdi headrace tunnel between chainage 2000 and 3400.

Degree of difficulties	Tunnel strain, %	Length, m	Horizontal convergence, cm	Possible consequences on applied rock support
Insignificant squeezing	< 1	980	< 7	No or very minor impact on applied support.
Minor squeezing	1 – 2.5	350	7 - 16	Cracks on applied shotcrete, slight yielding on rock bolts.
Severe squeezing	2.5 - 5	70	16 - 32	Slight buckling on steel ribs, cracks on applied shotcrete and yielding on rock bolts.
Very severe squeezing	5 - 10	-	32 - 64	Buckling to the steel ribs, wide cracks on shotcrete and severe yielding on rock bolts.
Extreme squeezing	> 10	-	> 64	Severe buckling on steel ribs, significant damage to applied shotcrete and extreme yielding on bolts.

Based on anticipated squeezing as shown in Table 6-12, a strategy can be made to tackle difficulties that may occur during tunnelling. One solution for tackling such difficulties is to increase the tunnel cross-section compensating the amount of squeezing.

6.4 WATER LEAKAGE

As discussed earlier, the rock masses in the Himalaya are highly fractured and deeply weathered. As a result, considerable temporary rock support has to be installed during tunnel excavation, but the use of full concrete lining after completion of excavation is also a tradition in the Himalaya. Hence, tunnelling through Himalayan rock mass has become very expensive, time consuming and in many cases economically unfeasible for hydro-

power schemes. The only way to solve this problem is to include temporary rock support as a part of the permanent support, and to use preinjection grouting to control water leakage. This concept was used in the recently constructed headrace tunnel of Khimti project by the consortium of NCC-Norway and Himal Hydro-Nepal (CCC, 2002).

One of most important aspects of the unlined / shotcrete lined water tunnel concept is control of water leakage while in operation at full hydrostatic pressure, and limiting the leakage to an appropriate volume (in Nepal defined as maximum 1 to 1.5 liters per minute per meter tunnel). The real difficulty, however, is the prediction and quantification of possible water leakage prior to tunnel excavation (during planning).

In the following, a probabilistic approach for predicting water leakage will be proposed based on data for Khimti. Before using this approach, an attempt will be made to establish an empirical relationship between specific leakage (q) and input parameters of the rock quality index (Q). Data on measured specific leakage (q) through exploratory holes drilled ahead of excavation to identify the need for preinjection grouting (Panthi and Nilsen, 2005a) and mapped input variables of the rock mass quality index (Q) in the headrace tunnel of the Khimti project are used for this purpose. Since the analysis will be based only on a single project of the Himalaya, it is acknowledged here that the uncertainties associated with this analysis will be considerable. Still, the approach is believed to have a considerable potential for this type of analysis.

6.4.1 Estimating correlation on specific leakage

The leakage through an unlined / shotcrete lined tunnel is mainly governed by hydrostatic head (h_{static}), degree of jointing and the discontinuity characteristics of the rock mass, see Figure 6-15 left.

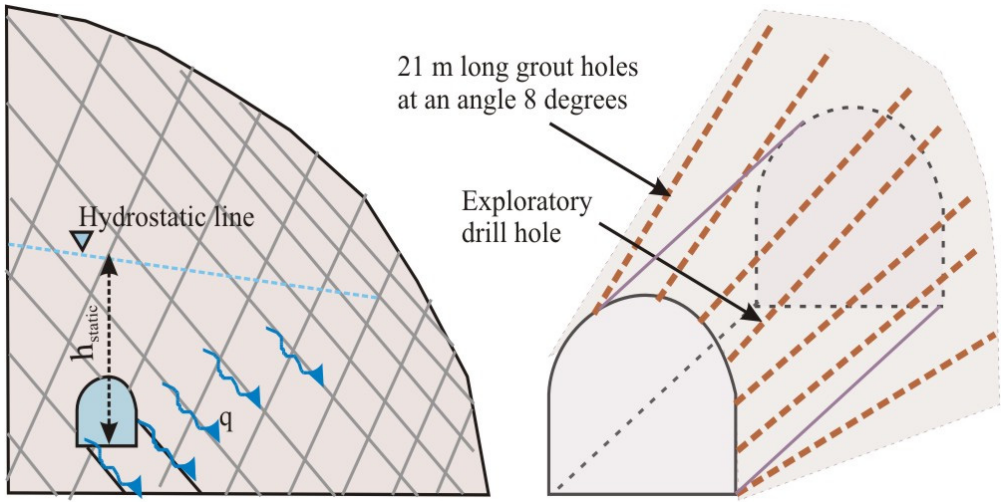

Figure 6-15. Principal illustration showing possible water leakage through an unlined / shotcrete lined tunnel (left), exploratory drill hole and grout curtain for preventing water leakage (right).

During excavation at Khimti, the specific leakage (q) was measured in an exploratory hole (approximately 18-21 meters long with an angle between 8 to 10 degrees relatively to the tunnel axis) drilled at the valley side of the tunnel as shown in Figure 6-15 right. The measured specific leakage in the drillhole may be considered as indicative for the specific leakage through the unlined / shotcrete lined tunnel during its operation at hydrostatic pressure.

For Khimti, the specific leakage (q) in the exploratory drillhole was expressed as:

$$q = \frac{V}{l \times t} \tag{6-3}$$

Where; q is the specific leakage in litres per minute per meter at an pressure 1.5 times hydrostatic head (1.5 represents factor of safety), V is the water volume in litres, l is the length of drillhole from the packer in meters (maximum 5 meters) and t is the time in minutes required to pump the water volume V.

Based on Equation 6-3, if the measured specific leakage (q) was more than one, it was concluded that there was a need for preinjection grouting.

After excavation of 2.5 kilometres of the Khimti headrace tunnel, it was realized that excessive leakage through the headrace tunnel might occur during operation. The main reason for such suspicion was the fact that the rock mass at the already excavated headrace tunnel sections was found to be highly fractured, see Section 4.3.1. Therefore, the principle explained above was introduced as a basis for preinjection grouting for approximately 4.2 kilometres of the Khimti headrace tunnel, see Figure 6-16.

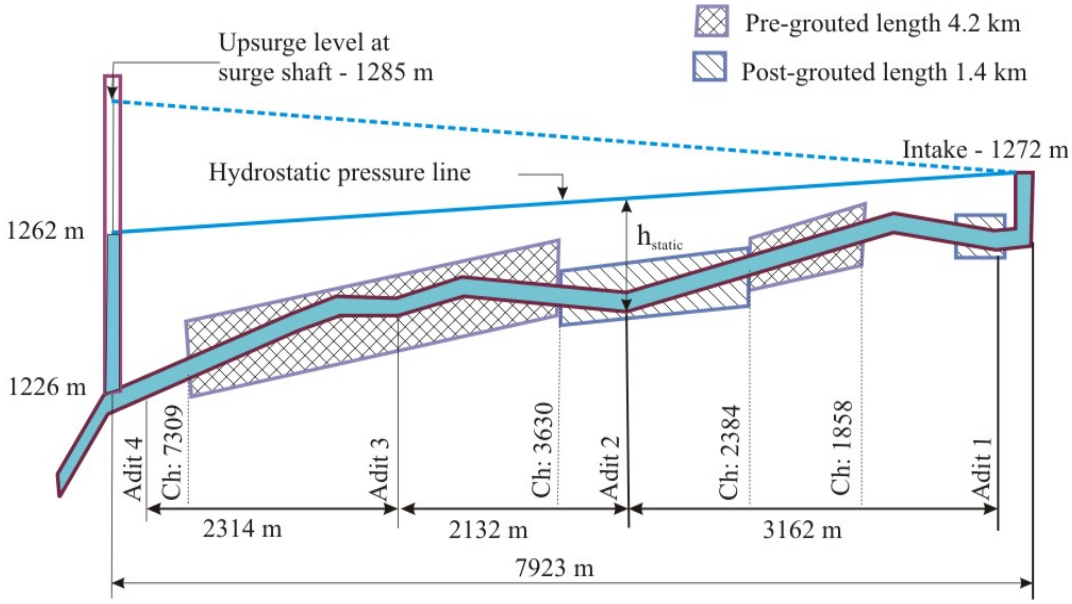

Figure 6-16. Khimti headrace tunnel profile showing hydrostatic pressure (h_{static}) line during operation and areas with preinjection and postinjection grouting. The figure is not in true scale.

It has been analyzed for Khimti whether the measured specific leakage (q) used for identifying the need for preinjection grouting, is interlinked with rock mass quality parameters. In particular, correlations between specific leakage (q) and jointing characteristics described by the Q-system, which was used to map the rock mass condition at Khimti headrace tunnel, have been checked.

The mapped jointing characteristics of the rock mass, pumping pressure (P) to identify specific leakage, measured specific leakage (q) and specific preinjection grout consumption (g_c) are summarized in Table 6-13. The table shows statistical distributions of these parameters representating their minimum, maximum and mean values and their standard deviations.

Table 6-13. Measured values of specific leakage (q), pumping pressure (P), hydrostatic head at operation (h_{static}) and jointing characteristics along the pre-grouted section of Khimti headrace tunnel.

Descriptions	Statistical distributions			
	Minimum	Maximum	Mean	Standard deviation
Discontinuity conditions:				
Rock quality designation (*RQD*)	10	85	40	25
Joint set number (J_n)	6	20	12	6
Joint roughness number (J_r)	0.5	3	1.5	0.7
Joint alteration number (J_a)	3	15	8	4.2
True hydrostatic head (h_{static}) in meters	19	39	29	6
Pumping pressure in bars (P)	2.9	5.8	4.4	1
Specific leakage (q) in litres per minute per metre	0	16	3.9	4.4
Specific grout consumption (g_c) in kg / m. tunnel	0	815	164	205

Note: Water pumping pressure through exploratory holes represents 1.5 times h_{static}.

In an attempt to find a correlation between specific leakage (q), hydrostatic head (h_{static}) and discontinuity characteristics of the rock mass, a regression analysis was performed by using different combinations of input variables of the Q-system. Figure 6-17 shows the results of regression analysis for different combinations of parameters.

A first attempt was made based on measured specific leakage, hydrostatic head and measured Q-values, see Figure 6-17a. As can be seen, no acceptable correlation was found. The second attempt was made by omitting J_w and *SRF* in the Q-value, assuming that these two input variables have very little influence on water leakage, see Figure 6-17b. As can be seen, the correlation has slightly improved, but is not satisfactory. The third attempt was made by reversing *RQD* and J_n, considering that the degree of jointing represented by J_n should increase leakage and high *RQD* on the other hand should reduce leakage. As shown in Figure 6-17c, the correlation improved considerably. The final attempt was made by omitting *RQD*, which gave a fairly good result with a correlation factor of 85 percent, see Figure 6-17d. This result is rather surprising since in theory, the *RQD* value that describes relative block size of rock mass, should have considerable effect on water leakage. A possible reason for the surprisingly small effect by *RQD* on leakage may be the fact that *RQD*

covers only a small part of the range of block size possible in the rock mass. For instance, in a tunnel located in highly jointed rock mass, if the spacing between most of the joints is just above 10 centimetres, the *RQD* value may be as high as 90. On the other hand, if the spacing between joints is slightly less than 10 centimetres, the *RQD* value may be as low as 10.

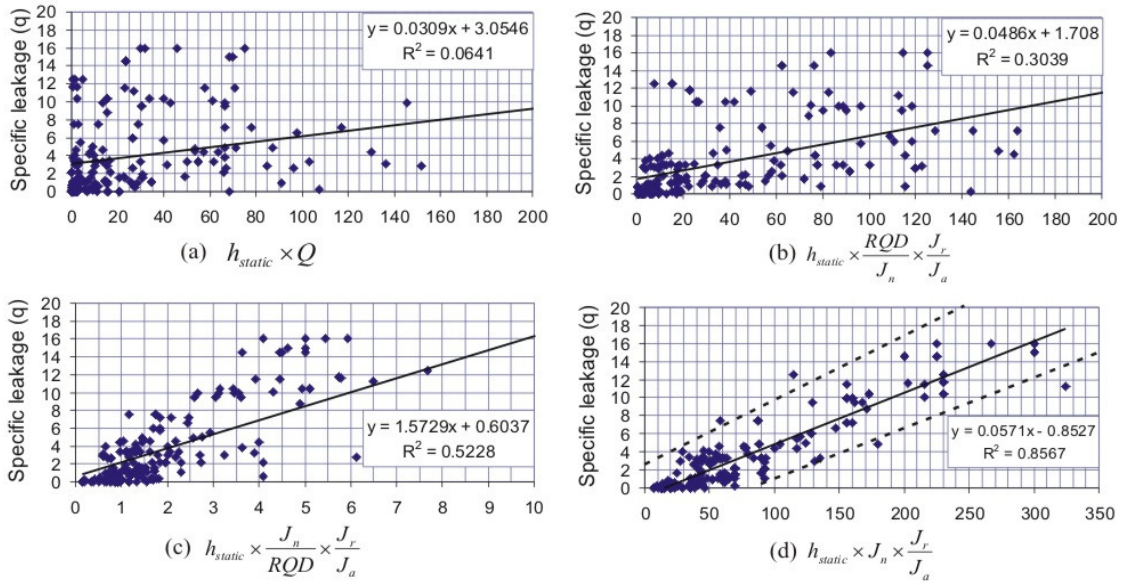

Figure 6-17. Correlations between specific leakage (q), hydrostatic height (h_{static}) and input variables of Q-system based on Khimti tunnel log and injection grouting records.

In the correlation represented by Figure 6-17d, there are four parameters that influence on the leakage; hydrostatic height (h_{static}), degree of jointing (J_n), joint roughness (J_r) and joint alteration (J_a). Three of these parameters are directly proportional to the leakage and therefore tend to increase leakage. Joint alteration is inversely proportional, and tends to reduce the leakage. This seems quite logical, because the higher the hydrostatic pressure and the more jointed the rock mass, the higher will be the possibility for large leakage, and the more altered and clay filled the joints are, the more impermeable the rock mass will be.

According to Figure 6-17d, the specific leakage in the tunnel (q_t) may roughly be estimated by the following equation:

$$q_t = f_a \times h_{static} \times \frac{J_n \times J_r}{J_a} \qquad (6\text{-}4)$$

Where; f_a is a joint permeability factor with unit litre per minute per sq. m. This factor is related to the permeability condition of joint sets and expresses connectivity between joint sets, joint spacing, aperture and infilling conditions. The factor f_a may vary from 0.05 to 0.12 (represents lower and upper line, respectively) depending upon the condition of dis-

continuity infilling. Lower values represent impermeable joints and higher values represent more open joints or joints filled with permeable material.

It needs to be emphasized here that the results shown in Figure 6-17 are based only on data for Khimti headrace tunnel. In this tunnel, the rock mass is highly fractured and has more than two prominent joints sets plus random joints, see J_n value in Table 6-13. Unless similar conditions are present, the uncertainty connected to the proposed correlation will be considerable.

6.4.2 Water leakage estimation

A probabilistic approach is used to estimate leakage based on Equation 6-4. The uncertainty analysis is carried out by using @Risk as described in Chapter 5. The postinjection grouted section of Khimti headrace tunnel between chainage 2384 and 3630 (near adit 2) is used for this purpose, see Figures 6-16. Through this tunnel section considerable volume of water leaked out during test water filling in early 2000. Approximately 200 litres of water per second leaked from adit 2 approximately 50 to 60 meters from the junction. Since no water leakage was observed around the concrete plug area, it was assumed that the leaking water was flowing in open joints. To control this leakage, an extensive postinjection grouting was performed in the ungrouted section upstream and downstream of adit 2 (CCC, 2002 and Panthi and Nilsen, 2005a), see Figure 6-16.

In terms of probabilistic approach, the specific leakage (q_t) defined by Equation 6-4 is considered as a factor which depends mainly on five variable input parameters; i.e. joint permeability factor (f_a), hydrostatic height (h_{static}), degree of jointing (J_n), joint roughness (J_r) and joint alteration (J_a). This means that the main principle of uncertainty analysis based on Equation 6-4 will be to characterize the uncertainties regarding these variable input parameters.

As Table 6-14 indicates, this section of headrace tunnel passes through highly fractured rock mass with an average J_n value of 12. The headrace tunnel mainly passes through mica gneiss, banded gneiss and sheared mica schist intercalations, see Figure 4-2. The discontinuities in the mica gneiss and banded gneiss are either open or filled with permeable silt material, while the occasional bands of sheared schist are rather impermeable in character. The unfavorable orientation of joint sets and the open character of joints are believed to be the main causes for the large leakage in this section of the headrace tunnel.

The statistical ranges of discontinuity characteristics calculated from geological tunnel logs, actual hydrostatic head at operation and specific leakage calculated according to Equation 6-4 are given in Table 6-14.

Table 6-14. Ranges of discontinuity characteristics, hydrostatic head, and specific leakage calculated based on Equation 6-4 by @Risk for Chainage 2384 – 3630 of Khimti headrace tunnel.

Descriptions	Statistical distributions				@Risk values
	Minimum	Maximum	Mean / most likely	St. dev.	
Discontinuity characteristics:					
Joint set number (J_n)	6	20	12	-	12.67
Joint roughness number (J_r)	0.5	3	2	0.5	2.00
Joint alteration number (J_a)*	15	2	4	2	4.22
Hydrostatic head (h_{static}) in meters	19	30	25	-	25.00
Permeability factor (f_a) in l / min / sq. m.	0.05	0.12	0.085	0.03	0.085
Specific leakage (q_t) in l / min. / m tunnel	0.2	108	12.75		12.76

Note: *Maximum number of J_a represents its minimum with respect to specific leakage and vice versa.

Definition of representative probability density function (pdf) plays a key role for uncertainty analysis based on @Risk. Probability density functions of variable input parameters of the Q-value are discussed in detail in Section 6.2, and similar argument are valid here too. A triangular probability density function is used for J_n, with most likely value 12 and minimum and maximum values 6 and 20, respectively. In blocky rock mass condition, J_r and J_a are assumed to cluster towards their mean, giving normal distributions. A triangular distribution is assumed for h_{static}, since the hydrostatic head changes linearly as shown in Figure 6-16. The factor f_a is assumed to have a mean value of 0.085 based on the fact that joint sets other than bands of intercalated schists within foliation joints are most permeable. Since the distribution pattern of f_a is not clearly known, it has been considered logical to use normal distribution as discussed in Chapter 5.

The @Risk uncertainty analysis model was run after assigning probability density functions (pdf) for each input variable of Equation 6-4 as shown in Table 6-11. The simulation settings of the @Risk model were specified as described in Section 6.3.2.2. The outcomes for the pseudo-randomly distributed specific leakage (q) achieved after simulation based on @Risk are shown in Figure 6-18 (see also Table 6-14).

The figure indicates an average specific leakage (q_t) of about 16 litres per minute per meter tunnel. This gives an overall leakage of approximately 350 litres per second through this section of the headrace tunnel. More importantly, the right hand diagram indicates specific leakage between 5 and 42 litres per minute per meter tunnel for a tunnel length of approximately 1120 meters (90 percent). The figure further illustrates that approximately 40 percent of the tunnel length (approximately 500 meters) has a specific leakage over 15 litres per minute per meter tunnel.

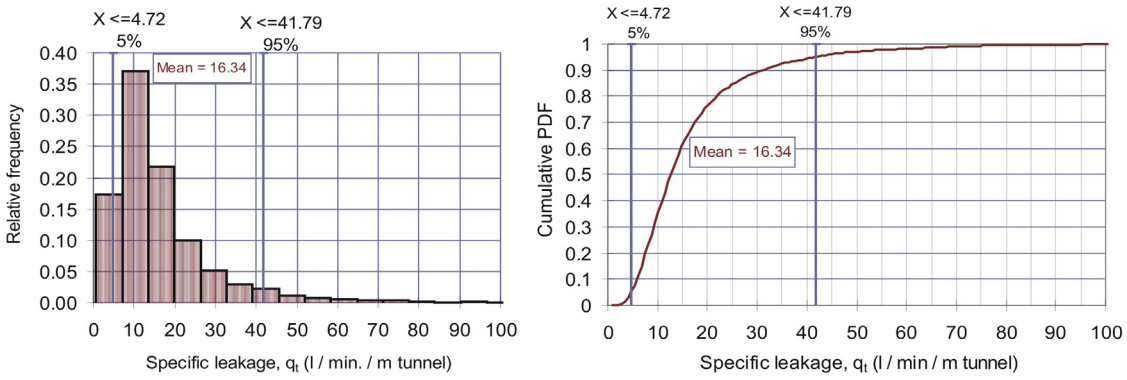

Figure 6-18. Distribution of specific leakage (q_t) between chainage 2384-3630, covering 1246 meter of the headrace tunnel from Adit 2.

To find the total leakage for the 1246 meter tunnel section, the average specific leakage (q_t) for each segment of tunnel (segment length defined by respective relative frequency of that segment multiplied by total tunnel length, in this case 1246 meters) is converted to total leakage for that segment. The calculated total leakage for each segment is than converted to cumulative leakage. The calculated cumulative leakage is shown in Figure 6-19.

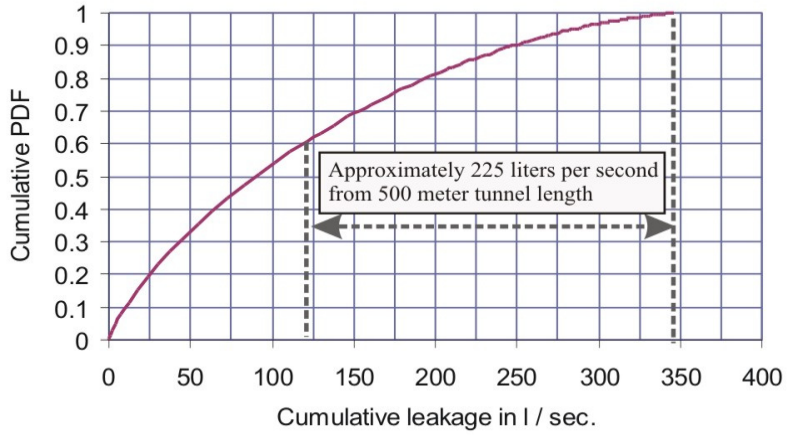

Figure 6-19. Calculated cumulative leakage for 1246 meter of the headrace tunnel near Adit 2.

As indicated in Figure 6-19, approximately 40 percent of the tunnel (cumulative curve above sixty percent) has estimated leakage of 225 litres per second (350 – 125). This 40 percent tunnel length covers approximately 500 meter tunnel length. In fact, this result is fairly close to what was observed during test water filling of the headrace tunnel. As mentioned earlier and also discussed by Panthi and Nilsen (2005a), 200 litres per second of water leaked from adit 2. To control this leakage an extensive postinjection grouting was carried out. During postinjection grouting special attention was given to the headrace tunnel section 300 meters upstream and 200 meters downstream adit 2.

This shows that the results of uncertainty analysis based on Equation 6-4 and discontinuity characteristics based on tunnel mapping (see Table 6-14) gave fairly good estimate of the leakage. This means that if reliable discontinuity data are available, it may be possible to carry out uncertainty analysis for estimating leakage from a planned unlined or shotcrete lined tunnel in similar geological conditions.

6.4.3 Estimating grout consumption

Estimating the quantity of cement necessary for preinjection grouting is very important for the unlined / shotcrete lined tunnel concept. Without such estimation, it is not possible to estimate the cost for injection grouting. Therefore, injection grouting data of the Khimti headrace tunnel have been used to investigate the correlation between specific leakage (q), grout pressure (P) and specific grout intake (g_c) for preinjection, see Figure 6-20.

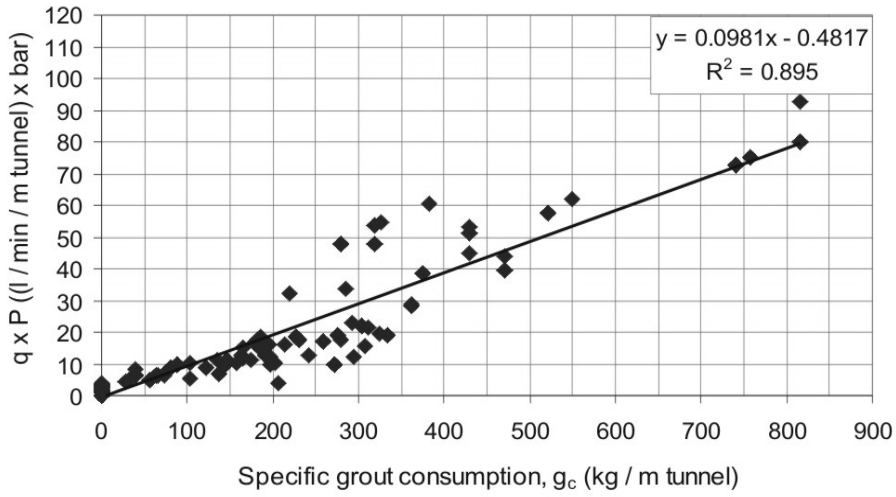

Figure 6-20. Correlation between specific leakage (q), grout pressure (P) and specific grout consumption (g_c).

As Figure 6-20 shows, a fairly good correlation is achieved that might be useful for estimating preinjection grout intake for future headrace tunnels built in similar ground conditions. Again it needs to be emphasized here that the results shown here are based on one single tunnel, Khimti headrace tunnel. In addition, the grout take is more difficult issue than given in the figure, which can be used only for projects where the grout mix, stop criterion and type of cement are the same as for Khimti.

6.5 CONCLUDING REMARKS

Based on the results for the cases discussed in this Chapter, it can be concluded that the probabilistic approach for evaluating rock mass quality, for estimating probability of tunnel squeezing and for assessing potential leakage through unlined / shotcrete lined tunnel has a great potential. It needs, however, to be emphasized here that covering all aspects of analy-

sis for all projects has been not possible within the scope of this thesis work. As indicated at the beginning of this Chapter, the stability issues have been prioritized based on main areas of uncertainties and available data information. The potential of this methodology for analyzing is further discussed on a more general basis in Chapter 7.

Chapter 7
Discussions

7.1 INTRODUCTION

Evaluating rock mass quality, predicting tunnel squeezing and estimating leakage have been the main issues of this research. As discussed in earlier chapters, these are the key issues for optimum and cost effective tunnelling through Himalayan rock mass. A probabilistic approach has been applied for analyzing geological uncertainties related to these issues.

Four tunnel cases (three recently constructed and one under construction) of Nepal Himalaya have been selected for the uncertainty analyses. Background information needed for the analyses has been collected and a comprehensive review of available data has been made. During field work for the last three summers, rock samples have been collected and laboratory testing has been carried out.

It needs to be emphasized that covering all areas of uncertainty for all project cases has been beyond the scope of this thesis. Decisions concerning what type of uncertainty analyses to be carried out for each case has been based on evaluation of what are the major areas of uncertainties, which data are available and what is the relevancy of such analysis for that particular case. The uncertainty analyses that have been carried out for respective tunnel cases are summarized in Table 7-1.

Table 7-1. Uncertainty issues covered for the respective tunnel cases.

Projects	Rock mass quality	Tunnel squeezing	Water leakage
Khimti I headrace tunnel	Yes	-	Yes
Kaligandaki "A" headrace tunnel	-	Yes	-
Modi Khola headrace tunnel	Yes	-	-
Middle Marsyangdi headrace tunnel	-	Yes	-

7.2 DEGREE OF CORRELATION

Due to the complex nature of rock mass behavior, it is not realistic to expect a perfect correlation between estimated and as-built conditions. Nevertheless, the probabilistic approach of analysis introduced in this thesis has given promising results. The degree of correlations between the results achieved by @Risk simulation for each type of uncertainty (Q-tunnel, ε_t and q) and actual conditions in the tunnel are classified in Table

7-2. This classification is subjective and the intention with the table is mainly to review the main conclusions of the analysis in Chapter 6. As can be seen in the table, good and fairly good degree of correlations have in most cases been found between simulated results achieved by @Risk model and the conditions in the tunnel.

Table 7-2. Degree of correlation between simulation results achieved by @Risk and conditions in the tunnel.

Type of uncertainty analysis	Projects	Analysis location	Degree of correlation		
			Good	Fair to good	Fair to poor
Rock mass quality (Q)	Khimti I	Chainage 1900 - 2200	X		
		Chainage 2200 - 2700	X		
		Chainage 3294 - 3900			X
	Modi Khola	Chainage 0 - 325		X	
		Chainage 325 - 1025	X		
Tunnel squeezing (ε_t)	Kaligandaki	Chainage 1964 - 4032	X		
	Middle Marsyangdi	Chainage 2000 - 3400	NA	NA	NA
Leakage (q)	Khimti I	Chainage 2384 - 3630		X	

Note: NA - not applicable. For Middle Marsyangdi tunnelling results are not yet available.

The results achieved for rock mass quality index (Q) have suggested that the assigned probability distribution functions (pdf) of each input variable of Q quite well reflect the ground conditions. The only location where relatively poor correlation has been achieved is for the headrace tunnel section between Chainage 3294 and 3900 of Khimti. A possible reason for relatively poor correlation here may be the fact that at this tunnel section the Q-values are highly scattered (ranging between 0.001 and 2, see Figure 6-5). This indicates that in rock mass with large variation in Q-value, it is not easy to assign probability distribution functions that give results close to real ground conditions. The most important aspect is however the mean value of Q in the tunnel (0.022), which is not very far from results achieved by @Risk (0.03), see Table 6-3.

The degree of correlation achieved concerning tunnel squeezing for Kaligandaki headrace tunnel is very good, see Figure 6-13. The availability of extensive instrumentation data on tunnel convergence, rock support pressure data and laboratory test results for this tunnel has made it possible to investigate the applicability of the assigned probability distribution functions (pdf) for each input variable of tunnel strain calculated according to Hoek and Marinos approach. The achieved good correlation has increased the confidence in predicting tunnel strain for the Middle Marsyangdi headrace tunnel.

With respect to uncertainty analysis of water leakage, the degree of correlation has been found to be fairly good. This analysis has been done by using a new equation proposed in this thesis on data from the Khimti headrace tunnel. It has to be emphasized, how-

ever, that since this has been used only for a single project and has not been tested for other tunnels, the degree of uncertainty here is considerable.

7.3 RELEVANCY OF THE PROBABILISTIC APPROACH

Identification and evaluation of the most sensitive input variables are the keys for successful use of the probabilistic approach of uncertainty analyses. In the following, the sensitivity and effect of variation in the value of each input variable related to the rock mass quality index (Q) and in the equations used for predicting tunnel squeezing and water leakage will be discussed.

7.3.1 Rock mass quality

The effect of variation on the value of each input parameter of quality index (Q) will be discussed here. The @Risk simulation results of assigned probability distribution of each of these input parameters for the three sections of Khimti headrace tunnel (Table 7-2) are used as basis for the discussions. As described in Chapter 6, these three sections of the headrace tunnel represent three different scenarios with respect to predicted and actual rock mass conditions, and are therefore believed to give valuable input for the discussion concerning sensitiveness of variation.

The discussions here will be focused mainly on the influence of degree of jointing, on the effect of intercalation of highly sheared bands of weak rocks within stronger rocks and on the effects of weathering and alteration, which are all factors that influence greatly on the overall rock mass quality in the Himalaya. Figure 7-1 shows the probability distributions of the value of each input parameter for rock mass quality index (Q) achieved by simulation based on @Risk. These probability distributions have been the inputs used in Chapter 6 for calculating the probability distribution of predicted and tunnel mapped rock mass quality indexes (Q) based on @Risk.

<u>*Weakness zone (Chainage 1900 – 2200):*</u> As shown in Figure 7-1, the simulated results of probability distribution for the values of J_n, J_r and J_a based on @Risk are very similar for predicted and actually mapped in the tunnel. This is logical, since in rock mass representating weakness or fracture zones it is not difficult to predict that the degree of jointing is generally high with a high number of joint sets. The roughness of the joint walls is generally smooth, slickensided and planar due to considerable alteration, weathering and shearing. As shown in the figure, there is some more deviation in the probability distributions of *RQD*, J_w and *SRF*, but the deviation is not very significant. These three parameters, however, show slightly more sensitivity than the other three, and generally should be estimated with care concerning statistical ranges.

<u>*Section with fairly good rock mass (Chainage 2200 – 2700):*</u> This is a tunnel section where fair to good quality rock mass was predicted, and the rock mass actually found in the tunnel was poor to fair, i.e. some deviation, but relatively close to predicted. Figure

7-1 shows that the simulated results of probability distribution achieved by @Risk are not very different for predicted and actually mapped parameters in the tunnel.

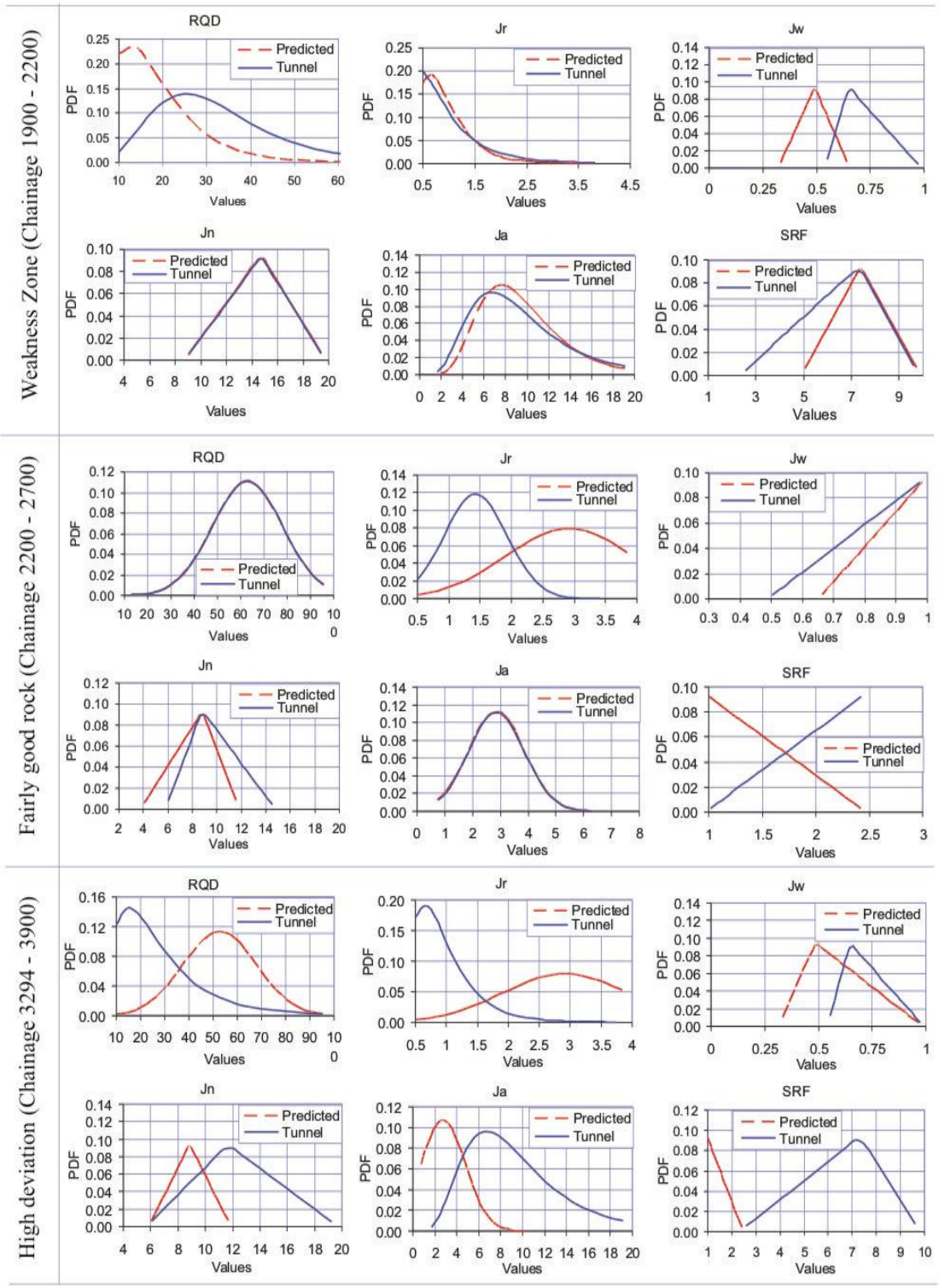

Figure 7-1. Probability distributions for each input parameter of Q in three sections of Khimti headrace tunnel based on @Risk.

As shown in Figure 7-1, the probability distributions for *RQD* and J_a are very similar, while small deviations can be seen in the probability distributions for J_n, J_w and *SRF* between predicted and actually mapped in the tunnel. However, for the probability distribution of J_r there is a considerable deviation, indicating high degree of sensitivity. The main reason for this greater deviation may be the fact that thin bands of mica schist intercalated with gneiss have caused joint surfaces to be more smooth and slickensided than was anticipated during planning.

Section with high deviation (Chainage 3294 – 3900): This is a tunnel section where fair to good quality rock mass was predicted, and the rock mass actually found was exceptionally poor to poor, i.e. the deviation was very considerable, see Figure 6-5. As shown in Figure 7-1, the simulated results of probability distributions for input variables of Q based on @Risk are very different for predicted and actually mapped in the tunnel. The only parameter that has positive value (better than predicted with respect to rock mass quality index Q) is the rating for J_w. The rating for other input variables are significantly more negative than predicted (as described in Chapter 6, higher rating values for the denominators J_n, J_a and *SRF* are considered negative since they cause reduction of Q-value). The considerable deviations in the ratings may be caused by the following:

1. The planning phase investigations were limited to surface mapping (Chapter 4). Very little exposed rock is found at the surface above this tunnel section, except for a very short length downstream Adit 2. During planning, the weathering depth below the surface was not believed to be greater than 20 meters (HPL, 1995) and similar rock mass as exposed in the Adit 2 area was believed to dominate. This resulted in overestimation on the overall rock mass quality.

2. Much more than expected, the rock mass along the tunnel was found to be highly weathered and altered. The weathering beyond Chainage 3450 was very deep and in some locations the much fractured rock mass had the character of decomposed soil (CCC, 2002; Panthi and Nilsen, 2005a and Chapter 4).

3. Beyond chainage 3450 and chainage 3900, thick bands (more than 1 meter thick) of highly sheared and extremely weak talcose mica schist intercalated within highly fractured gneiss was unexpectedly found in the tunnel.

Extreme jointing, high degree of weathering and alteration and intercalation of extremely weak talcose mica schist led to considerable reductions in the ratings of *RQD* and J_r, and considerable increases in the ratings of J_n, J_a and *SRF*. This resulted in reduction of overall rock mass quality index (Q).

From the discussions above it can be concluded that if the rock mass is well exposed on the surface, which is often the case in areas with steep topography, it should not be too

difficult to predict the ratings of input variables of the quality index (Q) by careful surface mapping.

The real challenge thus is the quantification of ratings for the input parameters of Q in areas where the rock mass is not exposed at surface. In such areas, the most difficult tasks are verification of weathering depth, evaluation of the extent of weathering and alteration, estimation of degree of jointing and possible intercalation of extremely weak rocks within stronger rocks.

If the rock is not exposed on the surface, engineering geological investigations such as core drilling and seismic investigations may help to some extent for evaluating the quality of the rock mass. During such investigation great focus must be placed on predicting the possible statistical ranges of each input variable used for the evaluation of rock mass quality.

7.3.2 Tunnel squeezing

The accuracy of uncertainty analysis regarding tunnel squeezing depends upon reliable estimation of the ranges of input variables associated with the method or equation used. Selection of representative probability distribution functions (pdf) for the respective input variables is very important in this respect.

In the following, the sensitivity and importance of reliable estimation on the value of each input variable related to Hoek and Marinos (2000) approach (Equation 3-12 and 3-14) will be discussed. As has been discussed in Section 6.3, the Hoek and Marinos approach requires reliable estimation of the ranges of three input variables; 1) rock mass strength (σ_{cm}), 2) overburden stress (γh), and 3) rock support pressure (p_i).

Figure 7-2 shows the probability distributions of the value of each of these input variables as simulated by @Risk, and based on assigned statistical ranges for each of them given in Table 6-9 and 6-11. The probability distributions shown in Figure 7-2 have been used as inputs for calculating the probability distribution of tunnel strain (ε_t) by @Risk for the respective cases.

As Figure 7-2 indicates, exponential probability distribution for inverse to overburden stress and normal probability distribution for rock mass strength and rock support pressure have been used in the uncertainty analysis. The squeezing analysis carried out for Kaligandaki headrace tunnel between chainage 1964 - 4032 have indicated fairly good correlation between tunnel strains calculated by @Risk and strains actually measured, see Figure 6-13. The achieved results suggest that Hoek and Marinos approach is fairly good for estimating tunnel squeezing.

The achieved results also suggest that the assigned probability distributions for the input variables are fairly representative and may be used for uncertainty analysis of tun-

nel squeezing at other projects. However, it needs to be emphasized here that the most crucial aspect lies in estimating reliable ranges of input variables; i.e. overburden stress, rock mass strength and rock support pressure.

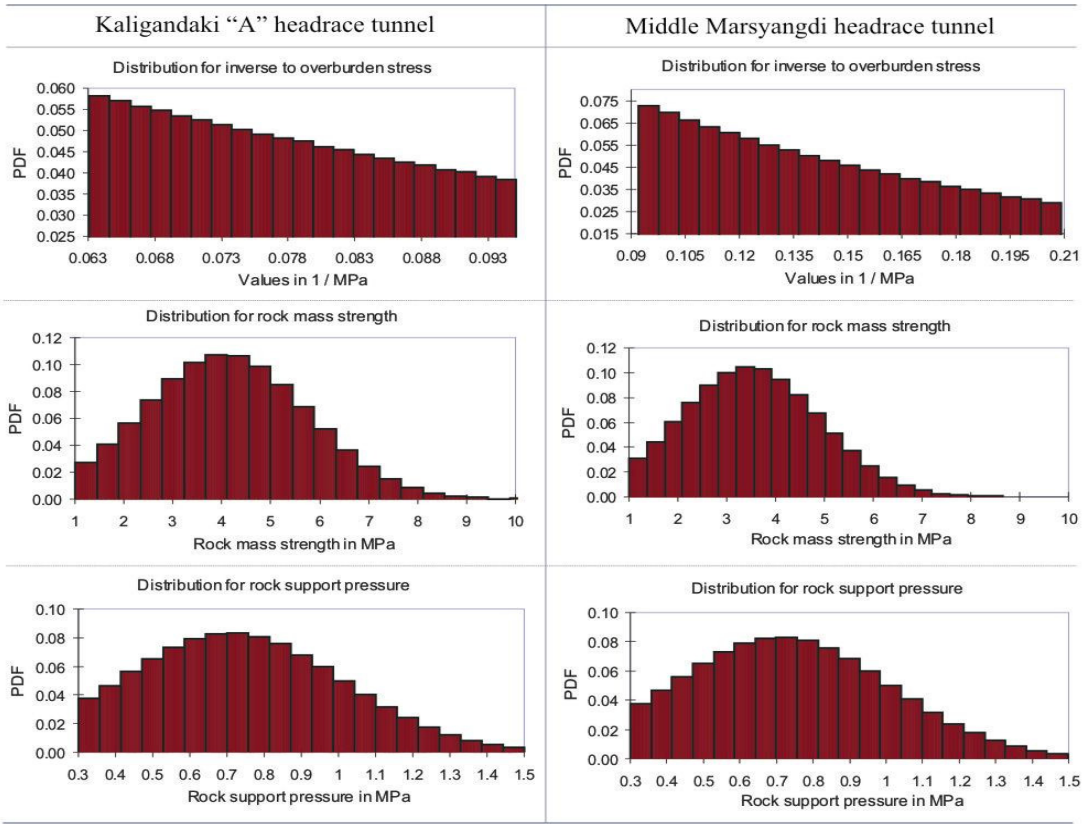

Figure 7-2. Probability distributions of the input variables for calculating tunnel strain as achieved by @Risk for the headrace tunnels of Kaligandaki and Middle Marsyangdi projects.

Estimating overburden stress is not a very difficult task since topographic maps are generally available during planning and design phases of any tunnel project. It is just a matter of calculating overburden height above the tunnel alignment with good accuracy. Depending upon the topography, overburden height calculated at intervals of approximately 50 meters or less will give fairly good results. Specific weight of the rock mass may be measured in laboratory or estimated based on literature review. The variation of specific weight is relatively small and has relatively little effect on overburden stress.

The most important and difficult part of squeezing analysis lies in the reliable estimation of rock mass strength. This input variable is the most sensitive for estimating tunnel strain based on Hoek and Marinos approach. Equation 3-1, representating a correlation between rock mass strength and intact rock strength, has been successfully used in this thesis for estimating the ranges of rock mass strength. The achieved results for tunnel strain based on this equation indicate fairly good approximation for the Kaligandaki

headrace tunnel. Therefore, this equation has been used also for predicting tunnel squeezing in the Middle Marsyangdi headrace tunnel.

Concerning rock support pressure, the only way to get reliable information about ranges of its values is to increase the database by field instrumentation, e.g. by pressure cell measurement. For Kaligandaki and Middle Marsyangdi, truncated lowest and highest values of 0.3 and 1.5 MPa, respectively, have been used for rock support pressure. This approximation has given fairly good fit between simulated results by @Risk and actually measured tunnel strain for the Kaligandaki headrace tunnel. Since the rock mass conditions are similar, analogous values have been used also for the Middle Marsyangdi headrace tunnel.

7.3.3 Water leakage

The preinjection grouting technique used in the Khimti headrace tunnel has demonstrated that it is possible to skip full concrete lining, and still have a leakage of acceptable value (Panthi and Nilsen, 2005a). In Section 6.4 of this thesis an attempt has been made to find a correlation between specific leakage and jointing characteristics of the rock mass defined by parameters of the Q-system. The suggested correlation has been achieved based on data from one single tunnel project of the Himalaya. The uncertainty analysis carried out based on the @Risk gave fairly good correlation for the headrace tunnel section of Khimti between chainage 2384 and 3630. At this tunnel section, no preinjection grouting was performed during excavation, and the extent of leakage was known by early water filling.

However, since only one project has been included in this analysis, it needs to be emphasized that the proposed correlation has a high degree of uncertainty if the geological conditions are not similar to those of Khimti. The only way to further test and improve this correlation is to add more data from other tunnelling projects of the Himalaya.

7.4 STRENGTH AND LIMITATIONS OF THE METHODOLOGY

Based on the attempt in this thesis to use probabilistic approach and @Risk for evaluating rock mass quality index (Q), tunnel strain (ε_t) and water leakage the main strength and usefulness of this approach may be described as follows:

1. The probabilistic approach of uncertainty analysis is very suitable for exploring and quantifying the probable distribution of each geological uncertainty under consideration.

2. The probabilistic approach helps to quantitatively describe and evaluate the significance of variation in the value of each input parameter.

3. The probabilistic approach of analysis makes it possible to foresee consequences of variation in the value of each input parameter and assess the risk posed by such variation.

4. The probabilistic approach is a tool which may also be very useful for back analysis and comparison between predicted and actually measured values of uncertainties in question.

There are, however also certain limitations and pitfalls which should be kept in mind while using this methodology:

1. It is a key for successful use of the probabilistic approach that the assigned probability distribution function of each input variable reflects the real situation. Thorough investigation and great care are therefore essential when selecting probability density functions.

2. The reliability of the method or equation used for uncertainty analysis should always be carefully examined.

3. The estimated statistical ranges of input parameters associated with the uncertainty in question should be as reliable as possible.

Provided that a careful approach as discussed above is followed, the probabilistic approach of uncertainty analysis may improve the reliability of prediction considerably. Use of this approach may reduce the discrepancies between predicted and actual rock mass conditions, and in addition the results of the probabilistic approach may be used for developing a strategy for tackling potential stability problems in a cost effective way. Most importantly, uncertainty analysis makes it possible to explore the influence of variations in the value of each input parameter, and to base engineering judgment on the variation of a range of values, rather than on a single value.

Chapter 8
Conclusions and recommendations

8.1 CONCLUSIONS

In the Himalaya, tunnel stability problems are mainly related to the existence of weak, highly deformed, highly schistose rock mass and high degree of weathering and fracturing of the rock mass. Evaluating rock mass quality, predicting stress induced problems, in particular tunnel squeezing, and predicting potential leakage during planning are key factors for successful tunnelling through Himalayan rock mass. For economically viable tunnelling it is therefore crucial to apply a methodology that makes it possible to analyze and foresee the consequences of these uncertainties. The probabilistic approach of uncertainty analysis for analyzing this has been the main achievement of this research.

The following conclusions can be drawn based on the research presented in this thesis:

1. Review of the geological conditions of the selected four tunnel cases has revealed considerable discrepancies between predicted and actual rock mass quality and also between predicted and as-built rock support. It has been revealed that there have been considerable variations in the type and level of investigations carried out for the tunnel cases. Generally, a thorough, stepwise investigation approach is recommended. It is also recommended that risk and uncertainty analysis should be performed at the pre-construction stage for realistic prediction and evaluation of rock mass quality and for analyzing potential instability conditions.

2. For analyzing stability problems associated with tunnelling through Himalayan rock mass conditions, uncertainty analysis based on the software program @Risk has been found very useful.

3. The proposed uncertainty analysis model has been successfully used for evaluating rock mass quality index (Q), for analyzing tunnel squeezing based on Hoek and Marinos approach and for predicting water leakage from unlined / shotcrete lined tunnel based on a correlation developed for Khimti headrace tunnel.

4. The results of the uncertainty analyses show fairly good degree of correlation between simulation results and conditions actually found in the tunnel. Thus, the proposed uncertainty analysis is believed to have a considerable potential for predict-

ing rock mass quality, tunnel squeezing and leakage estimation also for future tunnels in Himalayan rock mass conditions.

Generally, it is concluded that the best way to reliably analyze tunnel stability issues is to carry out uncertainty analyses as has been done in this thesis. Based on such analysis it is possible to foresee the effect of variation in the value of each input parameter related to the stability issue under consideration. Hence, the probabilistic approach of uncertainty analysis significantly improves engineering judgment. The rate of change in each uncertainty element makes it possible to minimize the degree of uncertainty and risk associated to that particular uncertainty. The results of uncertainty analysis also help in building a strategy for dealing with the consequences of variation in a more cost effective way, since such analysis quantifies the geological uncertainties that exist in the tunnel under consideration.

8.2 RECOMMENDATIONS

It needs to be emphasized that covering all uncertainty issues related to tunnelling through Himalayan rock mass conditions has not been possible within the scope of this thesis. Even though the probabilistic approach for uncertainty analysis of rock mass quality, tunnel squeezing and leakage has been successfully used for four cases in this thesis, the number of analyzed cases is still limited. In addition, the consequences of quantified uncertainties have not been assessed with respect to cost and time domain. Therefore, the following supplementary research is recommended for further documentation of the conclusions in this thesis:

1. Analysis of other relevant tunnel cases to increase the confidence and reliability. Particularly, verification of the proposed equation for estimation of leakage is very essential.

2. Analysis of the connection between quantified geological uncertainties and cost domain, which is an important aspect with respect to feasibility and risk in investment for tunnelling projects under consideration.

3. Assessment of the impact on construction time caused by geological uncertainties, which represents a very important aspect of successful tunnelling.

REFERENCES

Ajalloeian R. and Lashkaripour G. 2000. Strength anisotropies in mud rocks. *Bulletin of engineering geology and environment*, vol. 59, pp. 195-199.

Aydan O., Akagi T. and Kawamoto T. 1993. The squeezing potential of rocks around tunnels; theory and prediction. *Rock mechanics and rock engineering*, vol. 26 (2), pp. 137-163

Bajracharya B. B. and Panthi K. K. 2002. Rock support optimization in Himalayan tunnels. *Proceedings: ITA-AITES 2002 World Tunnelling Congress & 28th ITA General Assembly*. Sydney, pp. 461-467.

Bandis S. C. 1993. Engineering properties and characterization of rock discontinuities. *Comprehensive rock engineering, J. A. Hudson ed. Pergamon*, vol. 1, pp. 155-183.

Bandis S. C., Lumsden A. C. and N. R. Barton. 1981. Experimental studies of scale effects on the shear behavior of rock joints. *International journal of rock mechanics and mining sciences & geomechanics abstracts*, vol. 18, pp. 1-21.

Barton N. 1973. Review of a new shear strength criterion for rock joints. *Engineering geology*, vol. 7, pp. 287-332.

Barton N. 1974. A review of the shear strength of filled discontinuities in rock. *Norwegian geotechnical institute*, publication no. 105, 38 p.

Barton N. 1995. The influence of joint properties in modeling jointed rock masses. Keynote lecture. *8th congress of ISRM, Rotterdam Balkema*, vol. 3.

Barton N. 2001. Water and stress are fundamental to rock mass characterization and classification. Letter to the Editor. *ISRM news journal*, December 2001, 4 p.

Barton N. 2002. Some new Q-value correlation to assist in site characterization and tunnel design. *International journal of rock mechanics and mining sciences*, vol. 39, pp. 185-216.

Barton N. and Bandis S. 1990. Review of predictive capabilities of JRC-JCS model in engineering practice. *Proceedings: International conference on rock joints*, Balkema, Rotterdam.

Barton N. and Choubey V. 1977. The shear strength of rock joints in theory and practice. *Rock mechanics*, vol. 10, pp. 1-54.

Barton N., Bandis S. and Bakhtar K. 1985. Strength, deformation and conductivity coupling of rock joints. *International journal of rock mechanics and mining sciences & geomechanics abstracts*, vol. 22, pp. 121-140.

Barton N., Line R. and Lunde J. 1974. Engineering classification of rock masses for the design of tunnel support. *Rock mechanics*, vol. 6, pp 189-236.

Beacher G. B. 1972. Site exploration: A probabilistic approach. *Massachusetts Institute of Technology*. Ph.D. Thesis.

Beacher G. B. and Christian J. T. 2003. Reliability and statistics in geotechnical engineering. *John Wiley & Sons*, West Sussex, England, 605 p.

Beavis F. C. 1985. Engineering geology. *Blackwell scientific publication*, 231 p.

Beavis F. C., Roberts F. I. and Minskaya L. 1982. Engineering aspects of weathering of low grade metapelites in an arid climate zone. *Quaternary journal of engineering geo*logy, London, vol. 15, pp. 29-45.

Bieniawaski Z. T. 1973. Engineering classification of jointed rock masses. *Trans. S. Afr. Inst. Civ. Eng,* vol. 15, pp. 335-344.

Bieniawaski Z. T. 1978. Determining rock mass deformability: Experience from case histories. *International journal of rock mechanics and mining sciences & geomechanics abstracts*, vol. 15, pp. 237-247.

Bieniawaski Z. T. 1989. Engineering rock mass classifications. A complete manual for engineers and geologists in mining, civil, and petroleum engineering. *John Wiley & Sons, Inc.*, 251 p.

Bieniawaski Z. T. 1993. Classification of rock masses for engineering: The RMR-system and future trends. *Comprehensive rock engineering*, *J. A. Hudson ed.,* vol. 3, pp. 553-573.

Bieniawaski Z. T. and Van Heerden W. L. 1975. The Significance of in-situ tests on large rock specimen. *International journal of rock mechanics and mining sciences & geomechanic abstracts*, vol. 12, pp. 101-113.

Bieniawski Z. T. 1997. Quo vadis rock mass classification? Some thoughts on rating methods for tunnel design. *Felsbau (rock and soil engineering*), vol. 15, pp 177-178.

Borradaile G. 2003. Statistics of earth science data: their distribution in time, space and orientation. *Springer-Verlag Berlin Heideberg*, New York, 351 p.

Braathen A. and Gabrielsen R. H. 2000. Bruddsoner i fjell – oppbygning og definisjoner. *Norwegian geological survey (NGU). Gråsteinen,* vol. 7, 20 p.

Brattli B. 2002. Lecture notes on weathering. *MSc. course on hydropower development. Norwegian University of Science and Technology (NTNU)*, Norway.

Bray J. W. 1967. A study of jointed and fractured rock. Theory of limit equilibrium. *Felsmechanik und ingeneurgeologie (Rock mechanics and engineering geology)*, vol. 5, pp. 197-216.

Broch E. 1983. Estimation of strength anisotropy using the point load test. *International journal of rock mechanics and mining sciences & geomechanics abstracts,* vol. 20, pp. 181-187.

Broch E. and Sørheim S. 1984. Experience from the planning, construction and supporting of a road tunnel subjected to heavy rock-bursting. *Rock mechanics and rock engineering*, vol. 17, pp. 15-35.

Cai M., Kaiser P. K., Uno H., Tasaka Y. and Minami M. 2004. Estimation of rock mass strength and deformation modulus of jointed hard rock masses using the GSI system. *International Journal of rock mechanics and mining sciences*, vol. 41, pp. 3-19.

Carlsson A. and Olsson T. 1977. Variation of hydraulic conductivity in some Swedish rock types. *Proceedings: international symposium ROCKSTORE-77*, pp. 257-263.

Carosi R., Lombardo B., Musumeci G. and Pertusati P. C. 1999. Geology of the higher Himalayan crystalline in Khumbu Himal (Eastern Nepal). J*ournal of Asian earth sciences*, vol. 17, pp. 785-803.

Carranza-Torres C. and Fairhurst C. 2000. Application of the convergence confinement method of tunnel design to rock masses that satisfy the Hoek-Brown failure criteria. *Tunnelling and underground space technology*, vol. 15, pp. 187-213.

Casagrande A. 1965. Role of the "Calculated Risk" in earthwork and foundation engineering. *Journal of the soil mechanics and foundations division, proceedings ASCE*, vol. 91 (4), pp. 1-40.

Christian J. T., Ladd C. C. and Beacher G. B. 1994. Reliability applied to slope stability analysis. *Journal of geotechnical engineering, ASCE*, vol. 120 (12), pp. 2180-2207.

Civil Construction Consortium (CCC). 2002. Civil construction report. *Khimti I hydropower project*, volume I – main text.

Dahl F. (2003). DRI, BWI and CLI standard. *SINTEF*, 20 p.

Deoja B., Dhital M. and Wagner A. 1991a. Mountain risk engineering handbook. *International centre for integrated mountain development* (ICIMOD), Nepal.

Deoja B., Dhital M. and Wagner A. 1991b. Risk engineering in the Hindu Kush Himalaya. *International centre for integrated mountain development (ICIMOD)*, Nepal.

Department of Energy (DoE) .2003. South Asia regional overview. *Country analysis brief of the government of USA*. http://www.eia.doe.gov/emeu/cabs/sasia.html dated 29th September 2004.

Department of Road (DoR). 2004. Strategic road networks 1998 – 1999. *His Majesty's the Government of Nepal*. http://www.dormeu.gov.np dated 1st October 2004.

Einstein H. H. 2003. Uncertainty in rock mechanics and rock engineering – then and now. *Proceedings: the 10th congress of ISRM. ISRM 2003 – Technology roadmap for rock mechanics. South African Institute of Mining and Metallurgy,* pp. 281-293.

Einstein H. H. and Beacher G. B. 1982. Probabilistic and statistical methods in engineering geology, I. Problem statement and introduction to solution. *Rock mechanics supplement 12*, pp. 47-61.

Einstein H. H. and Beacher G. B. 1983. Probabilistic and statistical methods in engineering geology - specific methods and examples, part 1: exploration. *Rock mechanics and rock engineering*, vol. 19, pp. 47-61.

Einstein H. H., Labreche D. A., Markow M. J. and Beacher G. B. 1978. Decision analysis applied to rock tunnel exploration. *Engineering geology,* vol. 12, pp 143-161.

Fell R. 1993. Landslide risk assessment and acceptable risk. *Canadian geotechnical journal*, vol. 31, pp. 261-272.

Freeze R. A. and Cherry J. A. 1979. Ground water. *Prentice-Hall, Inc., Englewood Cliffs*, 553 p.

Galay V., Schreiev H. and Bestbier R. 2001. Himalayan sediments: Issues and guidelines. *CD-ROM- institutional development project. Water and energy commission secretariat (WECS), Ministry of Water Resources*, Nepal.

Gardner R. and Walsh N. 1996. Chemical weathering of metamorphic rocks from low elevations in the southern Himalaya. *Chemical geology*, vol. 127, pp. 167-176.

Gautem P. and Rosler W. 1999. Depositional chronology and fabric of Siwaliks group sediments in central Nepal from magneto-stratigraphy and magnetic anisotropy. *Journal of Asian earth sciences*, vol. 17, pp. 659-682.

Goel R. K. 2001. Status of tunnelling and underground construction activities and technologies in India. *Tunnelling and underground space technology*, vol. 16-2, pp 63-75.

Goel R. K., Jethwa J. L. and Paithankar A. G. 1995. Indian experience with Q and RMR systems. *Tunnelling and underground space technology*, vol. 10, pp. 97-109.

Goodman R. E. 1970. The deformability of joints. Determination of the in situ modulus of deformation of rock. *American society for testing and materials. Special technical publication*, 477, pp. 174-196.

Goodman R. E. 1989. Introduction to rock mechanics. *John Wiley & Sons*, 412 p.

Goodman R. E. 1993. Engineering geology. Rock in engineering construction. Second edition. *John Wiley & Sons*, 562 p.

Greminger M. 1982. Experimental studies of the influence of rock anisotropy on size and shape effects in point load testing. Technical note. *International journal of rock mechanics and mining sciences and geomechanics abstracts*, vol. 19, pp. 241-246.

Grimstad E. and Barton N. 1993. Updating the Q-system for NMT. Proceeding of the International Symposium on sprayed concrete – modern use of wet mix sprayed concrete for underground support, Fagernes. *Norwegian Concrete Association*, Oslo, Norway.

Grimstad E., Kankes K., Bhasin R., Magnussen A. W. And Kaynia A. 2003. *Proceeding of the international symposium on sprayed concrete,* September 2003, London.

Gudmundsson A., Fjeldskaar I. and Benner S. L. 2002. Propagation pathways and fluid transport of hydro-fractures in jointed and layered rocks in geothermal field. *Journal of volcanology and geothermal research*, vol. 116, pp. 257-278.

Guillot S. 1999. An overview of the metamorphic evolution in central Nepal. *Journal of Asian earth sciences*, vol. 17, pp.713-725.

Gupta A.S. and Rao K.S. 2000. Weathering effects on the strength and deformational behaviour of crystalline rocks under uniaxial compression state. *Engineering geology*, vol. 56, pp. 257-274.

Hagen T. 1968. Report on the geological survey of Nepal. Geology of the Thakkhola including adjacent areas. *Zurich memoires de la societe helvetique des sciences naturelles*, LXXXVI/1, 160 p.

Hagen T. 1969. Report on the geological survey of Nepal. Geology of the Thakkhola including adjacent areas. *Zurich memoire de la societe helvetique des sciences naturelles*, LXXXVI/2, 185 p.

Hatcher R. D. 1995. Structural geology. Principles, concepts and problems. *Prentice Hall, Englewood Cliffs, New Jersey,* 525 p.

Hawkins A. B. 1998. Aspects of rock strength. *Bulletins of engineering geology and environments*, vol. 57, pp. 17-30.

Helton J. C. and Davis F. J. 2003. Latin hypercube sampling and propagation of uncertainty in analyses of complex systems. *Reliability engineering and system safety*, vol. 81, pp. 23-69.

Himal Hydro (HH). 2001. Construction report. *Modi Khola hydroelectric project*. Nepal.

Himal Power Limited. 1995. Project definition report. *Khimti I hydropower project:* Nepal.

Hoek E. 1994. Strength of rock and rock masses. *ISRM news journal*, vol.2, pp4-16.

Hoek E. 1998. Practical rock engineering-2000 Edition. *Rocsciences: Hoeknotes 1998*. www.rocscience.com/roc/hoek/hoeknotes2000.html

Hoek E. 2001. Big tunnels in bad rocks. *ASCE journal of geotechnical and geoenvironmental engineering*, September 2001, pp. 726-740.

Hoek E. and Brown E. T. 1980. Underground excavation in rock. *Institute of mining and metallurgy*, London, 527 p.

Hoek E. and Brown E. T. 1997. Practical estimates of rock mass strength. *International journal of rock mechanics, mining sciences*, vol. 34, pp. 1165-1186.

Hoek E. and Marinos P. 2000. Predicting tunnel squeezing problems in weak heterogeneous rock masses. *Tunnels and tunnelling international*, vol. 32 (11 and 12), pp. 45-51 and pp. 34-36.

Hoek E., Marinos P. and Benissi M. 1998. Applicability of the geological strength index (GSI) classification for very weak and sheared rock masses. The case of the Athens schist formation. *Bulletin of engineering geology and environment*, vol. 57, pp. 151-160.

Hoek E., Torres C. C. and Corkum B. 2002. Hoek-Brown failure criterion – 2002 edition. *Proceedings North American rock mechanics society meeting*. Toronto, Canada.

Hudson J. A. 1989. Rock mechanics principles in engineering practice. *CIRIA ground engineering report: Underground construction*, 72 p.

Hudson J. A. 1993. Rock properties, testing methods and site characterization. *Comprehensive rock engineering, J. A. Hudson ed., Pergamo*n, vol. 3, pp. 1-39.

Hudson J. A. and Harrison J. P. 1997. Engineering rock mechanics. An introduction to the principles. *Pergamon,* 444 p.

Imam R. L., Davenport J. M. and Zeigler D. K. 1980. Latin hypercube sampling (A program user's guide). Technical report SAND79-1473. *Albuquerque, New Mexico: Sandia Laboratories*.

Indraratna B., Haque A. and Aziz N. 1999. Shear behavior of idealized joints under constant normal stiffness. *Geotechnique*, vol. 49-3, pp. 331-355.

ISRM. 1975. Report of the commission on terminology. *Lisbon.*

ISRM, 1978a. Suggested method for petrographic description of rocks. *International journal of rock mechanics and mining sciences & geomechanics abstracts*, vol. 15, pp. 43-45.

ISRM. 1978b. Suggested methods for the quantitative description of discontinuities in rock mass. *International journal of rock mechanics, mining sciences & geomechanics abstracts,* vol. 15, pp. 319-368.

ISRM, 1979a. Suggested methods for determining water content, porosity, density, absorption and related properties and swelling and slake durability index properties. *International journal of rock mechanics and mining sciences & geomechanics abstracts*, vol. 16, pp. 141-156.

ISRM, 1979b. Suggested methods for determining the uniaxial compressive strength and deformability of rock material . *International journal of rock mechanics and mining sciences & geomechanics abstracts*, vol. 16, pp. 135-140.

ISRM, 1985. Suggested method for determining point load strength. *International journal of rock mechanics and mining sciences & geomechanics abstracts*, vol. 22, pp. 51-60.

Joshi P. R. 2000. Importance of tunnelling for infrastructure development in Nepal. *Journal of Nepal geological society*, vol. 22, pp. 205-210

Karlsrud K. 2002. Control of water leakage when tunnelling under urban areas in the Oslo region. *Norwegian tunnelling society (NFF)*, publication 12, pp. 27-33.

Kassana L. B. and Nilsen B. 2003. Analysis of water leakage at lower Kihansi hydropower plant system in Tanzania, East Africa. *Waterpower XII - HCI publications*, pp. 1-12.

Kim B. H., Yang H. S. and Chung S. K. 2003. Revaluation of rock mass classification using multivariate analysis and estimation of tunnel support. *Proceedings: ISRM 2003 - Technology road map for rock mechanics. South African Institute of Mining and Metallurgy*, pp. 645-648.

Klootwijk C. T., Gee J. S., Smith G. M. and McFadden P. L. 1992. An early India-Asia contact: palaeomagnetic constraints from Ninetyeast Ridge ODP Leg 121. *Geology*, vol. 20, pp. 395-398.

Kovari K. 1998. Tunnelling in squeezing rock. *Tunnel*, vol. 5, pp. 12-31.

Lashkaripour G. R. and Dusseault M. B. 1993. A statistical study on shale properties: Relationships along principal properties. Proceedings: Probabilistic Methods in Geotechnical Engineering. *Li & Lo (eds), Balkema Rotterdam*, pp. 195-200.

Low B. K. 1997. Reliability analysis of rock wedges. *ASCE Journal of Geotechnical and geoenvironmental engineering*, vol. 123 (6), pp. 489-505.

Marinos V., Marinos P. and Hoek E. 2005. The geological strength index: application and limitations. *Bulletin of engineering geology and environment*, vol.64, pp. 55-65.

Martin C. D, Kaiser P. K. and Christiansson R. 2003. Stress, instability and design of underground excavations. *International journal of rock mechanics and mining sciences*, vol. 40, pp. 1027-1047.

McCutchen W. R. 1982. Some elements of a theory for in-situ stress. Technical note. *International journal of rock mechanics and mining sciences & geomechanics abstracts*, vol. 19, pp. 201-203.

Medhurst T. P. and Brown E. T. 1998. A study of the mechanical behaviour of coal for pillar design. *International journal of rock mechanics and mining sciences*, vol. 35, pp. 1087-1105.

Ministry of Water Resources (MoWR). 2003. Nepal country report presented by Minister for water resources His Majesty the Government of Nepal (HMGN). *Third World Water Forum*. Kyoto, Japan.

Ministry of Water Resources (MoWR). 1993. Feasibility study report by Butwal Power Company, Nepal and Norpower As, Norway. *Khimti I hydropower project*, volume I – main text.

Moores E. M. and Twiss R. J. 1995. Tectonics. *W.H. Freeman and Company*. New York.

Mugnier J. L., Leturmy P., Mascle G., Huyghe P., Chalaron E., Vidal G., Husson L. and Delcallau B. 1999. The Siwaliks of Western Nepal: Geometry and kinematics. *Journal of Asian earth sciences*, vol. 17, pp. 629-642.

Nasseri M. H. B., Rao K. S. and Ramamurthy T. 2003. Anisotropic strength and deformational behavior of Himalayan schist. *International journal of rock mechanics and mining sciences*, vol. 40, pp. 3-23.

National Planning Commission (NPC). 2003. Tenth plan. *His Majesty the Government of Nepal (HMGN)*. Unofficial translation from the webpage http://www.npc.gov.np dated 4th October 2004.

Nepal Electricity Authority (NEA). 1992. Detailed feasibility study. *Kaligandaki "A" hydroelectric project*, volume I – main report and volume III – appendices.

Nepal Electricity Authority (NEA). 1998. Upgrading of feasibility study. *Middle Marsyangdi hydroelectric project*.

Nepal Electricity Authority (NEA). 2000a. Completion report for headrace tunnel and surge tank. *Modi Khola hydroelectric project,* Parbat, Nepal.

Nepal Electricity Authority (NEA). 2000b. Tender design and preparation of tender documents. *Middle Marsyangdi hydroelectric project*. Basic design, volume 5 – geological report.

Nepal Electricity Authority (NEA). 2002a. Tender document - bill of quantities. *Middle Marsyangdi hydroelectric project*.

Nepal Electricity Authority (NEA). 2002b. Project completion report. Geology and geotechnical report, volume IV-A and geological drawings and exhibits, volume V-C. *Kaligandaki "A" hydroelectric project.*

Nepal Electricity Authority (NEA). 2004a. Kaligandaki "A" hydroelectric project.

Nepal Electricity Authority (NEA). 2004b. Tunnel geological log and registration of rock mass conditions. *Middle Marsyangdi hydroelectric project*. Unpublished.

Nepal Electricity Authority (NEA). 2004c. Point load strength test on lump samples. *Middle Marsyangdi hydroelectric project.* Unpublished.

Nikraz H. R. and Press M. 1993. Laboratory evaluation of the geotechnical design characteristics of the sandstone aquifers in the Collie Basin. Proceedings: Probabilistic methods in geotechnical engineering. *Li & Lo (eds), Balkema Rotterdam*, pp. 207-214.

Nilsen B. 1999. New trends in rock slope stability analysis. *Bulletin of engineering geology and environment*, vol. 58, pp. 173-178.

Nilsen B. and Palmstrøm A. 2000. Hand Book No. 2. Engineering geology and rock engineering. *Norwegian group for rock mechanics in cooperation (NBG) with Norwegian tunnelling society (NFF), Norway*, 249 p.

Nilsen B. and Thidemann A. 1993. Rock engineering. *Norwegian institute of technology (NTH), division of hydraulic engineering*. Hydropower development vol. 9, 156 p.

Nilsen B., Palmstrøm A. and Stille H. 1999. Quality control of a sub-sea tunnel project in complex ground conditions. *Proceedings of the world tunnel congress – challenges for the 21st century*, Oslo, Norway, pp. 137-145.

Nilsen B., Shrestha G. L., Panthi K. K., Holmøy K. H. and Olsen V. 2003. Classification Comparisons: RMR vs Q vs RMi. *Tunnels and Tunnelling International*, May 2003.

Norwegian Geotechnical Institute (NGI). 1997. Report on practical use of Q-method.

Palisade Corporation. 2002. Guide to using @Risk: Risk analysis and simulation add-in for Microsoft Excel. Version 4.5, 499 p.

Palmstrøm A. 1995. RMi – a rock mass characterization system for rock engineering purposes. PhD thesis. *Department of geology, University of Oslo*, 400 p. or *on* www.rockmass.net

Palmstrøm A. and Singh R. 2001. The deformation modulus of rock masses – comparison between the in situ test and indirect estimates. *Tunnelling and underground space technology*, vol. 16, pp. 115-131.

Panthi K. K. 1998. Direct link between Hetauda and Kathmandu - evaluation of proposed road tunnels, Nepal. *MSc thesis. Department of geology and mineral resources engineering. Norwegian University of Science and Technology (NTNU)*. Norway.

Panthi K. K. 2004. Tunnelling challenges in Nepal. *Proceeding: Norwegian national tunnelling conference "Fjellsprengningsteknikk Bergmekanikk / Geoteknikk 2004"*, Oslo, pp. 4.1-4.16.

Panthi K. K. and Gouro R. K. 2001. Technical auditing of civil works of the Kaligandaki "A" hydroelectric project. *Office of the Auditor General of Nepal*, Kathmandu.

Panthi K. K. and Nilsen B. 2005a. Significance of grouting for controlling leakage in water tunnels – a case from Nepal. *Proceedings: ITA-AITES 2005 world tunnelling congress & 31th ITA general assembly*, Istanbul, Turkey, pp. 931-937.

Panthi K. K. and Nilsen B. 2005b. Comparison between predicted and actual rock mass conditions: a review based on tunnel projects in Nepal. *Proceedings: Hydropower'05*, Stavangar, Norway, May 2005.

Pathak S. 2002. Probabilistic approach for rock slope stability analysis for Himalayan conditions – A contribution based on two Nepalese cases. Dr. Ing. *Thesis. Norwegian University of Science and Technology (NTNU)*, Norway.

Pathak S. and Nilsen B. 2004. Probabilistic rock slope stability analysis for Himalayan condition. *Bulletin of engineering geology and environment*, vol. 63, pp. 25-32.

Patrick J. O'B. 2001. Subduction followed by collision: Alpine and Himalayan examples. *Physics of the earth and planetary interiors*, vol. 127, pp. 277-291.

Paudel L. P. and Arita K. 2000. Tectonic and polymetamorphic history of the lesser Himalaya in central Nepal. *Journal of Asian earth sciences*, vol. 18, pp. 561-584.

Poudel T. R., Dangol V. and Sharma R. H. 1998. Construction phase engineering geological study in Modi Khola hydroelectric project, Nepal. *Journal of Nepal Geological Society*, vol. 18, pp. 343-355.

Prasad Y. 2003. Hydropower potential and future prospect. *National hydroelectric power corporation limited (NHPC), India*. Webpage: www.nhpcindia.com dated 15th January 2004.

Ramamurthy T. 1993. Strength and modulus responses of anisotropic rocks. *Comprehensive rock engineering*, *J. A Hudson ed., Pergamon,* vol. 1, pp. 313-329.

Rao N. P., Kumar M.R. and Tsukuda T. 2003. Current deformation of the Himalaya-Tibet-Burma seismic belt: inferences from seismic activity and strain rate analysis. *Journal of geodynamics*, vol. 36, pp. 485-496.

Regmi S. K. and Sitaula T. P. 2003. Krishnabhir slide a case study. *Proceedings: International seminar on sustainable slope risk management for roads*, March 2003, Kathmandu, pp. 156-163.

Rhardjo H., Aung K. K., Leong E. C. and Rezaur R. B. 2004. Characteristics of residual soils in Singapore as formed by weathering. *Engineering geology*, vol. 73, pp. 157-169.

Robyr M., Vannay J. C., Epard J. L. and Steck A. 2002. Thrusting, extension, and doming during the polyphase tectonometamorphic evolution of the high Himalayan crystalline zone in NW India. *Journal of Asia earth sciences*, vol. 22, pp. 221-239.

Rowland S. M. and Duebendorfer E. M. 1994. Structural analysis and synthesis. A laboratory course in structural geology. 2nd Edition. *Blackwell scientific publications,* 279 p.

Sarkar I. and Chander R. 2003. Role of static stress transfer in earthquake occurrence in the Himalaya. *Journal of Asia earth sciences*, vol. 22, pp. 59-65.

Serafim J. L. and Pereira J. P. 1983. Consideration of the geomechanics classification of Bieniawaski. *Proceedings: International symposium on engineering geology and underground construction*, pp. 1133-1144.

Sharma C. K. 1990. Geology of Nepal Himalaya and adjacent countries. *Sangeeta Sharma, Bishal Nagar*, Kathmandu, Nepal.

Shroder J. F. and Bishop M. P. 1998. Mass movement in the Himalaya: new insights and research directions. *Geomorphology*, vol. 26, pp. 13-35.

Singh B., Goel R. K., Jethwa J. L. and Dube A. K. 1997. Support pressure assessment in arched underground opening through poor rock masses. *Engineering geology*, vol. 48, pp. 59-81.

Singh B., Jethwa J. L., Dube A. K. and Singh B. 1992. Correlation between observed support pressure and rock mass quality. *Tunnelling and underground space technology*, vol. 7, pp. 59-74.

SINTEF. 1993. Determination of mechanical properties of rock by hydraulic fracturing and dilatometer tests for Kaligandaki "A" hydroelectric project. SINTEF rock and mineral engineering, Norway.

Steinar W. 1996. Tunnelling in squeezing rocks – case histories. *Rock mechanics and rock engineering*, vol. 29, pp. 211-246.

Stille H. and Palmstrøm A. 2003. Classification as a tool in rock engineering. *Tunnelling and underground space technology*, vol. 18, pp. 331-345.

Tang W. H. 1993. Recent developments in geotechnical reliability. Key note address. Proceedings: Probabilistic methods in geotechnical engineering. *Li & Lo (eds), Balkema Rotterdam*, pp. 3-27.

Tokheim O. and Janbu N. 1984. Flow rates of air and water from caverns in soil and rock. Proceedings: *ISRM-symposium on rock mechanics related to caverns and pressure shafts, Aachen, A. A. Balkema*, vol.3, pp. 1335-1343.

Tsidzi K. E. N. 1987. Foliation index determination for fine grained metamorphic rocks. *Bulletin of the international association of engineering geology*, vol 36, pp. 81-88.

United Nations Economic and Social Commission for Asia and Pacific (UNESCAP). 1996. Nepal country paper on infrastructure development. *The ministerial conference*, October 1996, New Delhi.

Upreti B. N. 1999. An overview of the stratigraphy and tectonic of the Nepal Himalaya. *Journal of Asian earth sciences*, vol. 17, pp. 577-606.

Whitman R. V. 2000. Organizing and evaluating uncertainty in geotechnical engineering. *Journal of geotechnical and geoenvironmental engineering, ASCE*, vol. 126 (7), pp. 583-593.

World Stress Map (WSM) *website:* www.world-stress-map.org

Wu T. H. and Kraft L. M. 1967. The probability of foundation safety. *Journal of the soil mechanics and foundations division, proceedings ASCE*, vol. 93 (5), pp. 213-230.

Wu T. H. and Kraft L. M. 1970. Safety analysis of slope. *Journal of the soil mechanics and foundations division, proceedings ASCE*, vol. 96 (2), pp. 609-630.

Appendices

Appendix A
Rock mass classification systems

A.1 INTRODUCTION

Rock mass classification systems are the means used extensively to quantitatively describe the quality of rock mass and to estimate rock support requirement at pre-construction phases. The use of rock mass classifications are also important during construction phases since they become decisive for monitoring, recording and comparing predicted and actual rock mass conditions (Bieniawski, 1997). However, as pointed out by Stille and Palmstrøm (2003), the risks for misuse in terms of both terminology and applications should always be kept in mind.

There are mainly two areas where rock mass classification systems have been widely used in Nepal Himalaya: 1) For evaluating rock mass conditions and estimating required rock support measures in tunnels during pre-construction and construction phases, and 2) for estimating rock mass properties such as deformation modulus and rock mass strength.

The Q-system (Barton et al, 1974) and the RMR-system (Bieniawski, 1973) are widely used rock mass classification systems in Nepal. In recent years, the RMi-system (Palmstrøm, 1995) and the GSI-system (Hoek, 1994) have also been used, particularly for estimating rock mass strength and deformability properties. These four rock mass classification systems are briefly discussed here with main emphasis on the Q-system, which has been used in this thesis as a basis for uncertainty and risk analysis.

A.2 Q-SYSTEM

Based on analysis and evaluation of approximately 200 tunnel cases, Barton et al (1974) of the Norwegian Geotechnical Institute (NGI) proposed the Q-system of rock mass classification. The Q-system gives useful correlation between Q-value and tunnel rock support. This method has got major updates in 1993 with the inclusion of data base from more than 1000 tunnel cases (Grimstad and Barton, 1993). Several papers have been published on the Q-system aiming to extend its applications in the estimation of rock mass properties (Barton, 2002 and Grimstad et al, 2003). In principle, this system is based on a numerical assessment of six different input parameters as defined by Equation A-1. The numerical estimation of these six input parameters according to Barton (2002) is presented in Table A-1.

$$Q = \frac{RQD}{J_n} \times \frac{J_r}{J_a} \times \frac{J_w}{SRF} \qquad \text{(A-1)}$$

Where; *RQD* is the rock quality designation, J_n is the joint set number, J_r *is the* joint roughness number, J_a is the joint alteration number, J_w is the joint water reduction factor, and *SRF* is the stress reduction factor.

Table A-1. Description of ratings for input parameters of Q-system (based on Barton, 2002).

RQD (Rock quality designation, %)		***J_n (Joint set number)***	
Very poor	0 - 25	Massive, no or few joints	0.5 - 1
Poor	25 - 50	One joint set	2
Fair	50 – 75	One joint set + random joints	3
Good	75 – 90	Two joint sets	4
Excellent	90 - 100	Two joint sets + random	6
<u>Notes:</u>		Three joint sets	9
(i) where RQD is reported or measured as ≤ 10 (including 0), a nominal value of 10 is used to evaluate Q.		Three joint sets + random	12
		Four or more joint sets, heavily jointed, sugar cube etc	15
(ii) RQD intervals of 5 i.e. 100, 95, 90 etc., are successfully accurate.		Crushed rock, earthlike	20
		<u>Note:</u> For tunnel intersections, use (3 x J_n) and for portals use (2 x J_n)	

J_r (Joint roughness number)			
(a) Rock wall contact		*(b) Rock wall contact before 10 cm shear*	
Discontinuous joints	4	Rough or irregular, undulating	1.5
Rough or irregular, undulating	3	Smooth, undulating	1
Smooth, undulating	2	Slickensided, undulating	0.5
Slickensided, undulating	1.5		
© No rock wall contact when sheared			
Zone containing clay minerals thick enough to prevent rock wall contact			1
Sandy, gravely or crushed zone thick enough to prevent rock wall contact			1
<u>Notes:</u> (i) Description refers to small-scale features and intermediate scale features, in that order (ii) Add 1.0 if the mean spacing of the relevant joint set is greater than 3 m. (iii) Jr = 0.5 can be used for planner, slickenside joints having lineations, provided these are oriented for minimum strength. (iv) Jr and Ja classification is applied to the joint set that is least favorable for stability both from the point of view of orientation and shear resistance, $\tau \approx \sigma_n \,.\, \tan^{-1}(J_r/J_a)$			

J_a (Joint alteration number)		
(a) Rock wall contact (no mineral fillings, only coatings)	*$ø_r$ (appr.)*	***J_a***
Tightly healed, hard, non-softening, impermeable filling i.e., quartz/epidote	-	0.75
Unaltered joint walls, surface staining only	25 - 35	1
Slightly altered joint walls, non-softening mineral coatings, sandy particles, clay free disintegrated rock ,etc.	25 - 30	2
Silty or sandy clay coatings, small clay fractions (non-softening)	20 - 25	3
Softening or low friction clay mineral coatings, i.e., kaolinite or mica. Also chlorite, talk, gypsum, graphite etc., and small quantities of swelling clay	8 - 16	4
(b) Rock wall contact before 10 cm shear (thin mineral fillings)		
Sandy particles, clay free disintegrated rock etc.	25 - 30	4
Strongly over-consolidated non-softening clay mineral fillings (continuous, but < 5mm thickness)	16 - 24	6

Medium or low over-consolidated non-softening clay mineral fillings (continuous, but < 5mm thickness)	12 - 16	8
Swelling clay fillings, i.e., montmorillonite (continuous, but < 5mm thick)	6 - 12	8 - 12
(c) No rock wall contact when sheared (thick mineral fillings)		
Zones or bands of disintegrated or crushed rock and clay	6 - 24	6, 8 - 12
Zones or bands of silty or sandy clay, small clay fraction (non-softening)	-	5
Thick, continuous zones or bands of clay	6 - 24	13 - 20

J_w (Joint water reduction factor)	*Approx. P (bars)*	***J_w***
Dry excavations or minor inflow, i.e., < 5 l/min locally	< 1	1
Medium inflow or pressure, occasional outwash of joint fillings	1 – 2.5	0.66
Large inflow or high pressure in competent rock with unfilled joints	2.5 - 10	0.5
Large inflow or high pressure, considerable outwash of joint fillings	2.5 - 10	0.33
Exceptionally high inflow or pressure at blasting, decaying with time	> 10	0.2 – 0.1
Exceptionally high inflow or pressure continuing without noticeable decay with time	> 10	0.2 – 0.1

<u>*Notes:*</u> (i) The last four factors are crude estimates. Increase J_w if drainage measures are installed. (ii) Special problems caused by ice formation are not considered. (iii) For general characterization of rock masses distance from excavation influences. The use of J_w = 1, 0.66, 0.5, 0.33, etc. as depth increases from say 0-5, 5-25, 25-250 to >250m is recommended, assuming that RQD/J_n is low enough (0.5-25) for good hydraulic connectivity.

SRF (Stress Reduction Factor)

(a) Weakness zones intersecting excavation, which may cause loosening of rock mass	*SRF*
Multiple occurrence of weakness zones containing clay or chemically disintegrated rock, very loose surrounding rock at any depth	10
Single weakness zone containing clay or chemically disintegrated rock (depth ≤ 50m)	5
Single weakness zone containing clay or chemically disintegrated rock (depth > 50m)	2.5
Multiple shear zones in competent rocks (clay free), loose surrounding rock at any depth	7.5
Single shear zone in competent rocks (clay free), (depth of excavation ≤ 50m)	5
Single shear zone in competent rocks (clay free), (depth of excavation > 50m)	2.5
Loose, open joints, heavily jointed or sugar cube etc. at any depth	5

<u>*Note:*</u> Reduce these values of SRF by 25 – 50 % if the relevant shear zones only influence but do not intersect the excavation.

(b) Competent rock, rock stress problems	σ_c / σ_1	σ_t / σ_c	*SRF*
Low stress, near surface, open joints	> 200	< 0.01	2.5
Medium stress, favorable stress condition	200 - 10	0.01 – 0.3	1
High stress, very tight structures. Usually favorable to stability, may be unfavorable for wall stability	10 - 5	0.3 – 0.4	0.5 - 2
Moderate slabbing after > 1 hour in massive rock	5 - 3	0.5 – 0.65	5 - 50
Slabbing and rock burst after a few minutes of excavation	3 - 2	0.65 - 1	50 - 200
Heavy rock burst and immediate dynamic deformations	< 2	> 1	200 – 400

<u>*Notes:*</u> (i) For strongly anisotropic virgin stress field (if measured): when $5 \leq \sigma_1 / \sigma_3 \leq 10$, reduce σ_c *to* $0.75\ \sigma_c$ and when $\sigma_1 / \sigma_3 > 10$, reduce σ_c *to* $0.5\ \sigma_c$. (ii) For general characterization of rock mass, overburden from excavation influences. The use of SRF 5, 2.5, 1 and 0.5 is recommended as depth increases from say 0-5, 5-25, 25-250 to > 250m respectively.

© Squeezing rock: plastic flow of incompetent rock under the influence of high rock pressure	σ_t / σ_c	*SRF*
Mild squeezing rock pressure	1 - 5	5 - 10
Heavy squeezing rock pressure	> 5	10 - 20

(d) Swelling rock: chemical swelling activity depending on pressure of water	*SRF*
Mild swelling rock pressure	5 - 10
Heavy swelling rock pressure	10 - 15

In the original version of Q-system, Barton et al (1974) defined rock mass quality in nine different classes ranging from 'exceptionally poor' to 'exceptionally good' and the Q-value was correlated with actually applied rock support measures in the tunnels. In 1993, Grimstad and Barton modified the Q-system, particularly its support chart and inclusion of squeezing conditions on the *SRF* rating. The most recent version of the support chart is shown in Figure A-1.

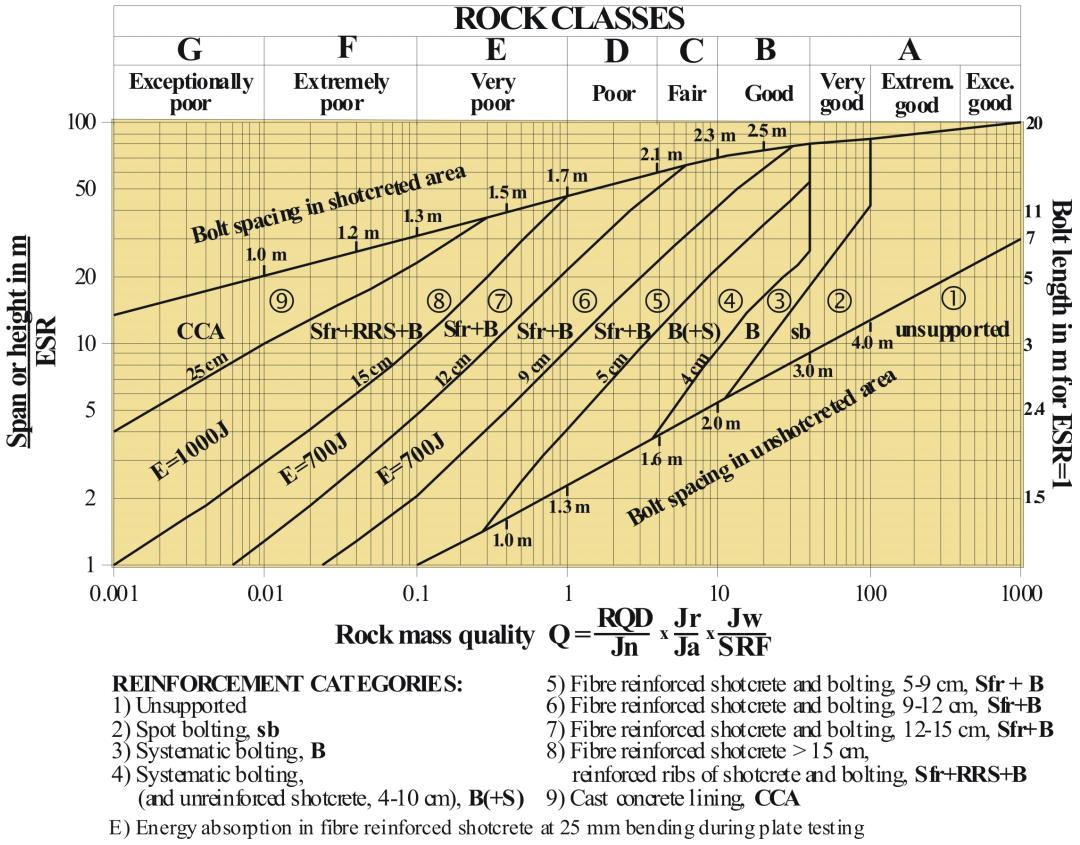

Figure A-1. Updated rock support chart for tunnels and caverns (after Grimstad et al 2003).

As can bee seen in Figure A-1, the rock support chart incorporates the equivalent excavation dimension, which is the ratio between the span or height of an underground opening and an excavation support ratio (ESR). According to NGI (1997), the ESR reflects the degree of safety and support required for the underground opening. Its value varies from 5 to 0.5 depending upon the type of underground excavation. For instance, an ESR value of 1.6 is used for water tunnels, permanent mine openings, adits and drifts and an ESR value of 1 for underground power house, road tunnels, railway tunnels, and civil defense chambers. For more details, reference is made to NGI (1997).

In the author's opinion, the main strength of the Q-system is the well described support chart, which is useful particularly for quantitative estimation of tunnel rock support at the pre-construction phase of the project, when there is a great need for reliable and trustworthy economic evaluation.

According to Stille and Palmstrøm (2003), the major criticism that the Q-system has received is connected to the SRF. This is because, as shown in Table A-1**,** it represents four complicated factors; weakness zones, stress influence in brittle, blocky and massive ground, stress influence in deformable (ductile) rock mass and swelling rocks. Barton (2001) argues that since the Q-system is an empirical design tool based on applied rock support of already completed project cases, it is logical that water and stress parameters are components of the classification systems.

A.3 RMR-SYSTEM

Bieniawaski already in 1973 introduced an empirical rock mass classification system called rock mass rating (RMR) system (also known as Geomechanics Classification). Over the years, this classification system has been modified as more case histories have become available. The last modification was made in 1989 (Bieniawaski, 1989). Basically, the RMR-system uses the following six parameters to classify a rock mass:

1. Uniaxial compressive strength of the rock
2. Rock quality designation (RQD)
3. Spacing of discontinuities
4. Condition of discontinuities
5. Ground water conditions and
6. Orientation of discontinuities

These classification parameters are evaluated by field measurements as shown in Table A-2 giving a numerical rating value to each parameter. The rating of each of these parameters is summarized to give a value of RMR, which can be used to define rock mass quality and its class. The RMR is also related to stand-up time as shown in Figure A-2.

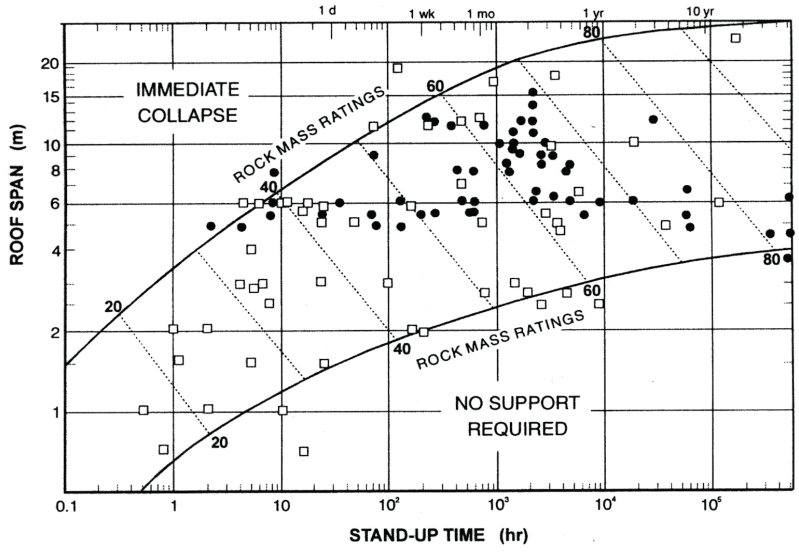

Figure A-2. Stand-up time of an underground opening as a function of roof span and RMR value (Bieniawaski, 1989).

Table A-2. RMR classification of rock mass (Bieniawaski, 1989).

A. Classification parameters and their ratings									
Parameters			Range of values or ratings						
1	Strength of Intact Rock	Point load strength index (MPa)	> 10	4 - 10	2 - 4	1 - 2	Low range uniaxial strength is preferred		
		Uniaxial compressive strength (MPa)	> 250	100-250	50-100	25-50	5- 25	1 - 5	< 1
	Rating		**15**	**12**	**7**	**4**	**2**	**1**	**0**
2	Drill core quality, RQD (%)		90-100	75-90	50-75	25-50	< 25		
	Rating		**20**	**17**	**13**	**8**	**5**		
3	Spacing of discontinuities (m)		> 2	0.6-2	0.2-0.6	0.06-0.2	< 0.06		
	Rating		**20**	**15**	**10**	**8**	**5**		
4	Condition of discontinuities	Length, persistence (m)	< 1	1-3	3-10	10-20	> 20		
		Rating	**6**	**4**	**2**	**1**	**0**		
		Separation (mm)	none	< 0.1	0.1-1	1-5	> 5		
		Rating	**6**	**5**	**4**	**1**	**0**		
		Roughness	very rough	rough	slightly rough	smooth	slickensided		
		Rating	**6**	**5**	**3**	**1**	**0**		
		Infilling (gouge) (mm)	none	hard filling		soft filling			
				< 5	> 5	< 5	> 5		
		Rating	**6**	**4**	**2**	**2**	**0**		
		Weathering	unweathered	slightly weathered	moderately weathered	highly weathered	decomposed		
		Rating	**6**	**5**	**3**	**1**	**0**		
5	Ground water	Inflow per 10 meter tunnel length (l/min)	none	< 10	10-25	25-125	> 125		
		ρ_w / σ_1	0	0.0.1	0.1-0.2	0.2-0.5	> 0.5		
		General conditions	dry	damp	wet	dripping	flowing		
		Rating	**15**	**10**	**7**	**4**	**0**		
		here, ρ_w is joint water pressure and σ_1 is major principle stress							
B. Rating adjustment for discontinuity orientation									
Tunnel alignment			very favorable	favorable	fair	unfavorable	very unfavorable		
Rating adjustment			**0**	**-2**	**-5**	**-10**	**-12**		
C. Rock mass classes determined from total ratings									
Rating			100-80	80-61	60-41	40-21	< 20		
Class No.			I	II	III	IV	V		
Description			Very good	Good	Fair	Poor	Very poor		
D. Meaning or rock mass classes									
Class No.			I	II	III	IV	V		
Average stand-up time			Can be estimated from Figure 4-4						
Cohesion of the rock mass (kPa)			> 400	3-400	2-300	1-200	< 00		
Friction angle of the rock mass (degrees)			< 45	35-45	25-35	15-25	< 15		

The main strength of the RMR-system is its relationship with the standup time, see Figure A-2, and its correlation with rock mass properties and with Hoek-Brown failure criterion to estimate constants such as *m* and *s*. The major deficiency is that its lacks a good system for prediction of rock support measures (Bieniawaski suggested a support table that is suitable only for a single sized tunnel with 10 meters span).

When using the RMR system at the planning and design phases, the rock mass is divided into structural regions with uniform features within each region. During tunnel excavation, the rating is generally related to the length of the blasting round or the recently excavated tunnel section.

A.4 RMi-SYSTEM

The rock mass index (RMi) is a rock mass characterization system developed by Palmstrøm in 1995. In principle it considers reduction in the intact rock strength caused by presence of joints. Thus, the RMi is meant to express approximate compressive strength of the rock mass as defined by Equation A-2 based on intact rock strength (σ_{ci}) and jointing parameters (JP) (Palmstrøm, 1995).

$$RMi = \sigma_{ci} \times JP = \sigma_{ci} \times 0.2\sqrt{jC} \times Vb^{D} \Rightarrow (D = 0.37 \times jC^{-0.2}) \qquad (2)$$

Where; σ_{ci} is the uniaxial compressive strength of intact rock measured on 50mm diameter sample, *Vb* is the block volume in cubic meters that can be measured at site by observation and $jC = jL \times jR / jA$ is the joint condition factors (a function of joint size and continuity factor jL, joint roughness factor jR and joint alteration factor jA).

The RMi-system is not used in any of the analysis discussed in this thesis, and therefore will not be discussed in any more detail here.

A.5 GSI-SYSTEM

When developing the Hoek-Brown failure criterion for rock mass in the late seventies, Hoek and Brown (1980) realized that there will be no meaning if such a criterion is not related to a rock mass classification system. They decided to relate it to RMR system. Before the 1990s the RMR system worked well in the criterion because most of the tunnel stability problems were in reasonable quality rock mass having RMR value between 30 to 70 under moderate stress conditions. However, it soon became obvious that the RMR system was difficult to apply for the estimating constants *m* and *s* for highly fractured rock mass with low RQD values (close to zero) and for very poor quality rock mass. To address this deficiency, Hoek (1994) introduced a new classification system called geological strength index (GSI). Since its development the GSI-system has been updated continuously and its use has increased significantly. In this system a GSI chart suggested by Hoek et al (1998) is the basis that incorporates very poor quality rock mass, see Figure A-3.

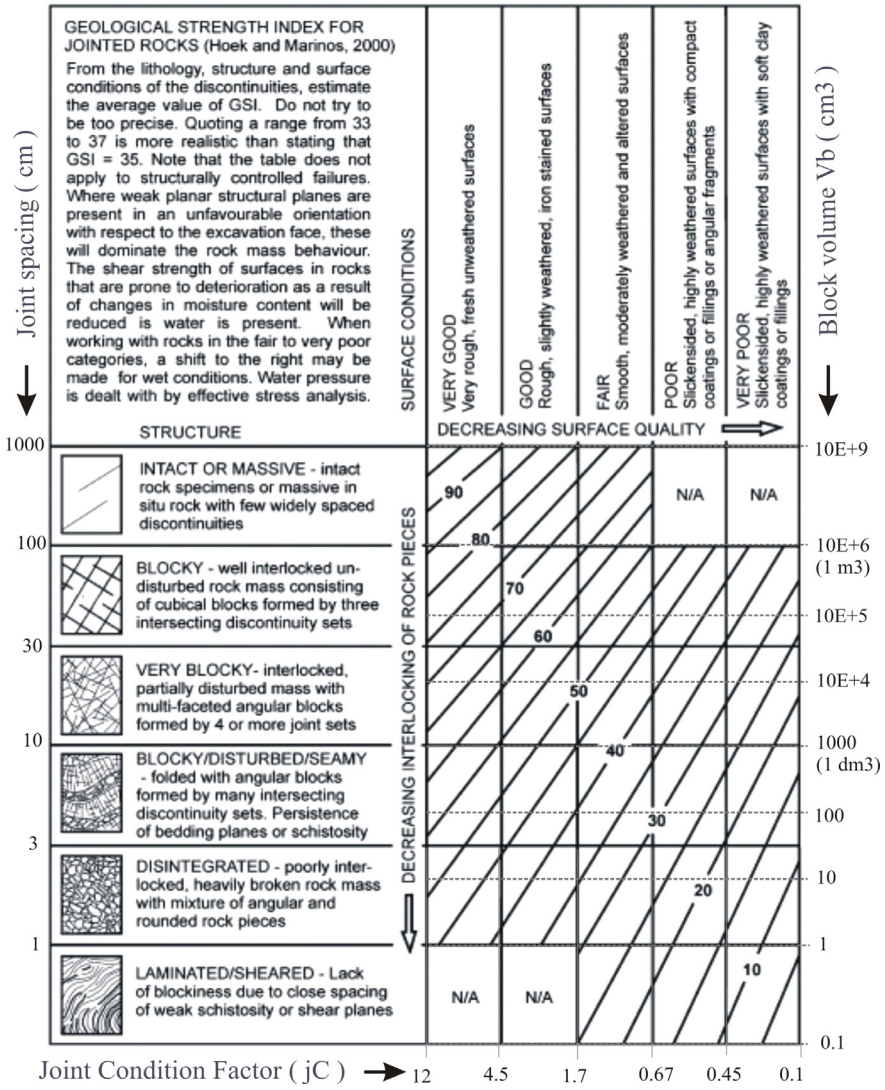

Figure A-3. General chart for GSI estimation from the geological observations (based on Cai et al, 2004 and Marinos et al, 2005).

The GSI system gives more emphasis on geological observations reflecting rock material and its geological structure. The basis of GSI classification is careful description of engineering geological conditions by qualitative judgment. As shown in Figure A-3, an attempt was made by Cai et al (2004) to incorporate quantitative description by adding the discontinuity features such as joint condition factor jC, block volume Vb and joint spacing. Marinos et al (2005) suggested that the quantification proposed by Cai et al should be limited to cases when these discontinuity properties can be easily measured.

The major strength of the GSI- system is its interconnection with rock mass strength (σ_{cm}), rock mass deformation modulus (E_{rm}) and constants *m* and *s* of Hoek-Brown failure criterion.

A.6 CONCLUDING REMARKS

All rock mass classification systems are empirical tools and are generally useful for evaluating rock mass quality and for estimating tunnel rock support during planning and design. The accuracy for estimating tunnel rock support and rock mass properties based on these systems however represent approximation and is difficult to evaluate. The Q-system, which is widely used, is believed most often to give a reliable estimation on rock support.

The usefulness and reliability of rock mass classification systems may be improved considerably if uncertainty and risk analysis is performed at an early stage of planning and design. Such analysis may help to judge the consequences of deviation between predicted and actual rock mass quality. The principle of such analysis is discussed in Chapter 6 of this thesis.

Appendix B
Laboratory and field test results

Table B-1. Mechanical properties of intact rock.

Rock Types	Project / Location	Core orientation with foliation	Dimensions		Mechanical properties						
			Diameter (d)	Length	Porosity	Density	Longitudinal sonic velocity	Young's modulus	Poisson's ratio	UCS (σ_c)	UCS (σ_{c50})
			mm	mm	%	gm / cm^3	m / sec	(E) GPa	v	MPa	MPa
Banded gneiss	Khimti I, Adit 1 (remains of blast)	Perpendicular	33	86	0.91	2.71	3420	28	0.11	50	46
			33	86	0.88	2.64	3957	23	0.13	51	47
			32	86	0.82	2.69	3786	23	0.11	60	55
		Mean	32.7	86.0	0.87	2.68	3721	25	0.12	54	50
		St. Deviation			0.05	0.04	274	3	0.01	6	5
Augen mica gneiss	Khimti, Adit 2 (remains of blast)	Perpendicular	33	86	0.66	2.76	3152	27	0.11	45	42
			33	86	0.86	2.78	3045	18	0.09	33	31
			33	86	0.75	2.65	2780	23	0.11	45	42
		Mean	33	86	0.76	2.73	2992	22	0.10	41	38
		St. Deviation			0.10	0.07	192	4	0.01	7	6
Siliceous Dolomite	Kaligandaki "A" (cores from desander slope)	Perpendicular	51	125	0.34	2.78	4845	61	0.15	290	291
			51	121	0.52	2.87	3878	60	0.11	231	231
			51	123	0.47	2.83	4227	50	0.10	274	274
		Mean	51	123	0.44	2.82	4317	57	0.12	265	265
		St. Deviation			0.09	0.04	490	6	0.03	31	31
Graphitic Phyllite	Kalgandaki "A" (cores from tunnel at intake side)	Perpendicular	45	113	0.42	2.78	4079	25	0.14	37	36
			45	109	0.44	2.79	3385	29	0.10	45	44
			45	112	0.48	2.77	3902	27	0.06	37	36

		Mean	45	111	0.45	2.78	3789	27	0.10	40	39
		St. Dev.			0.03	0.01	361	2	0.04	5	5
Quartzite	Modi Khola (naturally broken)	Perpendicular	33	86	0.25	2.59	5670	84	0.11	260	241
			33	86	0.23	2.62	5665	81	0.12	212	197
			33	86	0.18	2.60	5695	86	0.15	242	225
		Mean	33	86	0.22	2.60	5677	83	0.13	238	221
		St. Dev.			0.04	0.02	16	2	0.02	24	23
Quartzite	Middle Marsyangdi (remains of blast from power tunnel, adit 2 downstream)	Perpendicular	33	86	0.34	2.62	4782	49	0.10	210	195
			33	86	0.29	2.63	4693	46	0.11	218	202
			33	86	0.27	2.62	4732	43	0.10	185	172
		Mean	33	86	0.30	2.62	4736	46	0.10	204	190
		St. Dev.			0.04	0.01	45	3	0.01	17	16
Siliceous Phyllite	Middle Marsyangdi (remains of blast from power tunnel, adit 3 upstream)	Perpendicular	33	89	0.68	2.89	3735	13	0.05	46	43
			33	83	0.81	2.84	3828	13	0.05	45	42
			33	84	0.83	2.86	3540	15	0.05	36	33
		Mean	33	85	0.77	2.86	3701	14	0.05	42	39
		St. Dev.			0.08	0.03	147	1	0.00	6	5
Metasandstone	Middle Marsyangdi (cores from surge tank)	Perpendicular	48	118	0.68	2.65	4055	63	0.16	119	118
			48	104	1.04	2.64	3777	39	0.12	51	51
			48	104	0.71	2.67	3593	37	0.13	52	52
		Mean	48	109	0.81	2.65	3808	46	0.14	74	73
		St. Dev.			0.20	0.02	233	14	0.02	39	39

Table B-2. Slake-durability for various cycles of drying and wetting.

Number of cycles	MM quartzite	MM siliceous phyllite T2	MM siliceous phyllite T1	MM micaceous phyllite S1	MM micaceous phyllite T4	MM micaceous phyllite T3	MM micaceous phyllite S2	KGA graphite phyllite T2	KGA graphite phyllite S1	KHP banded gneiss	KHP mica gneiss
0	100.00	100.00	100.00	100.00	100.00	100.00	100.00	100.00	100.00	100.00	100.00
1	99.89	98.60	98.22	95.27	95.89	96.89	94.01	98.05	93.30	99.16	99.04
2	99.61	96.17	95.99	88.39	92.52	93.30	87.17	95.07	86.19	98.71	97.92
3	99.45	94.71	94.23	84.12	89.92	90.69	83.17	92.33	82.16	98.28	96.95
4	99.20	91.72	92.06	81.30	87.57	88.19	80.03	88.89	78.89	97.93	96.11

Note: 1. Sample location as per Table 4-4.
2. MM = Middle Marsyangdi, KGA = Kaligandaki "A" and KHP = Khimti

Table B-3. Measured N/NR Schmidt hammer rebound numbers at Middle Marsyangdi.

Rock types	Location	Measurement Direction	Measured rebound values															Mean	Standard deviation
Quartzite	Between chainage 0 to 500)	Perpendicular to foliation	58	59	52	50	50	48	54	56	59	57	56	52	52	48	59	54	4.2
			54	49	53	50	54	51	60	58	56	56	44	46	56	59	52		
			48	52	58	58	54	49	46	54	59	60	54	52	55	54	56		
			59	56	57	49	59	63	53	50	58	55	54	52	51	48	49		
			60	53	46	52	53	52	56	56	56	50	53	56	49	58	46		
Siliceous Phyllite	Between chainage 600 to 900 and 4050 to 4200	Perpendicular to foliation	28	18	35	28	34	32	33	36	36	28	26	31	29	17	30	29	5.3
			32	25	26	23	21	22	26	28	19	20	23	24	30	33	31		
			30	36	29	27	30	31	25	26	22	21	38	37	38	33	23		
			39	37	27	26	42	36	28	29	31	27	30	31	26	28	30		
			30	28	26	27	34	39	27	29	35	33	36	36	20	22	24		
			26	25	31	33	39	26	28	27	30	31	32	36	25	27	28		
Micaceous Phyllite	Between Jamitri and Khahare khola	Perpendicular to foliation	11	12	15	13	14	14	13	10	12	12	16	10	10	12	12	13	2.2
			13	15	10	14	11	13	13	10	14	13	12	14	15	10	16		
			17	16	12	12	10	17	12	13	18	15	17	16	13	14	16		
			16	13	10	12	15	13	13	10	12	14	12	15	16	13	12		
Metasand-stone	Between chainage 4500 to 5000	Perpendicular to foliation	38	33	53	50	50	59	35	39	46	45	33	30	48	52	48	40	8.0
			33	38	44	42	48	46	43	45	41	42	56	53	52	46	46		
			36	33	37	32	43	38	44	46	46	41	26	23	49	46	32		
			36	45	37	33	28	30	33	30	29	35	34	36	32	35	39		

Note: 1. Foliation planes are dipping 15 – 25 degrees towards northeast at the upstream end (in quartzite). Further downstream, in other rocks the dip angle increases gradually up to 35 degrees. 2. Minimum 5 hit at single location and each value represents the most frequent one.

Table B-4. Point load test results on lump samples conducted at site on regular basis (NEA, 2004c).

Rock types	No.	Dimensions				Load	Axial point load strength, I_s	Corrected point load strength, I_{s50}
		W	H	A	De			
		mm	mm	mm^2	mm	N	MPa	MPa
Quartzite (samples between chainage 0 and 500)	1	45	50	2250	54	20000	7.0	7.2
	2	52	54	2808	60	20500	5.7	6.2
	3	50	58	2900	61	19500	5.3	5.8
	4	39	45	1755	47	18000	8.1	7.9
	5	40	52	2080	51	23000	8.7	8.8
	6	35	50	1750	47	16000	7.2	7.0
	7	40	47	1880	49	16500	6.9	6.8
	8	40	42	1680	46	19000	8.9	8.6
	9	49	51	2499	56	20000	6.3	6.6
	10	40	41	1640	46	20000	9.6	9.2
	11	50	51	2550	57	21000	6.5	6.9
	12	50	52	2600	58	20000	6.0	6.4
	13	49	50	2450	56	19000	6.1	6.4
	14	45	50	2250	54	23000	8.0	8.3
	15	35	49	1715	47	17000	7.8	7.6
	16	43	52	2236	53	19000	6.7	6.9
	17	42	44	1848	49	20000	8.5	8.4
	18	41	45	1845	48	19000	8.1	8.0
	19	40	45	1800	48	18000	7.9	7.7
	20	40	44	1760	47	17500	7.8	7.6
	21	48	49	2352	55	20000	6.7	7.0
	22	40	42	1680	46	18000	8.4	8.1
	23	44	45	1980	50	19500	7.7	7.7
	24	43	44	1892	49	19000	7.9	7.8
	25	36	44	1584	45	18500	9.2	8.7
	26	43	43	1849	49	18500	7.9	7.8
	27	45	46	2070	51	19500	7.4	7.5
	28	40	45	1800	48	20500	8.9	8.8
	29	43	44	1892	49	18500	7.7	7.6
	30	48	50	2400	55	21500	7.0	7.4
	31	42	50	2100	52	21500	8.0	8.2
	32	45	46	2070	51	18500	7.0	7.1
Mean							7.5	7.6
Standard deviation							1.1	0.8

Rock types	No.	W	H	A	De	P	I_s	I_{s50}
		mm	mm	mm^2	mm	N	MPa	MPa
Siliceous and micaceous Phyllite (samples between chainage 600 and 900)	1	42	50	2100	52	7000	2.6	2.7
	2	48	50	2400	55	9000	2.9	3.1
	3	43	47	2021	51	8000	3.1	3.1
	4	42	42	1764	47	7000	3.1	3.0
	5	42	48	2016	51	7500	2.9	2.9
	6	47	50	2350	55	9000	3.0	3.1
	7	40	45	1800	48	6000	2.6	2.6
	8	38	40	1520	44	7000	3.6	3.4
	9	48	50	2400	55	10000	3.3	3.4
	10	40	44	1760	47	6000	2.7	2.6
	11	42	42	1764	47	5500	2.4	2.4
	12	40	43	1720	47	4000	1.8	1.8
	13	40	42	1680	46	5000	2.3	2.3
	14	41	42	1722	47	4000	1.8	1.8
	15	45	45	2025	51	5000	1.9	2.0
	16	50	53	2650	58	10000	3.0	3.2
	17	42	44	1848	49	8000	3.4	3.4
	18	43	45	1935	50	5000	2.0	2.0
	19	44	45	1980	50	8000	3.2	3.2
	20	42	45	1890	49	7000	2.9	2.9
	21	45	50	2250	54	8000	2.8	2.9
	22	47	50	2350	55	7500	2.5	2.6
	23	38	47	1786	48	5500	2.4	2.4
	24	38	42	1596	45	8500	4.2	4.0
	25	40	42	1680	46	7000	3.3	3.2
	26	50	50	2500	56	6500	2.0	2.2
	27	40	40	1600	45	4800	2.4	2.3
	28	48	50	2400	55	10000	3.3	3.4
	29	40	45	1800	48	6500	2.8	2.8
	30	42	50	2100	52	9500	3.5	3.6
	31	50	52	2600	58	8500	2.6	2.7
	32	52	53	2756	59	9500	2.7	2.9
	33	50	55	2750	59	9500	2.7	2.9
	34	43	48	2064	51	6800	2.6	2.6

Rock types	No.	W	H	A	De	P	I_s	I_{s50}
		mm	mm	mm^2	mm	N	MPa	MPa
Siliceous and micaceous Phyllite (samples between chainage 4050 and 4250)	35	46	52	2392	55	8000	2.6	2.7
	36	40	45	1800	48	7500	3.3	3.2
	37	44	46	2024	51	7500	2.9	2.9
	38	45	55	2475	56	8500	2.7	2.8
	39	45	50	2250	54	9000	3.1	3.2
	40	48	50	2400	55	7500	2.5	2.6
	41	52	55	2860	60	5500	1.5	1.6
	42	44	44	1936	50	4000	1.6	1.6
	43	43	48	2064	51	4500	1.7	1.7
	44	50	50	2500	56	6000	1.9	2.0
	45	45	60	2700	59	5000	1.5	1.6
	46	40	40	1600	45	4000	2.0	1.9
	47	42	40	1680	46	3600	1.7	1.6
	48	43	48	2064	51	4000	1.5	1.5
	49	58	50	2900	61	5000	1.4	1.5
	50	58	50	2900	61	5750	1.6	1.7
	51	48	50	2400	55	4850	1.6	1.7
	52	45	45	2025	51	5000	1.9	2.0
	53	45	50	2250	54	4500	1.6	1.6
	54	45	50	2250	54	4300	1.5	1.5
	55	46	42	1932	50	3500	1.4	1.4
	56	48	50	2400	55	4200	1.4	1.4
Mean							2.5	2.5
Standard deviation							0.7	0.7
Metasandstone (samples between chainage 4500 to 5000)	1	37	55	2035	51	7500	2.9	2.9
	2	42	45	1890	49	18500	7.7	7.6
	3	48	50	2400	55	21000	6.9	7.2
	4	41	43	1763	47	9000	4.0	3.9
	5	46	50	2300	54	17000	5.8	6.0
	6	40	52	2080	51	7000	2.6	2.7
	7	45	51	2295	54	20500	7.0	7.3
	8	40	48	1920	49	17000	7.0	6.9
	9	40	40	1600	45	7000	3.4	3.3
	10	40	40	1600	45	9000	4.4	4.2
	11	35	42	1470	43	11000	5.9	5.5

Rock types	No.	W	H	A	De	P	I_s	I_{s50}
		mm	mm	mm^2	mm	N	MPa	MPa
Metasandstone	12	48	55	2640	58	15000	4.5	4.8
	13	50	54	2700	59	14000	4.1	4.4
	14	42	45	1890	49	21000	8.7	8.7
	15	40	40	1600	45	16500	8.1	7.7
	16	40	42	1680	46	7500	3.5	3.4
	17	42	45	1890	49	10000	4.2	4.1
	18	42	42	1764	47	8000	3.6	3.5
	19	35	55	1925	50	17000	6.9	6.9
	20	48	52	2496	56	18000	5.7	6.0
	21	45	47	2115	52	5500	2.0	2.1
	22	48	52	2496	56	21000	6.6	7.0
	23	45	48	2160	52	12500	4.5	4.6
	24	38	42	1596	45	9500	4.7	4.5
	25	42	46	1932	50	8500	3.5	3.4
	20	48	52	2496	56	18000	5.7	6.0
Mean							5.1	5.1
Standard deviation							1.8	1.9

$$\sigma_{c50} = \frac{\sigma_c}{(50/d)^{0.18}}$$

$$D_e = \sqrt{4 \times A / \pi}$$

$$I_s = P / D_e^{\,2}$$

$$I_{s50} = (D_e / 50)^{0.45} \times I_s$$